Norsk institutt for luftforskning
Norwegian Institute for Air Research

Monitoring of greenhouse gases and aerosols at Svalbard and Birkenes in 2019

Annual report

Cathrine Lund Myhre, Tove Svendby, Ove Hermansen, Chris Lunder, Stephen M. Platt, Markus Fiebig, Ann Mari Fjæraa, Georg Hansen, Norbert Schmidbauer, Terje Krognes

NILU report 16/2020

NILU report 16/2020 Norwegian Environment Agency M-1797|2020	ISBN: 978-82-425-3018-9 ISSN: 2464-3327	CLASSIFICATION: A – Unclassified (open report)
DATE 22.10.2020	SIGNATURE OF RESPONSIBLE PERSON Ole-Anders Braathen, Viseadministrerende direktør (sign.)	NUMBER OF PAGES 152
TITLE Monitoring of greenhouse gases and aerosols at Svalbard and Birkenes in 2019 Annual report		PROJECT LEADER Wenche Aas NILU PROJECT NO. O-113007
AUTHOR(S) Cathrine Lund Myhre, Tove Svendby, Ove Hermansen, Chris Lunder, Stephen M. Platt, Markus Fiebig, Ann Mari Fjæraa, Georg Hansen, Norbert Schmidbauer, Terje Krognes		QUALITY CONTROLLER Kjetil Tørseth
REPORT PREPARED FOR Norwegian Environment Agency Postboks 5672 Sluppen, 7485 Trondheim		CONTRACT REF. Contract number 17078061

ABSTRACT

The report summarizes the activities and results of the greenhouse gas monitoring at the Zeppelin Observatory, situated on Svalbard in Arctic Norway, during the period 2001-2019, and the greenhouse gas monitoring and aerosol observations from Birkenes for 2009-2019.

NORWEGIAN TITLE

Overvåking av klimagasser og partikler på Svalbard og Birkenes i 2019: Årsrapport.

KEYWORDS

Greenhouse-gases/ Drivhusgasser	Aerosols/ Partikler	Climate gases/ Klimagasser	Halocarbons/ Halokarboner

ABSTRACT (in Norwegian)

Rapporten presenterer aktiviteter og måleresultater fra klimagassovervåkingen ved Zeppelin observatoriet på Svalbard for årene 2001-2019 og klimagassmålinger og klimarelevante partikkelmålinger fra Birkenes for 2009-2019

PUBLICATION TYPE: Digital document (pdf)	COVER PICTURE: Source: Kjetil Tørseth, NILU

Preface

This report presents the 2019 annual results from the national monitoring of greenhouse gas concentrations and climate-relevant particle properties. The observations are done at two atmospheric observatories; one regional background site in southern Norway and one Arctic site. The observations made are part of the national monitoring programme conducted by NILU- Norsk institutt for luftforskning (NILU) on behalf of The Norwegian Environment Agency. Additionally, the report includes results from Trollhaugen observatory in Antarctica. These measurements are not a part of the national monitoring programme, but receive direct support from the Norwegian Ministry of Climate and Environment.

The national monitoring programme comprises measurements of 46 greenhouse gases at the Zeppelin Observatory in the Arctic; and this includes a long list of halocarbons, which are not only greenhouse gases, but most of them are also ozone depleting substances. NILU initiated measurements of CH_4-isotope ($\delta^{13}C_{CH4}$) at Zeppelin in the year 2012 to provide more insight into Arctic sources of CH_4, and potential changes, as part of a project funded by the Norwegian Research Council. The continuation of these measurements was implemented in the Norwegian Monitoring programme in 2019. NILU upgraded and extended the observational activity at the Birkenes Observatory in Agder and from 2010, the national monitoring programme was extended to include aerosol properties (particle size, number, scattering and absorption properties) relevant for understanding the effects of aerosols on radiation.

The present report is the third of a series of annual reports in 2020, which cover the national monitoring of atmospheric composition in the Norwegian rural background environment. The other two reports focus on the atmospheric composition and deposition of air pollution of particulate and gas phase of inorganic constituents, particulate carbonaceous matter, ground level ozone and particulate matter (Aas et al, 2020), the second presents the monitoring of the ozone layer and UV (Svendby et al, 2020).

Participation in international programmes is crucial for quality assurance and quality control of the Norwegian measurement data and instruments. Data from this report contribute to, and benefit from, the European Research Infrastructure ACTRIS (*Aerosols, Clouds, and Trace gases Research InfraStructure*) and ICOS (*Integrated Carbon Observation System*). Additionally, data and results support and benefit from EMEP (European Monitoring and Evaluation Programme) under CLRTAP (Convention on Long-range Transboundary Air Pollution), and AGAGE (Advanced Global Atmospheric Gases Experiment).

All measurement data presented in the current report are public and can be received by contacting NILU, or they can be downloaded directly from the database: http://ebas.nilu.no.

A large number of persons at NILU have contributed to the current report, including those responsible for sampling, technical maintenance, chemical analysis and quality control and data management, in particular, Tove Svendby, Ove Hermansen, Chris Lunder, Markus Fiebig, Georg Hanssen, Stephen M. Platt, Terje Krognes, Ann Mari Fjæraa and Norbert Schmidbauer.

NILU, Kjeller, 30 September 2020
Cathrine Lund Myhre
Senior Scientist, Dep. Atmospheric and Climate Research

Contents

Sammendrag

Denne årsrapporten beskriver aktivitetene og hovedresultatene fra delprogrammet "*Overvåking av klimagasser og aerosoler på Zeppelin-observatoriet på Svalbard og Birkenes-observatoriet i Aust-Agder, Norge*". Rapporten omfatter målinger av 46 klimagasser og inkluderer de viktigste naturlig forekommende drivhusgassene, syntetiske klimagasser og ulike partikkelmålinger som har høy relevans for klima. Mange av gassene har også sterk ozonnedbrytende effekt. For klimagassene er utvikling og trender for perioden 2001-2019 rapportert, i tillegg til daglige og årlige gjennomsnittsverdier. Programmet ble utvidet med 16 nye gasser i 2015. I 2016 ble programmet ytterligere utvidet med seks nye gasser etter modifisering av instrumenteringen ved Zeppelinobservatoriet: tre hydrofluorkarboner (HFC), sulfurylfluorid (SO_2F_2), halon H-2402 og nitrogentrifluorid (NF_3). For de nye komponentene er data innhentet og analysert tilbake til 2010. Resultatene for alle klimagassene er oppsummert i tabell 1 på side 10.

Målingene på Zeppelin-observatoriet gir informasjon om utviklingen i bakgrunnsnivåkonsentrasjonene av klimagasser i Arktis, og alle de 46 gassene i overvåkningsprogrammet blir målt her. Birkenes-observatoriet ligger i et område i Sør-Norge som kan være sterkt påvirket av langtransportert luftforurensning, i tillegg til påvirkning fra lokal vegetasjon. På Birkenesobservatoriet gjøres observasjoner av karbondioksid (CO_2) og metan (CH_4), samt omfattende målinger av klimarelevante egenskaper til aerosoler (partikler). Aerosoler måles også på Zeppelin og Trollhaugen (Antarktis), men måleprogrammene her er ikke like omfattende som på Birkenes.

Konsentrasjonene av alle de viktigste klimagassene har økt kraftig siden 2001, bortsett fra ozonnedbrytende klorfluorkarboner (KFK-er) og noen få andre halogenerte gasser som er regulert gjennom Montrealprotokollen. De fleste av disse har hatt en reduksjon, som vist i rapporten.

Observasjonene fra 2019 viser nye rekordhøye nivåer for de fleste klimagassene i overvåkningsprogrammet. Årlig midlere CO_2 konsentrasjon i 2019 var 411.9 ppm (parts per million) på Zeppelin og 416.1 ppm på Birkenes. Dette er økninger på henholdsvis 2.6 ppm og 0.9 ppm fra 2018og ny rekord på begge stasjoner.

Konsentrasjonen av metan var også i 2019 rekordhøy både på Birkenes og på Zeppelin, med årlige middelverdier på 1961.2 ppb (parts per billion) på Birkenes og 1952.9 ppb på Zeppelin. I forhold til 2018-nivået er dette en økning på Zeppelin på 14.1 ppb, den høyeste økningen noen gang registeret på et år. Det er også betydelig økning på Birkenes på 8.2 ppb.

Endringene i løpet av de siste ti årene er store i forhold til utviklingen av metannivået i perioden 1998-2005, da endringene var tilnærmet null både på Zeppelin og globalt. Ulike metankilder (for eksempel naturgass og våtmarker) har ulik isotop-signatur (det vil si forhold mellom isotoper). Isotopmålinger av CH_4 på Zeppelin viser en klar trend i $\delta^{13}C_{CH4}$ etter 2012. En nedadgående trend i $\delta^{13}C_{CH4}$, samtidig med en økning av metankonsentrasjonene, viser at det har vært endringer i metankildene eller opptaksprosessene i løpet av de siste 7 årene. Endringene i $\delta^{13}C_{CH4}$ på Zeppelin tyder på økte utslipp fra biosfæren (våtmarker) og/eller jordbruk. Data fra 2019 indikerer at denne endringen i kildesammensetning er i ferd med å flate ut.

Lystgass (N_2O) har store menneskeskapte kilder som jordbruk og bergverk, men også naturlige kilder. N_2O nådde også nytt rekordnivå i 2019. Den årlige middelkonsentrasjonen på Zeppelin var 332.1 ppb, en økning på 0.8 ppb siden 2018.

De syntetiske, menneskeskapte klimagassene som inngår i overvåkingsprogrammet på Zeppelin er fire klorfluorkarboner (KFK-er), tre hydroklorfluorkarboner (HKFK-er), og 11 hydrofluorkarboner (HFK-er), de to sistnevnte gruppene er KFK-erstatninger. I tillegg inngår tre haloner, en gruppe med åtte andre halogenerte klimagasser, samt fire perfluorerte karboner (PFK-er) med svært høyt globalt oppvarmingspotensial (GWP). Videre rapporteres sulfurylfluorid, svovelhexafluorid, og nitrogentrifluorid, hvorav de to siste er meget sterke drivhusgasser.

Generelt, avtar konsentrasjonen av KFK-gasser, mens de øvrige gassene øker da disse ofte er erstatningsgasser for KFK-ene. For et par ås siden ble det oppdaget ukjente og urapporterte utslipp av KFK-11 i Asia, noe som har redusert den markante, negative trenden i de globale målingene av KFK-11. Utviklingen i KFK-gassene gir likevel grunn til optimisme, fordi konsentrasjonen for de fleste av disse gassene er synkende. KFK-115 er et unntak, her ser vi en økning fra 2018-2019. Samtidig, økte konsentrasjonene av KFK-erstatningsstoffene, HKFK-er og HFK-er, i perioden 2001-2019. For HKFK-er har det riktignok vært en avtagende økning de siste årene, og i år ser vi en liten nedgang for HCFC-142b. Denne nedgangen startet i 2017, så det er andre året på rad. HCFC-141b øker igjen, etter nedgang i perioden 2017-2018. Konsentrasjonen av HFK-gassene har økt kraftig siden 2001, og den økende trenden ser ut til å fortsette med unntak av noen få. Konsentrasjonene av disse menneskeskapte HFK-ene er fortsatt svært lave, noe som betyr at bidraget til den globale oppvarmingen per i dag er lite, men gitt den ekstremt sterke økningen og bruken av disse gassene, er det viktig å følge utviklingen nøye i fremtiden.

Konsentrasjonene av PFK-er og svovelfluorider (SF_6 og SO_2F_2) er også lave. Et unntak er PFK-14, som hadde en årlig middelverdi på 86.1 ppt (parts per trillion) i 2019, en økning på 0.85 ppt fra 2018 (noe lavere enn året før). Konsentrasjonen av SF_6 bør også følges nøye, ettersom denne forbindelsen har en atmosfærisk levetid på 3 200 år og et GWP på hele 23 500. Denne forbindelsen har økt med hele 105% siden målingene startet på Zeppelin i 2001.

Aerosoler består av små partikler i atmosfæren. Partiklenes klimapåvirkning avhenger av mengden partikler og absorpsjonsegenskapene til enkeltpartiklene. Konsentrasjonen av partikler på Birkenes bestemmes i hovedsak av den langtransporterte luftforurensningen fra det kontinentale Europa, i tillegg til regionale og lokale vegetasjonskilder (biogene kilder). I 2019 ser vi episoder av langtransportert aerosol fra kilder i sentral Europa om vinteren, og fra skogbrann i Ukraina i august 2019. Siden oppstart av målingene på Birkenes i 2010, ser vi ingen trend i utviklingen av partikkelegenskapene (antall, absorpsjons- og strålingsspredningsegenskaper), noe som nylig ble bekreftet av en omfattende studie av trender i optiske partikkelegenskaper fra stasjoner over hele verden.

På Zeppelin er situasjonen litt annerledes. Ved å sammenstille våre aerosolmålinger med resultater fra andre samarbeidspartnere, finner vi en nedadgående trend i aerosol-absorpsjonen, noe som viser at konsentrasjonen av sot eller såkalt «*black carbon*» går ned. Observasjoner av den totale kolonnen av aerosoler over Ny-Ålesund (aerosol optisk dybde, AOD) viser økte konsentrasjoner om våren sammenlignet med resten av året. Dette fenomenet, som kalles arktisk dis (*Arctic haze*), skyldes transport av forurensning fra lavere breddegrader i løpet av vinteren/våren, hovedsakelig transport fra Europa og Russland. I 2019 ser vi transportepisoder av aerosol fra skogbrann fra øst-Europa (vest Sibirske steppe, Ukraina, vest Russland), som inkluderer det samme kildeområdet observert på Birkenes i August 2019.

Partiklene på Trollhaugen i Antarktis er preget av naturlige storskalaprosesser med en veldig konstant årssyklus. En episode observert i 2019 om vinteren skyldes luftmasser påvirket av utslipp fra en nabo-stasjon 360 km til øst.

Summary

This annual report describes the activities and main results of the programme "*Monitoring of greenhouse gases and aerosols at the Zeppelin Observatory, Svalbard, and Birkenes Observatory, Aust-Agder, Norway*". The report comprises the measurements of 46 climate gases up to 31 December 2019; including the most important naturally occurring well-mixed greenhouse gases, synthetic greenhouse gases, reactive short lived gases as volatile organic compounds (VOCs), and CO in addition to various particle properties with high relevance to climate. Many of the gases also have strong ozone depleting effects. The development and trends for the period 2001-2019 are reported, in addition to daily and annual mean observations. In 2015, the programme was extended to include 16 new climate gases, all with measurements analysed back to 2010. In 2016 the programme was further extended with six more species after modification of the instrumentation at the Zeppelin Observatory: three hydrofluorocarbons (HFCs), sulphuryl fluoride (SO_2F_2), halon H-2402 and nitrogen trifluoride (NF_3). The main results for 2019 for all climate gases are summarized in Table 1.

The measurements at Zeppelin Observatory provide the trends in background level concentrations of climate gases in the Arctic, and all the 46 climate gases in the programme are monitored at this site. Birkenes Observatory is located in an area of Southern Norway highly influenced by long-range transport of pollutants from the European continent. At Birkenes the influence of local vegetation/terrestrial interactions is also important. Carbon dioxide (CO_2) and methane (CH_4) measurements are undertaken at Birkenes, in addition to a comprehensive aerosol measurement programme. Aerosol measurements are also performed at Zeppelin and Trollhaugen (Antarctica), although less extensively than the Birkenes measurements.

The concentrations of all main greenhouse gases have been increasing since 2001, except for the ozone-depleting chlorofluorocarbons (CFCs) and a few halogenated gases regulated through the successful Montreal Protocol.

The observations from 2019 show new record high levels for most climate gases measured. The annual average CO_2 concentration in 2019 was 411.9 ppm at Zeppelin and 416.1 ppm at Birkenes. The increases from 2018 are 2.6 ppm and 0.9 ppm, respectively.

The concentration of CH_4 also reached new record high levels in 2019 at Birkenes, and Zeppelin, with annual mean concentrations of 1961.2 ppb at Birkenes and 1952.9 ppb at Zeppelin. These levels represent new record annual increase at Zeppelin of 14.1 ppb. At Birkenes, the increase was 8.2 ppb. For the isotopic signature of CH_4, a clear trend in $\delta^{13}C_{CH4}$ is evident after 2012. The observed negative shifts in ambient $\delta^{13}C_{CH4,}$ and increases in the CH_4 ambient mixing ratio at the same time, imply changes in the balance of sources and potentially sinks. The developments in $\delta^{13}C_{CH4}$ observed at Zeppelin suggest increases in biosphere and/or agriculture (wetland or ruminant) emissions. For 2019 the data are indicating a more stable distribution among the sources.

The N_2O concentration at Zeppelin was also at a record high in 2018. The annual mean concentration was 332.1 ppb, an increase of 0.8 ppb since 2018.

The synthetic manmade greenhouse gases included in the monitoring programme at Zeppelin are 4 chlorofluorocarbons (CFCs), 3 hydrochlorofluorocarbons (HCFCs), and 11 HFCs – the last two being CFC substitutes. In addition three halons, a group of 8 halogenated gases, and 4 perfluorinated carbons (PFCs) with very high global warming potentials are included. Furthermore, sulphurhexafluorid, nitrogen trifluoride and sulphuryl fluoride were reported for the first time in 2016. Particularly the two first are extremely strong greenhouse gases.

Recently, new and previously unreported CFC-11 emission sources were discovered in Asia, which have slowed down the rate of CFC-11 decrease globally. Still, the development of the CFC gases measured at Zeppelin is very encouraging as the concentrations of the dominating species are declining. CFC-115 is an exception. We see an increase in the concentration of this compound. Contrary to the CFCs, the

CFC substitutes HCFCs and HFCs have increased over the period 2001-2019. For the HCFCs, a relaxation in the upward trend has been observed the last years, and HCFC-142b shows a small decrease the last 2 years. However, for HFCs a strong increase is observed since 2001, and the increasing trend is continuing. The contribution from these manmade gases to global warming is small today, as the concentrations of HFCs are still very low. However, given the extremely rapid increase in the use of these gases, it is crucial to follow their development in the future.

Atmospheric concentrations of PFCs and sulfuryl fluoride (SO_2F_2), sulphur hexafluoride (SF_6) are also low. An exception is PFC-14, which had a mixing ratio of 86.1 ppt in 2019, an increase of 0.85 ppt since 2018. SF_6 should also be followed closely, as this compound has an atmospheric life time of 3 200 years and an extremely high GWP of 23 500. This compound has increased by 105% since 2001.

Aerosols consist of small particles in the atmosphere. They can have warming or cooling effects on climate, depending on the amount of particles and their properties. Aerosol loads and properties at Birkenes are mainly influenced by long-range transport of air pollution from continental Europe, combined with regional sources like biogenic particle formation. Episodes visible in 2019 originate from long-range transport of winter emissions from Central Europe, and from forest fire emissions in Ukraine in August 2019. Since the start of physical and optical aerosol observations at Birkenes in 2010, we don't see any significant trend in aerosol properties, which is consistent with a recent study of aerosol optical property trends covering the whole globe.

At Zeppelin the situation is different. By comparing our aerosol absorption data collected at Zeppelin with data from collaborating institutes, a decreasing trend is observed, indicating a decrease of "black carbon" at Zeppelin. Observations of the total amount of aerosol particles in the atmosphere above Ny-Ålesund (aerosol optical depth) show high concentrations during springtime compared to the rest of the year. This phenomenon, called Arctic haze, is due to transport of pollution from lower latitudes accumulating in the Arctic atmosphere during winter/spring. In 2019, we can connect observed aerosol transport episodes to forest fire events in Eastern Europe (Western Siberian Plain, Ukraine, western Russia), which includes the same source region observed at Birkenes in August 2019.

The aerosol at Trollhaugen, Antarctica, is characterised by natural, hemispheric scale processes with a very constant annual cycle. An episode observed in Winter 2019 can be connected to emissions from a neighbouring station 360 km east of Troll.

Table 1: Key findings; Greenhouse gases measured at Zeppelin, Ny-Ålesund; lifetimes in years[1], global warming potential (GWP over 100 years, when available[1]), annual mean concentrations for 2019 and their long term trends per year over the measurement period. CO_2 and CH_4 are also measured at Birkenes. Concentrations are in ppm (parts per million) for CO_2, ppb (part per billion) for CH_4, CO, and N_2O, and ppt (parts per trillion) for the other gases. The trend method is described in appendix II.

Component		Life-time	GWP	Annual mean 2019	Annual change mean since last year	Trend /yr
Carbon dioxide - Zeppelin	CO_2	**	1	411.9	+2.6	+2.5
Carbon dioxide - Birkenes				416.1	+0.9	+2.5
Methane - Zeppelin	CH_4	12.4	28	1952.9	+14.4	+6.2
Methane - Birkenes				1961.2	+8.2	+8.4
Carbon monoxide	CO	few months	-	115.4	+1.8	-1.2
Nitrous oxide	N_2O	121	265	332.1	+0.79	+0.98
Chlorofluorocarbons						
CFC-11	CCl_3F	45	4 660	228.1	-1.02	-1.79
CFC-12	CF_2Cl_2	640	10 200	505.7	-3.17	-2.51
CFC-113	CF2ClCFCl2	85	13 900	70.1	-0.52	-0.64
CFC-115	CF_3CF_2Cl	1 020	7 670	8.8	+0.08	+0.02
Hydrochlorofluorocarbons						
HCFC-22	$CHClF_2$	11.9	1 760	255.7	+1.88	+5.81
HCFC-141b	$C_2H_3FCl_2$	9.2	782	25.7	+0.17	+0.53
HCFC-142b	CH_3CF_2Cl	17.2	1 980	23.1	-0.12	+0.54
Hydrofluorocarbons						
HFC-125	CHF_2CF_3	28.2	3 170	32.3	+3.42	+1.65
HFC-134a	CH_2FCF_3	13.4	1 300	114.8	+6.26	+5.14
HFC-152a	CH_3CHF_2	1.5	506	10.5	+0.24	+0.43
HFC-23	CHF_3	228	12 400	33.2	+1.35	+1.04
HFC-365mfc	$CH_3CF_2CH_2CF_3$	8.7	804	1.31	+0.03	+0.07
HFC-227ea	CF_3CHFCF_3	38.9	3 350	1.76	+0.16	+0.12
HFC-236fa	$CF_3CH_2CF_3$	242	8 060	0.20	+0.02	+0.01
HFC-245fa	$CHF_2CH_2CF_3$	7.7	858	3.53	+0.27	+0.21
HFC-32	CH_2F_2	5.2	677	25.2	+3.72	+2.15
HFC-4310mee	$C_5H_2F_{10}$	16.1	1 650	0.30	+0.01	+0.01
HFC-143a	CH_3CF_3	47.1	4 800	25.5	+1.64	+1.53
Perfluorinated compounds						
PFC-14	CF_4	50 000	6 630	86.10	+0.85	+0.89

* The measurements of these components have higher uncertainty. See Appendix I for more details.

[1] From Scientific Assessment of Ozone Depletion: 2010 (WMO, 2011b) and the 4th Assessment Report of the IPCC, Hodnebrog et al (2013)

** Carbon dioxide does not have a specific lifetime because it is continuously cycled between the atmosphere, oceans and land biosphere and its net removal from the atmosphere involves a range of processes with different time scales.

Component		Life-time	GWP	Annual mean 2019	Annual change mean since last year	Trend /yr
PFC-116	C_2F_6	10 000	11 100	4.91	+0.09	+0.09
PFC-218	C_3F_8	2600	8 900	0.69	+0.02	+0.01
PFC-318	c-C_4F_8	3200	9 540	1.80	+0.07	+0.06
Sulphurhexafluoride	SF_6	3 200	23 500	10.14	+0.34	+0.29
Nitrogen trifluoride	NF_3	500	16 100	2.22	+0.23	+0.20
Sulphuryl fluoride	SO_2F_2	36	4 090	2.63	+0.11	+0.10
Halons						
H-1211	$CBrClF_2$	16	1 750	3.37	-0.08	-0.07
H-1301	$CBrF_3$	65	7 800	3.39	+0.012	+0.02
H-2402	$CBrF_2CBrF_2$	20	1 470	0.41	0.00	-0.01
Halogenated compounds						
Chloromethane	CH_3Cl	1	12	507.97	-6.39	-0.37
Bromomethane	CH_3Br	0.8	2	6.78	+0.20	-0.16
Dichloromethane	CH_2Cl_2	0.4	9	58.89	-1.84	+1.93
Trichloromethane	$CHCl_3$	0.4	16	12.20	-2.50	+0.24
Carbon tetrachloride	CCl_4	26	1730	78.02	-0.76	-0.95
Trichloroethane	CH_3CCl_3	5	160	1.71	-0.29	-1.81
Trichloroethene	$CHClCCl_2$	-	-	0.16	-0.12	-0.02
Tetrachloroethene	CCl_2CCl_2	-	-	2.27	-0.02	-0.11
Volatile Organic Compounds (VOC)						
Ethane	C_2H_6	Ca 78 days[#]		1602.45	+77.51	-
Propane	C_3H_8	Ca 18 days[#]		454.71	-44.63	-
Butane	C_4H_{10}	Ca 8 days[#]		140.09	-3.43	-
Pentane	C_5H_{12}	Ca 5 days[#]		43.77	+4.85	-
Benzene	C_6H_6	Ca 17 days[#]		61.11	-1.77	-
Toluene	$C_6H_5CH_3$	Ca 2 days[#]		18.87	-2.08	-

[#]*The lifetimes of VOC are strongly dependant on season, sunlight, other components etc. The estimates are global averages given in C. Nicholas Hewitt (ed.): Reactive Hydrocarbons in the Atmosphere, Academic Press, 1999, p. 313. The times series for these are short and the trend is very uncertain.*

Monitoring of greenhouse gases and aerosols at Svalbard and Birkenes in 2019

Annual report

1 Introduction to monitoring of greenhouse gases and aerosols

1.1 The monitoring programme in 2019

The purpose of the monitoring programme is to study the long-term development of climate gases and aerosols (particles). Measurements are performed at three sites and the results are used as contributions to European and global observation networks.

The atmospheric monitoring programme presented in this report focuses on the concentrations of greenhouse gases and on selected particle physical and optical properties relevant for the understanding of climate change. Sampling sites are at Svalbard in the Norwegian Arctic (Zeppelin Observatory), where observations are considered to be representative for well-mixed background concentration levels, and a second site in southern Norway (Birkenes Observatory), where observations are more influenced by regional and local sources (Figure 1). A third site is in the Antarctic (Trollhaugen station).

Figure 1: Location of NILU's atmospheric supersites measuring greenhouse gases and aerosol properties.

The main objectives are to quantify the levels of the main greenhouse gases including ozone depleting substances, describe the relevant optical and physical properties of aerosols, and document their development over time. Measurements of the greenhouse gas concentrations and aerosol properties are core data for studies and assessments of climate change, and also crucial in order to evaluate mitigation strategies and their effectiveness. The Norwegian monitoring sites are located in areas where the influence of local sources is minimal, hence the sites are representative for a wider region allowing detection of long-term changes in atmospheric composition.

1.2 The measurements in relation to research and policy agreements

The Norwegian greenhouse gas and aerosol monitoring programme is set up to meet national and international needs for greenhouse gas and aerosol measurement data, both for the scientific community, national environmental authorities and global policy making.

Greenhouse gases: The Paris Agreement was negotiated and adopted by consensus at the 21st Conference of the Parties of the UNFCC in Paris on 12 December 2015. The Paris Agreement entered into force on 4 November 2016. As of September 2020 189 of the 197 Parties to the Convention, have

ratified the Protocol[2]. The crucial aim of the Paris agreement is to keep the increase in the global average temperature to well below 2°C compared to pre-industrial levels and to pursue efforts to limit the temperature increase to 1.5°C. The EU Heads of State and Governments agreed in October 2014 on the headline targets and the architecture for the EU framework on climate and energy for 2030. The agreed targets include a cut in greenhouse gas emissions by at least 40% by 2030 compared to 1990 levels[3], and this is also set in the Norwegian "*Klimaloven*"[4].

Ozone depleting substances and their replacement gases: In 1987 the Montreal Protocol was signed and entered into force in 1989 in order to reduce the production, use and eventually emission of the ozone-depleting substances (ODS). The amount of most ODS in the troposphere is now declining slowly and is expected to be back to pre-1980 levels around year 2050. It is central to follow the development of the concentration of these ozone depleting substances in order to verify that the Montreal Protocol and its amendments work as expected. The development of the ozone layer above Norway is monitored closely, and the results of the national monitoring of ozone and UV is presented in "*Monitoring of the atmospheric ozone layer and natural ultraviolet radiation: Annual report 2019*" ([5]Svendby et al. 2020). The ozone depleting gases and their replacement gases are also strong greenhouse gases making it even more important to follow the development of their concentrations.

To control the new replacement gases, a historical agreement was signed on 15 October 2016 when negotiators from 197 countries agreed to reduce the production and consumption of hydrofluorocarbons (HFCs). The agreement was finalized at the United Nations meeting in Kigali, Rwanda, aiming to reduce the use of HFCs by more than 80% over the course of the twenty-first century. The agreement in Kigali represents an amendment of the 1987 Montreal Protocol. The HFCs can be up to 10000 times as effective at trapping heat compared to carbon dioxide. Today HFCs account for a small fraction of the greenhouse-gas emissions and have had limited influence on the global warming up to now. However, the use of HFCs is growing rapidly and the projected HFC emission could contribute up to 0.5°C of global warming by the end of this century if not regulated (Xu et al., 2013). The agreement in Kigali is an amendment to the Montreal Protocol and entered into force in January 2019 and is now legally binding for the countries that have ratified the amendment.

1.3 The ongoing monitoring programme and the link to networks and research infrastructures

In response to the need for monitoring of greenhouse gases and ozone depleting substances, the *Norwegian Environment Agency* and *NILU – Norwegian Institute for Air Research* first signed a contract commissioning NILU to run a programme for monitoring greenhouse gases at the Zeppelin Observatory, close to Ny-Ålesund in Svalbard in 1999. This national programme now includes monitoring of 46 greenhouse gases and trace gases at the Zeppelin Observatory in the Arctic, many of them also ozone depleting substances. In 2009, NILU upgraded and extended the observational activity at the Birkenes Observatory in Aust-Agder. From 2010, the Norwegian Environment Agency/NILU monitoring programme was extended to also include the new observations from Birkenes of the greenhouse gases CO_2 and CH_4 and selected aerosol observations particularly relevant for the understanding of climate change. Relevant components are also reported in "*Monitoring of long-range transported air pollutants in Norway, annual report 2019*" [5](Aas et al. 2020), this includes particulate and gaseous inorganic constituents, particulate carbonaceous matter, ground level ozone and particulate matter for 2019.

[2] https://unfccc.int/process/the-paris-agreement/status-of-ratification
[3] Details here: http://ec.europa.eu/clima/policies/strategies/2030/ and here http://www.consilium.europa.eu/uedocs/cms_data/docs/pressdata/en/ec/145397.pdf
[4] https://lovdata.no/dokument/NL/lov/2017-06-16-60
[5] Norwegian Environment Agency monitoring reports

The location of both sites are shown in Figure 1, and pictures of the sites are shown in Figure 2. The unique location of the Zeppelin Observatory at Svalbard, together with the infrastructure of the scientific research community in Ny-Ålesund, makes it ideal for monitoring the global changes of concentrations of greenhouse gases and aerosols in the atmosphere. There are few local sources of emissions, and the Arctic location is also important as the Arctic is a particularly vulnerable region. The observations at the Birkenes Observatory complement the Arctic site. Birkenes Observatory is located in a forest area with few local sources. However, the Observatory often receives long-range transported pollution from Europe and the site is ideal to analyse the contribution of long range transported greenhouse gases and aerosol properties.

Figure 2: The two atmospheric observatories included in this programme, Zeppelin above and Birkenes to the left. A 75 m high mast was installed at Birkenes in 2020.

Data and results from the national monitoring programme are also included in various international programmes. Both sites contribute to EMEP (European Monitoring and Evaluation Programme) under the CLRTAP (Convention on Long-range Transboundary Air Pollution). Data from the sites are also reported to CAMP (Comprehensive Atmospheric Monitoring Programme) under OSPAR (the Convention for the Protection of the marine Environment of the North-East Atlantic, http://www.ospar.org), AMAP (Arctic Monitoring and Assessment Programme http://www.amap.no), WMO/GAW (The World Meteorological Organization, Global Atmosphere Watch programme, http://www.wmo.int) and AGAGE (Advanced Global Atmospheric Gases Experiment).

Zeppelin and Birkenes are both included in two central European environmental research infrastructures (RI) focusing on climate forcers and air quality. International collaboration and harmonisation of these types of observations are crucial for improved processes understanding and satisfactory quality of data to assess trends. The two central RIs are ICOS (Integrated Carbon Observation System, https://www.icos-ri.eu) focusing on the understanding of carbon cycle, and ACTRIS (Aerosols, Clouds, and Trace gases Research InfraStructure, www.actris.eu) focusing on short-lived aerosol climate forcers and related reactive gases, and clouds. This participation in these RIs ensure required quality of the data with harmonised methods and measurements across Europe and also a global link to have comparable data and results on global scale. This is essential to reduce the uncertainty in trends and in the observed levels of the wide range of climate forcers. Overall, the networks EMEP and AGAGE, and the research infrastructures ACTRIS and ICOS are crucial for quality assurance and quality control of the Norwegian measurement data and instruments. All measurements included in this report follow the protocols, methodology and recommendations of these frameworks. This is a prerequisite for harmonised and comparable data on both European and global scale, see Table 2 at page 17. (Additionally, the implementation of Norwegian measurements in ICOS through the ICOS-Norway[6] project is described in the Appendix II.)

NILU hosts the data centres of the European Monitoring and Evaluation Programme (EMEP), ACTRIS and the WMO Global Atmosphere Watch (GAW) World Data Centre for Aerosol (WDCA) and GAW-World Data Centre for Reactive Gases (WDCRG), and numerous other projects and programs (e.g. AMAP, HELCOM). Data reported from these frameworks are accessible and can be downloaded directly from the EBAS data base: http://ebas.nilu.no. All data from the national monitoring programme and from these frameworks are reported to this database, and through this accessible for all types of users. It is important to highlight that NILU's work in ACTRIS and also hosting the WMO GAW World Data Centres for Aerosols and reactive trace gases, among many other synergy effects, ensures efficient dissemination of the data on atmospheric aerosol properties collected within the Norwegian climate monitoring programme, to the scientific community. Among others, ACTRIS develops a primary standard for calibrating instruments measuring aerosol absorption, one of the properties of atmospheric black carbon, and develop quality standards for measuring the aerosol particle size distribution in order to further improve assessments of aerosol climate forcing. Another project relevant in this context is *ENVironmental Research Infrastructures building Fair services Accessible for society, Innovation and Research* (ENVRI-FAIR) [7] project. ENVRI-FAIR is an umbrella project for all environmental research infrastructures funded or supported by the EU under H2020. The objective is to make data FAIR, which means "*FAIR—**F**indable, **A**ccessible, **I**nteroperable, **R**eusable* (Wilkinson et al, 2016). One of its goal is to put data from the atmospheric, marine, tectonic, and biosphere domains into a common context by making the data interoperable, i.e. visible in common services. The efforts started with achieving this goal first within the atmospheric domain, and NILU is leading the implementation of FAIRness within the atmospheric domain, across all European Research Infrastructures.

Compiled key information on the national monitoring programme is listed in Table 2. From 2015 the programme was extended with 16 new greenhouse gases and reactive trace gases, mainly HFCs and

[6] https://no.icos-cp.eu
[7] http://envri.eu/envri-fair/

non-methane hydrocarbons. For some of those, quality assured measurements were possible to retrieve from the start in 2010. From 2016 also NF_3 and 4 PFCs and SO_2F_2 were added. More detailed information on the monitoring programme and measurement frequencies are provided in Appendix II. For the measurements of aerosol properties more details are presented in chapter 3.

Table 2: Summary of the measurement programme, run by NILU, at Birkenes and Zeppelin Observatory. The green colour indicates the extension and components added to the program in 2016.

Component	Birkenes Start	Zeppelin Start	International network, QA programme in bold	Comment
Trace gases				
CO_2	2009	2012	**ICOS**	Measured at Zeppelin since 1988 by Univ. Stockholm. By NILU at Zeppelin since 2012, now included in the programme. Qualified as ICOS class 1 site since 2017. ICOS labelling in 2020 for Birkenes
CH_4	2009	2001	**ICOS**	ICOS labelling and implementation in 2017 for Zeppelin, 2020 for Birkenes
N_2O	-	2009	**ICOS**	ICOS labelling and implementation in 2017
CO	-	2001	**ICOS**	ICOS labelling and implementation in 2017
Ozone (surface)	1985	1989	**EMEP**	Reported in Aas et al. 2020.
CFCs		2001/ 2010 and later	**AGAGE**	*The measurements marked "*": these components are not within the required precision of AGAGE, but a part of the AGAGE quality assurance programme. This is related to the measurements in the period 2001-2010, before the installation of the Medusa instrument. After 2010, the measurements are with the same precision as the rest of the measurements in the AGAGE network. The compounds marked in green were included in the national monitoring programme from 2015, with harmonised time series and measurements back to 2010 when the Medusa instrument was installed at Zeppelin.
CFC-11*				
CFC-12*				
CFC-113*				
CFC-115*				
HCFCs				
HCFC-22				
HCFC-141b				
HCFC-142b				
HFC-125				
HFC-134a				
HFC-152a				
HFCs				
HFC-125				
HFC-134a				
HFC-152a				
HFC-23				
HFC-227ea				
HFC-236fa				
HFC-245fa				
HFC-365mfc				
HFC-32				
HFC-4310mee				
HFC-143a				
PFCs				
PFC-14				
PFC-116				
PFC-218				
PFC-318				
Halons				
H-1211				
H-1301				
H-2402				

Component	Birkenes Start	Zeppelin Start	International network, QA programme in bold	Comment
Trace gases				
Other chlorinated				
CH_3Cl				
CH_3Br				
CH_2Cl_2				
$CHCl_3$				
CCl_4				
CH_3CCl_3				
$CHClCCl_2$*				
CCl_2CCl_2*				
Other fluorinated				
SF_6		2001		
NF_3		2016		
SO_2F_2		2010		
VOCs		2010		
C_2H_6 – ethane			**ACTRIS,** EMEP	VOCs were included in the national monitoring programme from 2015, but the measurements are harmonised back to 2010.
C_3H_8 – propane				
C_4H_{10} – butane				
C_5H_{12} – pentane				
C_6H_6 – benzene				
$C_6H_5CH_3$ – toluene				
Aerosol measurements				
Absorption properties	2009	2015	**ACTRIS,** EMEP	Measured by Univ. of Stockholm at Zeppelin, New from late 2015
Scattering properties	2009	-	**ACTRIS,** EMEP	Measured by Univ. of Stockholm at Zeppelin
Number Size Distribution	2009	2010	**ACTRIS,** EMEP	Reported in Aas et al. 2019; M-1395/2019.
Cloud Condensation Nuclei	2012	-	**ACTRIS**	Zeppelin: In collaboration with Korean Polar Research Institute
Aerosol Optical depth	2010	2007	**AERONET, GAW-PFR**	Birkenes: AERONET, Ny-Ålesund: GAW-PFR
PM_{10}	2001		**EMEP**	Reported in Aas et al. 2019; M-1395/2019.
$PM_{2.5}$	2001		**EMEP**	
Chemical composition -inorganic	1978	1979	**EMEP**	
Chemical composition - carbonaceous matter	2001		**EMEP**	

1.4 Greenhouse gases, aerosols and their climate effects

The Intergovernmental Panel on Climate Change's (IPCC's) Fifth Assessment Report (IPCC AR5) and the contribution from Working Group I "*Climate Change 2013: The Physical Science Basis*" was published in September 2013. This substantial climate assessment report presents evidence of past and projected future climate change from numerous independent scientific studies ranging from observations of the climate system, paleoclimate archives, theoretical studies on climate processes and simulations using climate models. Their main conclusion was:

> *"Warming of the climate system is unequivocal, and since the 1950s, many of the observed changes are unprecedented over decades to millennia. The atmosphere and ocean have warmed, the amounts of snow and ice have diminished, sea level has risen, and the concentrations of greenhouse gases have increased"*
> *(IPCC, Summary for policy makers, WG I,* 2013)

Their conclusions are based on a variety of independent indicators, some of them are observations of atmospheric compositional change. The overall conclusion with respect to the development of the concentrations of the main greenhouse gases is:

> *"The atmospheric concentrations of carbon dioxide, methane, and nitrous oxide have increased to levels unprecedented in at least the last 800,000 years. Carbon dioxide concentrations have increased by 40% since pre-industrial times, primarily from fossil fuel emissions and secondarily from net land use change emissions. The ocean has absorbed about 30% of the emitted anthropogenic carbon dioxide, causing ocean acidification"*
> *(IPCC, Summary for policy makers, 2013)*

In particular, Chapter 2, "*Observations: Atmosphere and Surface*", presents all types of atmospheric and surface observations, including observations of greenhouse gases since the start of the observations in mid-1950s and changes in aerosols since the 1980s. The IPCC AR5 report was the first time long term changes of aerosols were included in the report, based on global and regional measurement networks and satellite observations. The main conclusion with respect to development of the aerosol levels is that **"***It is very likely that aerosol column amounts have declined over Europe and the eastern USA since the mid-1990s and increased over eastern and southern Asia* since 2000" (Hartmann et al, 2013). This is important since the net effect of aerosols is atmospheric cooling, counteracting the effect of greenhouse gases. The changes in Europe and the USA are mainly due to mitigation strategies of e.g. sulphur, while the emissions are increasing rapidly in Asia, including increasing emissions of the warming component black carbon.

The basic metric to compare the effect of the various climate change drivers is radiative forcing (RF). RF is the net change in the energy balance of the Earth system due to some imposed change. RF provides a quantitative basis for comparing potential climate response to different changes. Forcing is often presented as the radiative change from one time-period to another, such as pre-industrial to present-day. For many forcing agents the RF is an appropriate way to compare the relative importance of their potential climate effect. However, rapid adjustments in the troposphere can either enhance or reduce the perturbations, leading to large differences in the forcing driving the long-term climate change. In the AR5 IPCC report it was also introduced a new concept, the effective radiative forcing (ERF). The ERF concept aims to take rapid adjustments into account, and is the change in net TOA (Top Of Atmosphere) downward radiative flux after allowing for atmospheric temperatures, water vapour and clouds to adjust, but with surface temperature or a portion of surface conditions unchanged (Myhre et al, 2013b). Figure 3 shows the RF and ERF of the main components referring to a change in the atmospheric level since 1750, pre-industrial time.

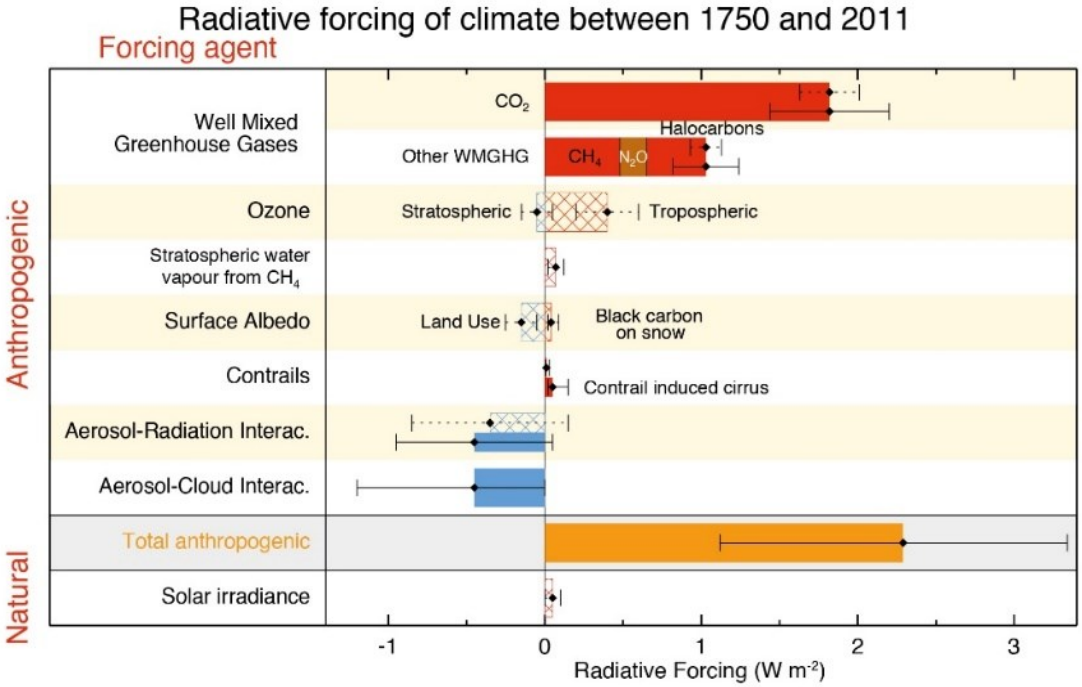

Figure 3: Bar chart for RF (hatched) and ERF (solid) for the period 1750–2011. Uncertainties (5 to 95% confidence range) are given for RF (dotted lines) and ERF (solid lines). (Taken from Myhre et al, 2013b).

Total adjusted anthropogenic forcing is 2.29 W m^{-2}, [1.13 to 3.33], and the main anthropogenic component driving this is CO_2 with a total RF of 1.82 W m^{-2}. The net direct and indirect effect of aerosols are cooling and calculated to -0.9 W m^{-2}. The diagram in Figure 4 shows a comparison in percent % of the various contribution from the long-lived greenhouse gases to the total forcing of the well-mixed greenhouse gases, based on 2011 levels.

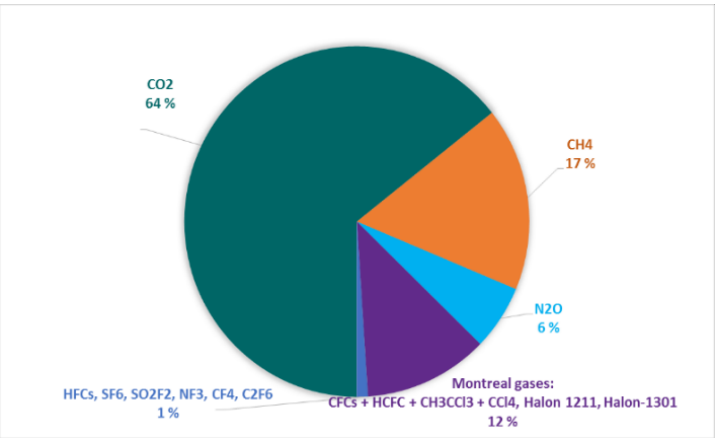

Figure 4: The contribution in % of the well-mixed greenhouse gases to the total forcing of the well-mixed greenhouse gases for the period 1750-2011 based on estimates in Table 8.2 in Chap 8, of IPCC (Myhre et al, 2013b).

An interesting but complex and more detailed picture of the influence of various emissions on the RF is illustrated in Figure 5. This Figure shows the forcing since 1750 by emitted compounds, to better illustrate the effects of emissions and potential impact of mitigations.

As seen, the number of emitted compounds and changes leading to RF is larger than the number of compounds causing RF directly. This is due to indirect effects, in particular components involved in atmospheric chemistry that affect e.g. CH_4 and ozone. Emissions of CH_4, CO, and NMVOC all lead to excess CO_2 as one of the end products, and this is the reason why the RF of direct CO_2 emission is slightly lower than the RF of abundance change of CO_2 in Figure 3. Note also that for CH_4, the contribution from emissions is estimated to be almost twice as large as that from the direct effect of the CH_4 concentration change, 0.97 W m^{-2} versus 0.48 W m^{-2} shown in Figure 3 and Figure 5 respectively. This is because emission of CH_4 leads to ozone production (shown in green colour in the CH_4 bar in Figure 5), stratospheric water vapour, CO_2 (as mentioned above), and importantly affects its own lifetime. As seen from the Figure, there is also a particularly complex picture of the effects of aerosols. Black carbon, originating from both fossil fuel, biofuel and biomass burning, heats the atmosphere. The direct effect of black carbon from fossil and biofuel is +0.4 W m^{-2}, while black carbon from biomass burning has zero net effect due to cooling from co-emitted organic carbon aerosol.

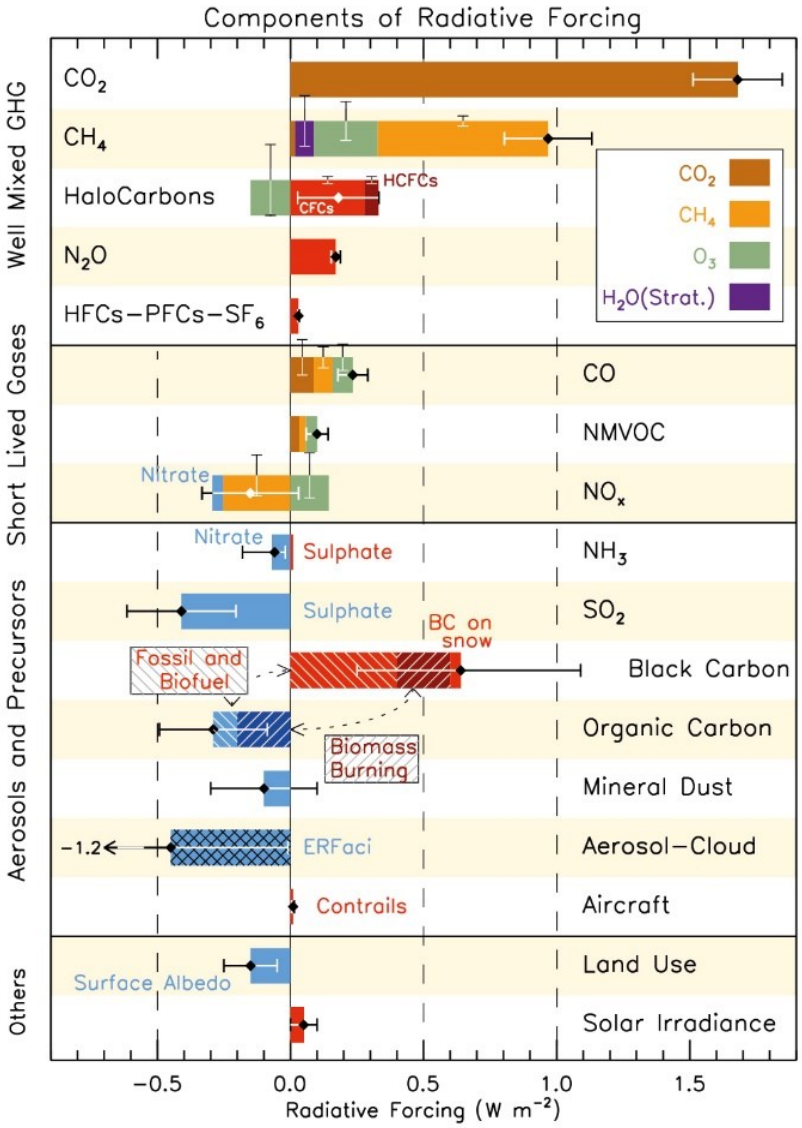

Figure 5: *RF bar chart for the period 1750–2011 based on emitted compounds (gases, aerosols or aerosol precursors) or other changes. Red (positive RF) and blue (negative forcing) are used for emitted components which affect few forcing agents, whereas for emitted components affecting many compounds several colours are used as indicated in the inset at the upper part the figure. The vertical bars indicate the relative uncertainty of the RF induced by each component. Their length is proportional to the thickness of the bar, that is, the full length is equal to the bar thickness for a ±50% uncertainty. The net impact of the individual contributions is shown by a diamond symbol and its uncertainty (5 to 95% confidence range) is given by the horizontal error bar. ERF aci is ERF due to aerosol–cloud interaction. BC and OC are co-emitted, especially for biomass burning emissions (given as Biomass Burning in the figure) and to a large extent also for fossil and biofuel emissions (given as Fossil and Biofuel in the figure where biofuel refers to solid biomass fuels) (The Figure is taken from Myhre et al, 2013b).*

Additionally, there is a small heating effect of black carbon on snow (0.04 W m^{-2} since 1750). The total effect of black carbon on snow since 1750 is currently in the order of a one-year increase of CO_2 concentration in the atmosphere (around 2 ppm).

1.4.1 Revisions of forcing estimates of carbon dioxide, methane, and nitrous oxide

In 2016 there was an important study publishing revised radiative forcing of carbon dioxide, methane, and nitrous oxide. This resulted in a significant revision of the methane radiative forcing, and minor changes in the others. To reduce uncertainty, more accurate forcing estimates were included and the global warming potential, using consistent methodology with IPCC and earlier estimates, was revised. For CH_4 this resulted in **25% stronger forcing, 32 vs 28 times CO_2, than given in the IPCC Fifth Assessment Report**, due to inclusion of the shortwave and near-infrared bands of CH_4, improved knowledge about water vapour absorption, more detailed models (*Etminan et al., 2016*). Figure 6 is taken from Etminan et al (2016) and show the revised estimates, compared to the old as included in IPCC AR5. The estimates are based on concentration development as in representative concentration pathway (RCP[8]) RCP8.5 from IPCC AR5.

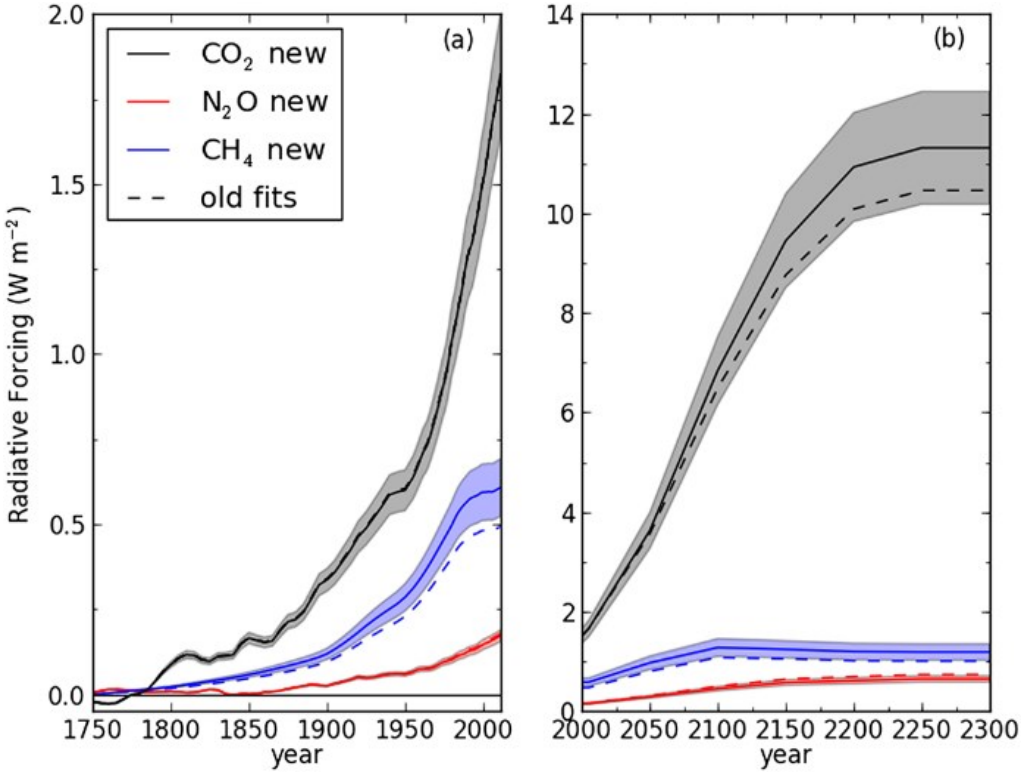

Figure 6: Radiative forcing of CO_2, N_2O, and CH_4 concentration change: (a) from 1755 to 2011 and (b) from 2000 to 2300, using RCP8.5 concentrations from IPCC AR5 relative to preindustrial value (280 ppm of CO_2, 275 ppb of N_2O, and 750 ppb of CH_4) using old and new expressions. Shading for the new expressions indicates the estimated radiative uncertainty in the forcing (Etminan et al, 2016).

[8] https://en.wikipedia.org/wiki/Representative_Concentration_Pathways

2 Observations of climate gases

NILU measures 46 climate gases at the Zeppelin Observatory at Svalbard and 2 at Birkenes, in addition to surface ozone reported in Aas et al., 2020. The results and analyses of the climate gas measurements are presented in this chapter. Furthermore, observations of CO_2 for the time period 1988-2012 at Zeppelin performed by the Stockholm University - Department of Environmental Science and Analytical Chemistry (ACES), are included in this report.

Table 3 summarises the main results for 2019 and the trends over the period 2001-2019. The table also includes 2019 global annual mean values given in Bulletin of the American Meteorological Society (BAMS) (Dlugokencky et al., 2019).

Table 3: Greenhouse gases measured at Zeppelin and Birkenes; lifetimes in years, global warming potential (GWP) for 100 year horizon and annual mean for 2019, change last year, and trends per year over the measurement period. Red is increasing and blue is decreasing trends. Global means for 2019 taken from Bulletin of the American Meteorological Society Bulletin of the American Meteorological Society Bulletin of the American Meteorological Society Bulletin of the American Meteorological Society (Dlugokencky et al., 2020) are included for comparison. All concentrations are mixing ratios in ppt, except for methane, nitrous oxide and carbon monoxide (ppb) and carbon dioxide (ppm).

Component		Life-time	GWP	Global mean BAMS 2019	Annual mean 2019	Absolute change last year	Long term trend /yr
Carbon dioxide - Zeppelin	CO_2	-	1	-	411.9	2.6	2.5
Carbon dioxide - Birkenes					416.1	0.9	2.5
Methane - Zeppelin	CH_4	12.4	28	-	1952.9	14.4	6.2
Methane - Birkenes					1961.2	8.2	8.4
Carbon monoxide	CO	A few months	-	-	115.4	1.8	-1.2
Nitrous oxide	N_2O	121	265	-	332.1	0.79	0.98
Chlorofluorocarbons							
CFC-11	CCl_3F	45	4 660	226.5	228.1	-1.02	-1.79
CFC-12	CF_2Cl_2	640	10 200	501.5	505.7	-3.17	-2.51
CFC-113	CF2ClCFCl2	85	13 900	69.7	70.1	-0.52	-0.64
CFC-115	CF_3CF_2Cl	1 020	7 670	-	8.8	0.08	0.02
Hydrochlorofluorocarbons							
HCFC-22	$CHClF_2$	11.9	1 760	246.8	255.7	1.88	5.81
HCFC-141b	$C_2H_3FCl_2$	9.2	782	24.4	25.7	0.17	0.53
HCFC-142b	CH_3CF_2Cl	17.2	1 980	22.0	23.1	-0.12	0.54
Hydrofluorocarbons							
HFC-125	CHF_2CF_3	28.2	3 170	29.1	32.3	3.42	1.65
HFC-134a	CH_2FCF_3	13.4	1 300	107.8	114.8	6.26	5.14
HFC-152a	CH_3CHF_2	1.5	506	6.9	10.5	0.24	0.43
HFC-23	CHF_3	228	12 400	32.5	33.2	1.35	1.04
HFC-365mfc	$CH_3CF_2CH_2CF_3$	8.7	804	1.01	1.31	0.03	0.07

Component		Life-time	GWP	Global mean BAMS 2019	Annual mean 2019	Absolute change last year	Long term trend /yr
HFC-227ea	CF_3CHFCF_3	38.9	3 350	1.56	1.76	0.16	0.12
HFC-236fa	$CF_3CH_2CF_3$	242	8 060	-	0.20	0.02	0.01
HFC-245fa	$CHF_2CH_2CF_3$	7.7	858	-	3.53	0.27	0.21
HFC-32	CH_2F_2	5.2	677	19.2	25.2	3.72	2.15
HFC-4310mee	$C_5H_2F_{10}$	16.1	1 650	-	0.30	0.01	0.01
HFC-143a	CH_3CF_3	47.1	4 800	23.8	25.5	1.64	1.53
Perfluorinated compounds							
PFC-14	CF_4	50 000	6 630	85.5	86.10	0.85	0.89
PFC-116	C_2F_6	10 000	11 100	4.85	4.91	0.09	0.09
PFC-218	C_3F_8	2600	8 900	0.69	0.69	0.02	0.01
PFC-318	$c\text{-}C_4F_8$	3200	9 540	1.76	1.80	0.07	0.06
Sulphurhexafluoride	SF_6	3 200	23 500	9.96	10.14	0.34	0.29
Nitrogen trifluoride	NF_3	500	16 100	-	2.22	0.23	0.20
Sulphuryl fluoride	SO_2F_2	36	4 090	-	2.63	0.11	0.10
Halons							
H-1211	$CBrClF_2$	16	1 750	3.25	3.37	-0.08	-0.07
H-1301	$CBrF_3$	65	7 800	3.28	3.39	0.012	0.02
H-2402	$CBrF_2CBrF_2$	20	1 470	0.40	0.41	0.00	-0.01
Halogenated compounds							
Chloromethane	CH_3Cl	1	12	546.5	507.97	-6.39	-0.37
Bromomethane	CH_3Br	0.8	2	6.56	6.78	0.20	-0.16
Dichloromethane	CH_2Cl_2	0.4	9	-	58.89	-1.84	1.93
Trichloromethane	$CHCl_3$	0.4	16	-	12.20	-2.50	0.24
Carbon tetrachloride	CCl_4	26	1730	78.4	78.02	-0.76	-0.95
Trichloroethane	CH_3CCl_3	5	160	1.60	1.71	-0.29	-1.81
Trichloroethene	$CHClCCl_2$	-	-	-	0.16	-0.12	-0.02
Tetrachloroethene	CCl_2CCl_2	-	-	-	2.27	-0.02	-0.11
Volatile Organic Compounds (VOC)							
Ethane	C_2H_6	Ca 78 days*		-	1602.45	77.51	-
Propane	C_3H_8	Ca 18 days*		-	454.71	-44.63	-
Butane	C_4H_{10}	Ca 8 days*		-	140.09	-3.43	-
Pentane	C_5H_{12}	Ca 5 days*		-	43.77	4.85	-
Benzene	C_6H_6	Ca 17 days*		-	61.11	-1.77	-
Toluene	$C_6H_5CH_3$	Ca 2 days*		-	18.87	-2.08	-

#The lifetimes of VOC are strongly dependant on season, sunlight, other components etc. The estimates are global averages given in C. Nicholas Hewitt (ed.): Reactive Hydrocarbons in the Atmosphere, Academic Press, 1999, p. 313. The times series for these are short and the trend is very uncertain.

Most greenhouse gases and other climate gases have numerous sources, both anthropogenic and natural. Trends and future changes in concentrations are determined by their sources and sinks, and in section 2.1 observations and trends of the monitored greenhouse gases with both natural and anthropogenic sources are presented in more detail. In Section 2.2 the detailed results of the ozone depleting substances with purely anthropogenic sources are presented.

For annual trend calculations we have used the method described in Appendix II. In order to estimate uncertainties we have applied an updated method taking auto-correlated errors in the fitted model residuals into account. Appendix II also includes a description of the measurements at the Zeppelin and Birkenes Observatories in more detail. Generally, Zeppelin Observatory is a unique site for observations of changes in the background level of atmospheric components. All peak concentrations of the measured gases are significantly lower here than at other sites at the Northern hemisphere, due to the station's remote location. Birkenes is closer to the main source areas. Further, the regional vegetation is important for regulating the carbon cycle, resulting in much larger variability in the concentration level compared to the Arctic region.

2.1 Climate gases with natural and anthropogenic sources

The annual mean concentrations for all gases included in the programme for all years are given in Appendix I, Table A 1 at page 116 All the trends, uncertainties and regression coefficients are found in Table A 2 at page 119. Section 2.1 focuses on the measured greenhouse gases that have both natural and anthropogenic sources.

2.1.1 Carbon dioxide (CO_2)

Key findings for CO_2: *The CO_2 concentrations have increased all years subsequently, in accordance with accumulation of gas in the atmosphere and the global development and increase in anthropogenic emissions. The annual CO_2 means in 2019 reached new record levels: 411.9 ppm at Zeppelin and 416.4 ppm at Birkenes. The increases from 2018 to 2019 are 2.6 ppm and 0.9 ppm, respectively. In general, the CO_2 increase has been high last years and it is urgent to understand the reasons, including the impact of natural sources and sinks on the annual variations.*

Carbon dioxide (CO_2) is the most important anthropogenic greenhouse gas with a radiative forcing of 1.82 W m^{-2} since the year 1750, (Myhre et al., 2013b). Etminan et al. (2016) presented revised forcing estimates for all main greenhouse gases (see more information in section 1.4.1 at page 23), and confirmed the forcing estimates for CO_2, with only minor changes.

The strong forcing is due to the increase in concentrations over the years. CO_2 is the end product in the atmosphere of the oxidation of all main organic compounds, and it has shown an increase of more than 50 % since the preindustrial times. This is mainly due to emissions from combustion of fossil fuels and land use change.

On Emissions

The Global Carbon Project http://www.globalcarbonproject.org estimates yearly updates on the emissions. CO_2 emissions from fossil fuel burning (including oil, gas, coal and flaring) and cement production increased by 0.9 % per year from 1990 – 2000. Then for the next 10 years period the increase was 3.0% per year from 2000-2010, and recently from 2010-2018 it is 0.9% per year. Emissions are projected to relax in 2018 to 0.6%. The global growth is driven by the underlying changes at the country level, in particular the total emissions in China and India are increasing.

It is worth noting that fossil CO_2 emissions will likely be more than 4% higher in 2019 than the year of the Paris Agreement in 2015 and 62% higher in 2019 than the year of the 1st IPCC report in 1990.

The measurements

NILU started CO_2 measurements at the Zeppelin Observatory in 2012 and the results are presented in Figure 7, together with the time series provided by ITM, University of Stockholm, back to 1988. ITM provides all data up till 2012 and we acknowledge the effort they have been doing in monitoring CO_2 at the site. After upgrading Birkenes in 2009, there are continuous measurements of CO_2 and CH_4 from mid May 2009 also at this site.

The atmospheric daily mean CO_2 concentration measured at the Zeppelin Observatory for the period mid 1988-2018 is presented in Figure 7 (upper panel), together with the 2009-2019 time series for Birkenes in the lower panel.

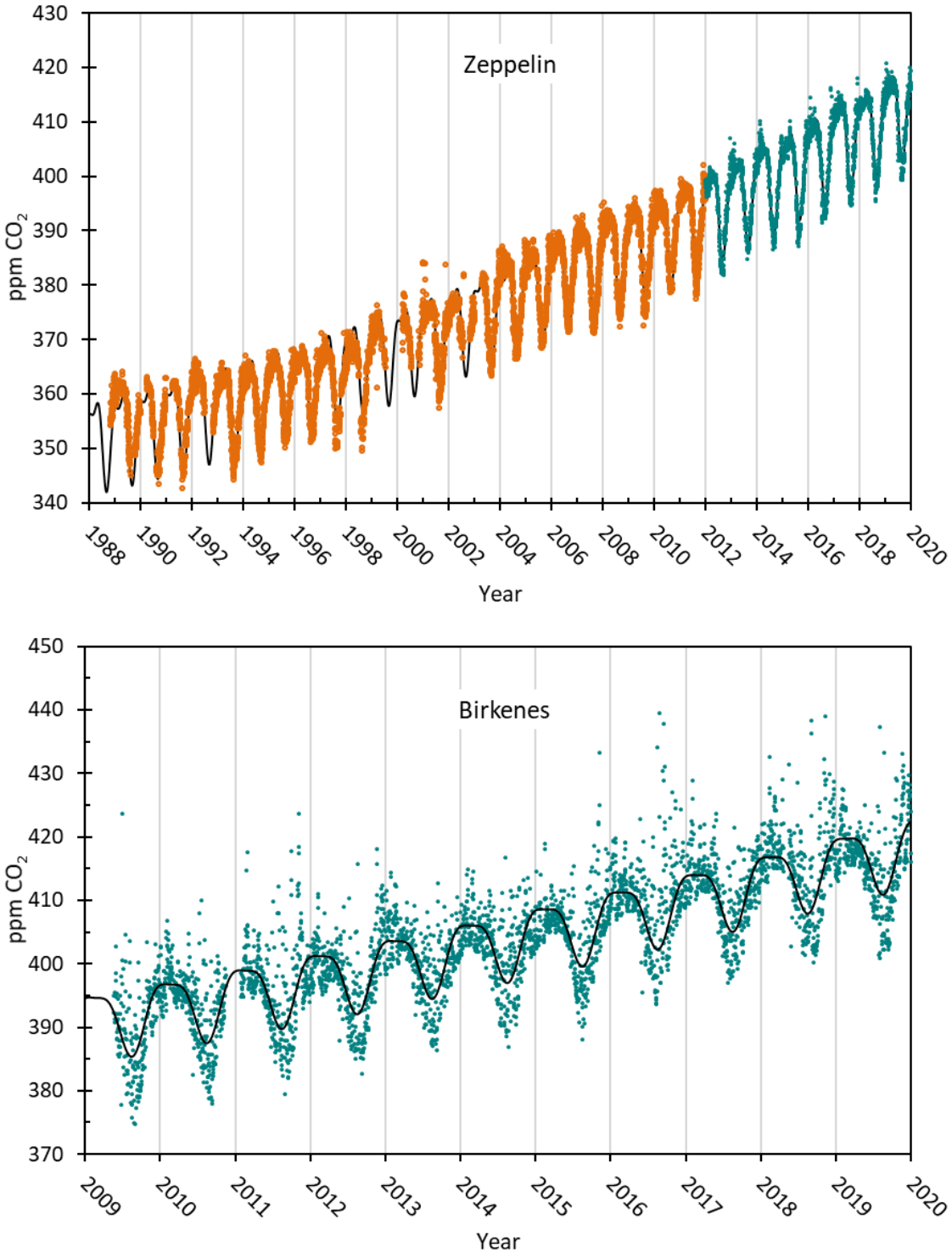

Figure 7: The atmospheric daily mean CO_2 concentrations measured at the Zeppelin Observatory for the period mid 1988-2019 are presented in the upper panel. Prior to 2012, ITM University of Stockholm provided all data, shown in orange. The green dots represent measurements from the Picarro instrument installed by NILU in 2012. CO_2 measurements at Birkenes are shown in the lower panel, the green dots are daily mean concentrations.

The results show continuous increase since the start of the observations at both sites. As can be seen there is larger CO_2 variability at Birkenes than Zeppelin. At Zeppelin the largest variability is during winter/spring, whereas Birkenes has large variability all year around. In summer there is also a clear

diurnal variation with high values during the night and lower values during daytime (not shown). This is mainly due to changes between plant photosynthesis and respiration, but also the general larger meteorological variability and diurnal change in planetary boundary layer, particularly during summer, contributes to larger variations in the concentrations. In 2020, NILU installed a 75 m mast, to also measure above the trees (see the appendix and Figure 67 included there at page 140) to limit these influences.

In addition to the diurnal variations, there are also episodes with higher CO_2 levels at both sites due to long range transport of pollution. In general, there are high levels when the meteorological situation results in transport from Central Europe or United Kingdom at Birkenes, and from central Europe or Russia at Zeppelin.

The maximum daily mean CO_2 value in 2019 at Birkenes was 437.0 ppm, measured on 4 August. During this period the wind direction and atmospheric circulation pattern indicate that air was transported from Eastern Europe, then shifting to central part of Norway. At Zeppelin the highest daily mean value in 2019 was 420 ppm, measured 16 January. This day the air at Zeppelin had been transported from central parts of Russia.

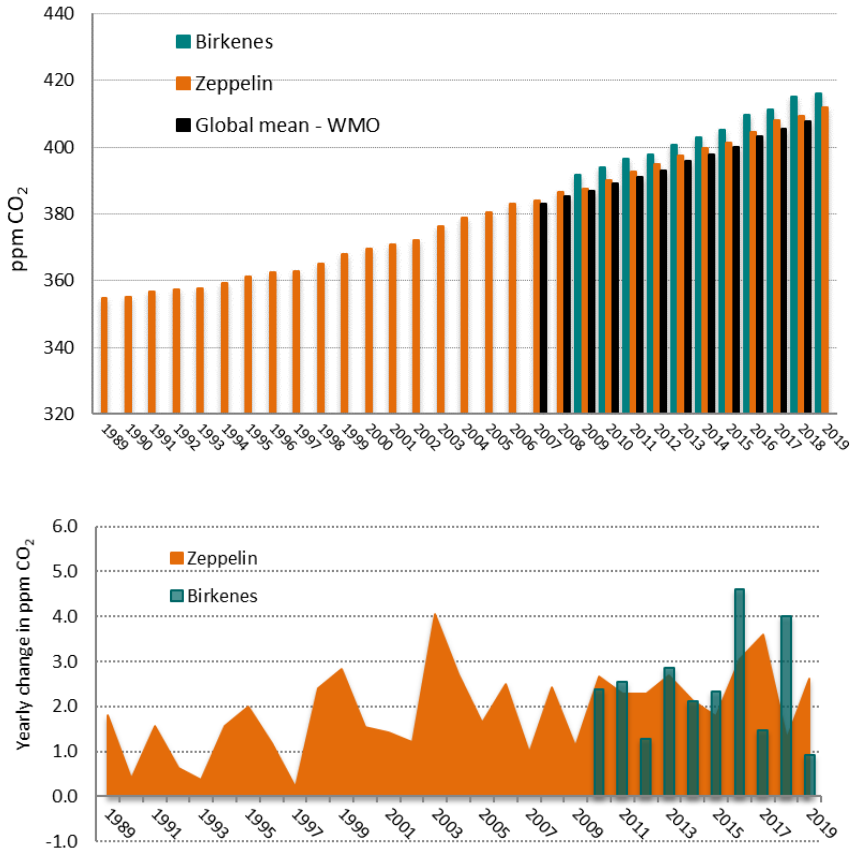

Figure 8: Upper panel: the annual mean concentrations of CO_2 measured at Zeppelin Observatory for the period 1989-2019 shown in orange. Prior to 2012, ITM University of Stockholm provides all data. The annual mean values from Birkenes are shown as green bars. The global mean values as given by WMO (2019) are included in black. The yearly annual increase are shown in the lower panel, orange for Zeppelin, green for Birkenes.

Figure 8 shows the development of the annual mean concentrations of CO_2 measured at Zeppelin for the period 1988-2019 (in orange) together with the values from Birkenes (in green) for the period

2009-2019. The global annual mean values as given by WMO (WMO, 2019) are in black. The yearly annual changes at Zeppelin and Birkenes are shown in the lower panel.

The annual mean CO_2 values at Birkenes and Zeppelin are higher than the global annual mean value as there are more anthropogenic sources and pollution at the Northern hemisphere. The mixing of air between the two hemispheres takes time, ca 2-3 years. The annual CO_2 mean in 2019, shown in Table 3 and Figure 8 (upper panel), was 416.1 ppm and 411.9 ppm at Birkenes and Zeppelin, respectively. The annual CO_2 changes illustrated in Figure 8, lower panel, shows an increase of 2.6 ppm at Zeppelin from 2018 to 2019. At Birkenes the CO_2 increase from 2018 to 2019 was 0.9 ppm, which is relatively low compared earlier years and Zeppelin. The global mean annual CO_2 increase from 2018 to 2019 is not yet published, but preliminary analyses suggest that the increase is in line with earlier year (it was 2.2 ppm from 2017- 2018).

Trend analyses based on method described in Appendix II show that CO_2 at Birkenes and Zeppelin increased by 2.5 ppm/yr, at both locations. This corresponds to an increase of ca 0.6 %/yr. These trend analyses are based on data from Picarro instruments, only (which were installed by NILU in 2012). If we use the entire Zeppelin time series back to 1988, the trend is less pronounced (~0.5%/yr), indicating that the CO_2 increase has intensified over the last decade.

It is interesting to note that in 2018, Europe experienced one of the worst droughts of the 21st century. The extensive heatwave and drought in 2018 had a negative impact on vegetation across Western and Northern Europe. An exceptionally long period of high temperatures and little precipitation resulted in an unprecedented browning of vegetation. It also meant that Europe's vegetation took up limited or no CO_2 from the atmosphere in that year. We are not able to see the direct sign of this at e.g. Birkenes, but it is well documented (Thompson et al, 2020, Ramonet et al 2020).

A paper in Nature Geoscience (Myhre et al, 2017) comments on the relation between CO_2 forcing and the CO_2 concentrations. Halfway to a doubling in the CO_2 concentration since 1750 is 417 ppm, which will be reached before 2025 with current CO_2 growth rates. However, with a global mean CO_2 abundance in 2017 at 405.5 ppm the halfway point to a doubling of CO_2 in terms of radiative forcing has already been reached. Hence, at CO_2 concentrations between 393 ppm and 417 ppm we are more than a halfway to a doubling of CO_2 in terms of radiative forcing, but not in concentration.

2.1.2 Methane (CH_4)

Key findings for Methane: *In 2019 the mixing ratios of methane increased to new record levels at Zeppelin with the strongest increase ever over one year, and significant increase was detected Birkenes. At Zeppelin the annual mean value reached 1952.9 ppb, which is a record yearly increase of 14.4 ppb since 2018. At Birkenes the annual mean value in 2019 was 1961.2 ppb, 8.2 pbb higher than previous year. The strong increase in methane concentrations and change are of great concern as the processes are not understood, and it can be due to climate feedback emission processes.*

Methane (CH_4) is the second most important greenhouse gas from human activity after CO_2. The IPCC reported a radiative forcing is 0.48 W m^{-2} since 1750 and up to 2011 (Myhre et al., 2013b), but as high as 0.97 W m^{-2} for the emission based radiative forcing (Figure 5, page 22) due to complex atmospheric effects. Etminan et al. (2016) presented revised forcing estimates for all main greenhouse gases (see section 1.4.1 at page 23), and for CH_4 this resulted in 25% stronger forcing than given in the IPCC Fifth Assessment Report, increasing from 0.48 W m^{-2} to 0.61 W m^{-2}. This emphasises the importance of understanding the development and changes in CH_4.

In addition to being a dominant greenhouse gas, methane also plays central role in atmospheric chemistry. The atmospheric lifetime[9] of methane is approx. 12 years, when indirect effects are included, as explained in section 1.4, for the direct effects ca 9-10 years.

The average CH_4 concentration in the atmosphere is determined by a balance between emission from the various sources and reaction and removal by free hydroxyl radicals (OH) to produce water and CO_2. A small fraction is also removed by surface deposition. Since the reaction with OH also represents a significant loss path for the oxidant OH, additional CH_4 emission will consume additional OH thereby increasing the CH_4 lifetime, implying further increases in atmospheric CH_4 concentrations (Isaksen and Hov, 1987; Prather et al., 2001).

The concentration of CH_4 was, after a strong increase during the 20th century, relatively stable over the period 1998-2006 (Dalsøren et al, 2016). The global average change was close to zero for this period, also at Zeppelin. Since 2005 a strong increase in the CH_4 levels is evident from our observations both at Zeppelin and Birkenes as well as observations at other sites, and in the global mean (WMO, 2019).

On Emissions

The Global Carbon Project http://www.globalcarbonproject.org rereleased new and updated emission estimates and global methane budget 15 July 2020. The emission estimates are for 2017, and also compared to mean emissions for the period 2000-2006. According to the Global Carbon Project and the underlaying peer-reviewed papers (Saunois et al, 2020 and Jackson et al. 2020) the distribution between natural and anthropogenic sources CH_4 is approximately 40% natural sources, and 60% of the sources are direct result of anthropogenic emissions. The main anthropogenic sources include emissions from agriculture (e.g. rice paddies, ruminant animals), waste and extraction and combustion of fossil fuels (oil, gas and coal). CH_4 is the principal component of natural gas and e.g. leakage from pipelines; off-shore and on-shore installations are a known source of atmospheric CH_4. The main natural sources are tropical, boreal and Arctic wetlands, freshwater systems (lakes and rivers), and geological sources like geological sources such as terrestrial and marine seeps and volcanoes.

Of natural sources there is a large unknown potential methane source under the ocean floor, so called methane hydrates and seeps.

Global Carbon Project report that the increasing anthropogenic methane emissions arise equally from agricultural and fossil fuel sources. Despite rapidly warming air temperatures (World Meteorological Organization 2019), methane emissions from northern high-latitude systems (>60°N) were virtually unchanged in 2017 relative to the average value for 2000–2006. Other regions contributed the most to greater methane emissions in 2017 compared with 2000–2006. These were Africa and the Middle East; China; and South Asia and Oceania increased their emissions. Here, agriculture and waste contributed 60% of this increase and fossil fuels the remaining 40%, with a slight decrease estimated for biomass and biofuel burning. It is worth noting that Europe is the only region with a slight decrease in CH_4 emissions in 2017 compared to the period 2000-2006.

Wetlands and freshwater systems more broadly are the largest source of methane but also the greatest source of uncertainty to the global methane budget. Furthermore, a large unknown amount of carbon is captured in the permafrost layer in Siberia and North America and this might be released as CH_4 if the permafrost layer thaws as a feedback to climate change. The balance between the release of CO_2 and CH_4 from thawing permafrost, will depend on the precipitation and changes in moisture.

The measurements

Figure 9 shows daily mean observations of CH_4 at Zeppelin since the start in 2001 (upper panel) and Birkenes since start in 2009 (lower panel). As can be seen from the figures there has been an increase in the concentrations of CH_4 at both sites the last years, and in general the concentrations are higher

[9] Time taken to decay to 1/e, 1/2.7, of original levels

at Birkenes than at Zeppelin. The highest ambient CH_4 concentration ever detected at Zeppelin, 2022 ppb, was measured on the 16th January 2019, same days as CO_2 had its peak value. The transport pattern on this day indicates a strong influence from central Russia. Fugitive emissions from Russian gas installations are normally the source of such high CH_4 values.

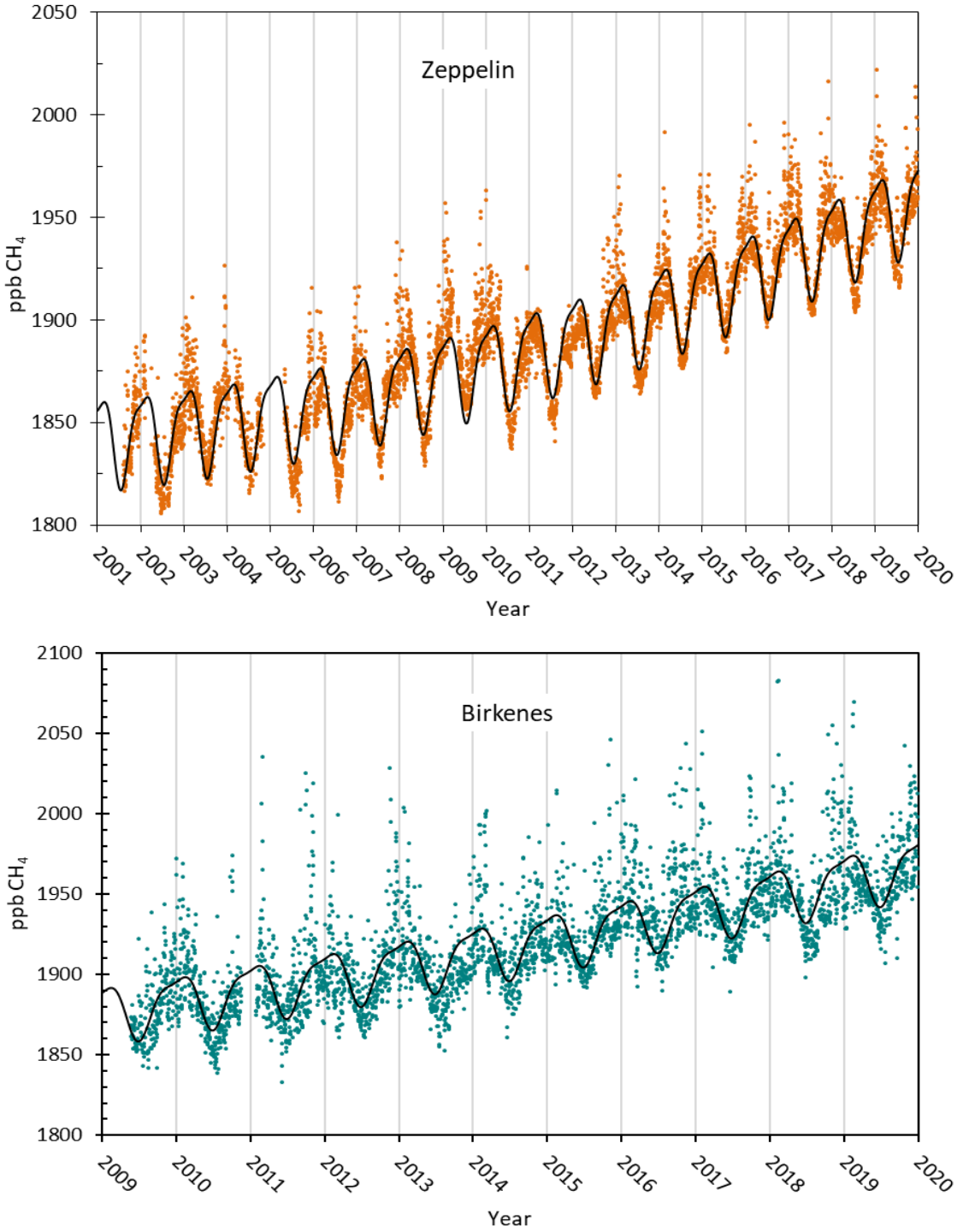

Figure 9: *The upper panel shows observations of daily averaged methane mixing ratio for the period 2001-2019 at the Zeppelin Observatory. The black solid line is empirical fitted methane mixing ratio. The lower panel shows the daily mean observations for Birkenes (green dots).*

The maximum CH_4 daily mean value recorded at Birkenes in 2019 was 2069 ppb, measured 18 February.

For both Zeppelin and Birkenes, the seasonal variations are clearly visible, although stronger at Birkenes than Zeppelin. This is due longer distance to the sources at Zeppelin, and thus the sink through reaction with OH dominates the variation. The larger variations at Birkenes are explained by both the regional sources in Norway, as well as a stronger impact of pollution transported from central Europe or UK. For the daily mean in Figure 9, the measurements show very special characteristics in 2010 and 2011 at Zeppelin. There is remarkably lower variability in the daily mean in 2011 with fewer episodes than the typical situation in previous and subsequent years (e.g. summer/autumn 2012). This seems to be due to less impact of episodes from Northern Russia (Thompson *et al*, 2017). A similar situation is evident also in 2018 at Zeppelin, resulting in less increase than expected and reported at other sites, including Birkenes.

At Zeppelin there are now 19 years of data for which the trend has been calculated. To retrieve the annual trend in methane for the entire period the observations have been fitted by an empirical equation, shown as the black solid line in Figure 9. This corresponds to a trend of 6.2 ppb/yr or 0.3%/yr. For Birkenes, shown in Figure 9 lower panel, the time series is shorter and the trend analysis is less accurate. The trend calculations demonstrate a CH_4 increase of 8.4 ppb/yr (0.4%/yr) for the period 2009-2019.

The annual methane increase over the last years is visualised in Figure 10, showing the CH_4 annual mean concentration at Zeppelin for the period 2001-2019 (orange) and Birkenes for the period 2009-2019 (green). The global mean values given by WMO from 2005-2018 (WMO, 2019) are included for comparison. The big difference between global mean, and the observations at Zeppelin and Birkenes is due to the fact that most emissions are in the Northern hemisphere.

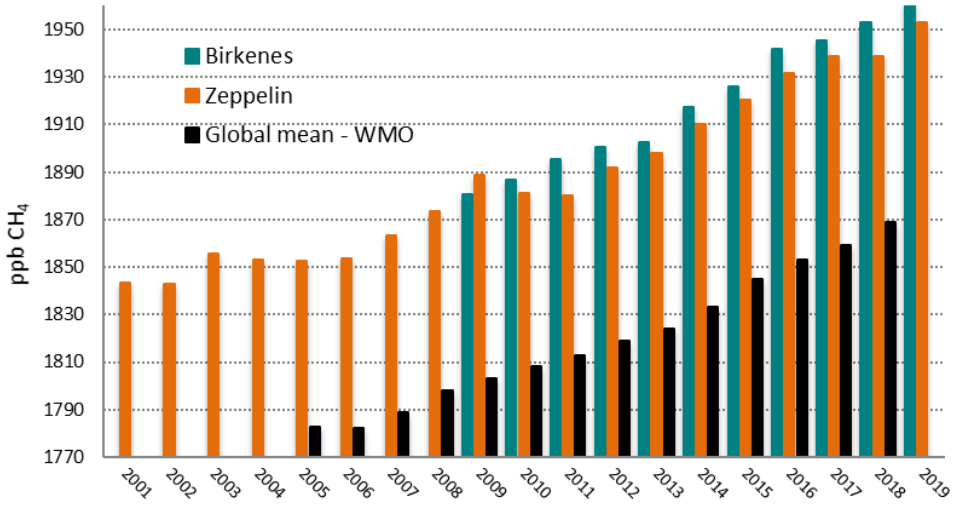

Figure 10: Development of the annual mean mixing ratio of methane in ppb measured at the Zeppelin Observatory (orange bars) for the period 2001-2019, Birkenes for the period 2010-2019 in green bars, compared to global mean provided by WMO as black bars (WMO, 2019).

The annual means are based on the measured methane values, however, model fitted values are used to fill in gaps if measurements are missing. Figure 10 demonstrates a gradual increase in the concentrations of methane at both Zeppelin and Birkenes the last decade. The annual mean

concentrations in 2019 were 1952.9 and 1961.2 at Zeppelin and Birkenes, respectively. For Birkenes, there is an increase of 8.2 ppb since 2018. For Zeppelin, it is even stronger, 14.4 ppb since 2018. This is the highest annual increase ever detected at Zeppelin since the measurements stated in 2001. It is worth noting that for the year 2017-2018, the situation was different with a decrease of 0.4 ppb. The increase since 2005 at Zeppelin is 100 ppb (approx. 5.2 %) which is high compared to the development of the methane mixing ratio for the period 1999-2005, both at Zeppelin and globally.

2.1.2.1 Transport pattern of air to the Zeppelin Observatory and analysis of the change yearly variation

The decrease in methane levels at Zeppelin from 2017 to 2018 was surprising, since other stations including Birkenes showed an increase, and we made a more in-depths analysis of this to explore the reason. To analyse the data further, we performed an analysis and assessment of the source regions of the air masses arriving at Zeppelin in the period 2001-2018. Analyses of the air mass origin are important for the understanding of the observed levels of both the gases and aerosols. We analysed the origin of the air arriving at Zeppelin in 2018 and compared to previous years. Air mass trajectories are calculated using the FLEXTRA trajectory model (http://www.nilu.no/trajectories/) and using meteorological data provided from European Centre for Medium Range Weather Forecasts (ECMWF). 7 days backward trajectories from ECMWF have been used to investigate the major transport pathways to Svalbard and Zeppelin.[10] The origin of the air arriving at Zeppelin is categorised in following 6 sectors:

- **Arctic region:** Clean Arctic air: Air mass trajectories with all trajectory points north of 65°N (sector 1 in Figure 11)
- **Atlantic sector:** Clean marine air: Air mass trajectories with all trajectory points between 10°W and 70°W and from south of 65°N. (sector 2 in in Figure 11)
- **North American sector:** Polluted air: If at least 50% of the trajectory points are between 70°W and 180°W, and from south of 65°N. (sector 3 in Figure 11)
- **European sector:** Polluted air: If at least 50% of the trajectory points were between 10°W and 30°E, and from south of 65°N. (sector 4 in in Figure 11)
- **Russian sector:** Polluted air: If air mass trajectories with all points between 30°E and 180°E and from south of 65°N. (sector 5 in *Figure 11*).
- **Undefined sector:** The trajectories that could not be allocated to any of the sectors defined above. This amounts to approximately 25% of the total

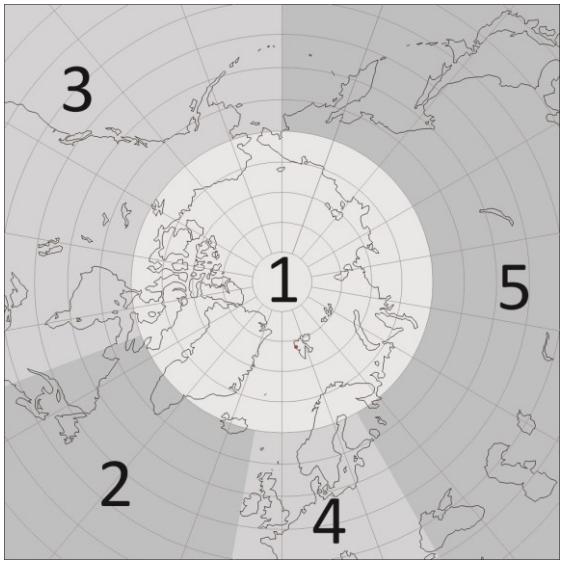

Figure 11: The sectors used to classify the air arriving at the Zeppelin Observatory. 1 is Arctic sector, 2 is Atlantic sector, 3 is North American sector, 4 is European sector and 5 is Russian sector.

[10] The spatial resolution is T106, which correspond to a latitude/longitude resolution of 1x1 degrees, the temporal resolution is 6 hours, and 91 levels (60 levels before February 2006) are available in the vertical direction. The data sets used are so-called analysis, which is a combination of observations and numerical calculations. This includes measurements from satellites, radio sondes, buoys, weather stations, etc. which are assimilated into a meteorological model that produce an estimate of the state of the atmosphere at a given time.

Air from the Arctic and Atlantic sector are assumed to contain minimal influence of pollution, as there are almost no industrial sources in these areas, and one can say that the air is 'clean', although there are increasing industrial activity in the northern part of Russia.

Figure 12 shows the share of polluted and clean air arriving at the Zeppelin observatory for the years 2002-2019. The analysis shows that in 2006, 2008 and 2018 the fraction of air arriving at Zeppelin categorized as clean marine and Arctic air was higher than the previous years, and for 2018 in particular air for the Russian sector is lower (27 % of the days). In 2019, this is back to normal (46%) and we also see a stronger increase in CH_4 at Zeppelin associated to emissions from this region. The 2 years before 2016-2017 the site experienced higher influence of polluted air masses from the Russian sector (40 and 48%). For 2018, an analysis of the seasonal variations show that this lower impact of Russian sector was particularly evident in winter and early spring. This is the time of year with highest levels, and most frequent pollution episodes, so lack of transport of pollution in this period have strong impact on the annual mean.

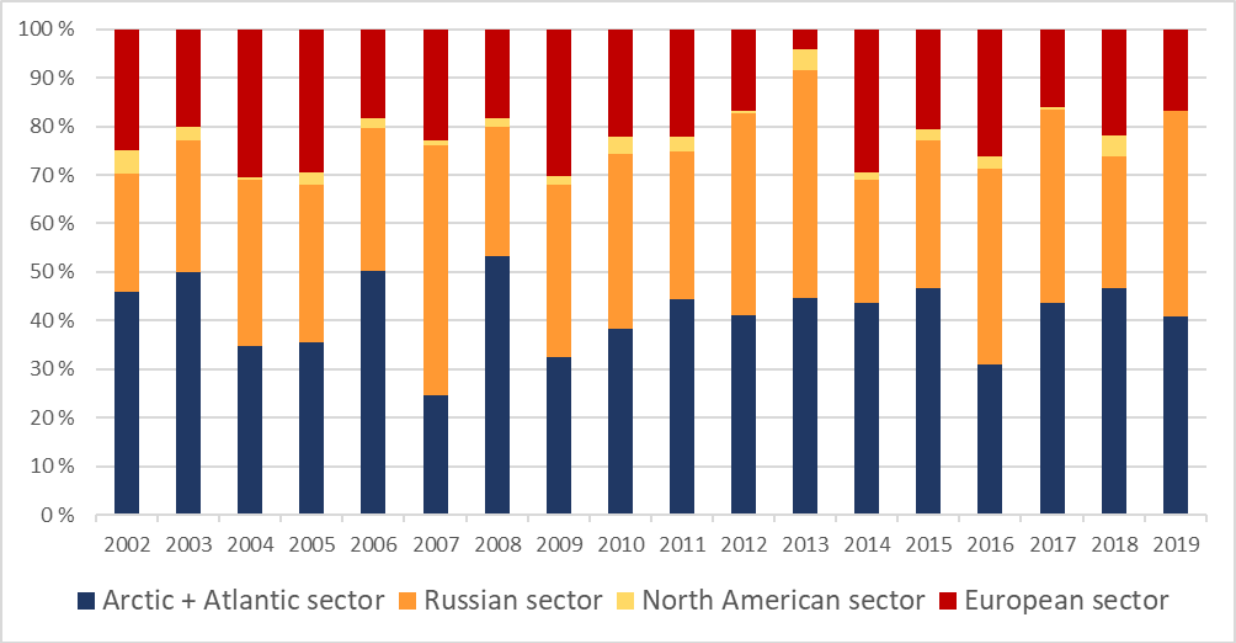

Figure 12: The percentage of polluted and clean air arriving at Zeppelin in the period 2002-2019 from the various sectors.

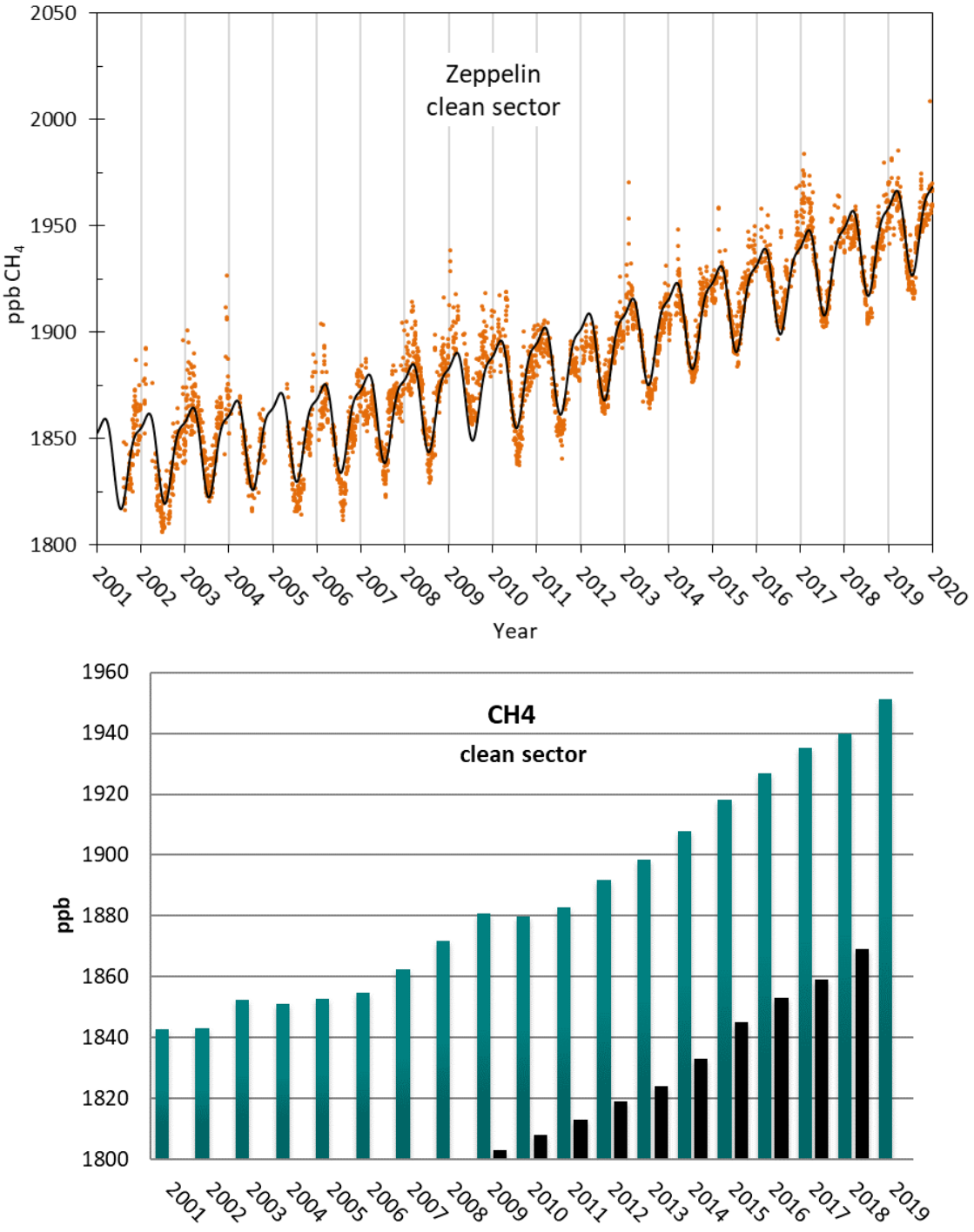

Figure 13: Upper panel: Daily mean CH_4 at Zeppelin for the days when the air comes from Arctic and north Atlantic sector. Lower panel; The annual mean, only taking days with air from Arctic and north Atlantic sector into account.

Figure 13 shows the daily mean CH_4 at Zeppelin for the daily and annual mean only taking days from Arctic and north Atlantic sector into account when the air comes from Arctic or Atlantic sectors.

The change in annual mean from 2017 to 2018, only taking the Arctic and north Atlantic sector change into account is +4.7 ppb. For 2018-2019 this was 11.3 ppb, which is very high.

To summarise, the increase at Zeppelin from 2018 to 2019 is again strong, and the enhanced methane concentrations and change are of great concern. The surprising development in 2018 was due to metrological conditions. This result also emphasises the need to consider atmospheric transport in order to understand trends in methane.

2.1.2.2 *Observations of the atmospheric $\delta^{13}C_{CH4}$ and discussion of potential change in CH4 sources*

The isotopic signature of CH_4 (expressed as $\delta^{13}C_{CH4}$) varies by emission source (France et al., 2016, see Figure 14) and measurements of the isotopic signature provides very valuable information for the understanding of the development of CH_4 sources, complementing other measurements (e.g. CH_4, CO and ethane). As can be seen from Figure 14 the isotopic signatures of CH_4 from e.g. biomass burning is different from natural gas. Leaks from gas installations, world-wide, both onshore and offshore might be an increasing source. Hence, it is essential to find out if the increase since 2005 is due to high emissions from point sources, or if it is caused by newly initiated processes releasing methane to the atmosphere e.g. the thawing of the permafrost layer or processes in the ocean, both related to permafrost and others. As a part of a research project under Norwegian Research Council (2011-2013[11]) NILU initiated measurements of $\delta^{13}C_{CH4}$ at Zeppelin in the year 2012 to provide more insight into Arctic sources of CH_4, and potential changes. The continuation of these measurements was implemented into the Norwegian Monitoring programme in 2017. Figure 15 shows the full time series of $\delta^{13}C_{CH}$ since May 2012 (red dots) to the end of 2019[12], together with ambient CH_4 concentrations (blue line) measured at the Zeppelin Observatory. The observations are mainly 2 times per week, performed in the morning. (For details about the measurements, see Appendix II).

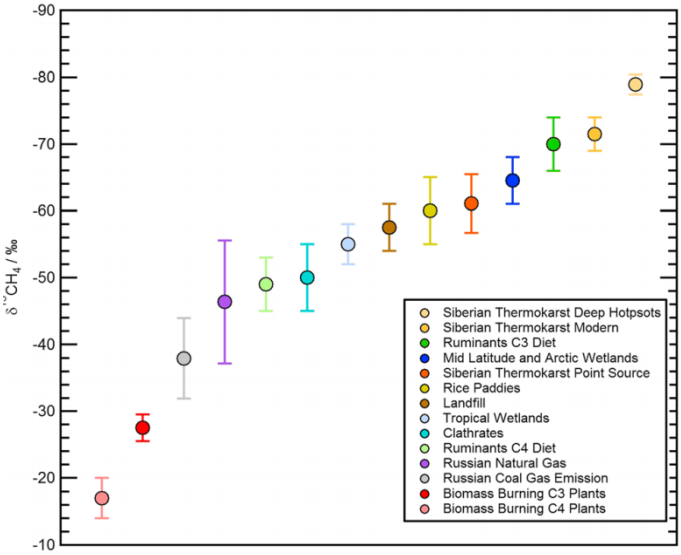

Figure 14: Isotopic ranges of $\delta^{13}C_{CH4}$ for a variety of CH4 sources as given in France et al, 2016.

A clear reduction (shift towards more negative values) in $\delta^{13}C_{CH4}$ is evident after 2012, parallel to the increase in the ambient concentration. Back in the 1980's, $\delta^{13}C_{CH4}$ shifted to more positive values, indicative of gas leaks and coal emissions (as $\delta^{13}C_{CH4}$ of fossil fuels is slightly higher than the ambient average), but it seems that increases in CH_4 concentrations since 2005 have been accompanied by a negative shift in $\delta^{13}C_{CH4}$, as illustrated in Figure 15 until the start of 2019.

[11] https://www.forskningsradet.no/prosjektbanken/#/project/NFR/207587

[12] Note that due to corona restrictions and lockdown, December data are not available at the time of the writing of the report. The sampling is done, and samples are sent for analyses in UK, but delayed in the special situation.

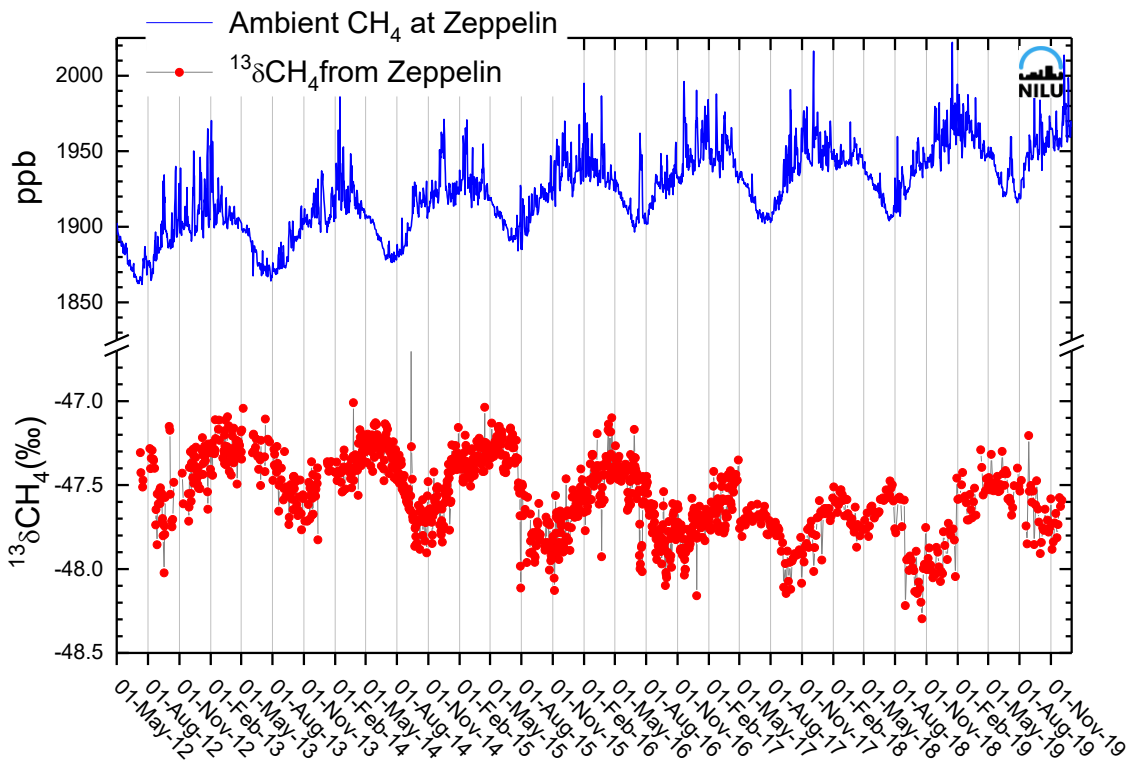

Figure 15: Long term measurements of methane (CH_4, blue) and the ^{13}C isotopic signature of CH_4 ($\delta^{13}C$-CH_4, red) at the Zeppelin Observatory, Svalbard 78°N.

These recent negative shifts in ambient $\delta^{13}C_{CH4}$, and increases in the CH_4 mixing ratio imply changes in the balance of sources and sinks, i.e. since changes in total fossil fuel emissions cannot account for a negative shift they also cannot entirely account for increases in the mixing ratio. Hence the development in $\delta^{13}C_{CH4}$ observed at Zeppelin suggests a role for biosphere and/or agriculture (wetland or ruminant) emissions, since these do have strongly negative $\delta^{13}C_{CH4}$ compared to ambient values and fossil sources. Changes in the sink strength (reaction with hydroxyl radicals, OH) is also a possibility. It is worth noting that as the major sink for almost all atmospheric Volatile Organic Compounds (VOCs), (not only CH_4), changes in OH would have profound implications for the whole atmosphere. There are a few signs of that. Ethane and methane are emitted together from fossil oil and gas sources, and the global decrease in ethane supports the hypothesis that wetland changes is a large contributor to the change in CH_4. Additionally, recent and ongoing scientific discussions point in the direction of increased emissions from wetlands located both in the tropical region and in the Arctic region. Thawing of permafrost, both in terrestrial regions and in marine region, might introduce new possible methane emission sources initiated by the temperature increase the last years in the Arctic region, but the new revised methane budget does not support this (see section 2.1.2). Interestingly, from 2019 there is no change in the isotopic shift, or it might even be a reversed from previous years. This indicates that the relative change among sources has stopped, at least for this period

Gas hydrates at the sea floor are widespread in thick sediments in this area between Spitsbergen and Greenland. These gas hydrates can decompose if temperatures increase or pressure decreases. Hence, if the sea bottom warms or sea level decreases (e.g. due to raising of the sea bed as the Greenland Ice sheet melts), this might initiate further emissions from this source. This was the core of the large polar research project *MOCA - Methane Emissions from the Arctic OCean to the Atmosphere: Present and*

Future Climate Effects[13], which started at NILU in October 2013, and was finalized spring 2017. Some of the results from this is included in the section 2.1.2.3 at page 39.

To summarise, isotopic signatures provide very valuable data for understanding the development of the source of CH_4, but careful interpretation of observational data and emission inventories is required before assigning observed shifts to a particular source. The observations in 2019 indicates that a relative change among sources have stopped, at least for this period. This further demonstrates the need for observational data on emission fluxes from the large natural reservoirs. There is most likely a combination of causes explaining the increase in methane the last years, and the dominating reason is not clear. A possible explanation is increased methane emissions from wetlands and agriculture, both in the tropics as well as in the Arctic region, in addition to increases in emission from the fossil fuel industry in some areas, but this alone cannot explain the development in the isotopic signature of CH_4 at Zeppelin.

2.1.2.3 Methane from Arctic Ocean to the atmosphere?

A comprehensive research project "*MOCA - Methane Emissions from the Arctic OCean to the Atmosphere: Present and Future Climate Effects*" ended in 2017 focusing on methane from Arctic Ocean to the atmosphere. This was a collaboration with CAGE (The Centre for Arctic Gas Hydrate, Environment and Climate, at UiT The Arctic University of Norway) and Cicero, but lead by NILU. The driving questions for MOCA were:

I. What is the status and current release of methane from marine seep sites and methane hydrates in the Arctic Ocean, and specifically around Svalbard?

II. How are these processes depending on trends in sea temperature and annual variations?

III. Where are the most important areas in the Arctic Ocean which could constitute a possible source of atmospheric methane, now and in the future?

IV. What is the present CH_4 emission from the seabed to the atmosphere?

V. What is the most likely change in flux, the next 50 and 100 years under realistic climate scenarios? And what is the global effect of this?

VI. What is the ocean temperature threshold for large changes in emission of methane from hydrates?

What are gas hydrates?

Large amounts of natural gas, mainly methane, are stored in the form of hydrates in continental margins worldwide, particularly, in the Arctic. Gas hydrate consists of ice-like crystalline solids of water molecules encaging gas molecules, and is often referred to as 'the ice that burns'.

What are seeps?

Cold seeps are locations where hydrocarbons are emitted from sub-seabed gas reservoirs into the ocean. This can be both from petroleum reservoirs and methane hydrates. The illustration is gas bubbles rising 800 m up from Vestnesa Ridge, offshore Svalbard (Smith et al. 2014).

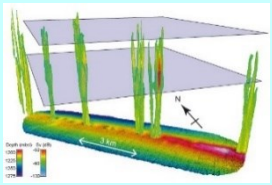

http://cage.uit.no

In this project we used integrated approaches to answer these questions. Figure 16 shows the exploratory platforms involved. Comprehensive measurement campaigns involving ship, aircrafts and Zeppelin have been performed. Additionally we used models both atmospheric chemistry, methane hydrates modelling at sea floor, and climate models.

[13] http://moca.nilu.no/

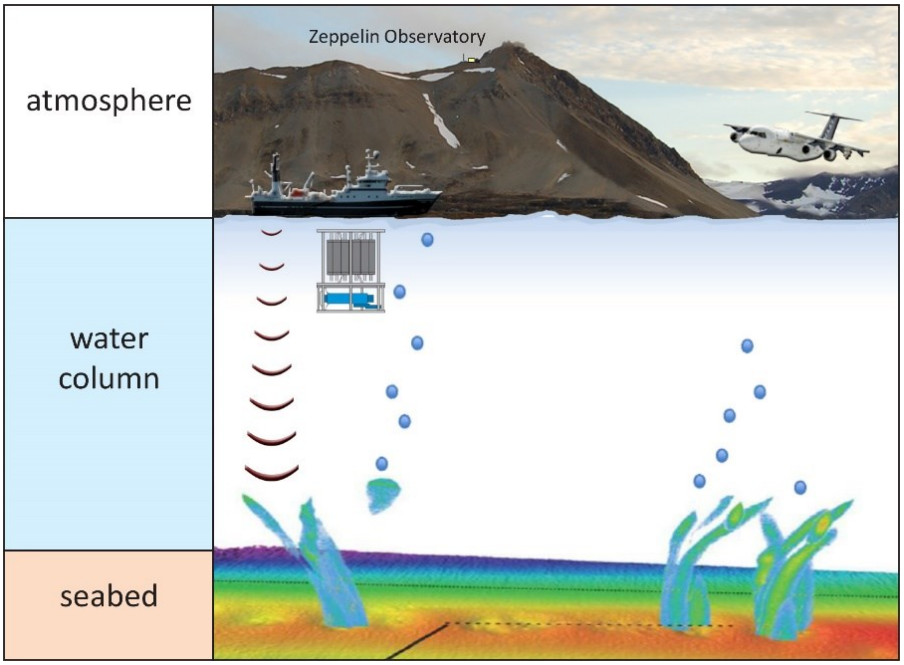

Figure 16: Field campaign and measurement platforms at the sea floor, in the water column, and in the atmosphere west of Svalbard in June-July 2014. Seeps on the seafloor, represented here by swath bathymetry, release gas bubbles that rise through the water column. The Research Vessel Helmer Hanssen detected gas bubbles and collected water samples at various depths, and provided online atmospheric CH4, CO and CO2 mixing ratios and discrete sampling of complementary trace gases and isotopic ratios. The Facility of Airborne Atmospheric Measurements (FAAM) aircraft measured numerous gases in the atmosphere, and an extended measurement programme was performed at the Zeppelin Observatory close to Ny-Ålesund. Data from Zeppelin was used for comparison to detect possible oceanic sources.

The main message from MOCA is that CH_4 gas released from the Arctic seabed can lead to an increased methane concentration in the ocean, but surprisingly, very little of the methane gas rising up through the sea appears to reach the atmosphere in the summer. This was an important message to bring to the debate on the state of the ocean and atmospheric system in the Arctic. It is important to emphasize that the Arctic has in recent years experienced major changes and average temperatures well above normal values, and this can change and also be different in other time of the year. Summer was in focus in this work. We used different state-of-the art models to assess and understand the variation in Arctic methane, to investigate potential oceanic sources in various regions, in particular methane hydrates and cold seeps. Results are presented in Myhre et al. (2016), Pisso et al. (2016), Dalsøren et al (2018), Thompson et al (2017), and Platt et al (2018) some information can be found here: http://forskning.no/havforskning-klima-arktis/2016/05/metan-slipper-ikke-ut-av-polhavet-om-sommeren.

In the last paper, Platt et al (2018) we identified a hotspot region where methane is being emitted from the ocean above an area north of Svalbard with active subsea seeps. We found a small flux, below the constraints for emissions established in Myhre et al. (2016), Pisso et al. (2016). Further investigation revealed that meteorological conditions at the time were favourable for measurements of ocean fluxes at the ship location (relatively stagnant air). In Platt et al (2018) we also demonstrated, via comparison to gridded emission fields, that apart from the single observation of an ocean flux, baseline excursions in Arctic atmospheric methane mixing ratio are well explained by land based emissions from wetlands, biomass burning, and anthropogenic activities.

2.1.3 Nitrous Oxide (N_2O)

Key findings Nitrous Oxide: *N_2O is a strong greenhouse gas and contributes ~6% to the total forcing of well-mixed greenhouse gases since 1750. N_2O is also the major source of the ozone-depleting NO and NO_2, thus the component is influencing the stratospheric ozone layer. The global mean level of N_2O has increased from around 270 ppb prior to industrialization and up to an average global mean of 331 ppb in 2019. At Zeppelin the annual mean N_2O level was 332.1 ppb in 2019.*

Nitrous Oxide (N_2O) is a greenhouse gas with both natural and anthropogenic sources. The sources include oceans, tropical forests, soil, biomass burning, cultivated soil and use of particular synthetic fertilizer, and various industrial processes. There are high uncertainties in the major soil, agricultural, combustion and oceanic sources of N_2O. Also frozen peat soils in Arctic tundra is reported as a potential source (Repo et al., 2009), but studies identify tropical and sub-tropical regions as the largest source regions (Thompson et al, 2013). N_2O is an important greenhouse gas with a radiative forcing of 0.17 W m^{-2} since 1750, contributing around 6 % to the overall well-mixed greenhouse gas forcing over the industrial era. N_2O is also the major source of the ozone-depleting nitric oxide (NO) and nitrogen dioxide (NO_2) in the stratosphere, thus the component is also influencing the stratospheric ozone layer (WMO, 2018).

In 2009, NILU installed a new instrument at Zeppelin measuring N_2O with high time resolution of 15 minutes. The instrument was in full operation in April 2010 and the results for 2010-2019 are presented in Figure 17. The annual mean N_2O value at Zeppelin was 332.1 ppb in 2019, an increase of 0.8 ppb from the 2018 annual mean value. N_2O has increased from around 270 ppb prior to industrialisation and up to an average global mean of 331.1 ppb in 2019 (WMO, 2019).

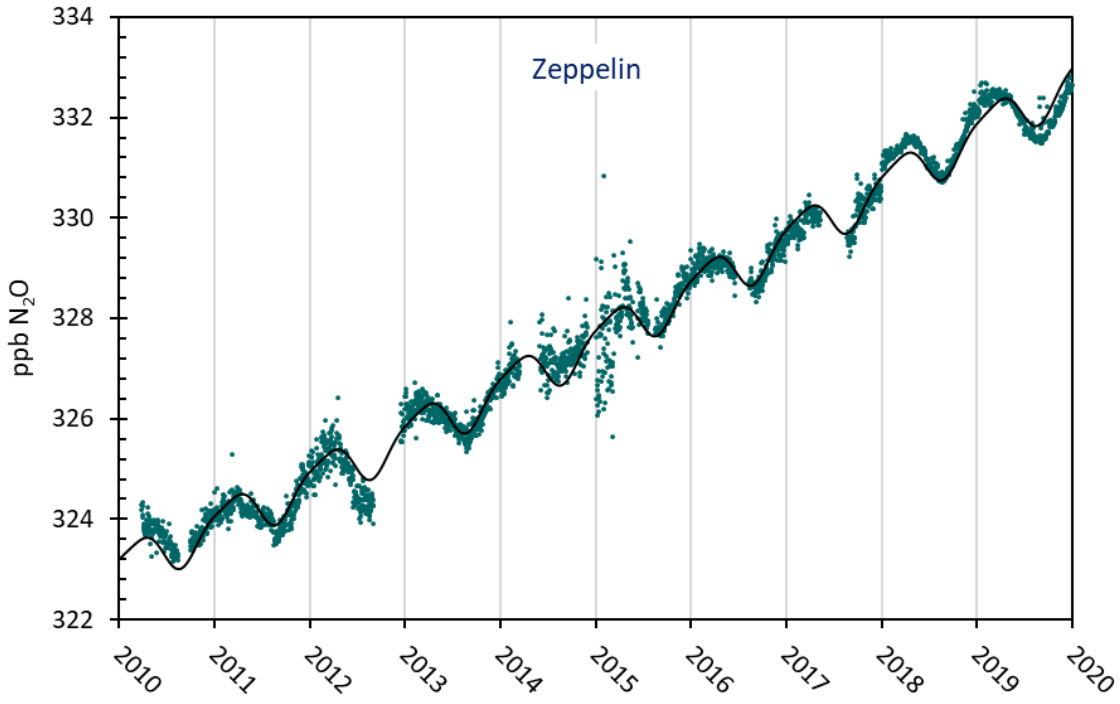

Figure 17: Measurements of N_2O at the Zeppelin Observatory for 2010-2020.The black line is empirical modelled N_2O mixing ratio.

As seen from Figure 17 there has been a gradual increase in N_2O at Zeppelin since the measurements started in 2010. For the period 2010-1019 the overall trend is 0.98 ppb/yr, an increase of 0.3%/yr.

Figure 18 shows annual average concentrations of N_2O measured at Zeppelin for the periods 2010-2019. The global annual means of N_2O (WMO, 2019) are included as a black bars for comparison. The concentrations at Zeppelin are slightly higher than the global means.

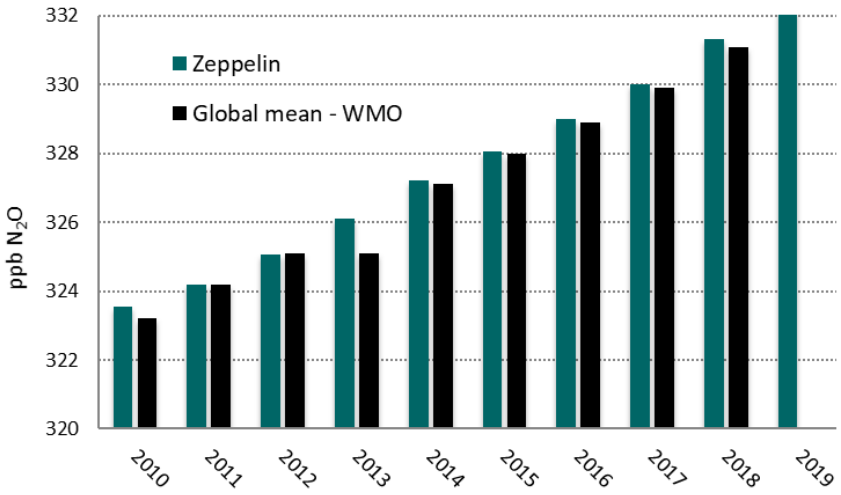

Figure 18: Annual mean concentration of N_2O at the Zeppelin Observatory for 2010-2019.

2.1.4 Volatile organic compounds (VOC)

Key findings – VOCs: *The VOCs are short lived greenhouse gases with low direct greenhouse gas effects, however, they have an indirect climate effect as they influence the levels of e.g. aerosols, ozone, and CO. Furthermore, they are important for surface ozone. Six different VOCs have been measured at Zeppelin since September 2010. The annual mean concentrations vary from one year to another and for most compounds it is not possible to draw any conclusions about developments and trends at this early stage.*

Volatile Organic Compounds (VOCs) represent a large group of carbon-based compounds that have a high vapour pressure and easily evaporate at room temperature. VOC oxidation contributes to the production of tropospheric ozone and influences photochemical processes, both impacting climate and air quality. Sources of VOCs (here ethane, propane, butane, pentane, benzene and toluene) are both natural (mostly geological but also from wildfires) and anthropogenic (fossil fuels). CH_4 and VOCs are co-emitted from oil and natural gas sources, for CH_4 to ethane the mass ratio varies from 7 to 14 (Helmig et al, 2016). The atmospheric ethane budget is not fully understood, and state-of-the-art atmospheric models underestimate ethane-mixing ratios, implying that current emission inventories require additional sources to balance the global atmospheric ethane budget.

Helmig *et al*. (2016) showed, from long-term observations of ethane from a global network that concentrations are increasing (since circa 2010), and that there is a strong latitudinal gradient, with the highest abundances observed in the Arctic, and a steep decline towards the south. They concluded that emissions from North American oil and natural gas development are the primary cause of increasing concentrations in recent years. However, there might be other factors. Another study by Nicewonger et al. (2016) used analysis of polar ice cores to estimate the pre-industrial emissions and concluded that natural ethane emissions from geologic seeps contributed significantly to the preindustrial ethane budget, and Etiope and Ciccioli (2009) suggested that a substantial part of the

missing ethane source can be attributed to gas seepage (classified as geologic seeps), but they did not include the Arctic in their study.

A study in Nature Geoscience performed under the MOCA project (see section 2.1.2.3) unveils a need of revising previous ethane and propane emissions studies, as these emissions have been underestimated by more than 50%. Such a revision could in turn improve our understanding of the forceful and related methane emissions (Dalsøren et al, 2018).

There has been large progress recently in the access to quality assured measurements of VOC under ACTRIS, with high time resolution. In a study by Dalsøren et al (2018) recent atmospheric measurement data from a number of sites are compared with the simulations from an atmospheric chemistry transport model, and found that a substantial increase of the emissions is needed to match the model predictions. Dalsøren et al (2018) showed that substantial geologic emissions are necessary to reproduce observations of preindustrial ethane concentrations. This provides an important constraint on both preindustrial and current natural emission budgets, reducing the relative contribution of fossil sources.

In 2010 a Medusa-GCMS instrument was installed at Zeppelin, which made it possible to perform online VOC measurements. Figure 19 shows the daily mean observations of the four non-methane hydrocarbons included in the programme in 2010: ethane, propane, butane and pentane.

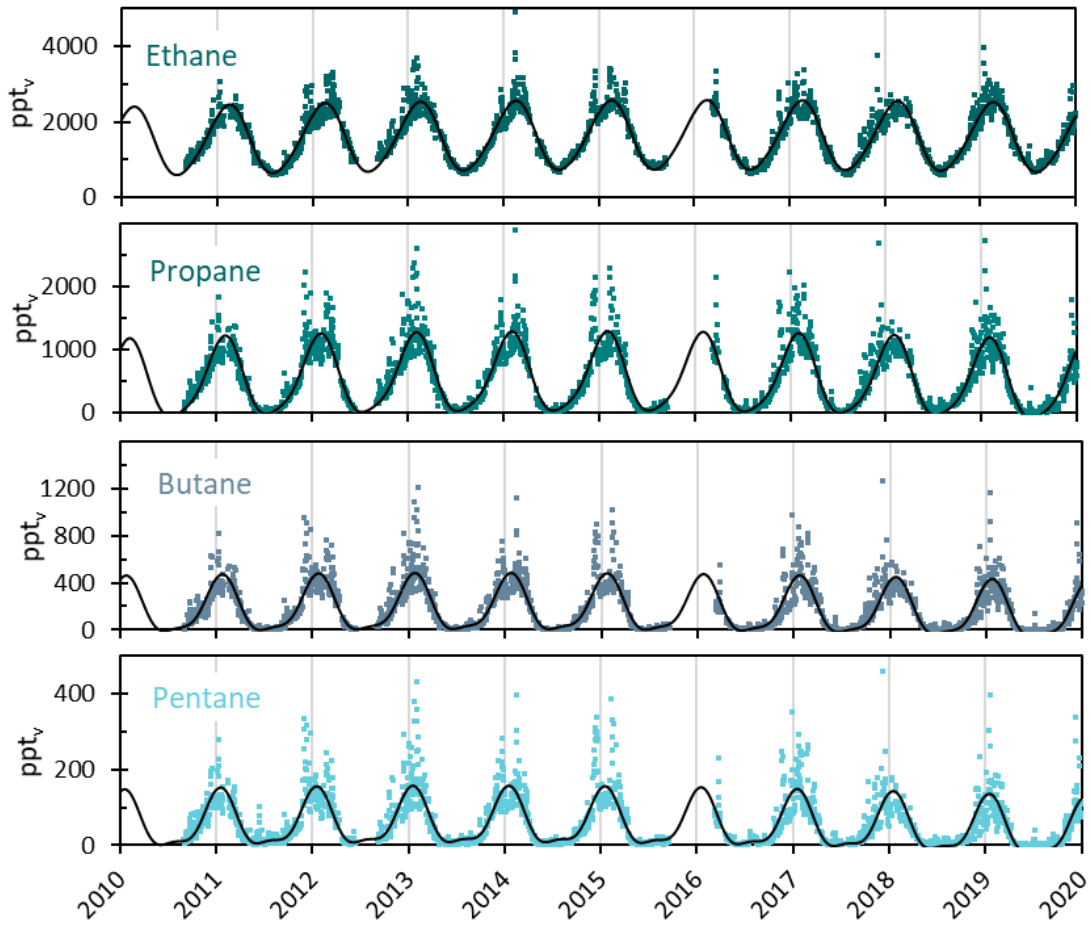

Figure 19: Observations of daily averaged mixing ratios of ethane, propane, butane, and pentane for the period September 2010 – 2019 at the Zeppelin Observatory. The black line is empirical modelled mixing ratio.

Due to the short lifetimes, ranging from a few days for pentane to 2-3 months for ethane, the annual cycles are very strong and are regulated by OH reactions. The annual mean from 2011 to 2019 are shown in Figure 20.

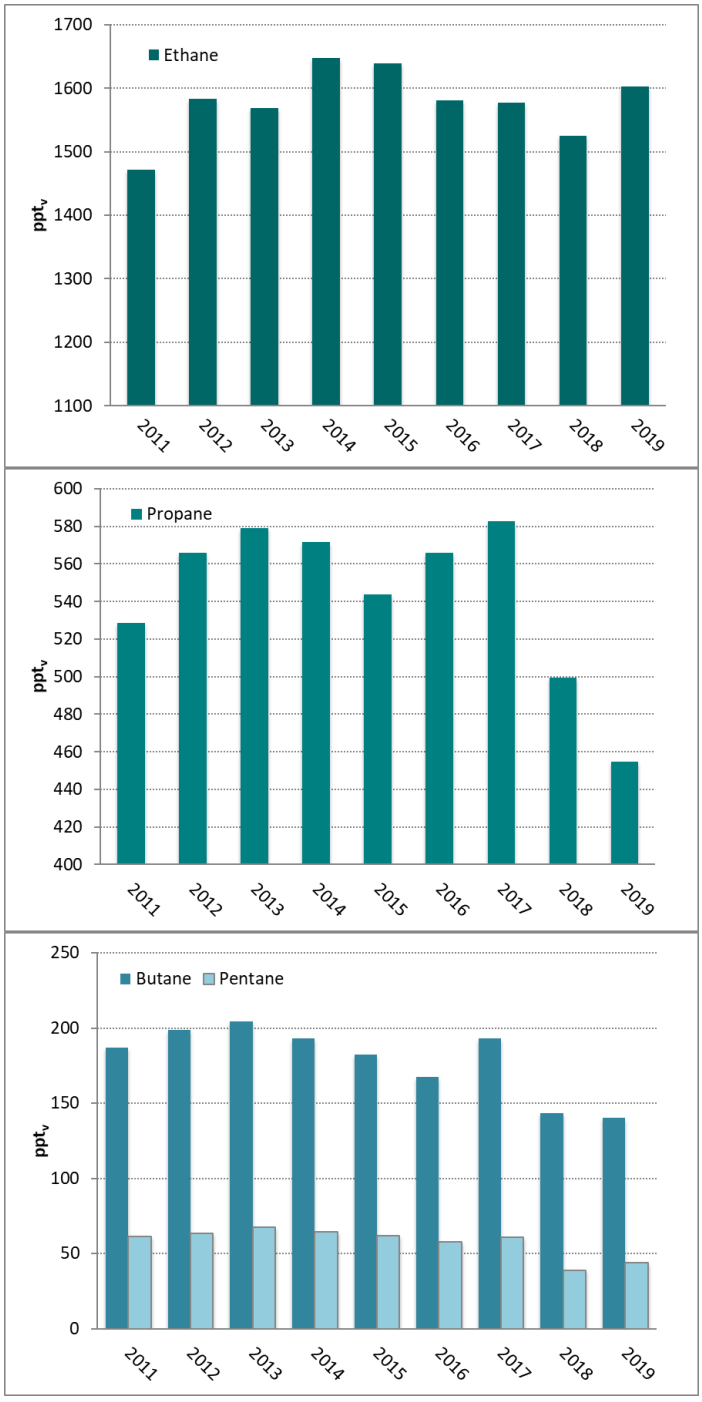

Figure 20: Development of the annual means of the measured non-methane hydrocarbons at the Zeppelin Observatory for the period 2011-2019. Upper panel in dark green: ethane, mid-panel propane, and lower panel butane and pentane. All concentrations are in ppt.

As seen from the figure the annual mean concentrations vary from one year to another and for most compounds it is not possible to draw any conclusions about development and trend. However, for all these compounds, there is a decrease from 2017-2018, but then an increase in ethane from 2018-2019. The decrease from 2017-2018 should be interpreted in light of the drought, and fewer transport episodes from Central-Europe during wintertime.

At Zeppelin we aim to measure two other aromatic VOCs, benzene and toluene, which belong to a group of VOCs found in petroleum hydrocarbons, such as gasoline. These compounds have attracted much attention since benzene are considered carcinogens, but they are also relevant for climate. The VOCs have relatively short atmospheric lifetimes and small direct impact on radiative forcing. However, anthropogenic secondary organic aerosols (SOA) are formed from photo oxidation of benzene and toluene (Ng et al., 2007), which indirectly impacts the climate (negative forcing). The SOA formation from these VOCs is most effective under low-NO_x conditions and when ambient concentration of organic aerosols is high. Thus, benzene and toluene influence climate through their production of secondary organic aerosols and their involvement in photochemistry, i.e., production of O_3 in the presence of light.

Figure 21 shows the daily mean observations of benzene and toluene at Zeppelin for the period 2010-2018. After an upgrade of the Medusa-GCMS in fall 2017, the benzene and toluene values became unrealistic low. Thus, the measurements performed after 4. October 2017 are flagged as "missing", but available again now fall 2019, after improvement of the instrument.

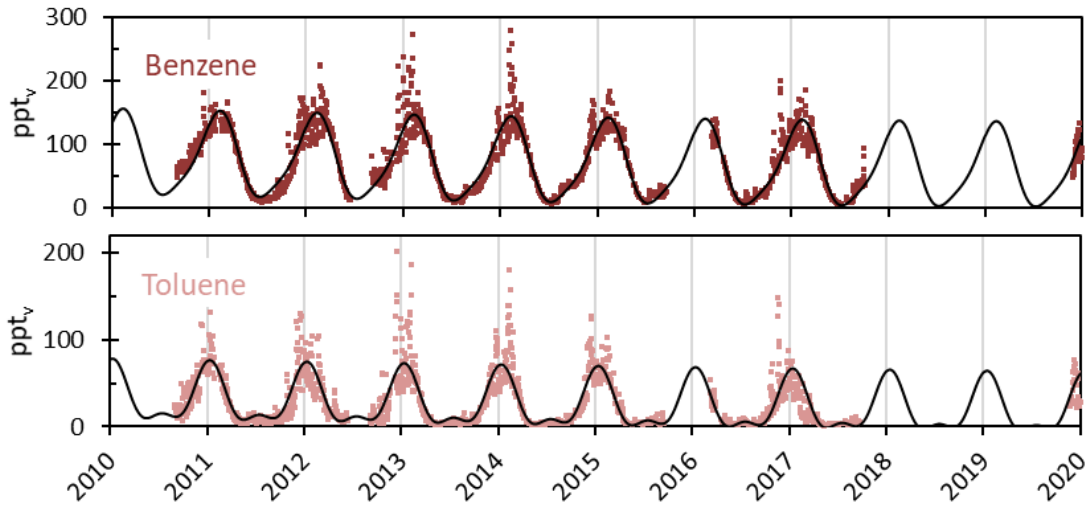

Figure 21: Observations of daily averaged mixing ratio of benzene (upper panel) and toluene (lower panel) for the period September 2010 – 2019 at the Zeppelin Observatory. The black line is empirical modelled mixing ratio.

As can be seen from the figure there are strong annual variations, mainly explained by the reactions induced by sunlight. The annual means of benzene and toluene for the period 2011-2019 are presented in Figure 22. The figure shows a declining tendency for both compounds, but unfortunately no annual mean values are calculated from the measurements in 2018. The shaded bars in Figure 22 indicates that the annual means in 2018 and 2019 are based on model values only (i.e. the black curve in Figure 21).

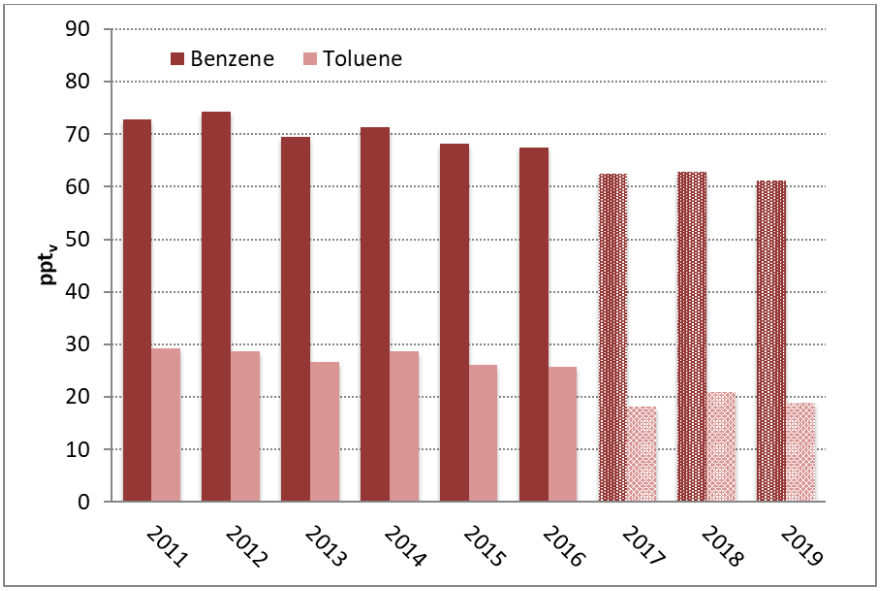

Figure 22: Development of the annual means of benzene (brown) and toluene (light red) for the period 2011 – 2019 at the Zeppelin Observatory. All concentrations are in ppt. Note that benzene and toluene in 2017-2019 mainly are based on model data.

2.1.5 Carbon monoxide (CO)

Key findings CO: *CO is not a direct greenhouse gas, but it is still considered as a climate gas as it regulates the levels of methane and ozone. CO is also an excellent tracer for long-range transport of smoke from fires. CO has been measured at Zeppelin since 2001. For the period 2001-2019 a decreasing trend of -1.3 ppb/yr is recorded. In 2019 there were strong CO transport episodes registered at Zeppelin traced back to fires in Siberia.*

Atmospheric carbon monoxide (CO) has both natural and anthropogenic sources. CO is produced when various organic gases are oxidized, such as methane, VOCs emitted from fossil fuel, and gases from biomass burning. Additionally, emissions from plants and ocean are important sources. CO is not considered as a direct greenhouse gas, as it does not absorb terrestrial thermal IR energy strongly enough. However, CO is able to modulate the level of methane and production of tropospheric ozone, which are both very important greenhouse gases. Hence, CO is considered as a climate relevant gas although not a greenhouse gas. CO is closely linked to the cycles of methane and ozone and it also plays a key role in the control of OH radicals.

CO at Zeppelin is included in the current monitoring programme and the observed CO mixing ratios for the period September 2001-2019 are shown in Figure 23.

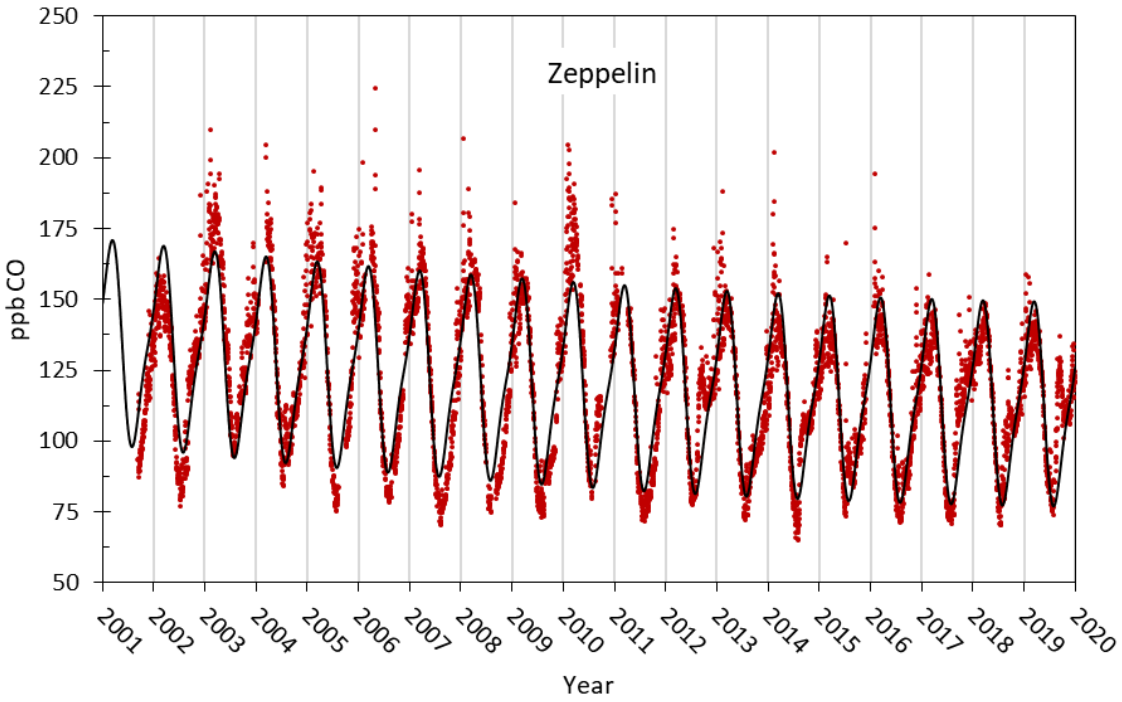

Figure 23: Observations of carbon monoxide (CO) from September 2001 to 2019 at the Zeppelin observatory. Red dots: daily averaged observed mixing ratios. The solid line is the empirical fitted mixing ratio.

The concentrations of CO show characteristic seasonal variations with a clear annual cycle with a late winter (February/March) maximum and a late summer (August) minimum. This seasonal cycle is driven by variations in OH concentration as a sink, emission by industries and biomass burning, and transportation on a large scale. As seen from the figure there are also peak values which are due to long-range transport of polluted air to Zeppelin and the Arctic. The highest mixing ratio of CO ever observed at Zeppelin is 225 ppb, measured on the 2nd of May 2006. This peak value was due to agricultural fires in Eastern Europe. In general, CO is an excellent tracer for transport of smoke from fires (biomass burning, agricultural- or forest fires).

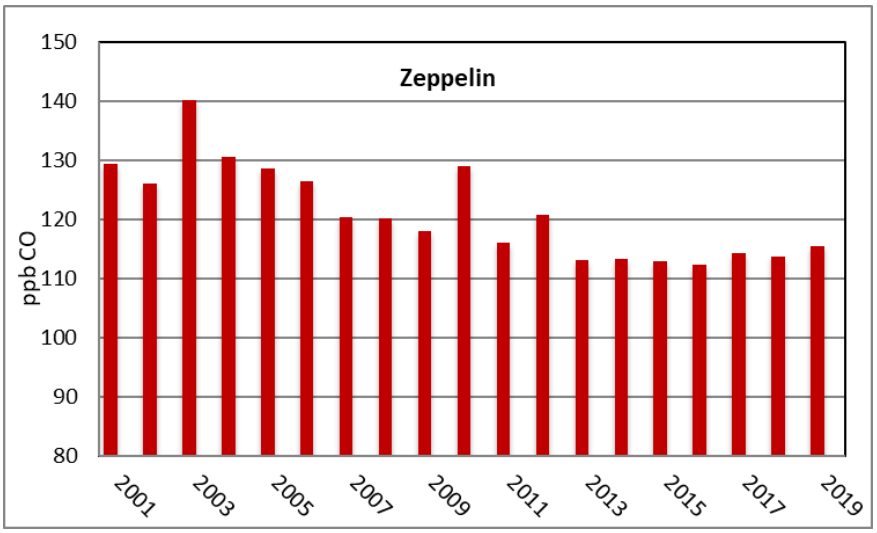

Figure 24: Development of the annual means of CO measured at the Zeppelin Observatory for the period 2001-2019. The concentrations are in ppb.

The development of the annual CO means at Zeppelin for the period 2001-2019 is presented in Figure 24. In general the CO concentration at Zeppelin shows a decrease during the period 2003 to 2009, and stable levels the last years with a small peak in 2010. For the period 2001-2019 a trend of -1.2 ppb/yr is calculated. There were no episodes with extreme CO concentrations in 2018. However, analysis of the data from the year 2019 is more interesting, as there were heavy fires in Siberia, in particular, this year. There was also a large increase in fires in Amazonas in 2019 and elsewhere in the southern hemisphere, and this might influence even the observations at Zeppelin.

An unprecedented amount of wildfires have been raging in various regions of the Arctic, including Greenland and Alaska in the US. They have been caused by record-breaking temperatures and lightning, fuelled by strong winds. These fires emit significant smoke and particulates harmful pollutants and toxic gases into the atmosphere, which make their way across the Bering Sea to the U.S. and Canada. According to the WMO, fires in the Arctic released around 50 mega tonnes of carbon dioxide in June alone – equivalent to Sweden's total annual emissions. In summer 2019, Siberia saw wildfires on a massive scale across the countryside. We can also see the high CO concentration during summer time at Zeppelin in Figure 23, better shown in the next figure. The image shown is captured from space on 28 July 2019 (European Space agency (ESA)). According to ESA almost three million hectares of land are estimated to have been affected. This Copernicus Sentinel-3 image shows a number of fires, producing plumes of smoke.

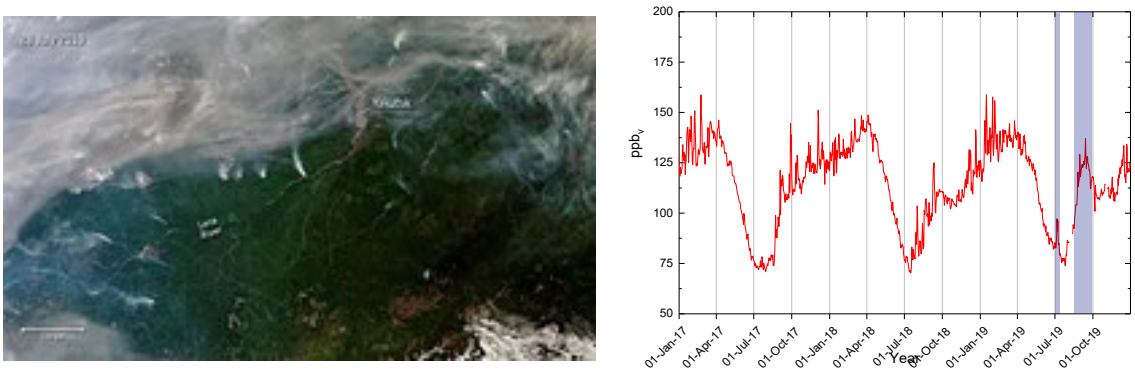

Figure 25: An unprecedented amount of wildfires have been raging in various regions of the Arctic, including Greenland and Alaska in the US. The picture to the left is from Sentinel-3, the plot to the right is CO at Zeppelin for 2017-2019. The blue bars show when there are high CO concentration for the season, highly impacted by the fires.

2.1.6 Chloromethane at the Zeppelin Observatory

***Key findings - Chloromethane**: The atmospheric concentration of chloromethane is relatively stable. The gas has a dominating natural origin and is not regulated through the Kyoto or Montreal protocols. The annual mean CH_3Cl concentration at Zeppelin has decreased by ~-1.3% since 2001.*

Chloromethane (also called methyl chloride, CH_3Cl) is the most abundant chlorine containing organic gas in the atmosphere. It contributes approximately 16% to the total chlorine from the well-mixed gases in the troposphere (WMO, 2014b), and through this a strong contributor to ozone depletion. The main sources of chloromethane are natural, and the dominating sources include ocean, biomass burning, fungi, wetlands, rice paddies, and tropical forests. Due to the dominating natural sources, this compound is not regulated through the Montreal or the Kyoto protocols. To reach the stratosphere,

the lifetime in general needs to be above the order of 2-4 years, but this is also dependent on the source strength and the regional distribution of the gas. Chloromethane has a relatively high mixing ratio and contributes to the stratospheric chlorine burden.

The result of the measurements of this gas for the period 2001-2019 is shown in Figure 26. The lifetime of chloromethane is only one year, resulting in large seasonal fluctuations due to rapid changes in emission, as shown in Figure 26.

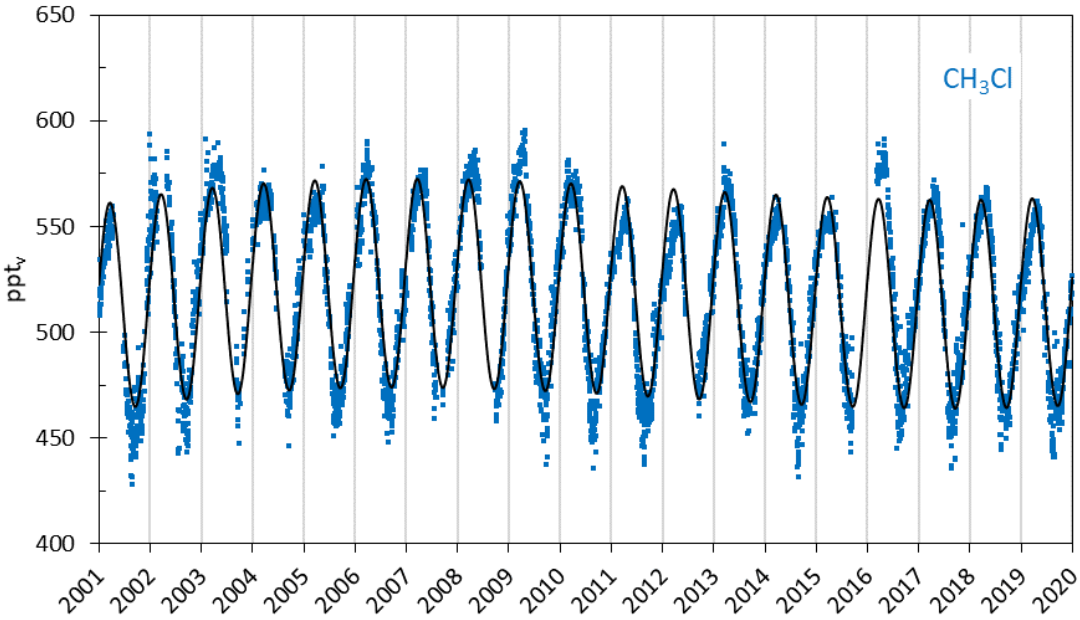

Figure 26: Observations of chloromethane, CH_3Cl, for the period 2001-2019 at the Zeppelin Observatory. Blue dots: daily averaged concentrations from the observations, solid line: empirical fitted mixing ratios.

The annual means of chloromethane for the period 2001-2019 are shown in Figure 27. Days with missing observations are filled with empirical fitted data. Only small changes have been observed since the measurements started in 2001. The trend for the period 2001-2019 is -0.37 ppt/yr (-1.3% for the entire period). From 2002 to 2009 the annual mean chloromethane concentrations were relatively stable at a level around 520 ppt, but since 2009 there has been larger variability and a decreasing tendency, except from 2016 where the annual mean value was 10 ppt higher than previous year. The black bars in Figure 27 shows that the global annual means in 2016-2019 (Hall et al., 2017 and 2020; Dlugokencky et al., 2018 and 2019) were 30-40 ppt (6-7%) higher than the annual mean values at the Zeppelin Observatory. This is likely explained by strong emission sources in the tropics, resulting in increased CH_3Cl mixing ratios towards lower latitudes (Umezawa et al., 2014). Zeppelin is less affected by this, due to the short lifetime.

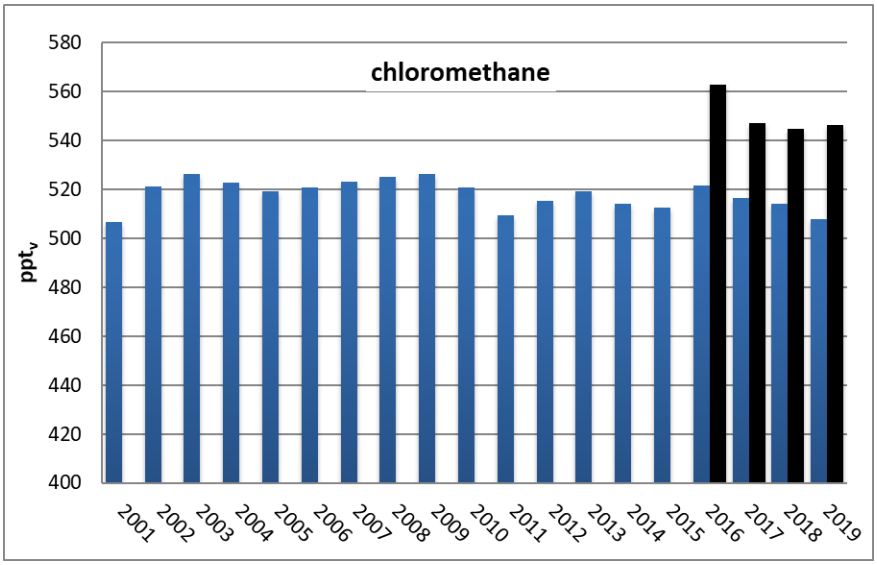

Figure 27: Development of Chloromethane annual means measured at the Zeppelin Observatory for the period 2001-2019. Global annual means for 2016-2019 are included as black bars. All units are in ppt.

2.1.7 Bromomethane at the Zeppelin Observatory

Key findings - Bromomethane: *The atmospheric concentration of CH_3Br at Zeppelin has decreased by ~25% since the observations started in 2001. The decrease is a result of the implementation of the Montreal Protocol. However, CH_3Br has many natural sources with uncontrolled fluctuations from one year to another.*

Bromomethane (also called Methyl bromide, CH_3Br) is an important reservoir for atmospheric bromine, which reacts with ozone to deplete the ozone layer. CH_3Br has both natural and anthropogenic sources. The natural sources such as the ocean, plants, and soil, can also be a sink for this gas. The primary anthropogenic source of bromomethane has been from its use as a fumigant, e.g. for pest control and pesticide in the control of weeds. Other anthropogenic sources of CH_3Br include the combustion of leaded gasoline, biomass burning, and emissions from certain crop species. Even though bromomethane is a natural substance, the additional contribution from anthropogenic sources contributes to the man-made depletion of the ozone layer. Total organic bromine from halons and bromomethane peaked in the mid-1990s, but the tropospheric concentration has decreased by ~25% over the past 20 years. Also, the stratospheric abundance of bromide has started to decrease (WMO, 2018).

The result of the daily averaged observations of bromomethane for the period 2001-2019 is shown in Figure 28. Bromomethane is a greenhouse gas which is twice as strong as CO_2 and has a lifetime of 0.8 years (Myhre et al, 2013b). The short lifetime explains the strong annual and seasonal variations of this compound.

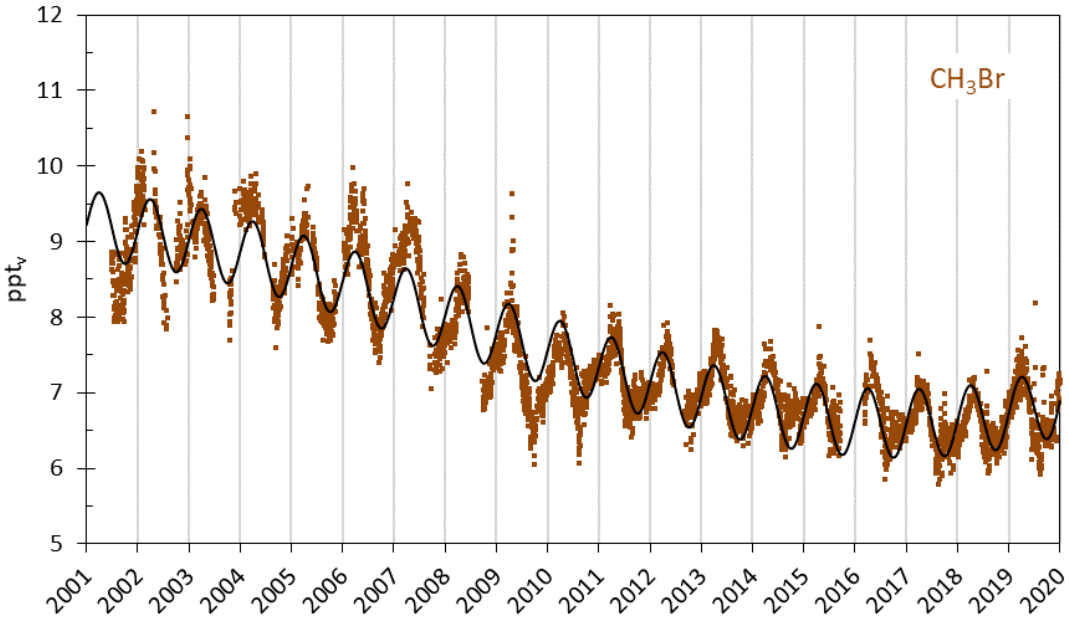

Figure 28: Observations of Bromomethane, CH_3Br, for the period 2001-2019 at the Zeppelin Observatory. Brown dots: daily averages mixing ratios from the observations, solid line empirical fitted mixing ratios.

The development of the annual means for the period 2001-2019 is presented in Figure 29. For this period there is a trend in the mixing ratio of -0.16 ppt/yr. The overall observed change since 2001 is -2.3 ppt, i.e. -25%. In 2019 the annual mean CH_3Br concentration was 6.8 ppt, which is slightly higher than the mean values from the previous two years. In general, the decline in bromomethane is explained by considerable reduction in emissions; The uses of CH_3Br has decreased steadily as a result of the implementation of the Montreal Protocol, from over 50 000 tonnes/yr in the late 1990s to about 4 000 tonnes/yr in 2012 (WMO, 2014b).

The global mean mixing ratios published by BAMS in "State of the Climate" (Dlugokencky et al., 2018 and 2019; Hall et al., 2017 and 2020), presented by the black bars in Figure 29, were ~6.6 ppt in both 2017, 2018 and 2019. This is close to the annual mean values observed at the Zeppelin Observatory.

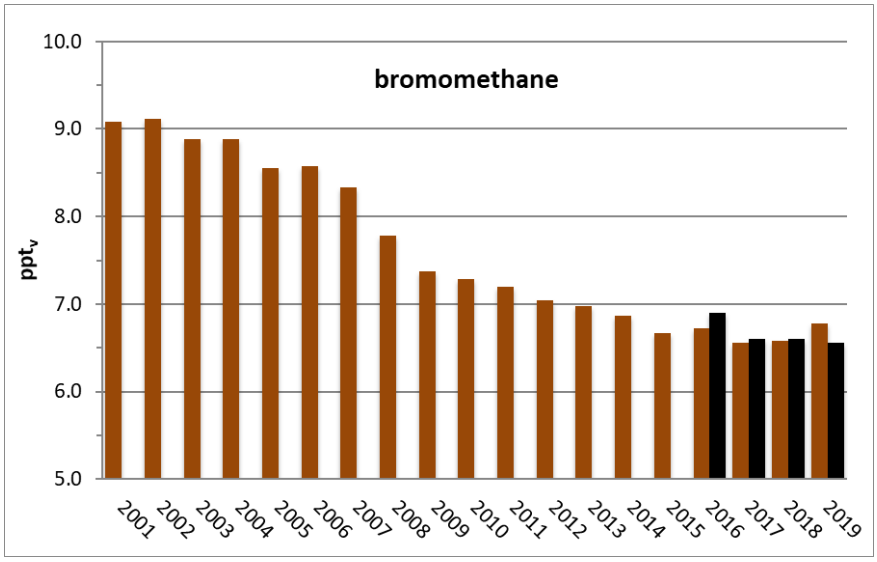

Figure 29: Development of the annual means of bromomethane measured at the Zeppelin Observatory for the period 2001-2019. The global annual mean for 2016-2019 are included as black bars.

2.2 Greenhouse gases with solely anthropogenic sources

The gases presented in this chapter have solely anthropogenic sources. These man-made greenhouse gases include CFCs, HCFCs, HFCs, SF_6, NF_3, SO_2F_2 and halons, and most of these gases did not exist in the atmosphere before the 20th century. Although the gases have much lower concentration levels than most of the natural gases mentioned in the previous section, they are strong infrared absorbers, many of them with extremely long atmospheric lifetimes resulting in high global warming potentials (see Table 3). As a group, the gases contribute to around 12% to the overall global radiative forcing since 1750 in according to the AR5 IPCC report (Myhre et al, 2013b). The annual mean concentrations for all years and all gases included in the monitoring programme are given in Appendix I (Table A 1, page 116), whereas trends, uncertainties and regression coefficients are found in Table A 2.

Some of these gases are ozone depleting, and consequently regulated through the Montreal protocol. Especially chlorine and bromine from CFCs, HCFCs and halons contribute to the depletion of the ozone layer, allowing increased UV radiation to reach the earth's surface, with potential impact not only on human health and the environment, but on agricultural crops as well. In 1987 the Montreal Protocol was signed in order to reduce the production and use of these ozone-depleting substances (ODSs) and the amount of ODSs in the troposphere reached a maximum around 1995. The amount of most ODSs in the troposphere is now declining slowly and the concentrations are expected to be back to pre-1980 levels around year 2050. In the stratosphere the peak ODS level was reached around year 2000. According to WMO (2018) the amount of Equivalent Effective Stratospheric Chlorine (EESC) declined by about 9% in the Polar regions and 13-17% in Mid-latitude regions from mid 1990s to 2016.

There are two generations of substitutes for the CFCs. The first generation is included in the Montreal protocol as they also deplete the ozone layer. This comprises the HCFCs listed in Table 3. The second-generation substitutes, the HFCs, are included in the Kyoto protocol and in the amendment to the Montreal Protocol agreed in Kigali in 2016. The general situation now is that the CFCs are declining, while their substitutes are increasing, and some of them are increasing rapidly.

2.2.1 Chlorofluorocarbons (CFCs) at Zeppelin Observatory

Key findings - CFCs: *The development of the CFC levels at Zeppelin is promising and in good accordance with the compliance of the Montreal protocol. The concentrations of CFC-11, CFC-12 and CFC-113 are all declining, and the mixing ratios of these gases are reduced with approximately 12.5%, 8.2% and 14.1% since 2001, respectively. However, recent studies have shown that the rate of decline in CFC-11 has slowed down by ~50% after 2012, both globally and at Zeppelin. This is probably related to unreported emissions in China. Also, CFC-115 has increased by 5.3% since 2001 and the increase has intensified after 2013. This can also be related to Chinese emissions.*

In total, four chlorofluorocarbons (CFCs) are measured and analysed at the Zeppelin observatory: CFC-11, CFC-12, CFC-113, and CFC-115. These are the main ozone depleting gases. The anthropogenic emissions started around the 1930s, and all these compounds were restricted in the Montreal protocol from 1987. The main sources of these compounds were foam blowing, aerosol propellant, temperature control (refrigerators), solvents, and the electronics industry. The highest production of the CFCs was in around 1985 and maximum emissions were in around 1987. The lifetimes of these compounds are long. From 45 to over one thousand years (see Table 3) and combined with strong infrared absorption properties their GWPs are high.

Figure 30 shows the daily averaged observed mixing ratios of the four CFCs. Before 2010/2011 the instrumentation for measurements of CFCs at Zeppelin was not in accordance with recommendations and criteria of AGAGE, and consequently there are relatively high uncertainties in the observations of these compounds, see also Appendix I. From September 2010, new and improved instrumentation was installed at Zeppelin, providing more accurate observations of CFCs. The higher precisions are clearly

visualised in Figure 30, but due to several severe instrumental problems in 2013/14, 2015/16 and 2019 there are some periods without CFC measurements[14].

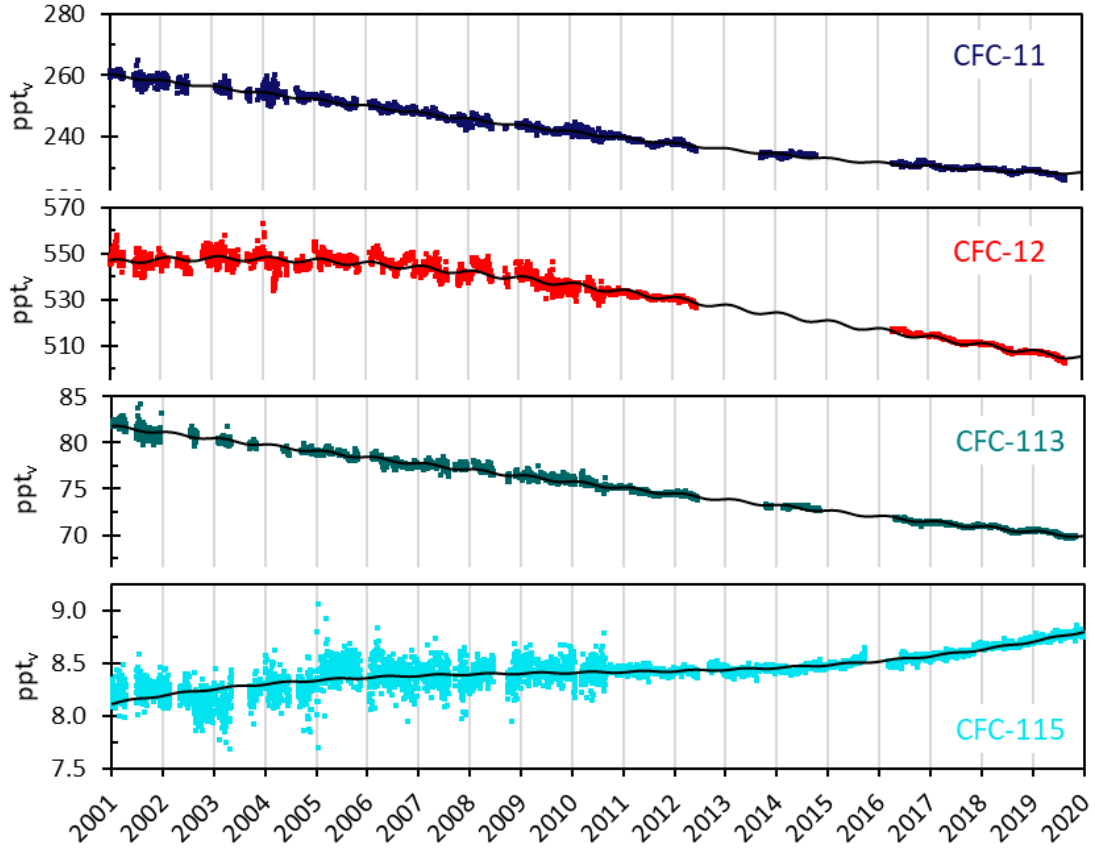

Figure 30: Daily averaged mixing ratios of the monitored CFCs at the Zeppelin observatory for the period 2001-2019: CFC-11 (dark blue), CFC-12 (red), CFC-113 (green) and CFC-115 (light blue). The solid lines are empirical fitted mixing ratios.

The trends per year for CFC-11, CFC-12 and CFC-113, given in Table 3, are all negative. The decreases are -1.8, -2.5, and -0.6 ppt/yr for CFC-11, CFC-12 and CFC-113, respectively. For the compound CFC-115 the trend is still slightly positive, +0.02 ppt/yr, and there has also been a small increase the last few years, after a stable period. It should be noted that the ambient concentration of CFC-115 is relatively low compared to CFC-11 and CFC-12, but it has a very long lifetime of 1020 years, which limits our ability to reduce the abundance in the atmosphere. In total, the development of the CFC levels at the global background site Zeppelin is promising and in accordance with the compliance of the Montreal protocol.

Recent studies have shown that the rate of decline of atmospheric CFC-11 concentrations has slowed down by about 50% after 2012 (Rigby et al., 2019). This is caused by new production and unreported CFC-11 emissions in China, strongly inconsistent with the Montreal Protocol agreement. Also, studies from Vollmer et al. (2018) conclude that a large fraction of the current global emissions of CFC-115 originate from the Chinese mainland. This demonstrates the importance of maintaining good monitoring networks, both to detect possible changes in ODSs, but also to detect possible effects of climate change on the ozone layer.

[14] *The instrumentation is not in accordance with recommendations and criteria of AGAGE for measurements of the CFCs and there are larger uncertainties in the observations of this compound, see also Appendix I. This is also why these compounds are particularly sensitive to instrumental problems.*

The 2001-2019 annual means for all the observed CFCs at Zeppelin are shown in Figure 31. Also, the global annual means in 2016 – 2019 as reported in "State of the Climate", BAMS (Dlugokencky et al., 2018 and 2019; Hall et al., 2017 and 2020) are included as black bars for comparison. As can be seen, the observed concentrations at Zeppelin are close to the global mean for these compounds, as the lifetimes are long and there are hardly any present-day emissions.

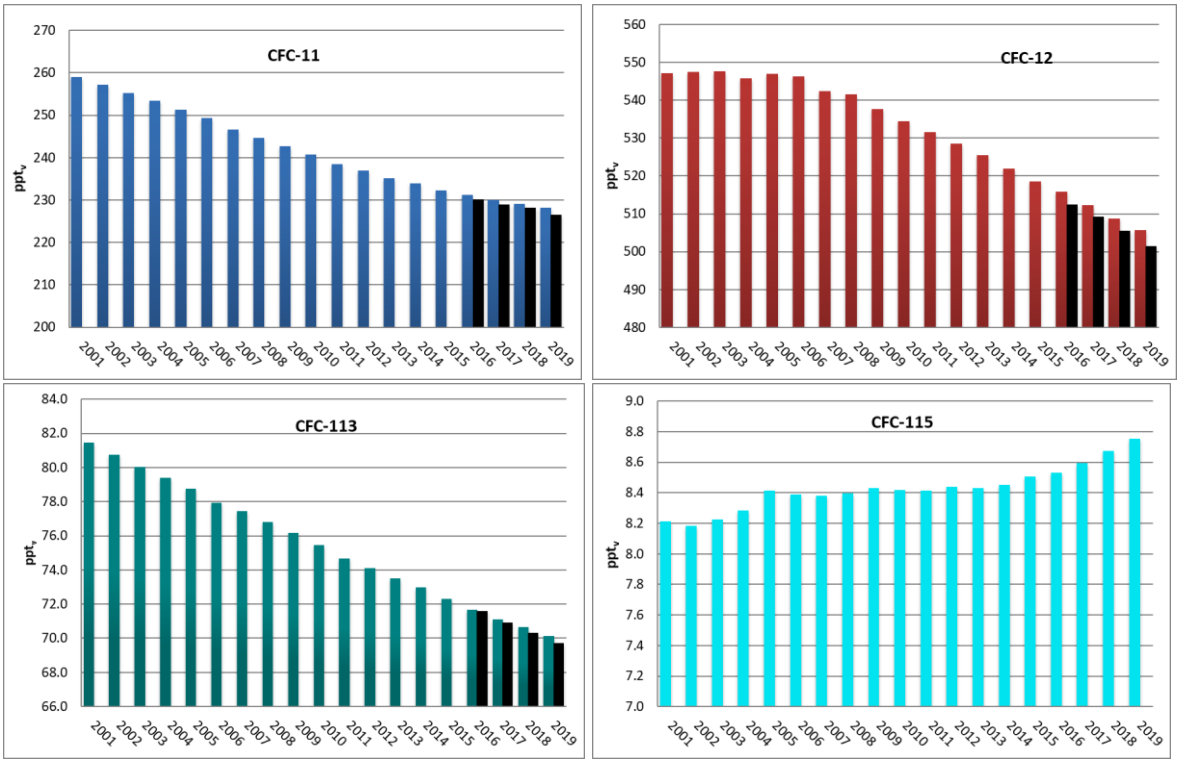

Figure 31: Development of CFC annual means at the Zeppelin Observatory for the period 2001-2019. Upper left panel: CFC-11, upper right panel: CFC-12, lower left panel: CFC-113, lower right panel: CFC-115. See Appendix I for data quality and uncertainty. The global annual means for 2016-2019 are included as black bars. All units are in ppt.

According to WMO (2018) the global mean mixing ratio of CFC-11 (from the AGAGE network) decreased with approximately 1.3 ppt/yr from 2015 to 2016. This is in accordance with the measurements at Zeppelin. As mentioned above, the rate of atmospheric CFC-11 decline slowed down after 2012. At Zeppelin the average rate was -2.1 ppt/yr prior to 2012 and -1.3 ppt/yr after 2012. CFC-12 (the red diagram) has a very high GWP, 10200, and it is also the most abundant CFC. This makes CFC-12 a very potent greenhouse gas. The global mean estimates from the AGAGE network, show that the atmospheric mixing ratio of CFC-12 decreased at a rate of -0.7%/yr from 2015 to 2016 (WMO, 2018). This fits well with our observations at Zeppelin the last years. CFC-12 had a maximum around 2003-2005, but there has been a clear reduction over the last years: 41 ppt since 2005.

2.2.2 Hydrochlorofluorocarbons (HCFCs) at Zeppelin Observatory

Key findings - HCFCs: *The CFC substitutes HCFC-22, HCFC-141b and HCFC-142b have increased significantly since the measurements started at Zeppelin in 2001. HCFC-22 has a growth rate of 5.8 ppt/yr, whereas HCFC-141b and HCFC-142b have average growth rates of 0.5 ppt/yr. From 2001 to 2019 HCFC-22, HCFC-141b and HCFC-142b increased by 61%, 53% and 61%, respectively. HCFC-22 is still increasing, but the rate has slowed down. The situation is even more positive for HCFC-141b and HCFC-1412b, where concentrations have declined the last three years.*

Hydrochlorofluorocarbons, HCFCs, represent the first generation of replacement gases for CFCs. The lifetimes are rather long, see Table 3, but although not as stable and persistent in the atmosphere as CFCs, they can still end up in the stratosphere where they can destroy the ozone layer. Consequently, the gases are regulated through the Montreal protocol. The Norwegian monitoring programme includes three HCFC species: HCFC-22, HCFC-141b and HCFC-142b. These compounds are mainly used as refrigerants, foam blowing agents and solvents. The use of the gases worldwide is now frozen, but they are yet not completely phased out. All the gases potentially have a strong warming effect, depending on their concentrations and absorption properties, i.e. their GWPs (see Table 3). HCFC-142b has the highest GWP, with a warming potential 1980 times stronger than CO_2, per kg gas emitted.

The daily averaged observations of the three HCFCs are shown in Figure 32 for the period 2001-2019.

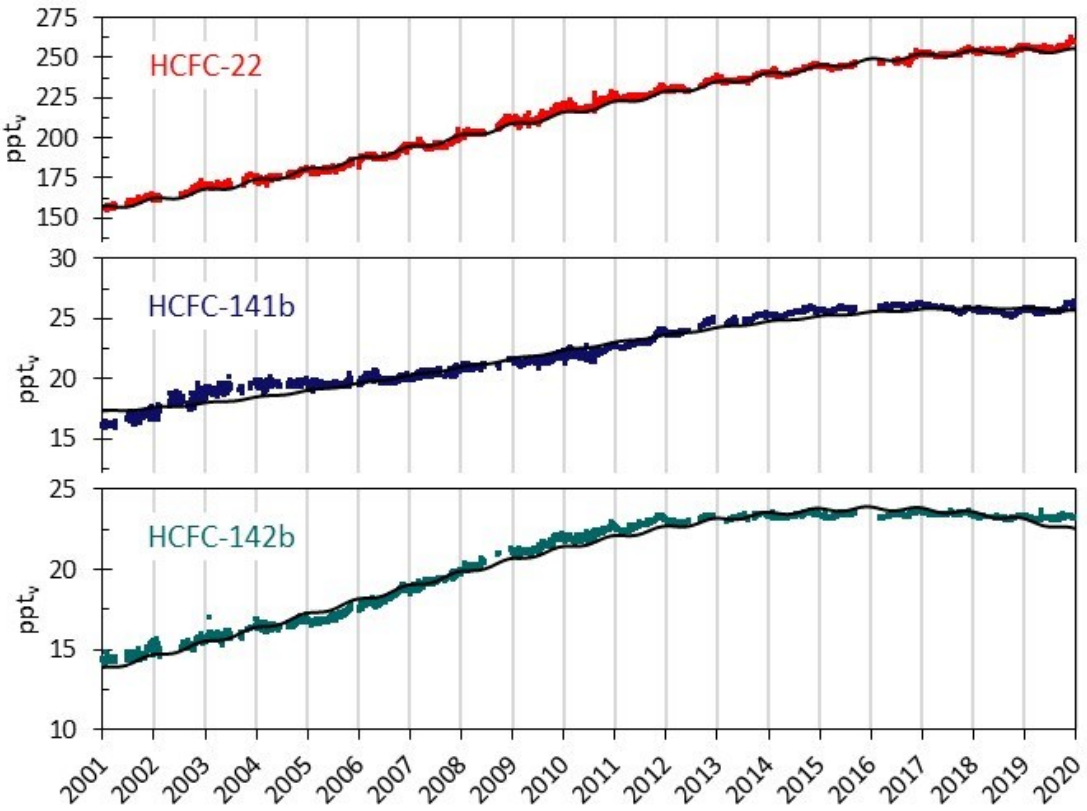

Figure 32: Daily averaged mixing ratios of the monitored HCFCs for the period 2001-2019 at the Zeppelin observatory: HCFC-22 (red), HCFC-141b (dark blue), and HCFC-142b (green). The solid lines are empirical fitted mixing ratios. All units are in ppt.

HCFC-22, HCFC-141b and HCFC-142b are all increasing over the period 2001-2019. HCFC-22 is the most abundant HCFC species and has been increasing at a rate of 5.8 ppt/yr over the period 2001-2019. The

concentration of the two other compounds, HCFC-141b and HCFC-142b, are a factor of ten lower than HCFC-22, and the increase in absolute annual means are also a factor of ten lower; HCFC-141b and HCFC-142b both increase by 0.5 ppt/yr over the period 2001-2019. However, the development is encouraging for HCFC-141b and HCFC-142b, which both have decreased after 2017. This is best illustrated in Figure 31, which shows the annual means for the full period. The rate of increase for HCFC-22 has also slowed down the last 3-4 years. Ten years ago, HCFC-22 increased by ~8 ppt/yr. From 2018 to 2019 the increase was reduced to 1.9 ppt/yr. With lifetimes in the order of 10-20 years, it is important to continue monitoring the development of the HCFCs for many years to come, as they have a significant influence on the ozone layer and are also strong greenhouse gases. The global annual means for 2016-2019 are included in Figure 31 as black bars (Hall et al. 2017 and 2020; Dlugokencky et al. 2018 and 2019). The observed concentrations at Zeppelin are 4-6% higher than the global means.

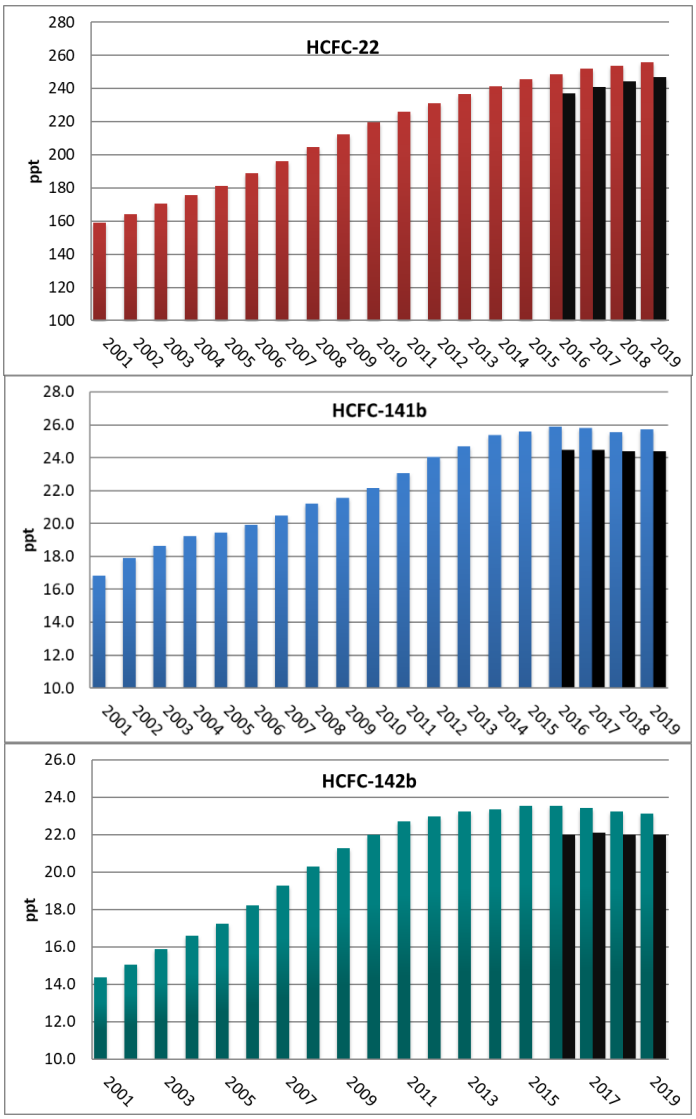

Figure 33: Development of the annual means of observed HCFCs at the Zeppelin Observatory for the period 2001-2019. HCFC-22 (red), HCFC-141b (blue), and HCFC-142b (green). The global annual means in 2016 to 2019 are included as black bars. All units are in ppt.

2.2.3 Hydrofluorocarbons (HFCs) at Zeppelin Observatory

Key findings - HFCs: *The hydrofluorocarbons (HFCs) have been introduced as replacements for the ozone depleting CFCs and HCFCs. They pose no harm to the ozone layer since they do not contain chlorine, but still they are strong greenhouse gases. The mixing ratios of HFC-125, HFC-134a, and HFC-152a have been measured at the Zeppelin observatory since 2001**,** and for the period 2001-2019 the concentrations have increased by 1379%, 448% and 301% since 2001, respectively. Eight new HFCs were introduced to the monitoring programme in 2015 and 2016: HFC-23, HFC-365mfc, HFC-227ea, HFC-236fa, HFC-245fa, HFC-32, HFC-143a, and HFC-4310mee. The mixing ratios of these gases are analysed back to 2010, showing an increase of 4-16%/yr, except for HFC-32 which increase by as much as 40%/yr. HFC-152a is the only HFC which has levelled off and stabilized,- for all the other HFCs the steep growth rate continued in 2019. The contribution from the HFCs to the global warming is still relatively small but given the rapid, in some cases apparently exponential, atmospheric increase it is crucial to follow the development of these gases. The phase-down of HFCs under the Montreal Protocol, agreed in Kigali in 2016, is important in curbing the growth in these gases*

The substances called HFCs are the so-called second-generation replacements of CFCs, which means that they are considered as better alternatives to the CFCs with respect to the ozone layer than HCFCs, as they do not contain chlorine or bromine. However, many of these compounds are strong greenhouse gases. 1 kg of HFC-23 is as much as 12 400 times more powerful greenhouse gas than CO_2 (see Table 3). The phase-down of HFCs under the Montreal Protocol was under negotiation for many years and the successful agreement in Kigali, October 2016, represented an important progress. Presently, the contribution to global warming posed by HFCs is very limited. However, most of the compounds are increasing rapidly. The compounds are strong infrared absorbers with high GWP (see Table 3, page 24), hence it is crucial to reduce future emissions.

For the period 2001-2019 three compounds have been measured at the Zeppelin Observatory: HFC-125, HFC-134a, and HFC-152a. HFC-125 is mainly used as a refrigerant and fire suppression agent. HFC-134a is used as a temperature control for domestic refrigeration and automobile air conditioners, whereas HFC-152a is used as a refrigerant and propellant for aerosol sprays and in gas duster products. Since 1990, when HFC-134a was almost undetectable in the atmosphere, the concentration of this gas has risen massively, and HFC-134a is currently the HFC with highest atmospheric concentration.

In 2015 five new HFCs were included in the Norwegian monitoring programme: HFC-23, HFC-365mfc, HFC-227ea, HFC-236fa, and HFC-245fa. In 2016 three additional HFCs were introduced to the programme: HFC-32, HFC-143a, and HFC-4310mee. All these species have been measured at Zeppelin since 2010, but they have not been analysed or reported to an international data base until 2016. The development of HFC-23 should be followed carefully, since this gas has a relatively high concentration and an extremely high GWP. HFC-23 is a by-product of the production of HCFC-22 and is also used in the semiconductor industry. In addition, it is a useful refrigerant and fire suppressant.

Generally, the new HFCs are used for refrigeration and air conditioning, foam blowing, and fire extinguishing. Both HFC-245fa and HFC-365mfc are substitutes for HCFC-141b in foam blowing applications. HFC-236fa is also a foaming agent, in addition to a fire suppression agent and a refrigerant. HFC-227ea is mainly used to suppress fire in data equipment and telecommunication facilities, and in protection of flammable liquids and gases. HFC-227ea is also used as an aerosol propellant in pharmaceutical dose inhalers for e.g. asthma medication.

The three new HFCs introduced to the monitoring programme in 2016, are mainly used for refrigeration (HFC-32 and HFC-143a). In addition, HFC-143a is applied as propellant in canned air products for cleaning electronic equipment. HFC-4310mee is mainly used as a cleaning solvent in the electronics industry.

The seasonal cycle in HFC mixing ratios are closely linked to the lifetimes and variations in the incoming solar radiation. HFC-152a has the shortest lifetime (1.5 year), and as seen in Figure 34 HFC-152a has the most distinct seasonal cycle. The gas is mainly destroyed in the lowest part of the atmosphere by photolysis and reactions with OH.

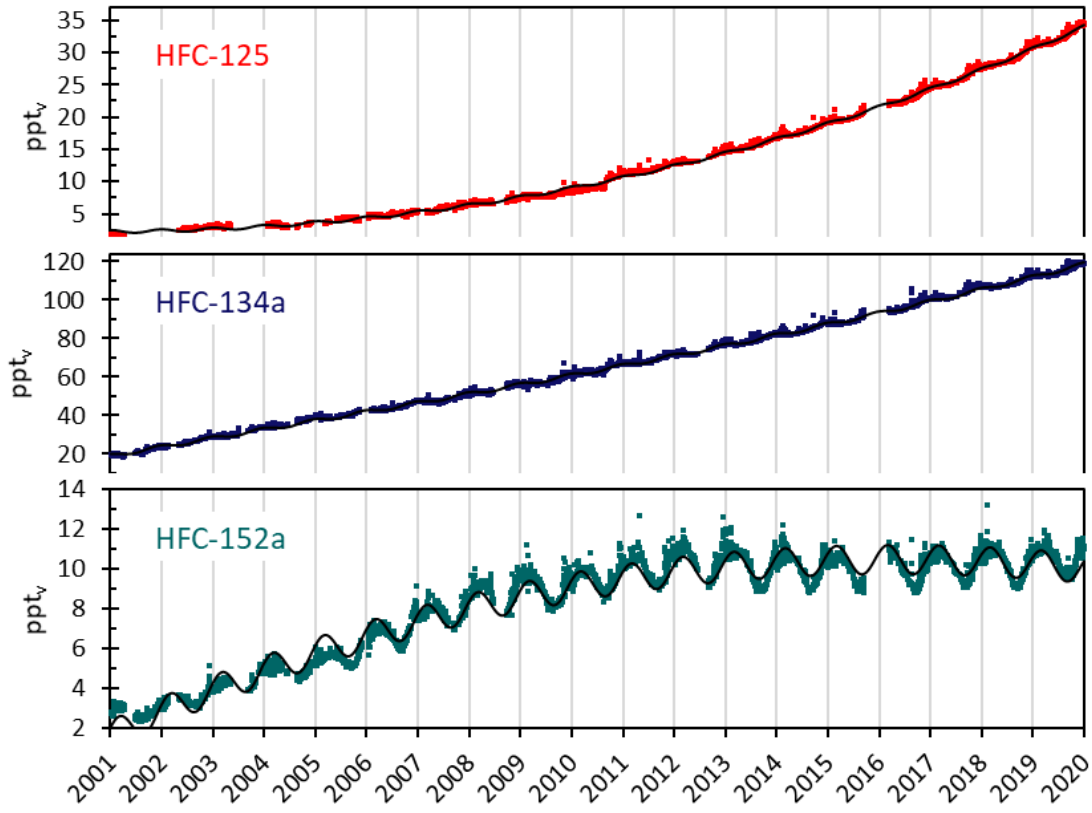

Figure 34: Daily averaged concentrations of the monitored HFCs for the period 2001-2019 at the Zeppelin observatory: HFC-125 (red), HFC-134a (dark blue), and HFC-152a (green).The solid lines are empirical fitted mixing ratios.

For the period 2001-2019 all HFCs shown in Figure 34 have increased significantly. HFC-134a has an increasing trend of 5.1 ppt/yr, which leaves this compound as the one with second highest change per year of the all the halocarbons measured at Zeppelin, next after HCFC-22. The mixing ratios of HFC-125, HFC-134a and HFC-152a have increased by as much as 1379%, 448% and 301% since 2001, respectively. For HFC-125 we can even see an accelerating trend. HFC-152a, however, is the only HFC where the rapid increase has levelled off and stabilized after 2012. This is partly due to the shorter lifetime and rapid response to emission changes. This is clearly illustrated in Figure 34 and Figure 36.

The eight new HFCs included in the programme in 2015 and 2016 are shown in Figure 35, which clearly demonstrates that the concentrations of all HFCs have increased steadily since 2010. The compounds generally increase by 4-16%/yr, except from HFC-32 which increases by as much as 40%/yr.

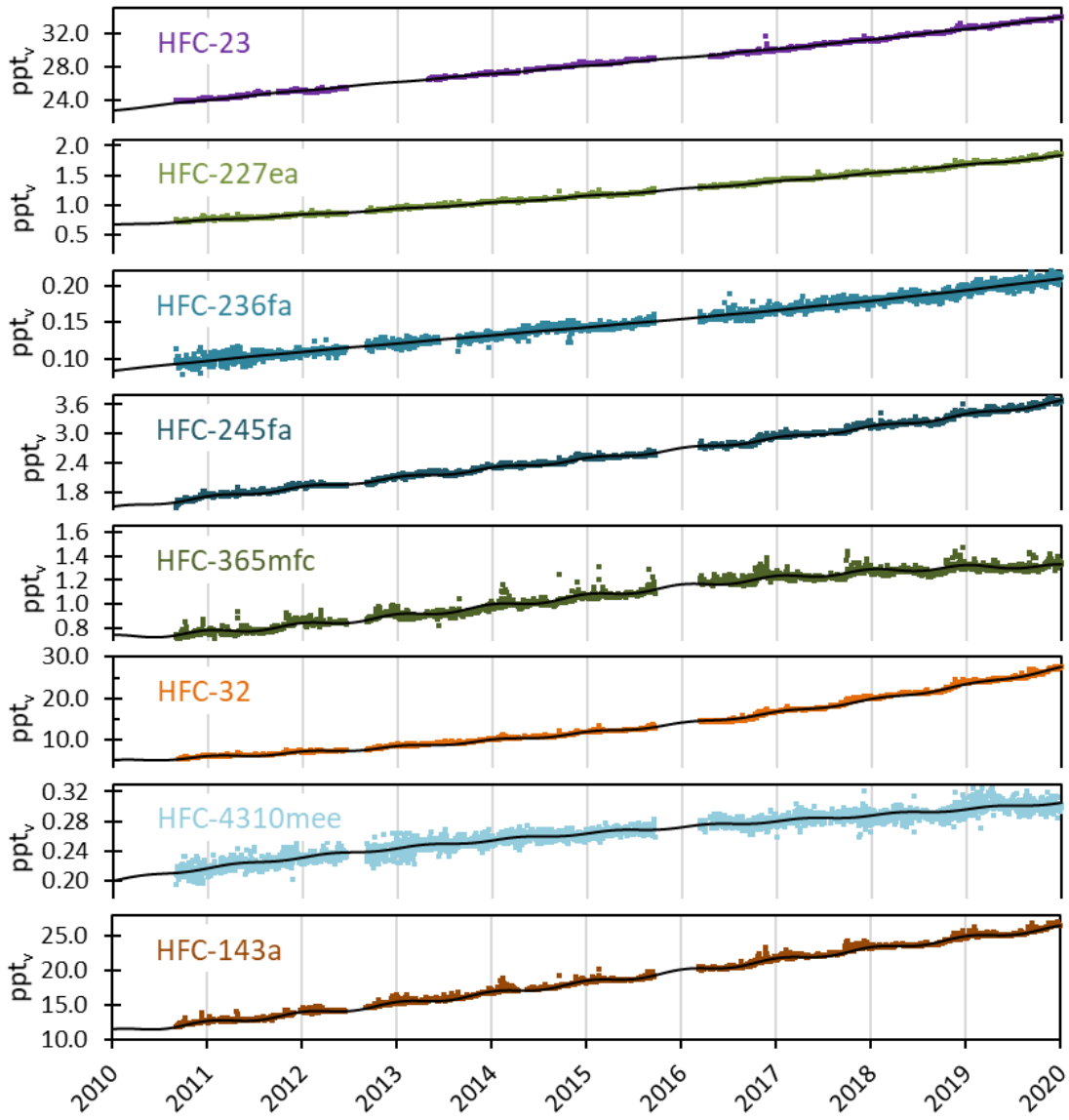

Figure 35: Daily averaged concentrations of monitored HFCs at the Zeppelin observatory for the period 2010-2019: HFC-23 (violet), HFC-227ea (light green), HFC-236fa (blue), HFC-245fa (dark blue), HFC-365mfc (dark green), HFC-32 (orange), HFC-4310mee (light blue), and HFC-143a (brown). The solid lines are empirical fitted mixing ratios.

The development of annual means of all reported HFCs are shown in Figure 36. The global annual means of 2016 -2019 as given in Hall et al. (2017; 2020) and Dlugokencky et al. (2018; 2019) are included as black bars for comparison. As for HCFCs the concentrations at Zeppelin are slightly higher than the global means. Also, the increasing tendency for most HFCs is clear, even if the concentrations are still very low, particularly for the new HFC-365mfc, HFC-245fa, HFC-236fa, HFC-227ea, and HFC-4310mee, with 3.3 ppt as maximum for HFC-245fa.

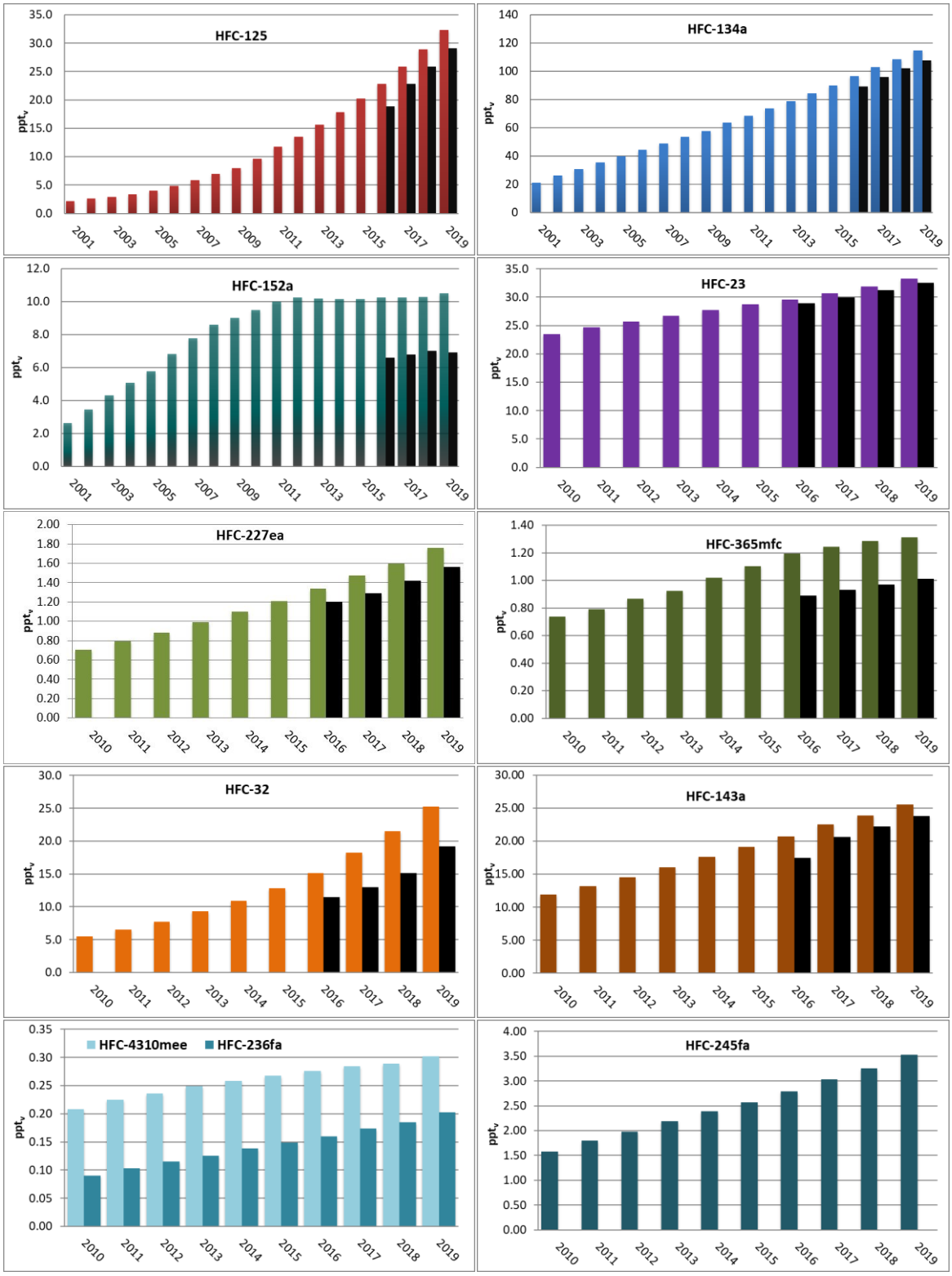

Figure 36: Development of the annual means of observed HFCs at the Zeppelin Observatory. For the period 2001-2019: HFC-125 (red), HFC-134a (blue), and HFC-152a (dark green). For the period 2010-2019: HFC-23 (violet), HFC-227ea (light green), HFC-365mfc (dark green), HFC-32 (orange), HFC-143 (brown), and light to dark blue: HFC-4310mee, HFC-236fa, and HFC-245fa. The global annual means in 2016-2019 are included as black bars, when available.

2.2.4 Halons measured at Zeppelin Observatory

***Key findings - Halons**: Halons are bromine containing halocarbons that contribute both to the depletion of the ozone layer and to global warming. Three halons are measured at Zeppelin: H-1211, H-1301, and H-2402. For H-1211 a maximum was observed in 2004, followed by a gradual decline. The concentration of H-1211 is ~23% lower today than when the measurements started in 2001. H-2402 has deceased by ~13% during the same period. H-1301, however, has increased by ~13% from 2001 to 2019, but no increase has been measured the last 4-5 years. According to the last Ozone Assessment (WMO, 2018) the stratospheric bromine concentration has now started to decrease.*

Halons are greenhouse gases containing bromine. Thus, regulations of halons are also important to protect the ozone layer. Actually, bromine is even more effective in destroying ozone than chlorine. The halons are regulated trough the Montreal protocol and the concentration of most substances are decreasing. The main source of halons has been fire extinguishers.

Previously, two halons were measured at the Zeppelin observatory: H-1301 and H-1211. In 2016 H-2402 was also included in the monitoring programme. H-2402 was used primarily in the former USSR and was the main halon fire suppressant in that region.

The ambient concentrations of the three halons are fairly low, all below 4 ppt. Figure 37 shows the daily average concentrations of the monitored halons at Zeppelin. The halon trend analyses, listed in Table 3 and visualized in Figure 37, show an increase for H-1301 during the period 2001-2019 and a decrease for H-1211. The concentration of H-1211 is ~23% lower today than when the measurements started in 2001, whereas H-1301 has increased by ~13%. However, the concentration of H-1301 has stabilized and no increase has been measured the last 4-5 years. The new compound, H-2402, shows a relaxation of ~13% from 2010 to 2019. The development of the annual means for all three compounds are shown in Figure 38.

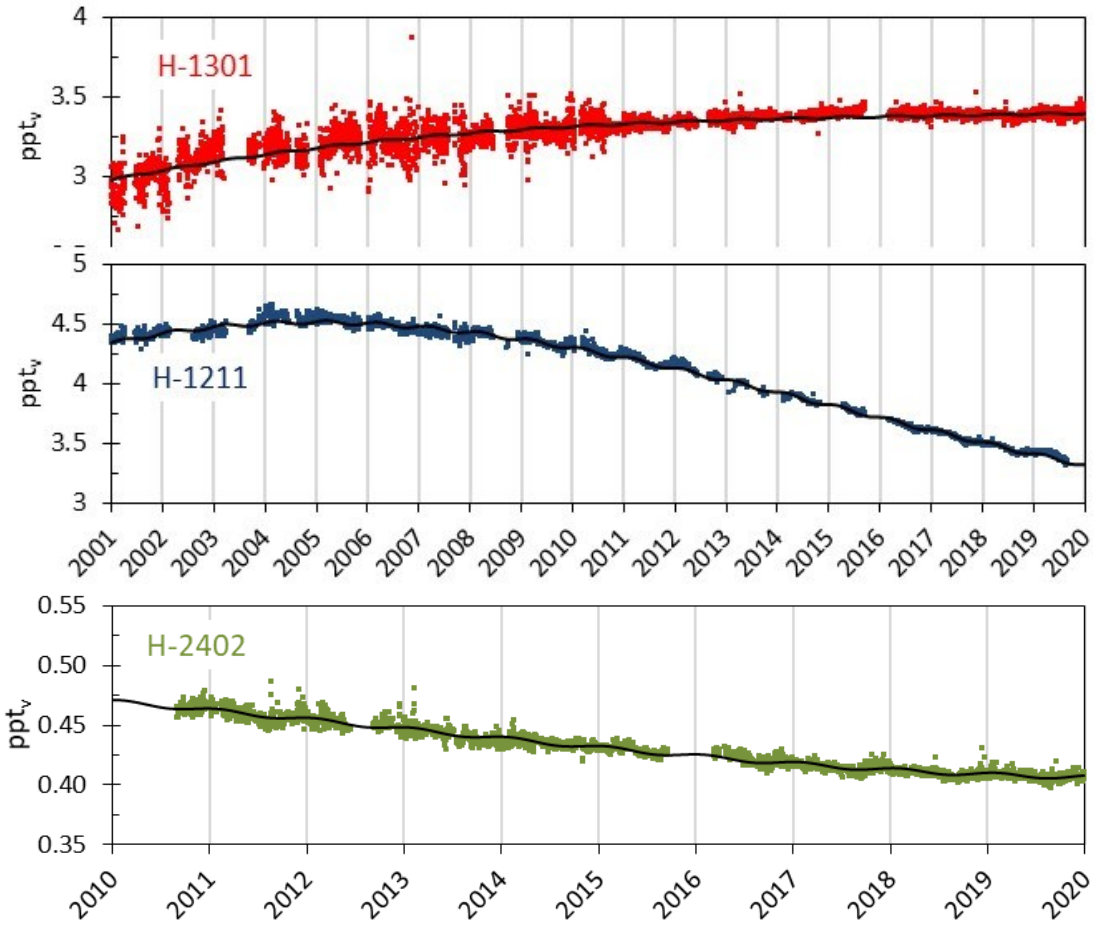

Figure 37: Daily averaged concentrations of the monitored halons at the Zeppelin Observatory. For the period 2001-2019: H-1301 (red) and H-1211 (blue). For the period 2010-2019: H-2402 (green). The solid lines are empirical fitted mixing ratios.

The annual means have not changed dramatically over the measured period, which is explained by low emissions and relatively long lifetimes (16 years for H-1211, 65 years for H-1301, and 20 years for H-2402). However, clear declines are evident for H-1211 and H-2402, which have the shortest lifetimes. According to the last Ozone Assessment report (WMO, 2018) the total stratospheric bromine concentration decreased by ~0.15 ppt/yr from 2012 to 2016.

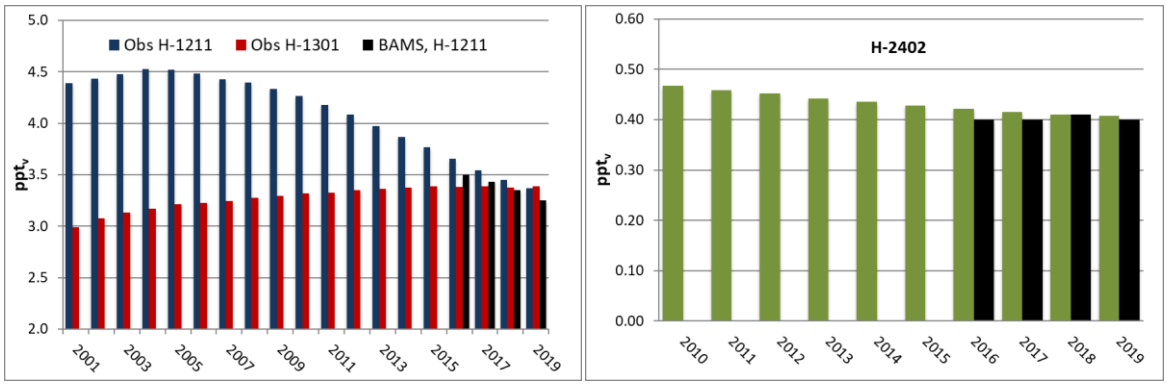

Figure 38: Development of the annual means of the observed halons at the Zeppelin Observatory. Red: H-1301, blue: H-1211, and green: H-2402. The global annual means in 2016 to 2019 are included as black bars. All units are in ppt.

2.2.5 Other chlorinated hydrocarbons at Zeppelin Observatory

***Key findings - Other chlorinated greenhouse gases**. In addition to chloromethane and bromomethane described in section 2.1.6 and 2.1.7, the following six chlorinated gases are measured at the Zeppelin Observatory: Trichloroethane (CH_3CCl_3), dichloromethane (CH_2Cl_2), trichloromethane ($CHCl_3$), trichloroethene ($CHClCCl_2$), tetrachloroethene (CCl_2CCl_2), and carbon tetrachloride (CCl_4). The concentration of most of these gases are decreasing. Possible exceptions are trichloromethane and dichloromethane, which increased significantly from 2007 to 2017. However, the last two years the annual mean concentrations of trichloromethane and dichloromethane at Zeppelin have decreased*.

This section describes the following components measured at the Zeppelin Observatory: Trichloroethane (also called methyl chloroform, CH_3CCl_3), dichloromethane (CH_2Cl_2), trichloromethane (also called chloroform, $CHCl_3$), trichloroethene (TCE, $CHClCCl_2$), and tetrachloroethene (PCE, CCl_2CCl_2). The daily average concentrations are shown in Figure 40. Additionally, a new compound was added to the monitoring programme in 2015; Carbon tetrachloride (CCl_4). The main sources of all these substances are solvents.

The global fraction of trichloroethane (CH_3CCl_3), which is controlled under the Montreal Protocol, has been declining steadily since the peak values in the early 1990s. In 2016 the global amount of CH_3CCl_3 reaching the stratosphere was reduced by 98% of its maximum value (WMO, 2018). The measurements at Zeppelin show that the concentration has decreased to 1.7 ppt in 2019, a reduction of 96% since the measurements started in 2001. Today trichloroethane contributes negligible to the atmospheric chlorine burden.

It is worth noting the strong increase in dichloromethane (violet) and trichloromethane (light blue) from 2007 to 2017, seen in Figure 39 and Figure 40. Dichloromethane has a lifetime of less than 6 months and responds rapidly to emissions changes, where about 90% has industrial origin. Its main applications are from paint strippers, degreasers and solvents; in foam production and blowing applications; and as an agricultural fumigant (WMO, 2011). The natural sources of dichloromethane, which account for ~10% of the total emission, is mainly from biomass burning and marine sources. At Zeppelin dichloromethane has increased by ~86% since 2001. However, the level has decreased the last two years and the annual mean concentration in 2019 was 2.3 ppt (~4%) below the peak value in 2017.

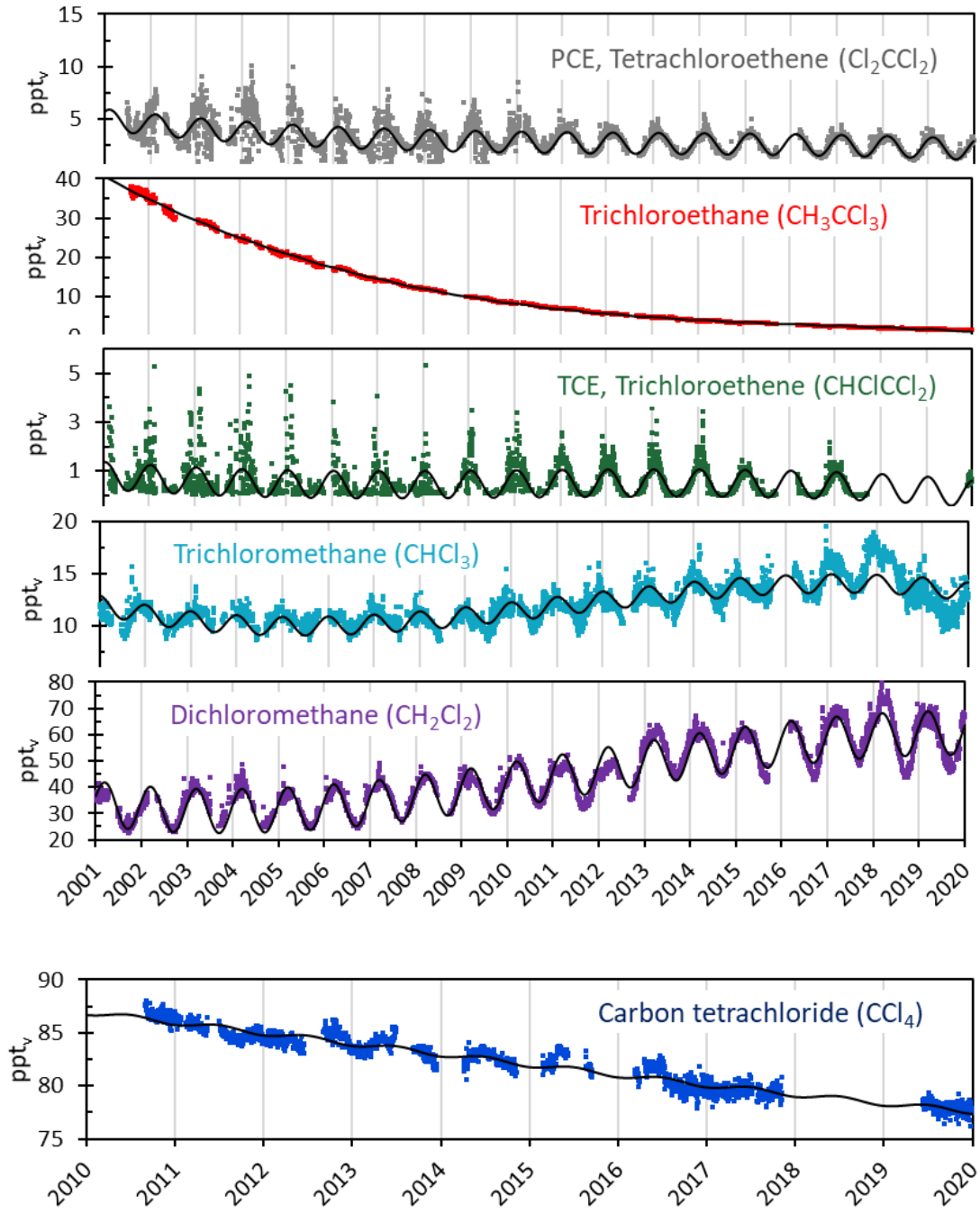

Figure 39: Daily averaged concentrations of chlorinated hydrocarbons at the Zeppelin observatory: For the period 2001-2019: Tetrachloroethene (grey), trichloroethane (red), trichloroethene (green), trichloromethane (light blue), and dichloromethane (violet). For the period 2010-2019: carbon tetrachloride (dark blue). Solid lines are empirical fitted mixing ratios.

Trichloromethane (light blue) has a lifetime of ~0.4 year, thus the response to emission changes is also relatively rapid. The annual mean value of trichloromethane at Zeppelin increased by 37% from 2001 to 2017 and similar increases were observed at other sites (e.g. Mauna Loa at Hawaii and Barrow in Alaska). Similar to dichloromethane, there has been a clear decrease in trichloromethane at Zeppelin the last two years, i.e. a decrease of 3.1 ppt (~20%). The reason for these rapid changes is not yet clear, but they might be explained by natural sources.

Even if trichloromethane and dichloromethane have relatively short lifetimes, modelling studies imply that chlorine from these compounds can reach the lower stratosphere and potentially destroy stratospheric ozone (Hossaini et al., 2017). Thus, sustained growth in these compounds might offset some of the gains achieved by the Montreal Protocol, further delaying recovery of Earth's ozone layer.

The atmospheric concentrations of trichloroethene (TCE; green) and tetrachloroethene (PCE; grey) are low, and the annual variabilities are quite high, especially before 2011 due to instrumental limitations (see appendix 2). This makes it difficult to draw conclusions about trends and development of these species. In 2019 the annual average concentrations of PCE was 2.3 ppt.

The concentration of carbon tetrachloride (CCl_4) has been measured at Zeppelin since 2010. This compound was once a popular solvent in organic chemistry, but because of its adverse health effects it is rarely used any more. Today CCl_4 is sometimes applied as a solvent for infrared spectroscopy. For the period 2010-2019 the annual mean values have decreased by 1.1%/yr, i.e. from 86.6 ppt in 2010 to 78.0 ppt in 2019.

It should be noted that no annual mean values of PCE and CCl_4 are calculated from the measurements in 2018. In addition, there is not enough data to calculate a reliable annual mean value for PCE in 2019. This is related to the upgrade of the Medusa-GCMS in 2017 (see Appendix II), which caused problems for these two compounds. Thus, the PCE and CCl_4 measured performed from October 2017 to the summer/fall 2019 are flagged as "absent".

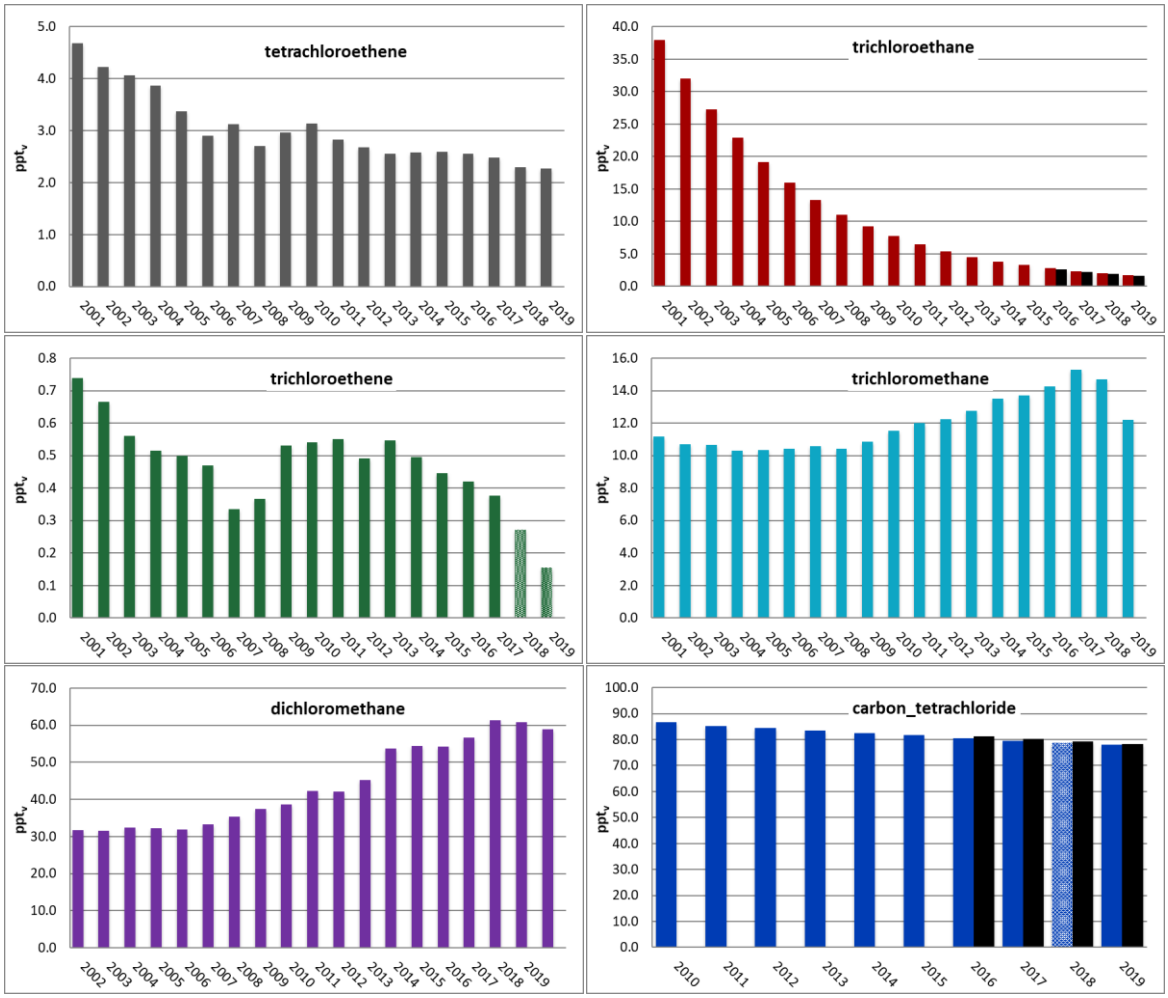

Figure 40: Annual means of the chlorinated hydrocarbons. Upper panel: tetrachloroethane (grey) and trichloroethane (red). Mid panel: trichloroethene (TCE, green) and trichloromethane (light blue). Lower panel: dichloromethane (violet) and carbon tetrachloride (CCl_4, dark blue). The global annual means for CH_3CCl_3 and CCl_4 in 2016-2019 are included as black bars, when available. All units are in ppt. Note that CCl_4 and TCE from 2018 and partly 2019 are based on model data.

2.2.6 Perfluorinated compounds at Zeppelin Observatory

Key findings – Perfluorinated compounds. *This group of compounds include SF_6, SO_2F_2, NF_3, PFC-14, PFC-116, PFC-218, and PFC-318. Generally, these compounds are extremely potent greenhouse gases, but their concentrations are still low. An exception is PFC-14, which had a mixing ratio of 86.1 ppt in 2019, an increase of 0.9 ppt since 2018. SF_6 should also be followed closely, as this compound has an atmospheric lifetime of 3 200 years and an extremely high GWP of 23 500. This compound has increased by 105% since 2001.*

Perfluorinated compounds belong to a group of long-lived greenhouse gases, and their contribution to the Earth's radiative forcing has increased over the past several decades. The impact of these highly fluorinated compounds on climate change is a concern because of their exceptionally long atmospheric lifetimes, as well as their strong absorption in the infrared "window" region (Baasandorj et al., 2012).

Up to 2015, the Norwegian national monitoring programme only included measurements of one perfluorinated compound, SF_6. However, other perfluorinated compounds are also very powerful greenhouse gases with atmospheric lifetimes up to 50 000 years (See Table 3) and with increasing concentrations in the atmosphere. NILU has from 2010 extended the monitoring of perfluorinated compounds at Zeppelin as we have new and improved instrumentation. Several of these compounds, so-called perfluorocarbons (PFCs), were included in the current monitoring programme from 2015, with analysis back in time to September 2010. Two additional compounds were included in the 2016 monitoring programme: Nitrogen trifluoride (NF_3) and Sulphuryl fluoride (SO_2F_2). For the latter compound data was analysed back to 2010. The instrument at Zeppelin was re-built and optimised in 2015 and 2016, which made it possible to measure NF_3. Thus, NF_3 data are only available from 2016.

2.2.6.1 Sulphurhexafluoride (SF6), Sulphuryl fluoride (SO_2F_2), Nitrogen trifluoride (NF_3)

Sulphurhexafluoride, SF_6, is an extremely strong greenhouse gas emitted to the atmosphere mainly from the production of magnesium and in the electrical industry for high-voltage circuit breakers, switch gears and other electrical equipment. Measurements of this component has been a part of the programme since 2001. The atmospheric lifetime of this compound is 3 200 years, and the global warming potential is 23 500, which means that the emission of 1 kg of SF_6 has a warming potential which is 23 500 times stronger than 1 kg emitted CO_2 (Myhre et al, 2013b).

Sulphuryl fluoride, SO_2F_2, has a lifetime of 36 years and a GWP of 4 090. SO_2F_2 is normally used as a pesticide fumigant for dried fruits, nuts, and other agricultural commodities that must be kept pest-free during storage. It is one of the most common replacements for bromomethane, an ozone-depleting substance whose use is being phased out.

Nitrogen trifluoride, NF_3, has a lifetime of 500 years and a GWP as high as 16 100, meaning that it also is an extremely strong greenhouse gas. NF_3 is used in the manufacturing of new generation solar panels, flat-screen televisions, touch-sensitive screens, and electronic processors. The use of NF_3 has widely increased in the past because of the rising demand in flat-screen televisions and microelectronics.

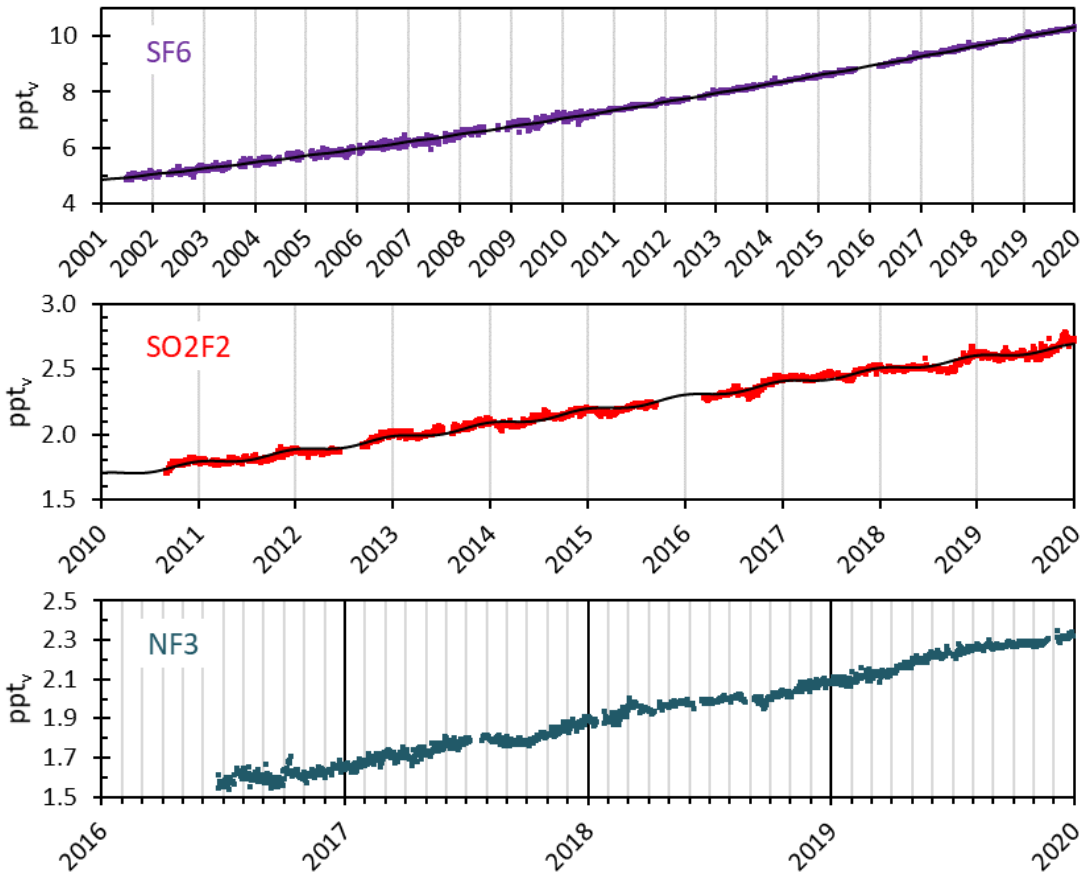

Figure 41: Daily averaged concentrations at the Zeppelin Observatory. Upper panel: SF_6 for the period 2001-2019. Middle panel: SO_2F_2 for the period 2010-2019. Lower panel: NF_3 from mid 2016 to 2019. Solid lines are statistical fitted mixing ratios.

The daily averaged concentrations of SF_6, SO_2F_2 and NF_3 are presented in Figure 41. SF_6 is increasing with a rate of 0.29 ppt/yr and has increased as much as 105% since the start of our measurements in 2001. The instrumentation before 2010 was not optimal for measurements of SF_6, thus there are higher uncertainties for this compound's mixing ratios than for most of the other compounds reported from 2001 to 2010 (see Appendix I).

The concentration of SO_2F_2 has also increased significantly the last years (see Figure 41). The total increase for the period 2010-2019 is 0.90 ppt (52%). No trend is derived for NF_3, as the measurements started in 2016. Daily average observations of NF_3 are visualized in Figure 41, lower panel, and the figure clearly demonstrates a gradual increase since the measurements started in June 2016. The annual average NF_3 concentration in 2019 was 2.22 ppt, an increase of 0.61 ppt (38%) from 2017.

Figure 42 shows annual average concentrations of SF_6 (left panel) and SO_2F_2 (right panel) measured at Zeppelin for the periods 2001-2019 and 2010-2019, respectively. The global annual means of SF_6 in 2016 - 2019 (Hall et al., 2017 and 2020; Dlugokencky et al., 2018 and 2019) are included as black bars for comparison. Again, the concentrations at Zeppelin are slightly higher than the global means.

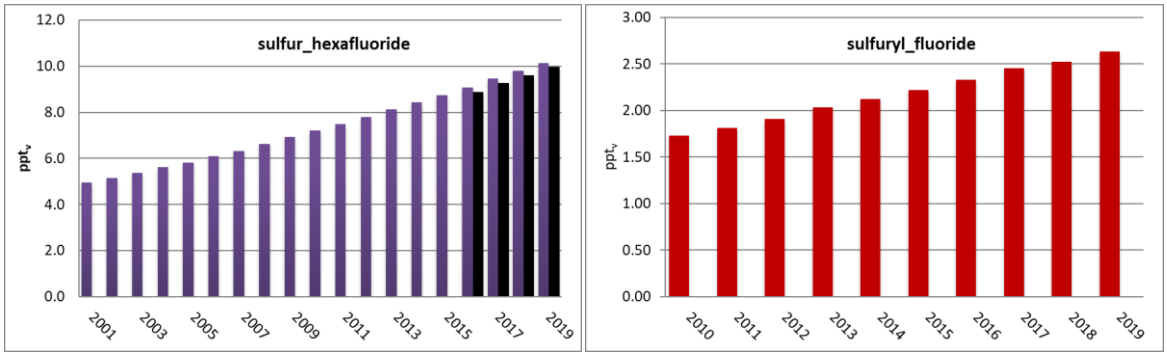

Figure 42: Annual means of SF_6 for the period 2001-2019 (left) and SO_2F_2 for the period 2010-2019 (right) at the Zeppelin observatory. The global annual means for SF_6 in 2016 to 2019 are included as black bars.

2.2.6.2 Perfluorocarbons or PFC's: PFC-14, PFC-116, PFC-218, PFC-318

Perfluorocarbons or PFCs are compounds that contain only carbon and fluorine. Four of these compounds are currently measured and reported at Zeppelin: PFC-14, PFC-116, PFC-218, and PFC-318. PFC-14, also called tetrafluoromethane or CF_4, is the most persistent PFC greenhouse gas with an atmospheric lifetime of 50 000 years and a greenhouse warming potential of 6 630. It is used as a low temperature refrigerant, in electronics microfabrication, and in neutron detectors. Another potent greenhouse gas is hexafluoroethane, PFC-116, which has an atmospheric lifetime of 10 000 years and a GWP of 11 100. The gas is used as an etchant in e.g. semiconductor manufacturing, and aluminium and the semiconductor manufacturing industries are the major emitters of PFC-116. Fraser et al. (2013) showed that the release of PFC-14 at Hydro's aluminium plant in Australia was 10 times greater than the release of PFC-116. Octafluoropropane, PFC-218, which has an atmospheric lifetime of 2 600 years and a GWP of 8 900, is also used in the electronics industry as a plasma etching material. In medicine, PFC-218 microbubbles reflect sound waves well and is used to improve the ultrasound signal backscatter. Octafluorocyclobutane, PFC-318, with an atmospheric lifetime of 3 200 years and a GWP of 9 540, is the third most abundant PFC in the atmosphere (Oram et al, 2012). Although a number of potential sources of PFC-318 have been reported, including electronic and semi-conductor industries, there remains a large discrepancy in the atmospheric budget.

The daily averaged concentrations of the PFCs measured at Zeppelin are shown in Figure 43. For the period 2010-2019 PFC-116, PFC-218 and PFC-318 increased by 2.1%/yr, 2.6%/yr and 4.5%/yr, respectively. For PFC-14 no data exist until October 2014, but the measurements in 2015 to 2019 indicate that the concentration of PFC-14 increases by ~1.1%/yr.

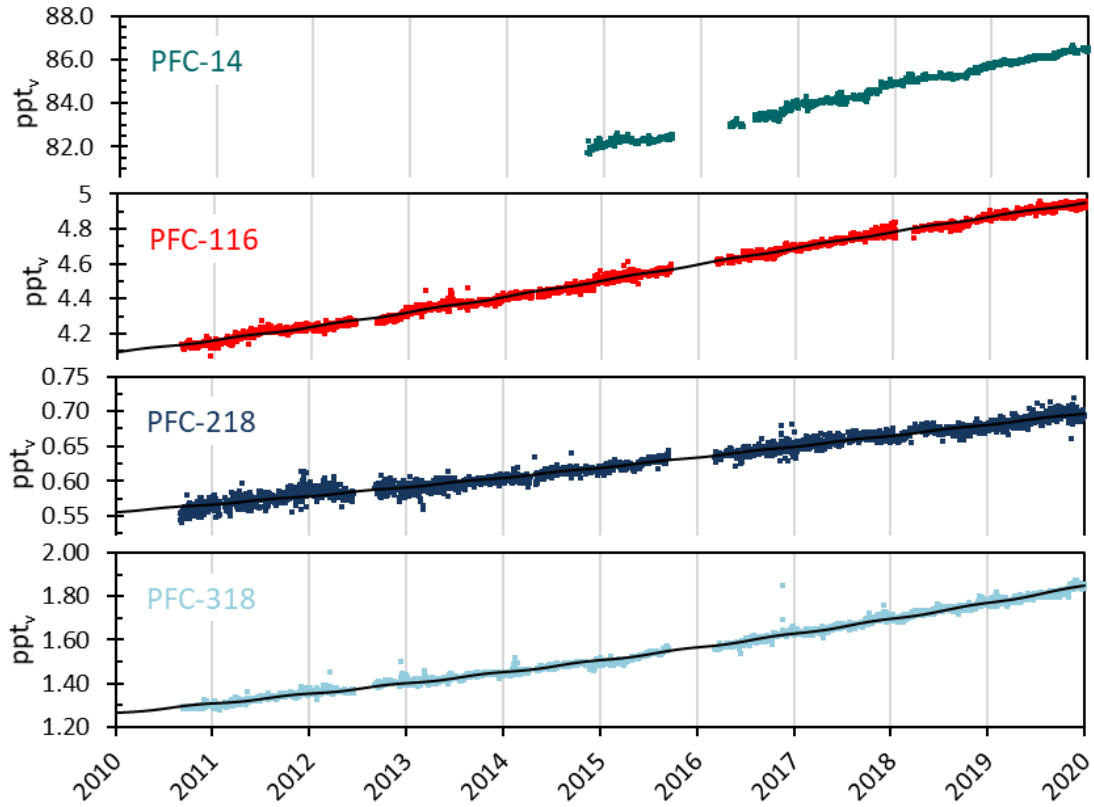

Figure 43: Daily averaged concentrations of perfluorocarbons at the Zeppelin observatory for the period 2010-2019: PFC-14 (green), PFC-116 (red), PFC-218 (dark blue), and PFC-316 (light blue). PFC-14 is only ranging back to autumn 2014. The solid lines are statistical fitted mixing ratios.

The development of the annual means of the PFCs are shown in Figure 44. For PFC-116 the global annual mean in 2016 to 2019 (Hall et al., 2017 and 2020; Dlugokencky et al., 2018 and 2019) are shown as black bars for comparison. The concentrations of most PFCs are relatively low. However, PFC-14 is an exception. With an annual mean concentration of 86.1 ppt in 2019, a lifetime of 50 000 years and GWP of 6 630, this is an important greenhouse gas that should be followed carefully.

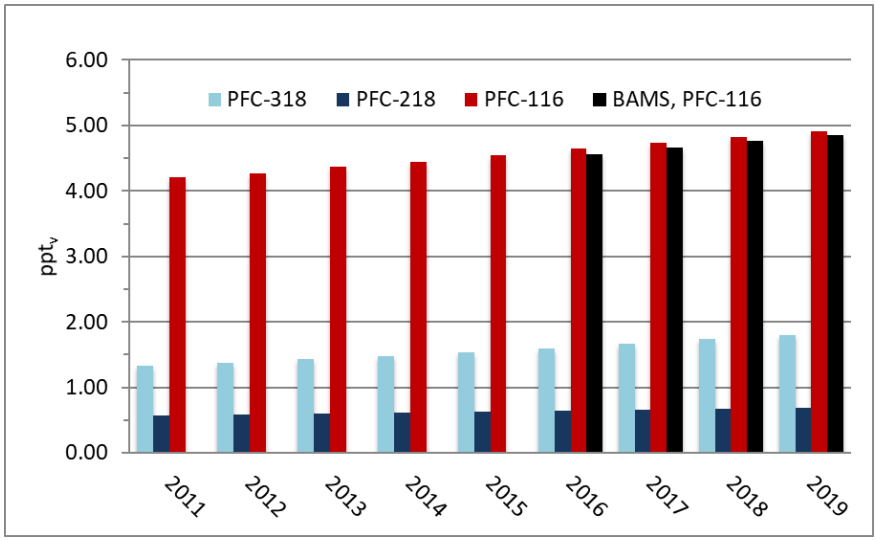

Figure 44: Annual mean concentrations of perfluorocarbons for the period 2010-2019 at the Zeppelin observatory: PFC-116 (red), PFC-218 (dark blue), and PFC-318 (light blue). The global annual means for PFC-116 in 2016 to 2019 are included as black bars.

3 Aerosols and climate

Atmospheric aerosol influences climate by scattering incoming solar radiation back into space, or absorbing the radiation. This so called direct aerosol climate forcing results mostly in cooling, but can be moderated if the aerosol itself absorbs solar radiation, e.g. if it consists partly of light absorbing carbon or light absorbing minerals. In this case, the aerosol warms the surrounding atmosphere. Atmospheric aerosol influences climate as outlined in section 1.4. Atmospheric aerosol particles also affect the reflectivity and lifetime of clouds, which is termed the indirect aerosol climate effect. The effect can be cooling as well as warming for climate, but in most cases, the cloud reflectivity and lifetime are increased, leading again to a cooling effect (see Figure 3). Figure 45 gives an overview of the main natural and anthropogenic sources of atmospheric aerosols, also described in detail the annual report of Aas et al. 2020 on long range transport of air pollution.

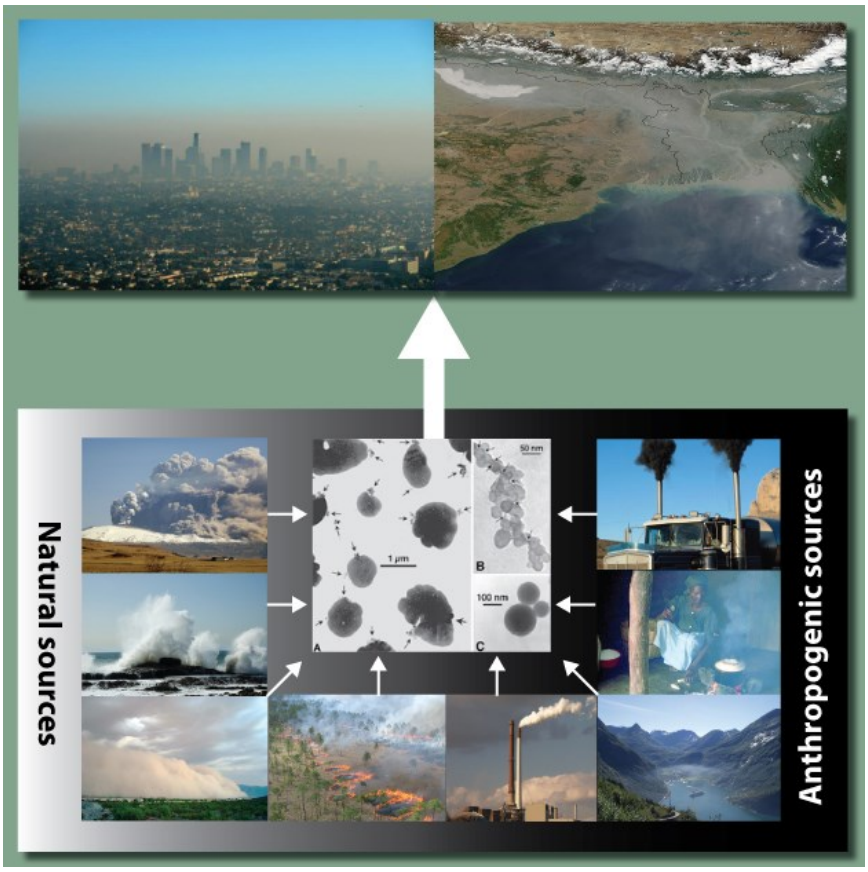

Figure 45: Illustration of the main natural and anthropogenic sources of atmospheric aerosols taken from Myhre et al (2013b). Top: local and large scale air pollution. Sources include (bottom, counter clockwise) volcanic eruptions (producing volcanic ash and sulphate), sea spray (sea salt and sulphate aerosols), desert storms (mineral dust), savannah biomass burning (BC and OC), coal power plants (fossil fuel BC and OC, sulphate, nitrate), ships (BC, OC, sulphates, nitrate), cooking (domestic BC and OC), road transport (sulphate, BC, VOCs yielding OC). Additionally, Biogenic VOC to SOA and primary biological (e.g. pollen) from vegetation is crucial. Center: Electron microscope images of (A) sulphates, (B) soot, (C) fly ash, a product of coal combustion (Posfai et al., 1999).

Uncertainties in assessing aerosol climate forcing hamper the attribution of changes in the climate system. IPCC AR5 (IPCC, 2013) has high confidence in stating that total atmospheric aerosol negative radiative forcing in the past, has offset a significant fraction of greenhouse gas radiative warming, although the magnitude is connected with uncertainty. Due to the decline of aerosol concentrations as reported in Tørseth et al (2012), Collaud Coen et al., (2013), and Asmi et al., (2013), and summarized in Hartmann et al. (2013) the total anthropogenic radiative forcing (from both greenhouse gases and aerosols) will be even larger, i.e. more warming, in the future, due to less negative forcing from cooling aerosols (sulphates etc.)

3.1 Analysis of in situ aerosol radiative properties around the world

Recently there has been comprehensive studies presenting global status and trends in aerosol properties using data and results from the national monitoring programme. Currently, scientists working on climate change and its effects around the world are busy with work and preparations running up to the publication of the 6th Assessment Report (AR6) of the UN Intergovernmental Panel on Climate Change (IPCC). While the final product, the Synthesis Report, is scheduled for publication in the first half of 2022, the report of Working Group I – The Physical Science Basis will be released already in 2021.
As input for IPCC AR6, numerous scientific articles reviewing and summarising the state of the atmosphere and its composition have been prepared, within the deadline of being submitted for publication by the end of 2019 to be considered for IPCC AR6. Different deadlines apply to publications on Covid-19 related issues. Among these articles are several initiated by the WMO Global Atmosphere Watch (GAW) programme and ACTRIS, in which the observations of aerosol properties at Zeppelin, Birkenes, and Trollhaugen are used.

1. Laj et al. 2020, entitled "*A global analysis of climate-relevant aerosol properties retrieved from the network of Global Atmosphere Watch (GAW) near-surface observatories*". This article gives an overview over the GAW station network measuring climate relevant aerosol particle properties at surface stations, with link to ACTRIS as quality assurance and quality control framework (see section 1.3on page 13). The properties observed comprise particle light scattering and absorption coefficient, particle number concentration and size distribution.

2. Collaud Coen et al. (2020), entitled "*Multidecadal trend analysis of in situ aerosol radiative properties around the world*". A subset of Laj et al., data from 52 stations worldwide is used in Collaud Coen et al., to provide a robust analysis of the long-term (>10 yr) trends of aerosol optical properties. This study contains a detailed discussion of trends in climate relevant optical aerosol properties, namely particle scattering, backscattering, and absorption coefficient, but also the derived properties single scattering albedo, scattering and absorption Ångström coefficient (see section 3.3 for a definition of these terms). Also, the evolution of trends and their causes are evaluated.

3. Gliß et al. (2020), entitled "*Multi-model evaluation of aerosol optical properties in the AeroCom phase III Control experiment, using ground and space based columnar observations from AERONET, MODIS, AATSR and a merged satellite product as well as surface in-situ observations from GAW sites*". The authors use synthetic observations generated by those climate models feeding into IPCC AR6, and compare them to corresponding real-world observations. Comparisons include aerosol optical depth by space and surface based remote sensing, as well as observations of aerosol optical properties from the GAW network.

4. Mortier et al. (2020), entitled "*Evaluation of climate model aerosol trends with ground-based observations over the last two decades - an AeroCom and CMIP6 analysis*". The authors take the trends discovered in atmospheric aerosol observations (aerosol optical depth from surface remote sensing, aerosol optical properties and mass of particulate matter from surface in situ stations), and investigate whether climate models can reproduce these. Since observations

aren't representative for the whole globe, they use the climate models to extrapolate the trends in the observations to the global level.

This series of publications demonstrates how time series of high-quality observations of atmospheric aerosol properties can feed into IPCCs Assessment Reports, contributing to improved understanding of climate change ongoing, and predictions. The value chain leads from data management and quality control by network participation, via trend assessment at the network level, to validation and improvement of model produced climate predictions. Key findings of the above publications include:

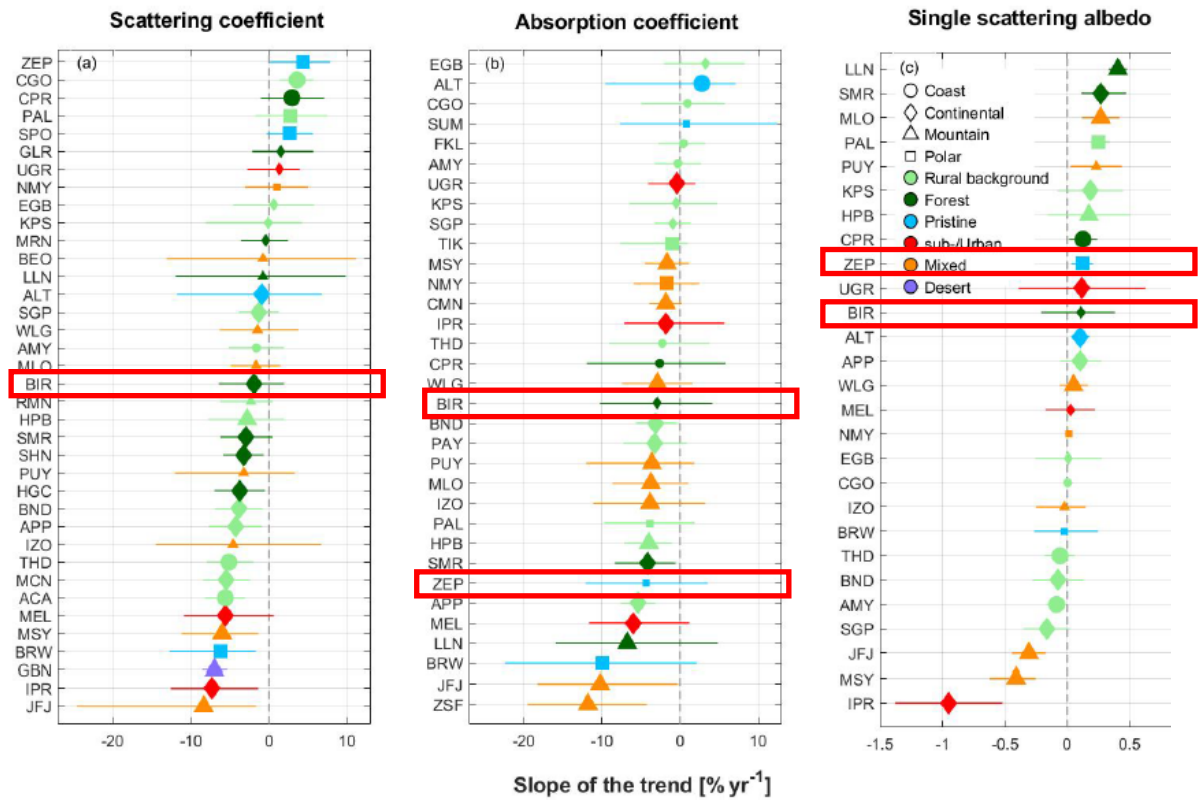

Figure 46: Annual trends for (a) the scattering coefficient, (b) the absorption coefficient, and (c) the single-scattering albedo derived for GAW stations providing 10-year time series ending in 2016–2018 (Laj et al 2020). The larger symbols represent statistically significant trends at 95% significance level (Collaud Coen et al., 2020). The lines are the 90% confidence limit upper and lower confidence limits. Colour codes and symbols describe the station footprint. The graph is from Laj et al. (2020), Figure 11. Data points generated from input data covered by this report are marked by red boxes.

Laj et al. (2020) report for the first time aerosol data from all operational GAW stations worldwide (approx. 90) are for a reference year, providing a unique and very robust view of the annual variability of some Essential Climate Variables. The current gaps in the GAW network are analysed and the paper provides the science-based requirements for the Global Climate Monitoring System.

- **Decreasing trends in particle scattering and absorption:** Collaud Coen et al. (2020) exploits data from Laj et al (2020) and the GAW network and finds decreasing trends in particle scattering and absorption. Collaud Coen et al. (2020) reports that trends of particle scattering and absorption over time first increasing, now decreasing. Scattering coefficient trends are decreasing in Europe and North America and are not statistically significant in Asia, whereas

polar stations exhibit a mix of increasing and decreasing trends. Absorption coefficients also exhibit mainly decreasing trends. The single scattering albedo (SSA) is a key variable co-determining the direct radiative impact of aerosol. SSA present positive trends in Asia and Eastern Europe and negative in Western Europe and North America leading to global positive median trend of 0.02%/yr, indicating a recently enhanced scattering contribution to aerosol forcing (having a cooling effect). The paper also reports the time dependence of trends for the optical particle properties at GAW stations. They find a tendency to increasing trends for particle scattering and absorption until the first decade of the 2000s, and decreasing trends thereafter. This likely reflects abatement strategies for pollution by particulate matter.

- **Climate models underestimate atmospheric particle load**: Gliß et al. (2020) find that climate models underestimate aerosol optical depth by 21%±17% relative to ground-based remote sensing, and by 17%-38% relative to observations from space. With respect to surface-level observations from the GAW network, climate models underestimate the particle scattering coefficient on average by 44%±22%, the particle absorption coefficient by 32%±34%. Models seem to overestimate water uptake by aerosol particles, as well as the average particle size, leading to higher aerosol lifetimes in the models than in reality.
- **Models capture trends in aerosol parameters scaling with particle load**: Despite the fact that climate models underestimate the magnitude of aerosol parameters scaling with particle load (Gliß et al., 2020) Mortier et al. (2020) show that they capture the trends in these parameters, at least in those regions of the globe covered by surface-based observations. This gives some confidence that these models represent these trends correctly also in other regions of the globe.

These studies provide an in-depth analysis of trends in surface in situ observations of atmospheric aerosol properties, to which the observations covered by this report contribute. They also investigate how well these trends are captured by climate models feeding into the upcoming IPCC AR6. While such in-depth studies usually coincide with these assessment reports, there now exist services which quantify such trends in observations, as well as the agreement with climate models, on a continuous basis. One such is operated by the Norwegian Meteorological Institute as part of the ACTRIS research infrastructure.[15]

3.2 Overview of aerosol observations at Zeppelin, Birkenes and Troll Observatory

This monitoring programme includes measurements of aerosol properties relevant for quantifying the direct and indirect aerosol climate effect from 3 observatories NILU operates: 1) Zeppelin Observatory (in collaboration with the Norwegian Polar Institute and Stockholm University); 2) Birkenes Atmospheric Observatory, Aust-Agder, Southern Norway; 3) Trollhaugen Atmospheric Observatory, Antarctica (observatory operated by NILU, main station operated by Norwegian Polar Institute). The observations cover the particle concentration as a function of particle size as physical aerosol property, as well as particle light scattering and absorption as a function of light wavelength, both optical aerosol properties.

Table 4 provides an overview over these and further observations of aerosol properties conducted at the named observatories, which are partly covered by other reports.

[15] https://actris.nilu.no/Content/trends

Table 4: Aerosol observations at Zeppelin, Birkenes and Troll Observatory. Those observations contributing to ACTRIS follow the ACTRIS recommendations. Parameters in green are funded by the Norwegian Environment Agency and Ministry of Climate and Environment and the rest is funded by NILU and other institutes.

	Zeppelin/Ny-Ålesund	Birkenes	Trollhaugen
Particle Number Size Distribution (PNSD) (fundamental to all aerosol processes)	fine mode (0.01 µm < D_p < 0.8 µm), NILU and in collaboration with Stockholm University	fine and coarse mode (0.01 µm < D_p < 10 µm)	fine mode (0.01 µm < D_p < 0.8 µm)
Number Size Distribution of Refractory Particles (proxy for BC PNSD)	fine mode (0.01 µm < D_p < 0.8 µm), NILU	---	---
Aerosol Scattering Coefficient (addressing direct climate effect)	spectral at 450, 550, 700 nm, in collaboration with Stockholm University	spectral at 450, 550, 700 nm	spectral at 450, 550, 700 nm
Aerosol Absorption Coefficient (addressing direct climate effect)	single wavelength at 525 nm, (Stockholm University); single wavelength at 670 nm (Stockholm University); 7-wavelength (Demokritos Athens); 7-wavelength (NILU)	spectral at 470, 522, 660 nm wavelength.; 7-wavelength (NILU)	spectral at 470, 522, 660 nm wavelength.
Aerosol Optical Depth (addressing direct climate effect)	spectral at 368, 412, 500, 862 nm in collaboration with WORCC	spectral at 340, 380, 440, 500, 675, 870, 1020, 1640 nm, in collaboration with Univ. Valladolid	spectral at 368, 412, 500, 862 nm
Aerosol Chemical Composition (addressing direct + indirect climate effect)	inorganic ions (ion chromatography), heavy metals (inductively-coupled-plasma mass-spectrometry)	main components (daily resolution, offline filter-based, ion chromatography), heavy metals (inductively-coupled-plasma mass-spectrometry)	inorganic ions and POPs (ion chromatography), discontinued from 2011 due to local contamination.
Aerosol Chemical Speciation (direct + indirect climate effect, source attribution, transport)	Particle main chemical species (hourly resolution, online mass spectrometry)	Particle main chemical species (hourly resolution, online mass spectrometry)	---
Particle Mass Concentration	---	$PM_{2.5}$, PM_{10}	PM_{10}
Cloud Condensation Nuclei (addressing indirect climate effect)	size integrated number concentration at variable supersaturation in collaboration with Korean Polar Research Institute	Size integrated number concentration at variable supersaturation	---

Parameters included in this report, are printed in green.

3.3 Observed optical properties of aerosols

Aerosol particle absorption and scattering is decisive for the cooling or warming effect of aerosol in climate. All types of particles are scattering solar radiation, but the higher the fraction of particle absorption, the more warming the aerosol becomes. The absorption depends on the particle composition; black carbon (e.g. soot) and minerals absorb radiation.

3.3.1 Optical aerosol properties measured at the Birkenes Observatory

Key findings aerosol optical properties Birkenes: *There are no trends in aerosol optical properties observed at Birkenes, agreeing with findings at other European stations and recent trend analyses (e.g. Collaud Coen et al., 2020). The aerosol scattering shows a stronger contribution of smaller particles in summer than in winter. The reason for these seasonal differences is that summer aerosol is influenced by biogenic emissions which tends to give large amounts of newly formed small particles. In contrast, aerosol absorption shows a higher contribution of smaller (newer) particles in winter than in summer, reflecting the winter contribution of wood burning for domestic heating.*

The comprehensive set of instruments observing in situ optical aerosol properties at Birkenes, describing the direct effect of aerosol on climate, has now been in operation since 2010. The parameters covered include the scattering coefficient σ_{sp} and the absorption coefficient σ_{ap} at various wavelengths. Figure 47 summarises the essence of these observations for the years 2010 – 2019 in time series of the observations themselves and relevant directly derived parameters. All properties are measured for particles with aerodynamic diameter $D_{p,aero} < 10$ µm and at relative humidity below 40%, thus avoiding water uptake by particles. This protocol follows the recommendations provided by ACTRIS. This is crucial to have comparable data at Zeppelin, Trollhaugen and Birkenes, and with other sites on European and global scale. For more details concerning measurement principles and quality assurance routines, please see Appendix II and Laj et al (2020). During data quality control, it was discovered that parts of the 2019 data of the integrating nephelometer, measuring the particle scattering coefficient σ_{sp}, are affected by a leak in the filter providing zero calibration air. To meet the quality standards, the affected data were removed from the dataset.

Panel a) of Figure 47 displays the time series of the scattering coefficient σ_{sp} at 450, 550, and 700 nm wavelength. Thin lines represent daily average values for the respective wavelength, whereas the heavy green line represents the running 8-week median for easier visibility of seasonal averages (green wavelength at 550 nm only for clarity). The σ_{sp} time series exhibits significant variability on the time scale of days, illustrating that particle load in an air mass varies significantly with air mass type and thus air mass origin, i.e. with the synoptic weather situation on a time scale of 1 – 3 days. When focussing on the graph of the running median, a slight seasonal variation can be detected, with values higher in summer than winter.

For optical aerosol properties, information is contained both in the absolute level and in the values at different wavelengths relative to each other. In order to make this spectral information accessible, the Ångström coefficient has been defined, that can be calculated for optical aerosol properties, both for scattering and for absorption. Higher values of the scattering Ångström coefficient correlate with higher concentration ratios of particles in the fine size range ($D_p < 1$ µm) as compared to the coarse size range ($D_p > 1$ µm). Moreover, the relative size of particles determining an optical aerosol property decreases with wavelength, i.e. smaller wavelengths "see" smaller particles in relative terms, larger wavelengths "see" larger particles. Already with these simple qualitative rules, many features exhibited by spectral aerosol optical property data in general and Ångström coefficient data in particular can be interpreted meaningfully.

Panel b) of Figure 47 shows the time series of the scattering Ångström coefficient $å_{sp}$, calculated from $\sigma_{sp}(\lambda)$, again as daily averages (thin line) and running 8-week median (heavy line). As with σ_{sp}, the strongest variability is associated to a time scale of 1-3 days, indicative of changes associated with air mass type, origin, and synoptic weather situation. Looking at the running median however, the seasonal cycle is more pronounced for $å_{sp}$ than for σ_{sp}, with $å_{sp}$ values around 1.1 in winter and 1.8 in summer. This indicates a stronger contribution of smaller particles, i.e. particles with D_p smaller than about 120 nm, to σ_{sp} in summer than in winter. This is consistent with number concentrations of particles in this size range exhibiting a similar seasonal cycle, as will be discussed below. The time series

of σ_{sp} and $\mathring{a}_{sp}$ don't show any trend, which is consistent with the findings for other European continental background stations at Jungfraujoch (Switzerland, mountain top), Hohenpeissenberg (Southern Germany, elevated boundary layer), and Pallas (Northern Finland, boreal background) (Collaud Coen et al., 2013). Also the range of σ_{sp} values encountered, 3 - 50 Mm^{-1} with an annual average of about 12.5 Mm^{-1}, is consistent with findings at comparable stations (Delene & Ogren, 2002).

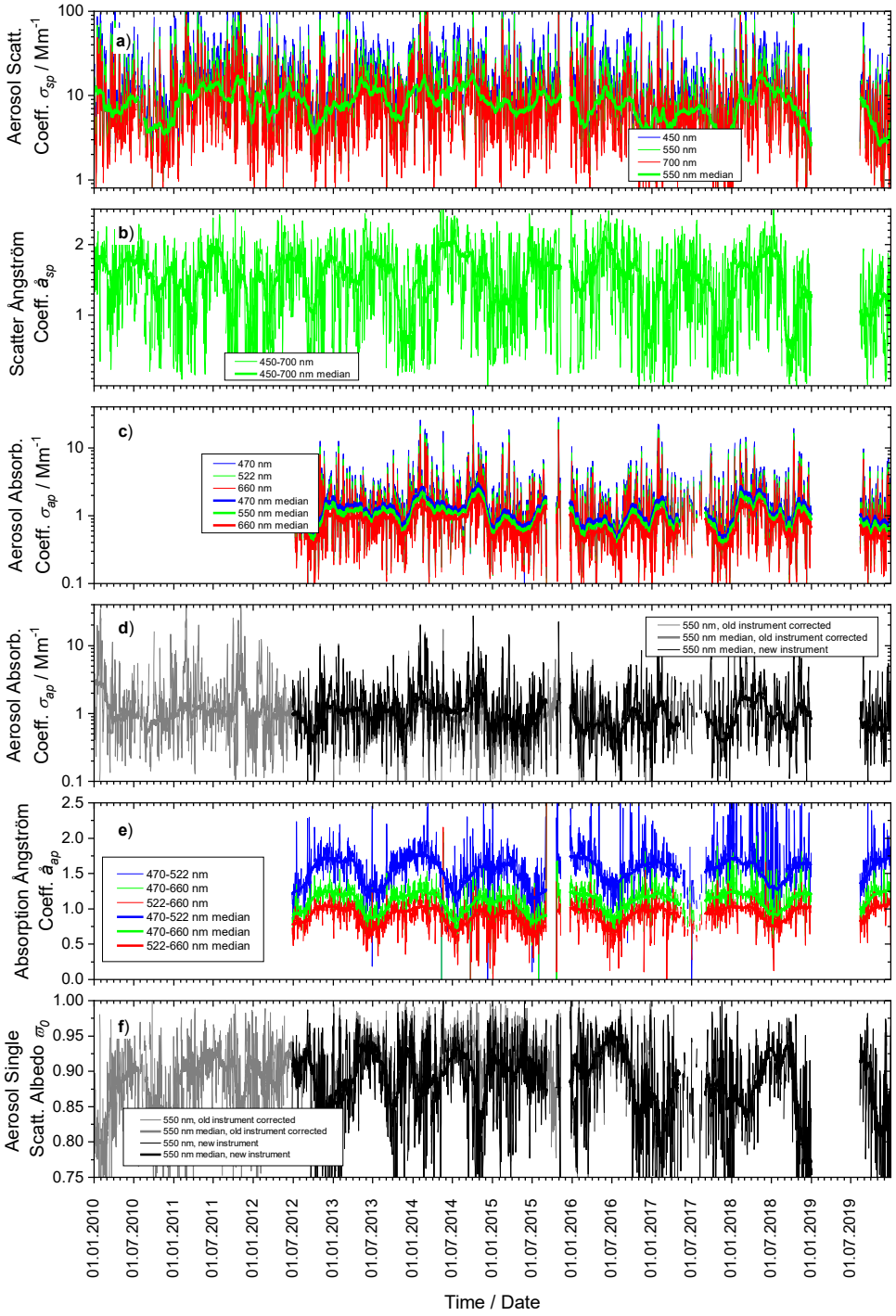

Figure 47: Time series of aerosol particle optical property daily means measured for 2010 - 2019 at Birkenes. Panel a) shows the aerosol scattering coefficient σ_{sp} at 450, 550, and 700 nm wavelength measured by integrating nephelometer. Panel c) the aerosol absorption coefficient σ_{ap} at 470, 522, and 660 nm wavelength measured by the newer filter absorption photometer, Panel d) the aerosol absorption coefficient σ_{ap} at 550 nm of the

older filter absorption photometer, shifted from the instrument wavelength at 525 nm for consistent comparison assuming an absorption Ångström coefficient of -1. Panels b) and e) show the derived properties scattering and absorption Ångström coefficient $å_{sp}$ and $å_{ap}$, respectively, while Panel f) depicts the single scattering albedo ϖ_0. All plots also depict the running 8-week medians of the respective properties as heavy lines to visualize seasonal variations. To demonstrate consistency between old and new filter absorption photometer, respective comparison lines are displayed.

The observations of the particle absorption coefficient σ_{ap} at Birkenes were upgraded in 2012 and in November 2017. All 3 concerned instruments use the same physical principle, tracking the change of attenuation of light that passes through a filter while the filter is loaded with sampled particles. The 2012 instrument measures σ_{ap} at 3 wavelengths (470, 522, 660 nm) with considerably less electronic noise and significantly better long-term stability than the previous instrument of 2010 with one wavelength (522 nm). The 2017 instrument extends the spectral range to 7 wavelengths (370, 470, 520, 590, 660, 880, 950 nm). Panel c) of Figure 47 displays the σ_{ap} time series of the 2012, 3-wavelength filter absorption photometer, Panel d) the data of the 2010 one wavelength instrument. For the 2010 instrument, the wavelength has been recalculated to the same green wavelength as observed by the nephelometer (550 nm) assuming an absorption Ångström coefficient of 1. Both panels use thin lines for daily averages, heavy lines for the running 8-week medians. The first year of data of the 2017 instrument have now been evaluated for consistency with the 2012 instrument (see Appendix II). The data of the 2 instruments show a correlation coefficient R^2 of 0.97, i.e. 97% of the variation in one instrument is explained by the variation in the other instrument. This ensures that the 2017 instrument will continue the σ_{ap} time series consistently.

Panel d) also displays the σ_{ap} running median time series of the 2012 filter absorption photometer (also recalculated to 550 nm wavelength) together with the data of the old instrument as an indicator for the goodness of overlap between the 2 instruments measuring the same property (see appendix II page 145 for more details).

Apart from the variation with synoptic transport and air mass origin, σ_{ap} does not seem to exhibit significant seasonal variation. The values of σ_{ap} are in the range of 0.3 – 4 Mm^{-1} with annual means around 1 Mm^{-1}.

In order to cover the largest possible time period, panel f) of Figure 47 shows the time series of the aerosol particle single scattering albedo ϖ_0 based on the time series of the older filter absorption photometer (grey lines), again daily averages (thin line) and 8-week running median (heavy line), together with the respective time series of the new instrument (black lines). The single scattering albedo ϖ_0 quantifies the fraction of light scattered by the particles rather than absorbed. It thus quantifies how absorbing the average aerosol particle is, with ϖ_0 values decreasing with increasing absorption of the average particle. For a purely scattering aerosol, ϖ_0 is 1, and decreases with increasing fraction of light absorbing components in the aerosol particle phase. The most prominent feature in the ϖ_0 time series is the pronounced annual cycle, varying between 0.86 – 0.96, with lower ϖ_0 values and higher particle absorption in winter. The annual cycle in ϖ_0 has been discussed in previous reports of the Birkenes aerosol dataset, and has been connected to the combustion of biomass in wood stoves for domestic heating in the winter season.

Panel e) of Figure 47 is based on data of the 2012 filter absorption photometer, measuring σ_{ap} at 3 wavelengths, as opposed to 1 wavelength with the 2010 instrument. Panel e) depicts the time series of the absorption Ångström coefficient $å_{ap}$ for all 3 wavelength pairs provided by the new instrument. For $å_{ap}$, the information on relative particle size concerns not the overall aerosol particle phase, but the fraction of absorbing particles. Thus, considering $å_{ap}$ data allows to investigate changes in source

and transport of the absorbing particle fraction in the aerosol. When looking at the $å_{ap}$ data in panel e) of Figure 47, an annual cycle is apparent that is opposite of the annual cycles seen in scattering Ångström coefficient $å_{sp}$ and single scattering albedo ϖ_0. Both $å_{sp}$ and ϖ_0 increase in summer as compared to winter, $å_{sp}$ because of a summer increase in small particles due to particle formation from biogenic precursors, ϖ_0 because of fewer combustion emissions in summer than in winter. For $å_{ap}$, values increase in winter as compared to summer, indicating, in relative terms, higher abundance of smaller absorbing particles in winter than in summer. This observation is consistent with assuming emissions from domestic heating by wood stoves to contribute to the Birkenes winter aerosol, which is the explanation for the decreased winter values of ϖ_0. The size of the absorbing aerosol particles increases with aerosol age. Consequently, a smaller size of the absorbing particles indicates a younger combustion aerosol and a closer combustion source, which is consistent with a scattered distribution of houses using wood stoves for heating, i.e. typical for Southern Norway. The previous instrument upgrade of aerosol absorption measurements in Birkenes has thus provided another indication for the contribution of wood stove emissions to the Birkenes winter aerosol. Further information can be expected from the additional upgrade extending the spectral range of particle absorption observations in November 2017.

3.3.2 Optical aerosol properties measured the Zeppelin Observatory

Key findings aerosol optical properties Zeppelin: *The aerosol absorption measurements at Zeppelin station are conducted in collaboration with the Greek Demokritos-Athens research institute, and continue a time series that has been in started 2001. The decreasing trend in aerosol absorption observed since 2001 by Eleftheriadis et al. (2009) has continued, and fits with the trend observed at other surface in situ stations in the Arctic (Coen et al., 2013; Collaud Coen et al., 2020). The spectral dependence of particle light absorption at Zeppelin indicates a contribution of absorbing components with spectral dependence due to chemical composition, e.g. brown carbon or mineral dust.*

The in situ optical properties of the particles at Zeppelin Observatory covered in this report are more limited as compared to Birkenes and Trollhaugen. NILU operates only one filter absorption photometer, an AE33 aethalometer, at Zeppelin measuring the absorption coefficient $\sigma_{ap}(\lambda)$ between 370-950 nm wavelength. A nephelometer providing the spectral scattering coefficient $\sigma_{sp}(\lambda)$ is also deployed at Zeppelin, but operated by Stockholm University, and data are therefore not available for this report. This excludes also calculation and discussion of the particle single scattering albedo.

Figure 48 summarises the 2015 – 2019 time series, i.e. 4.5 years, of spectral aerosol particle absorption coefficient $\sigma_{ap}(\lambda)$ data collected at Zeppelin Observatory since deployment of the aethalometer in June 2015. The top panel displays daily averaged $\sigma_{ap}(\lambda)$ data for all 7 wavelengths (thin lines), as well as running 8-week medians (bold lines), here only for 3 wavelengths to improve readability of the graph. The middle panel shows graphs of the absorption Ångström coefficient $å_{ap}$ for 3 wavelength pairs representing short wave end, long wave end, and full range of the measured wavelength spectrum. The $å_{ap}$ data are plotted as 8-week median only, since daily averages are too noisy due to the low particle load commonly observed at Zeppelin.

The 4.5 year time series of σ_{ap} (top panel of Figure 48) exhibits the same annual cycle as described already in the data of the other aethalometer instrument at Zeppelin collected in earlier years (Eleftheriadis et al., 2009), with lower values in summer and higher ones in winter. These variations have been attributed to changes in combustion aerosol sources caused by emissions from domestic heating in the relevant source regions, e.g. Northern and Central Russia (Law & Stohl, 2007). This pattern is moderated by incidents of emissions from large forest fires reaching the Arctic, which can increase aerosol particle absorption in episodes also in summer (e.g. Stohl et al., 2007). Absolute values

of σ_{ap} vary in the range of 0.02 – 2 Mm^{-1}at Arctic Zeppelin station, with median values roughly a factor of 5 lower than at boreal Birkenes, but a factor of 4 larger than at Antarctic Trollhaugen station.

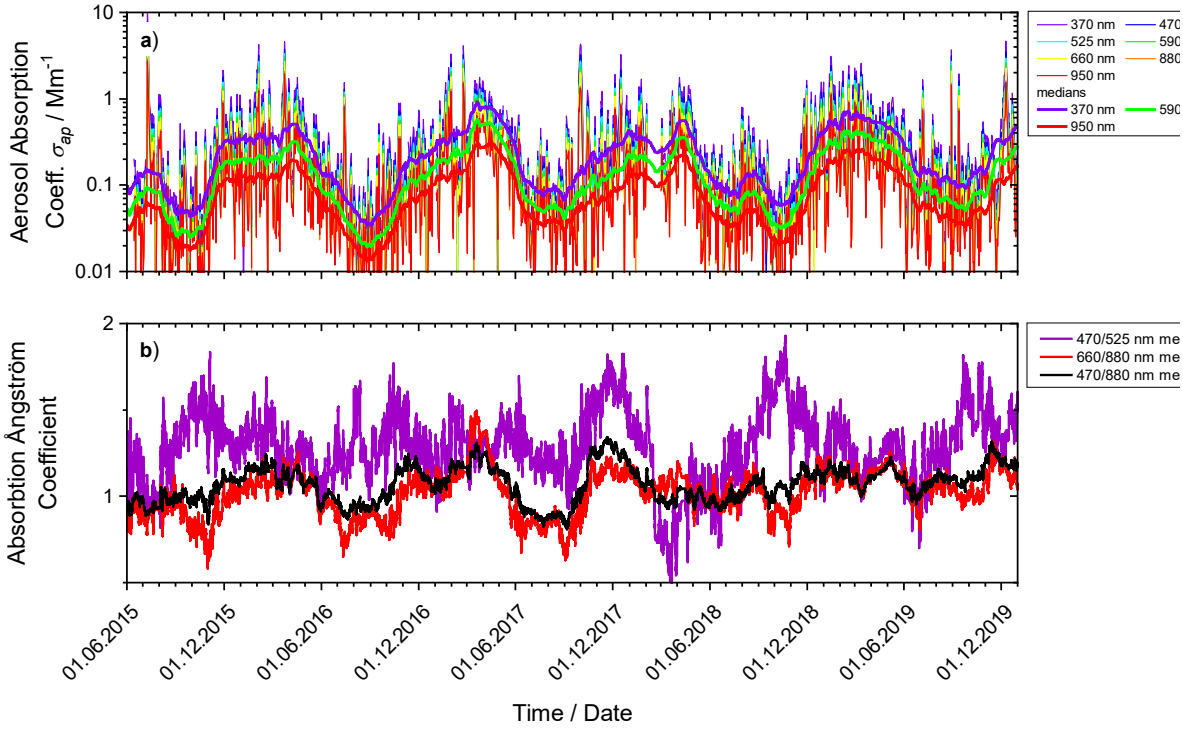

Figure 48: 2015 – 2019 time series graphs of data collected by the filter absorption photometer at Zeppelin Observatory since deployment in June 2015. Top: daily means of absorption coefficient at all 7 measured wavelengths (thin lines), and 8-week running medians for top, middle and bottom of observed spectral range (heavy lines). Bottom: 8-month running medians of absorption Ångström coefficient, top, bottom, and whole observed spectral range.

Also interesting in the data provided by the filter absorption photometer is the aerosol absorption Ångström coefficient $å_{ap}$. The $å_{ap}$ values exhibit a distinct spectral dependence on wavelength, with $å_{ap}$ for shorter wavelengths deviating to higher values as compared to $å_{ap}$ at larger wavelengths for periods of lower aerosol absorption, i.e. in summer. Such a behaviour can be caused by absorbing aerosol components that exhibit a spectral dependence in absorption, e.g. brown carbon or dust. For black carbon in contrast, $å_{ap}$ at shorter and larger wavelength agree at values around 1.

3.3.3 Optical aerosol properties measured at the Trollhaugen Observatory

Key findings aerosol optical properties Trollhaugen: *The length of the time series of data on optical aerosol properties at Trollhaugen is too short for drawing conclusions on trends. The annual cycle of the aerosol optical properties at Trollhaugen has been studied in detail, and is associated to a natural, hemispheric-scale atmospheric pattern. The same annual cycle with higher particle loads and larger particles in summer is observed also at other stations on the central Antarctic continent.*

This section covers the aerosol optical properties collected at the station after the relocation in January 2014 from the Troll main base to Trollhaugen located above and upwind of the previous location. At the location of the old station, up to 80% of the collected data were contaminated by diffuse (unavoidable) emissions from the main buildings, making the scientific value and interpretation of the data from the old location difficult.

At Trollhaugen station, the same comprehensive set of instruments for observing optical aerosol properties as used in Birkenes is deployed. These cover the spectral scattering coefficient $\sigma_{sp}(\lambda)$, the spectral absorption coefficient $\sigma_{ap}(\lambda)$, as well as the derived properties scattering and absorption Ångström coefficient $\mathring{a}_{sp}$ and $\mathring{a}_{ap}$, parameterising the wavelength dependence of σ_{sp} and σ_{ap}, as well as the single scattering albedo ϖ_0. Figure 49 summarises the corresponding data collected at Trollhaugen for the years 2014 – 2019.

Starting with the time series of $\sigma_{sp}(\lambda)$ in panel a) of Figure 49, a slight annual cycle can be observed, with superimposed peaks throughout the year. The peaks are associated with intrusions of marine air during storm episodes, while the annual cycle is caused by an annual cycle of the particle number size distribution (PNSD) in Antarctic background air, with higher particle loads and larger particles in summer. The same annual cycle in the PNSD also explains the annual cycle in the scattering Ångström coefficient $\mathring{a}_{sp}$ plotted in panel b). The scattering Ångström coefficient increases as the PNSD receives a relative peak at smaller particle sizes, which is the case in Antarctic background summer air.

An annual cycle can also be detected in the $\sigma_{ap}(\lambda)$ time series depicted in panel c) of Figure 49, even though the filter absorption photometer operates constantly around the detection limit. The minimum in the cycle occurs in Southern hemisphere winter when the Antarctic vortex decreases transport from lower latitudes through the lower and mid-troposphere. In the absorption Ångström coefficient $\mathring{a}_{ap}$ time series shown in panel d), the annual cycle is rather weakly pronounced, with the lowest values also occurring in winter.

The time series of the single scattering albedo ϖ_0 (panel e) of Figure 49) shows the highest values close to 1, i.e. almost no particle absorption at all, in Antarctic winter, coincident and consistent with the minimum in particle absorption. Lower ϖ_0 values, i.e. higher average particle absorption, occurs towards summer when the Antarctic continent is subject to stronger transport from mid-latitude sources through the lower part of the troposphere.

Optical aerosol properties are tightly connected to the physical aerosol properties, which is why they are ideally interpreted together. The annual cycle in the optical aerosol properties observed at Trollhaugen is caused by a corresponding annual cycle in the physical properties, which will be discussed in section 3.4.3.

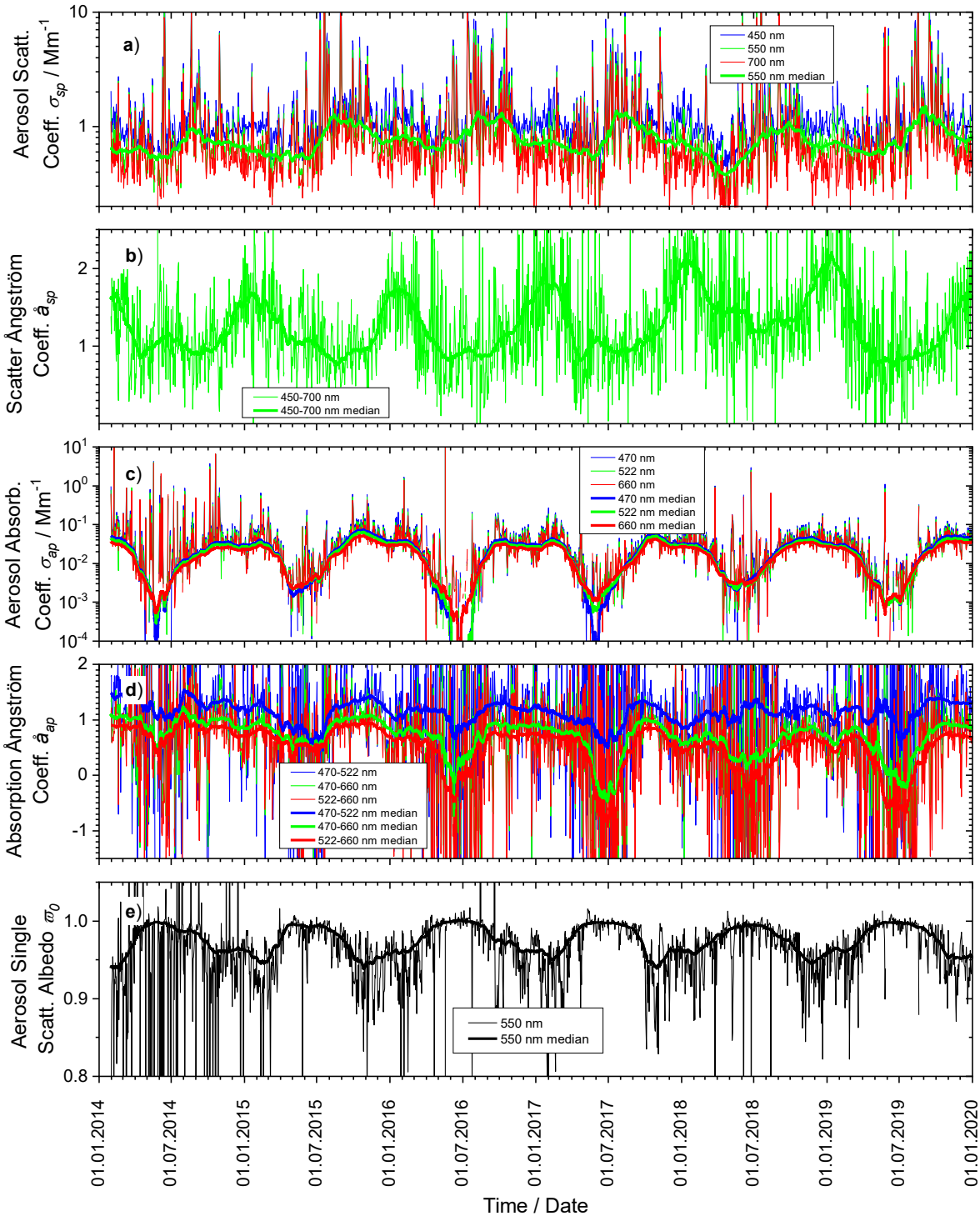

Figure 49: Time series of aerosol particle optical property daily means measured for 2014 - 2019 at Trollhaugen station. Panel a) shows the aerosol scattering coefficient σ_{sp} at 450, 550, and 700 nm wavelength measured by integrating nephelometer. Panel c) the aerosol absorption coefficient σ_{ap} at 470, 522, and 660 nm wavelength measured by filter absorption photometer. Panels b) and d) show the derived properties scattering and absorption Ångström coefficient $å_{sp}$ and $å_{ap}$, respectively, while Panel e) depicts the single scattering albedo ϖ_0. All plots also depict the running 8-week medians of the respective properties as heavy lines to visualize seasonal variations.

3.4 Measurements of particle number and size

3.4.1 Physical aerosol properties measured at the Birkenes Observatory

Key findings aerosol physical properties Birkenes: *Size segregated aerosol particle concentrations at Birkenes do not exhibit any obvious trend. This corresponds to findings obtained at other Nordic stations within ACTRIS and EMEP. The particle size distribution at Birkenes is governed by 5 major sources: 1) clean Arctic background aerosol; 2) Central and Eastern European aerosol; 3) Arctic haze; 4) fine fraction biogenic aerosol; 5) wood combustion aerosol from domestic heating. Episodes observed in winter and August 2019 can be traced to source regions in Central Europe (winter) and fires in Ukraine (August 2019).*

Figure 50 shows the time series of the particle number size distribution (PNSD) measured at Birkenes in 2019, separated into 4 different panels by season. In this plot type, the x-axis shows the time of the observation, whereas the y-axis shows the particle diameter D_p on a logarithmic scale. The logarithmic colour scale is the particle concentration, normalised to the logarithmic size interval, dN / dlog D_p. The use of logarithmic axis is common when displaying size information since both, particle diameter and particle concentration, tend to span several orders of magnitude while containing relevant information over the whole scale. In this report, the PNSD reported for Birkenes is intended to cover the whole size range between 0.01 – 10 µm by combining the information of 2 instruments, one each focussing on the fine (D_p < 1 µm) and coarse (D_p > 1 µm) size ranges, into a common PNSD product (see Appendix II for details). For the common PNSD product, both instruments need to agree in their overlap size range. At observation times when this criterion isn't met, the resulting PNSD is rejected, which can lead to gaps in the PNSD time series. This normally occurs predominantly in winter when the aerosol particles are absorbing, which affects the instrument covering the coarse size rage, an Optical Particle Size Spectrometer (OPSS). Existing operating procedures and quality standards defined by the European research infrastructure ACTRIS have been used (Wiedensohler et al., 2012), but cover only the fine particle size range.

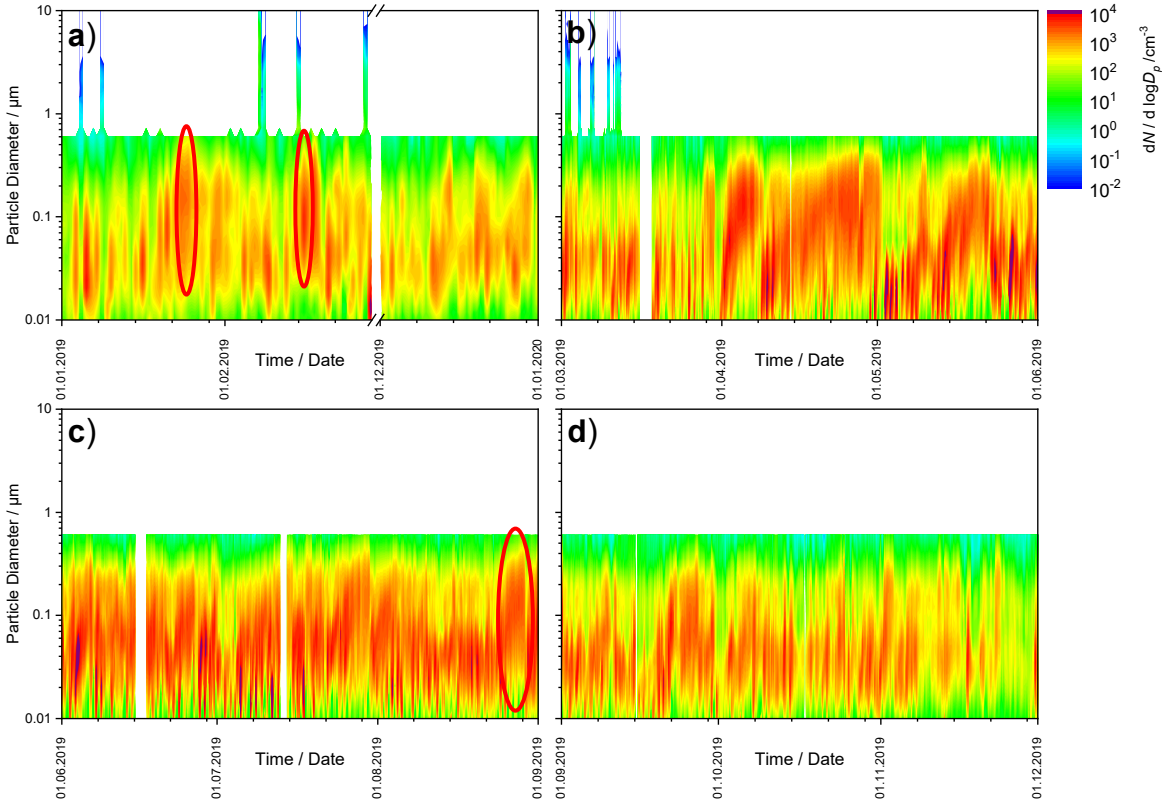

Figure 50: 2019 time series of particle number size distribution at Birkenes, panel a) winter, panel b) spring, panel c) summer, panel d) autumn. Episodes in winter and summer 2019 are marked by red oval shapes.

The OPSS follows a schedule of manufacturer calibrations, which is traceable only to a master unit, but not to an independent SI standard. This limits options for in-the-field QA and calibration measures using portable SI standards. In 2019, the OPSS experienced calibration issues and is therefore mostly excluded from analysis. This highlights the need for manufacturer independent, SI traceable calibration options. In this context, the role of station networks such as ACTRIS and WMO GAW cannot be overstated. For measuring the coarse-range PNSD, alternatives to the OPSS are currently being evaluated.

There doesn't exist any unique connection between the PNSD and air mass type, but the PNSD still is normally fairly characteristic for the air mass, and can serve, together with the single scattering albedo ϖ_0, and the scattering Ångström coefficient $\mathring{a}_{sp}$, as valuable indication of air mass origin, which at Birkenes shifts with the synoptic weather situation. Consequently, the information content of a PNSD time series plot is too high to be discussed in detail in this overview-type annual report. The PNSD and ϖ_0 observations reconfirm findings from earlier years on the dominant air mass types at Birkenes, which consist of: 1) clean Arctic background aerosol; 2) Central and Eastern European aerosol; 3) biogenic aerosol, i.e. vegetation emitted precursor gases condensing to the particle phase by photooxidation; 4) wood combustion aerosol from domestic heating.

Of particular interest in 2019 are episodes occurring in winter and summer. Visible in panel a) of Figure 50, the winter episodes around 23 January and 16 February are characterised by a PNSD dominated by a single accumulation mode peaking around 0.1 µm particle diameter. Aerosols exhibiting such a PNSD have been subject to intense auto-processing, either by being closed off from surrounding air, and/or by maintaining high particle concentrations under transport. By use of the trajectory model FLEXTRA, it is determined that the air masses corresponding to the 23 January event originate from Eastern Germany via Sweden, while the air masses connected to the 16 February event pass over Britain, Belgium, Switzerland, The Po valley, and Eastern France (in this order) before arriving at Birkenes. Thus, these episodes are caused by transport of Central European emissions. The summer episode around 28 August is connected by trajectory analysis to fires in Ukraine that month. Emissions from these fires are also observed at Zeppelin.

In order to condense the information in the PNSD time series, Figure 51 shows the time series of selected PNSD integrals, i.e. the concentration of particles falling into selected size intervals. The size intervals are chosen to represent characteristic processes governing the atmospheric aerosol (see Appendix II for more details): 1) the Aitken-mode size range, 0.02 – 0.1 µm; 2) the accumulation mode size range, 0.1 – 1 µm; 3) the coarse mode size range, 1 – 10 µm. The time series in Figure 51 represent daily averages over these PNSD integrals for the whole period since the Birkenes station upgrade in 2010, as well as the corresponding running 8-week medians to highlight seasonal variations. The respective size range integral particle concentrations are denoted N_{ait} for the Aitken mode, N_{acc} for the accumulation mode, and N_{coa} for the coarse mode.

As to be expected, the particle concentration in the Birkenes aerosol in absolute terms is dominated by the Aitken mode particles, followed by the accumulation mode. Also the most prominent feature in Figure 51 is exhibited by the particle concentrations in these 2 modes, a clear annual cycle caused by the same underlying physical process. In summer, the vegetation emits gaseous aerosol precursors, which are photo-oxidised and condense onto Aitken-mode particles or form those directly. These particles coagulate, increasing the concentration of accumulation mode particles. These same processes increasing N_{ait} and N_{acc} in summer are also responsible for increasing the scattering

Ångström coefficient $å_{sp}$ in summer. The processes controlling N_{coa} are decoupled from those controlling N_{ait} and N_{acc}. Coarse mode particles are formed from bulk material, their concentration is affected by wind speed (levitating dust, spores, pollen), snow cover, and rain (both inhibiting dust levitation).

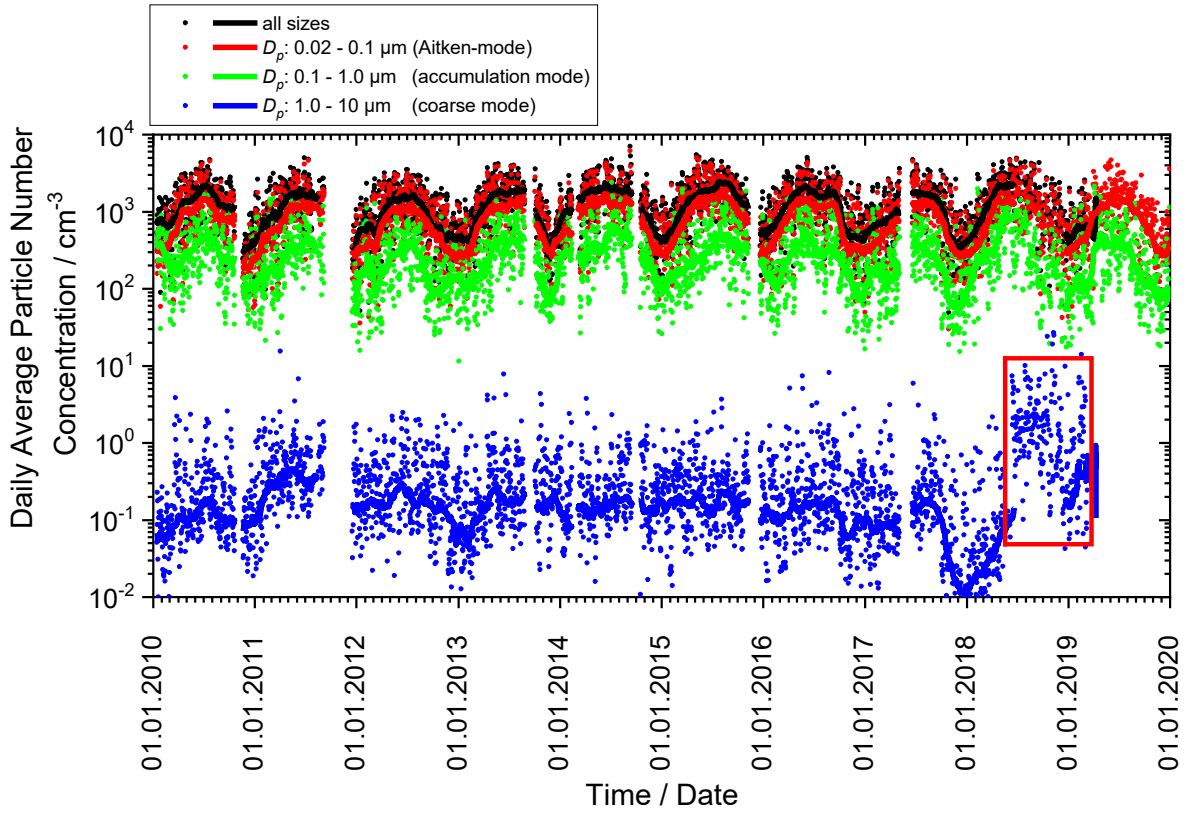

Figure 51: Birkenes 2010-2019 time series of particle number concentration integrated over selected size ranges representing the different physical processes governing the atmospheric aerosol. The dotted graphs represent daily averages of the respective size range, the lines the 8-week running median. The period where the OPSS, measuring the concentration of coarse size range particles, experienced calibration issues, is marked by a red box.

3.4.2 Physical aerosol properties measured in situ at the Zeppelin Observatory

Key findings aerosol physical properties Zeppelin: *Zeppelin particle size distribution data exhibit the well-known Arctic haze pattern. Trends in this pattern cannot be studied in this context due to too short the time series. Newly established observations of the particle size distribution in the refractory particle fraction can serve as indicator of aerosol processing time. An episode occurring at Zeppelin in July, August, and September 2019 can be traced back to fires in the Western Siberian Plain, Ukraine, and Western Russia, respectively.*

A Differential Mobility Particle Sizer (DMPS) instrument, measuring the particle number size distribution, was installed at Zeppelin in 2016 primarily to calibrate the ACSM instrument, but included continuous monitoring as an additional benefit. The same instrument type, operated in a different mode, is used to *measure* the particle number size distribution (PNSD) in the particle diameter range 0.01 µm – 0.8 µm at Birkenes and Trollhaugen stations. It was therefore decided to deploy the Zeppelin DMPS in the same way when not needed for calibrating the ACSM instrument.

As an additional feature, the Zeppelin DMPS has been upgraded late 2017 to also provide the PNSD of refractory (non-volatile) particles. The refractory particle fraction is often used as a proxy for the absorbing aerosol particle fraction, which will allow to study changes in particle absorption on a microphysical basis in the Arctic environment on a routine basis. The corresponding data are available in real-real-time with only 1 hour delay.

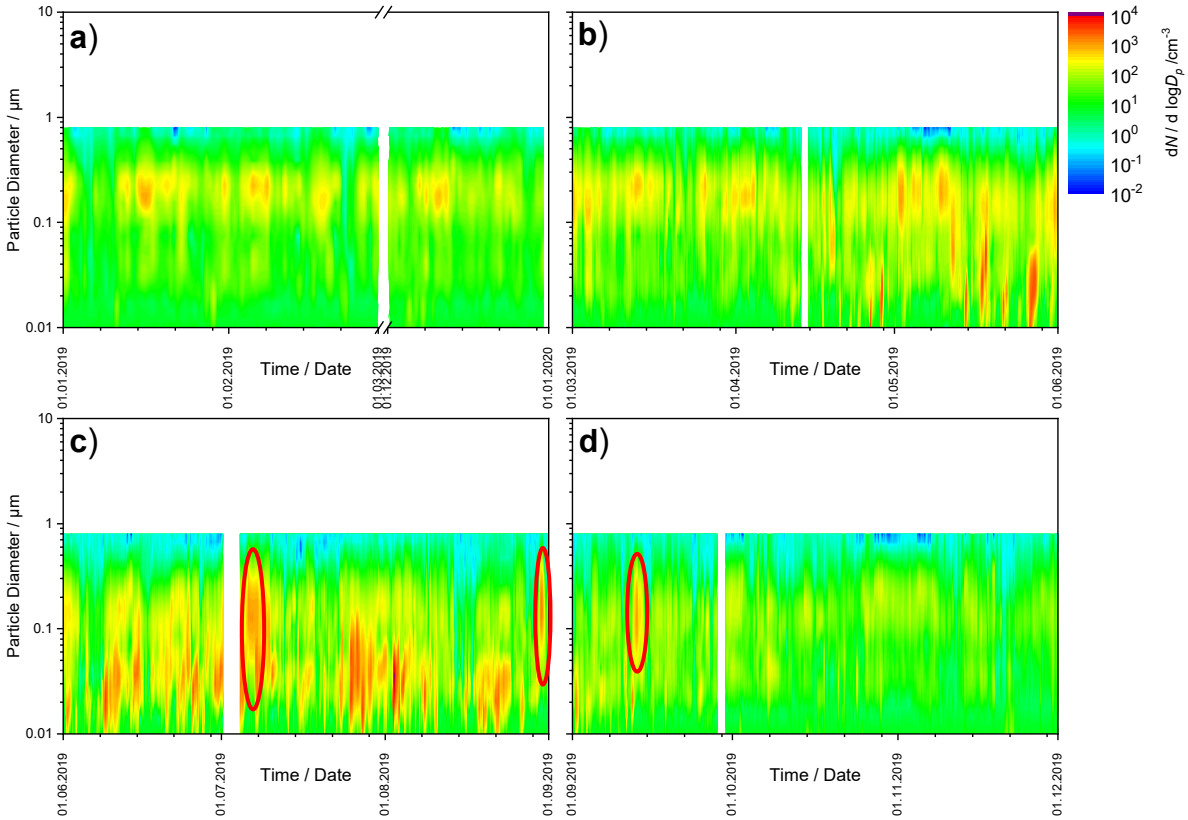

Figure 52: 2019 time series of particle number size distribution at Zeppelin, panel a) winter, panel b) spring, panel c) summer, panel d) autumn. Episodes occurring around 6 July, 30 August, and 13 September 2019 are marked with a red ovals.

At Zeppelin, the DMPS is not combined with an instrument covering the coarse particle size range larger 1 µm. This limits the available PNSD information the DMPS size range. Figure 52 presents the Zeppelin PNSD data available for this report for 2019 in the same way as for Birkenes and Trollhaugen, with one PNSD time series panel per season.

In contrast to mid-latitudes, air masses don't shift quite as rapidly at polar latitudes due to a smaller influence of frontal systems, making weather patterns more persistent at least in parts of the year. This allows to interpret the information on air mass types contained in PNSD data in more detail. Focussing in on Panel a) of Figure 52 displaying the PNSD data of winter 2018, periods with a uni-modal size distribution are visible. This means the PNSD is dominated by a single mode, in this case the accumulation mode with a peak around 0.25 µm particle diameter. Such a PNSD is typical of early-phase Arctic haze (Heintzenberg, 1980), which is also detectable in late autumn (Panel d) of Figure 52). Arctic haze is formed by auto-processing of aerosol particles trapped under the winter Arctic vortex while the particle mass increases from industrial emissions under the vortex (e.g. Law & Stohl, 2007).

The late spring and summer PNSD at Zeppelin (Figure 52 panels c) and d) is somewhat more variable than in winter due to less stable atmospheric conditions. Particle formation events can be observed,

with peak in the PNSD at particle diameters between 0.01 –0.02 µm. These are triggered by photo-chemical production of chemical species that condense into the particle phase, and don't find enough existing particle surface to condense on, thus forming new particles.

More unusual events can be observed in the 2019 Zeppelin PNSD data around 6 July, 30 August, and 13 September. The PNSD is dominated by a single mode peaking around 0.1-0.15 µm particle diameter. This indicates again strong auto-processing of the aerosol. Trajectory analysis and satellite observations of fires indicate fires in the Western Siberian Plain, Ukraine, and Western Russia, respectively, as sources of these events. Emissions from the August fire in Ukraine were also observed at Birkenes.

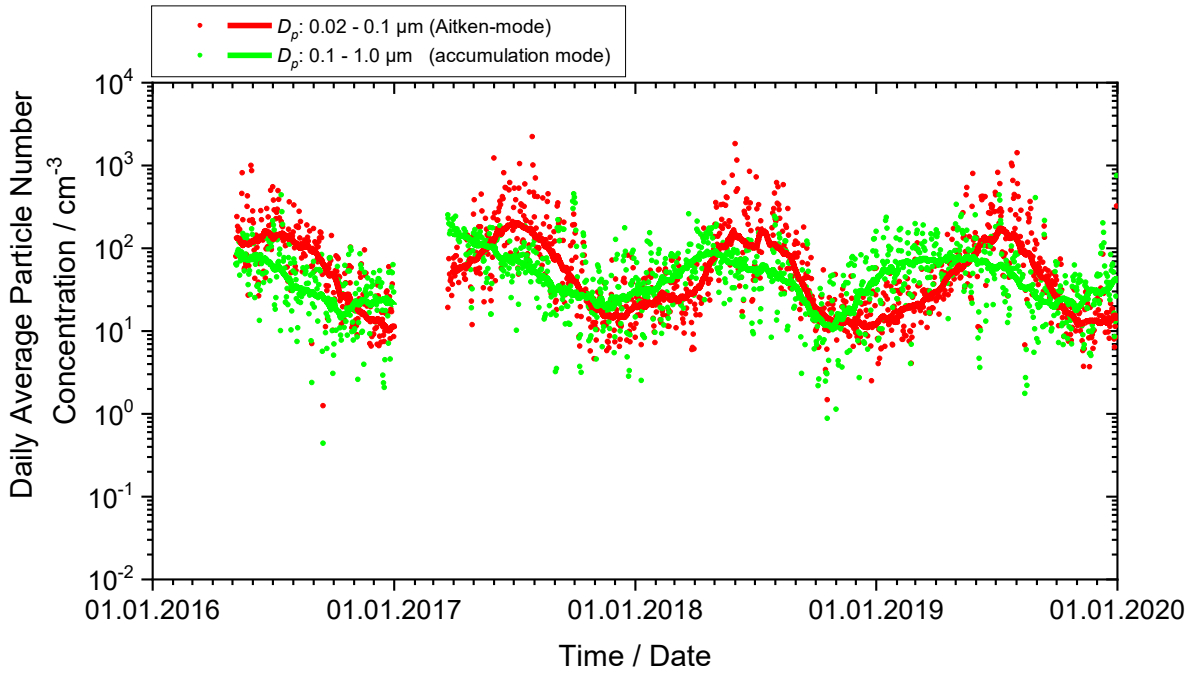

Figure 53: Zeppelin 2016-2019 time series of particle number concentration integrated over selected size ranges representing the different physical processes governing the atmospheric aerosol. The dotted graphs represent daily averages of the respective size range, the lines the 8-week running median.

Figure 53 summarises the 2016-2019 Zeppelin PNSD data by displaying time series of the PNSD size integrals for the Aitken mode N_{ait} (0.02 µm< D_p < 0.1 µm) and N_{acc} (0.1 µm< D_p < 0.8 µm). Apart from particle concentrations an order of magnitude lower than at boreal Birkenes, the most prominent feature of the graph is the point in early November where the N_{acc} running median becomes consistently larger than N_{ait} running median. This behaviour is typical for auto-processed aerosols, and occurs normally only for shorter events. At Zeppelin, this point marks the onset of the Arctic haze period. The Zeppelin DMPS experienced an outage in 2017 caused by a diaphragm failure in the sheath air pump. Though unfortunate, such failures can occur despite preventive maintenance.

Figure 54 displays the annual time series of the PNSD measured at Zeppelin in the non-volatile (refractory) particle fraction in 2019, again with one panel per season. The refractory particle fraction is measured by heating the aerosol sample to 250°C prior to measuring the PNSD. It can be considered as proxy for the BC particle fraction, but contains also mineral dust and condensed species which become non-volatile by charring or oligomerisation while the sample is heated.

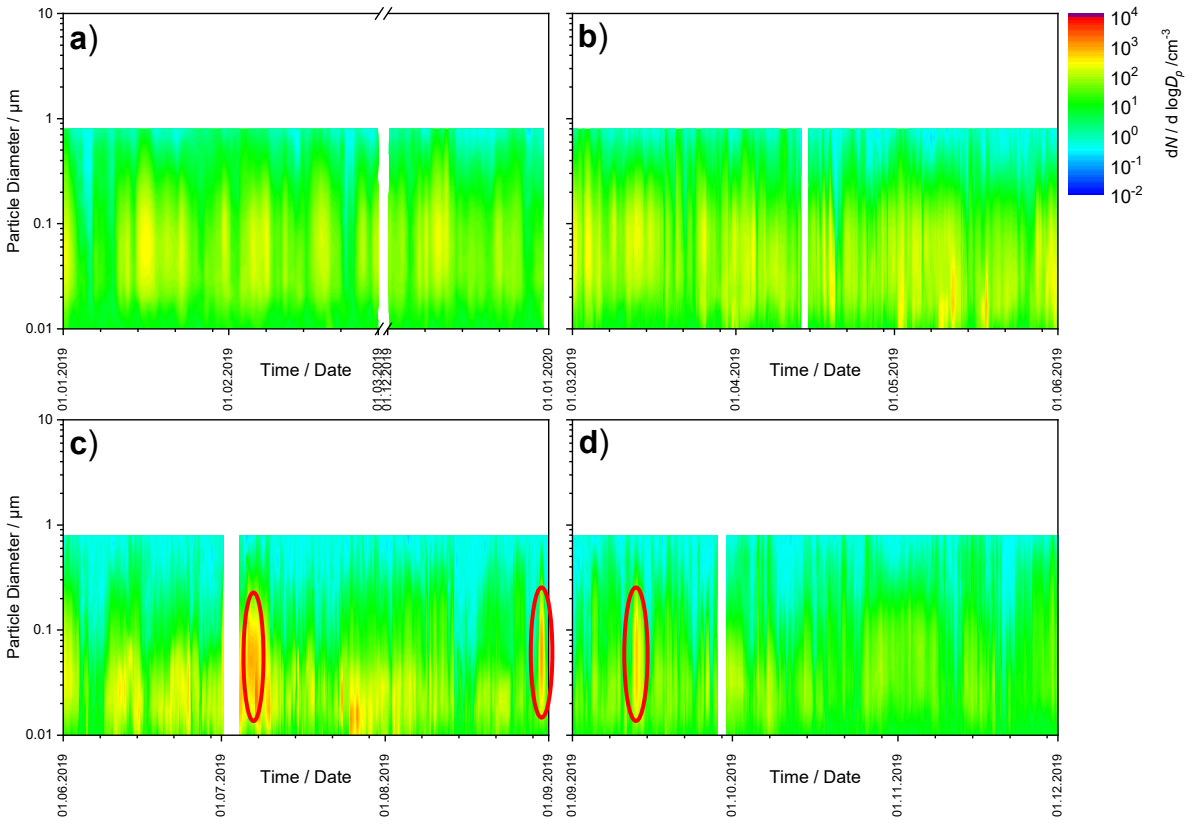

Figure 54: 2019 time series of particle number size distribution of the non-volatile particle fraction at Zeppelin, panel a) winter, panel b) spring, panel c) summer, panel d) autumn. Episodes occurring around 6 July, 30 August, and 13 September 2019 are marked with red ovals.

As most obvious distinction between the PNSD of the ambient aerosol (Figure 52) and the PNSD of the non-volatile aerosol fraction (Figure 54), the particle number concentration levels are around half-a-magnitude lower in the non-volatile as compared to the ambient aerosol. The PNSD is almost exclusively mono-modal, with the single mode peaking in the Aitken-size range between 0.25-0.5 µm particle diameter. The peak diameter increases with the auto-processing and lifetime of the aerosol. The refractory particle component increases in size due to coagulation, and not modulated by volatile particle components. The refractory particle fraction can even reveal aerosol age which would not be visible otherwise, as exemplified by the episodes around 6 July, 30 August, and 13 September, and marked by a red ovals in Figure 54. The fire episodes are marked by pronounced modes in the refractory particle PNSD. The peaks correspond to the episodes visible in the ambient aerosol PNSD (Figure 52).

Similar as before, Figure 55 summarises the 2018 Zeppelin PNSD data for the refractory particle fraction by displaying time series of the PNSD size integrals for the Aitken mode N_{ait} (0.02 µm< D_p < 0.1 µm) and accumulation mode N_{acc} (0.1 µm< D_p < 0.8 µm). As mentioned before, the overall level of N_{ait} and N_{acc} for the refractory particle fraction is roughly half an order of magnitude lower than for the respective counterparts in the ambient aerosol. An annual cycle might be visible, now confirmed by 2 years of data.

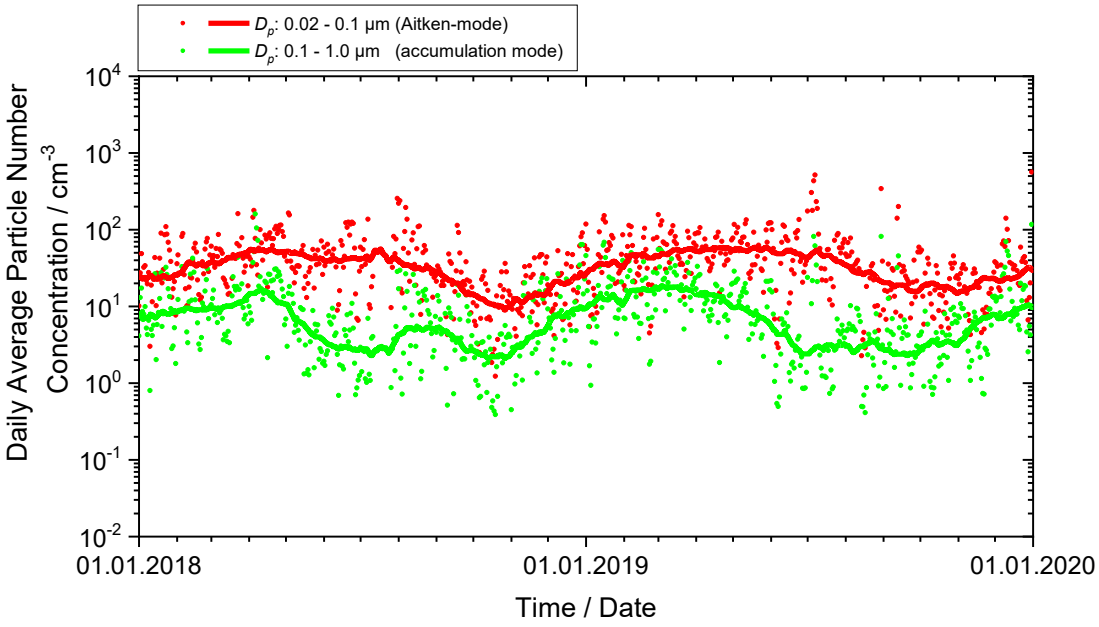

Figure 55: Zeppelin 2019 time series of number concentration in the refractory particle fraction integrated over selected size ranges representing the different physical processes governing the atmospheric aerosol. The dotted graphs represent daily averages of the respective size range, the lines the 8-week running median.

3.4.3 Physical aerosol properties measured in situ at the Trollhaugen Observatory

Key findings aerosol physical properties Trollhaugen: *The length of the time series of reliable data on the aerosol particle number size distribution at Trollhaugen is too short for drawing conclusions on trends. The annual cycle of the PNSD at Trollhaugen has been studied in detail, and is associated to a natural, hemispheric-scale atmospheric pattern. Antarctic background air descends over the Central continent from the upper troposphere / lower stratosphere. At that altitude, it has been transported to the pole after being uplifted (and cleaned by wet removal) at mid- or tropical latitudes. An episodes of mono-modal aerosol intrusion during winter can be connected to emissions form research stations 360 km east of Trollhaugen.*

In contrast to mid-latitudes, polar latitudes exhibit more stable atmospheric conditions with less influence of frontal systems. This is especially true for the Antarctic continent due to colder inland temperatures and the absence of land masses in the mid- to high-latitude Southern hemisphere that could disturb the atmospheric air flow, as compared to the Northern hemisphere. This makes air masses well-defined in these regions, and their associated aerosol properties easier to interpret than under shifting Northern mid-latitude conditions.

This section only covers data collected at the station after the relocation in January 2014 from the Troll main base to Trollhaugen located above and upwind of the previous location. At the old station location, up to 80% of the collected data were locally contaminated by diffuse (unavoidable) emissions from the main station buildings, making a statistically meaningful interpretation of the data from the old location difficult.

The DMPS system measuring the PNSD at Trollhaugen station has been re-built on–site during the station maintenance visit of January / February 2016, causing a gap in the PNSD time series in January 2016. After the re-built, the system conforms to the quality standards of the ACTRIS research infrastructure, and the observed size range has been extended from 0.03 – 0.8 µm to 0.01 – 0.8 µm, making it now suitable to study formation of new particles. As a consequence, absolute particle concentrations measured by the system before and after remodelling are not directly comparable. This disadvantage has been accepted in favour of a wider range of applications for the DMPS system.
Figure 56 plots the 2019 Trollhaugen PNSD data in the same way as for Birkenes. Due to the rather well-defined atmospheric conditions over the Antarctic continent, 2019 is again rather representative also for previous years. Please observe that the times for the panels are the same as for the Northern hemisphere stations, but that seasons in the Southern hemisphere are shifted by 6 months.

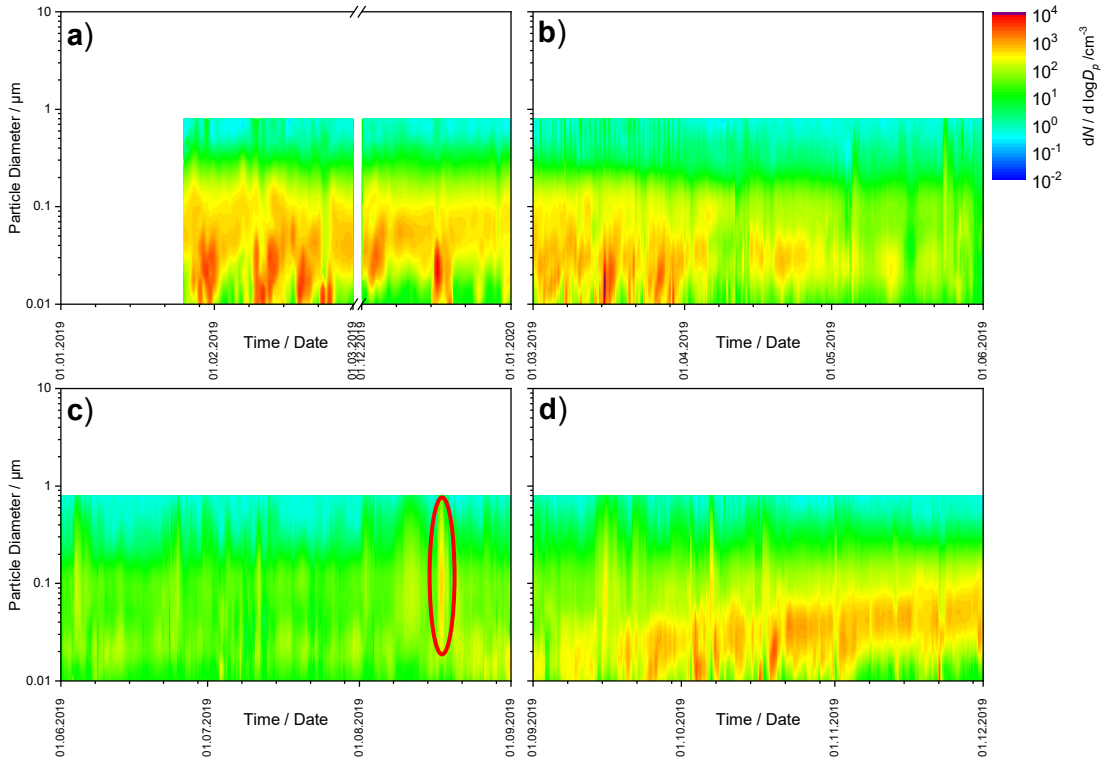

Figure 56: 2019 time series of particle number size distribution at Trollhaugen, panel a) Southern Hemisphere summer, panel b) autumn, panel c) winter, panel d) spring.

Even though the Antarctic continent is among the most pristine regions on the globe, new particle formation events triggered by photo-chemical oxidation of precursor substances can be observed in Antarctic summer. Formation of new particles is not a function of available condensable vapour alone, but also of the available particle surface. If the available particle surface becomes too small to accept the condensing vapour, new particles occur. This ratio doesn't depend on the absolute amount of aerosol particles. Thus, formation of new particles can occur anywhere on the globe.

A year-round feature observed at Trollhaugen is the intrusion of marine air associated with marine storms. These have been observed even at South Pole, and are visible in the PNSD when the particle concentration at the upper end of the particle size range increases.

The probably most prominent feature in the Trollhaugen annual PNSD time series data is the annual cycle visible in the background aerosol. Particle concentrations are low in winter over the whole observed PNSD size range, and nucleation events lacking. In spring, particle concentrations in the

diameter range 0.01 – 0.03 µm increase, and the central particle diameter of this peak increases throughout spring until reaching values around 0.09 µm in summer. Towards autumn and winter, the cycle reverses.

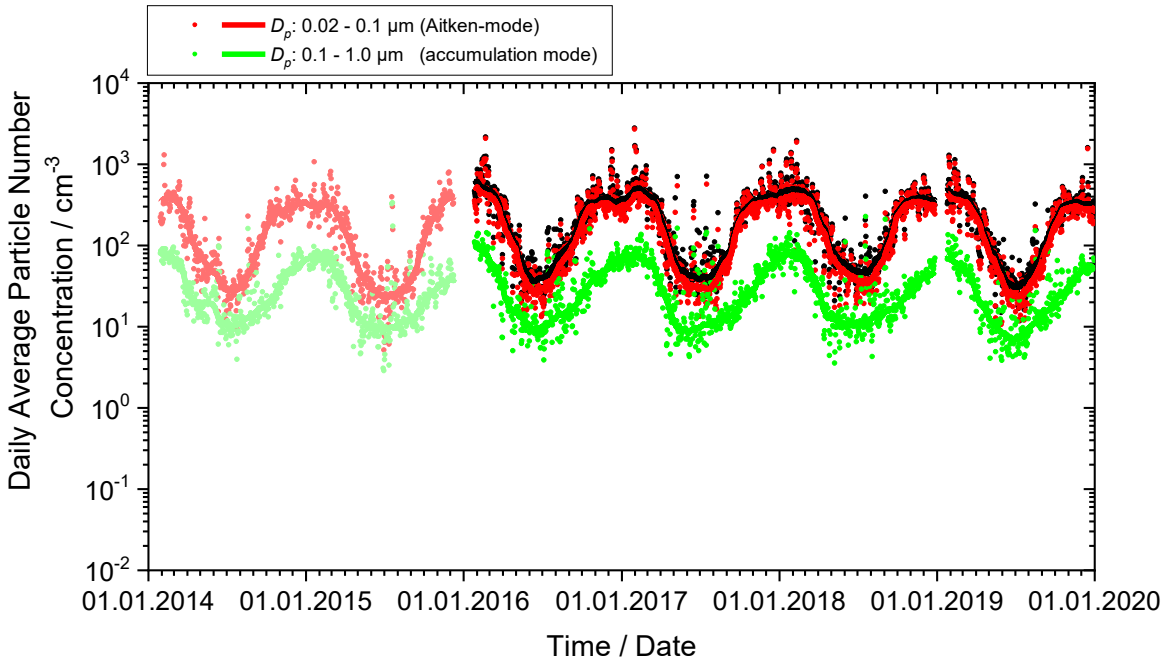

Figure 57: 2014-2019 time series of particle number concentration integrated over selected size ranges representing the different physical processes governing the atmospheric aerosol. The dotted graphs represent daily averages of the respective size range, the lines the 8-week running median. Data of the DMPS instrument prior to its upgrade are plotted in lighter colour as reminder that data before and after remodelling aren't directly comparable due to extension of the particle size range observed by the instrument.

This annual cycle in the Antarctic background PNSD is reflected by the PNSD size integrals for the Aitken mode N_{ait} (0.02 µm< D_p < 0.1 µm) and N_{acc} (0.1 µm< D_p < 0.8 µm) plotted in Figure 57, with higher particle concentrations in summer than in winter. A study based on data collected at Troll (Fiebig et al., 2014) connects the annual cycle to transport patterns seen by Antarctic background air. Antarctic background air descends over the central continent from the upper troposphere / lower stratosphere region, where it has been transported from mid-latitudes or even the tropics at the same altitude. At these lower latitudes, it had been uplifted by frontal conveyers (mid-latitudes) or tropical anvil clouds. The uplift process, associated with extensive wet removal of particles in the frontal or anvil cloud system, explains the cleanliness of the air.

Fiebig et al. (2014) raise the hypothesis that the annual cycle of the Antarctic background aerosol is caused by the annual variation of solar insolation seen by the air during this transport pattern. The hard UV radiation in the upper troposphere would oxidise water-insoluble vapours that survived wet removal during uplift of the air. The oxidation products would subsequently condense into the particle phase, causing the observed annual cycle in the Antarctic background PNSD.

In 2019, the PNSD at Trollhaugen exhibits an episode on 17 August 2019, characterised once more by a single accumulation mode peaking around 0.1 µm particle diameter. Footprint calculations with the Lagrangian transport model FLEXPART suggest emissions of the Antarctic research stations

Novolazarevskaya (Russia) and Maitri (India) 360 km east of Trollhaugen as sources, which can be seen against the pristine Antarctic background air.

3.5 Summary of physical and optical aerosol properties

Aerosol particle absorption and scattering are decisive for the cooling or warming effect of aerosols on climate. All types of aerosols are scattering solar radiation, but the higher fraction of aerosol absorption, the more warming is the aerosol. The absorption depends on the composition; black carbon (e.g. soot), certain organic compounds (brown carbon), and minerals absorb radiation. The number size distribution of the aerosol particles also determines the scattering properties. In order to summarise the measurements of physical and optical aerosol properties observed at Birkenes, Trollhaugen, and Zeppelin stations, annual and seasonal means of the main parameters are collected in Table A 3 for the physical parameters, and in Table A 4 for the optical parameters (see Appendix I)

Focussing first on the columns for Birkenes, Aitken-mode particle concentrations N_{ait} for the summer and winter show surprisingly little variation over the years. Relative to previous years, particle concentrations in 2019 for winter are close to the multi-year range, which applies also to summer concentrations. Similarly, spring N_{ait} concentrations are close to those for many previous years, whereas those for autumn are lower, but all still within the range seen in previous years. Variations of this kind are not unusual, and depend on the actual transition from winter to summer weather and vice versa. Late onset of summer weather in spring and early onset of winter weather in autumn will decrease the N_{ait} particle concentrations for these seasons. Also for the accumulation mode seasonal average particle concentrations N_{acc}, spring values are in the middle of the variability range, autumn values at the lower end, whereas summer and winter values don't show exceptional deviations.

At Birkenes, N_{ait} values for winter are typically around 33% of their summer values due to lack of biogenic particle production from the gas-phase. They depend on emissions from domestic heating, with higher values for colder winters. With spring and autumn as transition periods between the winter and summer extreme values, the variability of N_{ait} in these seasons depends on the pace of transition between summer and winter. The same tendencies apply to the accumulation mode particle concentration N_{acc}.

Coarse mode particle concentrations at Birkenes have a tendency to be up to a factor of 2 smaller in winter than in summer due to less crustal particle production with a snow-covered ground. Particle concentrations at Birkenes don't exhibit any obvious trend over time.

Aitken and accumulation mode particle concentrations at Trollhaugen are an order of magnitude lower than at Birkenes, reflecting the pristine conditions in Antarctica. Their pronounced annual cycle and its cause has been discussed in section 3.4.3. Both concentrations show little variability over the years, reflecting the fact that atmospheric composition in Antarctica is still mostly governed by natural processes whose large scale pattern changes slowly.

Zeppelin particle size distribution data exhibit the well-known Arctic haze pattern. Trends in this pattern cannot be studied in this context due to the short time series. Newly established observations of the particle size distribution in the refractory particle fraction can serve as indicator of aerosol atmospheric processing time. The spectral dependence of particle light absorption at Zeppelin indicates a contribution of absorbing components with spectral dependence due to chemical composition, e.g. brown carbon or mineral dust

The conclusion of no obvious trends applies also to the optical aerosol properties observed at Birkenes, and Trollhaugen, and is confirmed by the recent trend study of Collaud Coen et al. (2020), whereas Zeppelin aerosol absorption continues to show a decreasing trend (Eleftheriadis et al., 2009). At Birkenes, the annual and inter-annual variability is governed by the same processes mentioned when discussing the particle concentrations. More specifically, the aerosol is more absorbing in winter, and hence more warming, due to emissions from wood burning for domestic heating, which come on top of a baseline of absorbing aerosol emitted from traffic. This is reflected in higher particle absorption coefficient values in winter, and even more significantly in lower winter values of the single scattering albedo (lower meaning higher average particle absorption).

Episodes of long-range transport are visible at all 3 stations 2019, with sources of Central European winter emissions and fires in Ukraine (Birkenes), fires in Eastern Europe (Zeppelin), and emissions from neighbouring research stations (Trollhaugen).

3.6 Column optical aerosol properties measured by ground-based remote sensing

Ground-based remote sensing of the optical characteristics of aerosols in the atmospheric total column is conducted with multi-wavelength sun-photometers. A sun-photometer is oriented towards the sun to detect the solar radiation attenuated along the slant path from the top-of-atmosphere to the ground. The atmospheric aerosol load leads to a decrease in the solar radiation transmitted through the atmosphere. This decrease depends on the aerosol optical depth (AOD), which is given by the integral of the volume aerosol extinction coefficient along the vertical path of the atmosphere. The wavelength dependence of AOD, described by the Ångström exponent (AE) is a qualitative indicator of the particle size and contains information about the aerosol type. The larger the Ångström exponent, the smaller the size of the particles measured.

Photos of instruments used for monitoring of spectral resolved AOD at Birkenes and Ny-Ålesund, their main characteristics are given in Appendix II, and detailed tables with monthly data for all years are given in Appendix I.

3.6.1 Column optical aerosol properties measured by ground-based remote sensing at Birkenes Observatory

Key findings column-integrated optical aerosol properties Birkenes: *There is no statistically significant trend, neither in AOD nor in AE, in the eleven years of AOD observations at Birkenes. While AOD monthly means from January to June are close to or lower than the multi-year average, the July and August values are markedly higher than the long-term mean. AE means are very close to the long-term mean in all months covered except April.*

AOD measurements started at the Birkenes Observatory in spring 2009, utilizing an automatic sun and sky radiometer (CIMEL type CE-318, instrument #513). The retrieval method is that of the AERONET version 3 direct sun algorithm (for details: http://aeronet.gsfc.nasa.gov). Quality assured (Level 2) data are available for the eleven years of operation, 2009 - 2019. Due to technical and transport problems related to the annual calibration of the instrument at the University of Valladolid, Spain, measurements commenced only in the second half of April. New technical problems arose in October, which were not solved by the end of the year.

A second Cimel instrument (#1163) was purchased in summer 2018 and subsequently calibrated at the University of Valladolid in October 2018; it was installed at Birkenes in November 2018. Regular measurements started on 7 January 2019, and continued throughout 2019. During the analysis of the data in early 2020 it turned out that the instrument suffered technical problems and was contaminated

with dirt during two extended periods in 2019 (20 June – 25 July, 20 August – 5 November); no usable data are available from these periods. At present, the final approval of the 2019 measurements is still pending, and the results reported here are based on level 1.5 data.

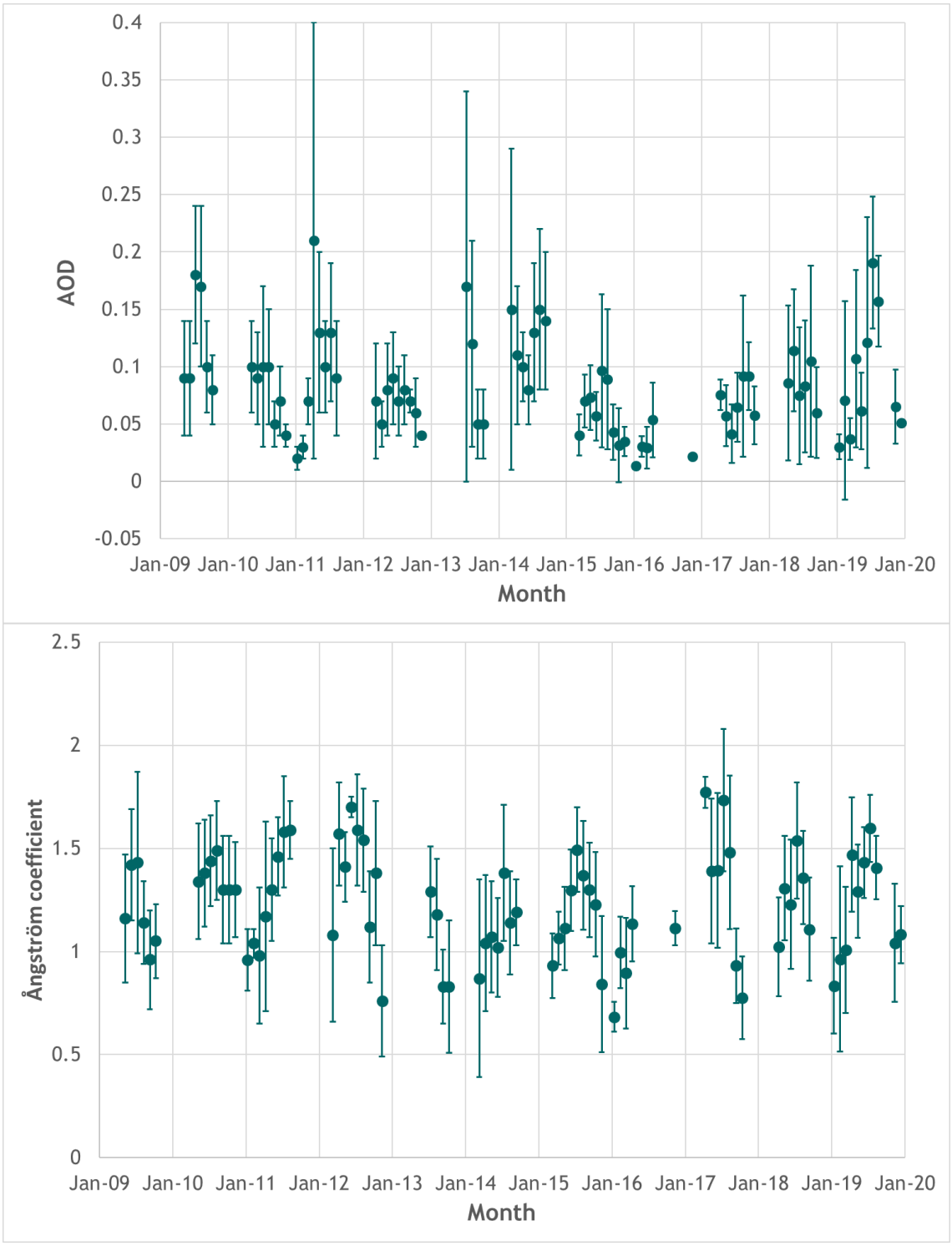

Figure 58: : 2009 - 2019 time series of aerosol optical depth (AOD) at 500 nm wavelength in the atmospheric column above Birkenes (upper panel) and (470 nm, 800 nm) Ångström exponent describing the AOD wavelength dependence (lower panel). Mean values and standard deviations are given.

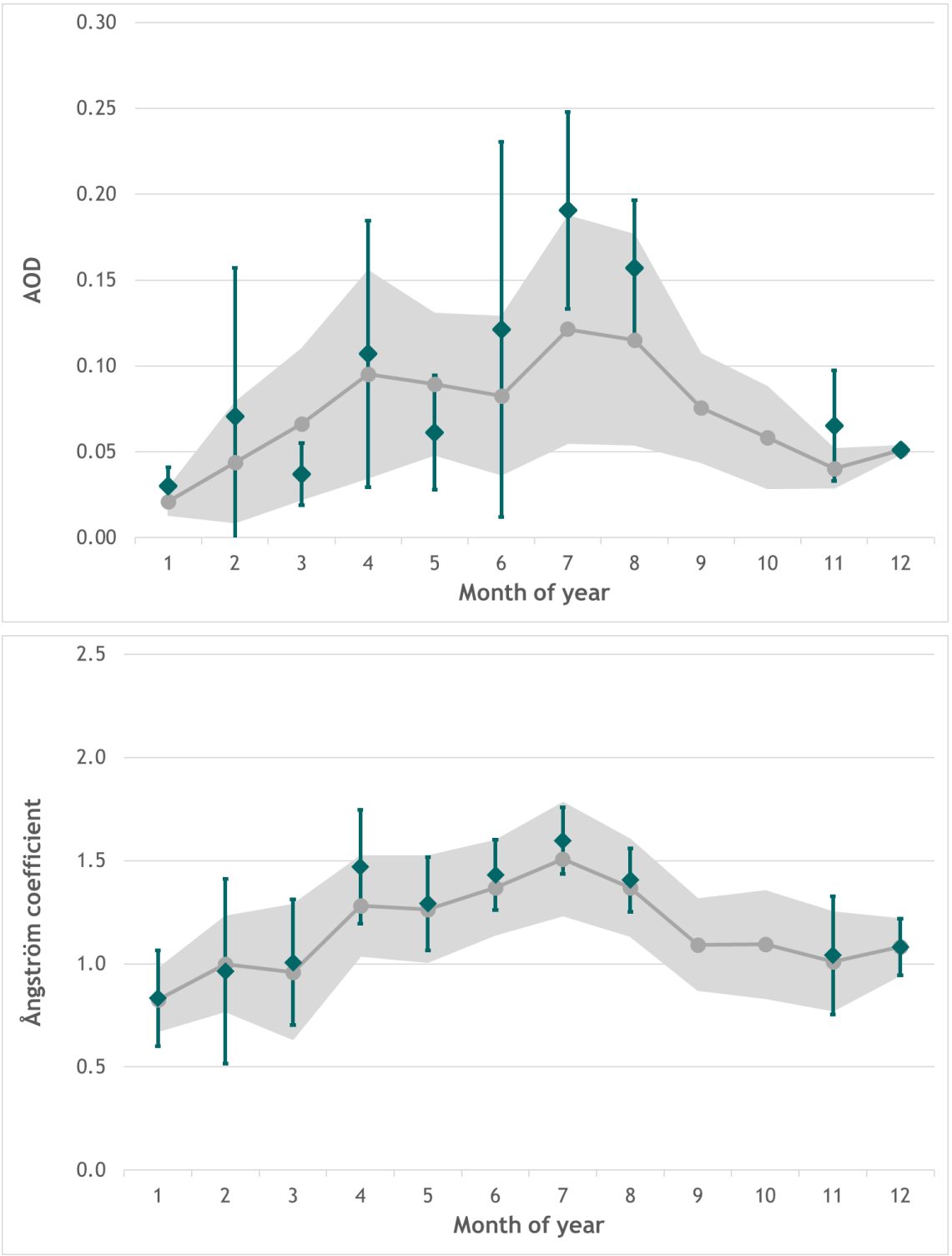

Figure 59: 2019 monthly mean aerosol optical depth (AOD) at 500 nm wavelength in the atmospheric column above Birkenes (upper panel) and (470, 800 nm) Ångström coefficient describing the AOD wavelength dependence (lower panel). Mean values and standard deviations are given. Values marked in grey are the mean and standard deviations for the time period 2009-2019.

The AOD and Ångström coefficient time series and seasonal variations for 2019 are shown in Figure 58 and Figure 59. The 2019 monthly mean and mean values for all years are shown in Table 5. Data for all

years are given in Appendix I. While AERONET calculates daily averages in case of more than 3 single measurements, we have used a minimum of 10 single measurements. However, in the monthly means we include all approved single measurements from the respective month instead of daily averages weighted with the number of single measurements included in the respective daily means. This yielded 107 daily means. There are no obvious (and statistically significant) trends visible in the 11-year series of AOD and AE monthly means.

Compared to central European observations, e.g. the Cabauw station in the Netherlands with AOD monthly means well above 1.0 for large parts of the year, the aerosol load at Birkenes is relatively low, but episodes with advected airmasses rich in pollution/aerosol load occur. In 2019, these episodes were rather frequent, but short-lived in the first half of the year. This resulted in monthly-mean AOD values at Birkenes close to the long-term means, but with large standard deviations in February, April and June. The July and August means were noticeably above the long-term means, but suffer from poor statistics due to the mentioned technical problems. For the first time we report a monthly mean for December (though with a low number of observations) which fits well with measurements in November and January. The highest monthly average AOD of 0.19 was observed in July (based on only five days of observations in a 7-day period at the end of the month), while the lowest monthly mean occurred in January with a value of 0.03. The largest AOD daily means occurred on June 4 (day 155) and April 4 (day 95) with values of around 0.44.

The Ångström exponent monthly means varied much less than AOD means and were close to the long-term means of the 12-year series throughout the year. On the other hand, the standard deviation of the monthly means was larger than the standard deviation of the multi-year means. This is due to a limited number of marked outliers (low AE values) in the period February – May.

Table 5: Monthly mean values for 2019 and mean for the time period 2009-2019, plus standard deviations, for aerosol optical depth (AOD) and Ångström exponent observed in Birkenes. In addition, the number of days with cloud free and quality assured observations are given.

Month/Year	Jan	Feb	Mar	Apr	May	Jun	Jul	Aug	Sep	Oct	Nov	Dec
Aerosol optical depth (AOD)												
2019	**0.03 ±0.01**	**0.07 ±0.09**	**0.04 ±0.02**	**0.11 ±0.08**	**0.06 ±0.03**	**0.12 ±0.11**	**0.19 ±0.06**	**0.16 ±0.04**			**0.07 ±0.03**	**0.05 ±0.003**
Mean 09-19	**0.02 0.01**	**0.04 ±0.04**	**0.07 ±0.04**	**0.10 ±0.06**	**0.09 ±0.04**	**0.08 ±0.05**	**0.12 ±0.07**	**0.12 ±0.06**	**0.08 ±0.03**	**0.06 ±0.03**	**0.04 ±0.01**	**0.05 ±0.003**
Ångström coefficient (Å)												
2019	**0.83 ±0.23**	**0.96 ±0.45**	**1.01 ±0.31**	**1.47 ± 0.28**	**1.29 ± 0.23**	**1.43 ± 0.17**	**1.60 ± 0.16**	**1.41 ± 0.15**			**1.04 ±0.29**	**1.08 ±0.14**
Mean 09-19	**0.83 ±0.15**	**1.00 ±0.23**	**0.96 ±0.33**	**1.28 ±0.24**	**1.26 ±0.26**	**1.37 ±0.23**	**1.51 ±0.27**	**1.37 ±0.24**	**1.09 ±0.22**	**1.09 ±0.26**	**1.01 ±0.24**	**1.08 ±0.14**
Number of days with cloud-free and quality assured observations (AERONET level 2)												
2019	**6**	**9**	**14**	**23**	**23**	**11**	**5**	**10**			**3**	**3**
Total 09-19	**14**	**20**	**74**	**95**	**160**	**160**	**171**	**143**	**85**	**60**	**15**	**3**

3.6.2 Column optical aerosol properties measured by ground-based remote sensing at Ny-Ålesund

Key findings *column-integrated optical aerosol properties Ny-Ålesund: In 2019, Ny-Ålesund monthly mean AOD values in most months were close to or smaller than the long-term means. However, in the period July-September, they were more than 2 standard deviations larger than the long-term means. The reason for this is very probably the large-scale boreal forest fires in both Northern Eurasia and North America which were prominent and persistent throughout the 2019 summer season.*

In 2002, Physikalisch-Meteorologisches Observatorium Davos/World Radiation Center (PMOD/WRC), in collaboration with NILU, started AOD observations in Ny-Ålesund (at the Sverdrup station, 46 m a.s.l.) as part of the global AOD network on behalf of the WMO GAW program. A precision filter radiometer (PFR) measures the extinction in four narrow spectral bands at 368 nm, 415 nm, 500 nm and 862 nm. Data quality control includes instrumental control like detector temperature and solar pointing control as well as objective cloud screening. Ångström coefficients are derived for each set of measurements using all four PFR channels. Calibration is performed annually at PMOD/WRC. Quality assured data are available at the World Data Centre of Aerosols (WDCA), hosted at NILU (see https://ebas.nilu.no). In order to calculate a daily average, at least 50 single measurements are required.

In Ny-Ålesund, the solar elevation is less than 5° before 4 March and after 10 October, limiting the period with suitable sun-photometer observations to the spring-summer-early autumn. In 2019, first usable sun-photometer observations were made on 1 April, while the last usable measurement series was taken on 1 October; reliable AOD values are available on 80 days. The AOD and Ångström coefficients time series of monthly means and standard deviation since the start of measurements in 2002 are shown in Figure 60, while the 2019 values on the background of the average data and their standard deviation from the whole 18-year period (including 2019) are shown in Figure 61. The 2019 monthly mean values and standard deviations for all years are given in Table 6. Data for all years are given in Appendix I.

In order to fill the long data gap during the Arctic winter, a PFR version making use of the moonlight around full moon (Lunar PFR) has been developed and tested by PMOD/WRC since 2015. In 2018, the Lunar PFR was integrated in the Svalbard Integrated Arctic Earth Observing Network (SIOS), and data are made available also for monitoring purposes. In 2019, lunar observations were performed in January and February; autumn/winter observations were not obtained due to a technical failure, which could be resolved in January 2020. These data are included in Figure 60 and Figure 61, as well as in the data tables.

The 2019 observations reveal a situation which has occurred repeatedly in recent years, namely very low AOD values in late winter and spring, but clearly elevated AOD in summer and early autumn. However, in 2019 the high-AOD observations in summer were not limited to few days, but persisted over weeks, leading to the highest July and August monthly means ever observed with values of 0.20 and 0.19, respectively. Also the September monthly mean was rather large (about 2 standard deviations above the long-term mean), but not the highest observed so far. The highest AOD daily mean of 0.45 was observed on 7 July 2020. The lowest monthly mean was observed in June with a value of 0.05. In contrast to AOD, Ångström exponent monthly means showed no prominent features and were all within the standard deviations of the long-term means.

The lunar PFR data from January and February appear reasonable compared to (the few) previous winter observations and somewhat lower than the more frequent March observations. However, the number of observations in these months is still too low to draw any quantitative conclusions.

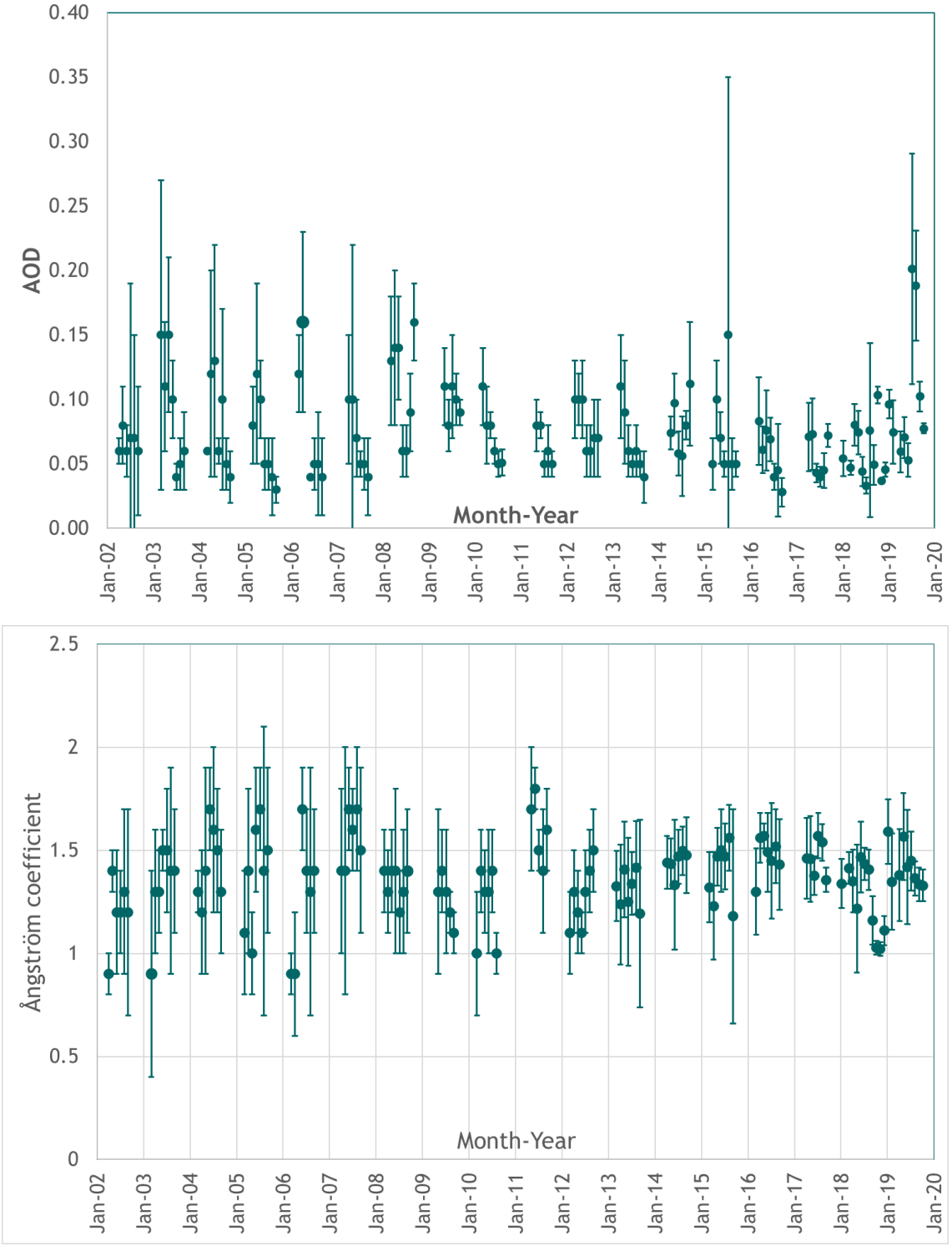

Figure 60: 2002 - 2019 time series of aerosol optical depth (AOD) at 500.5 nm wavelength in the atmospheric column above Ny-Ålesund (upper panel) and Ångström coefficient (lower panel). Monthly mean values and standard deviations are given.

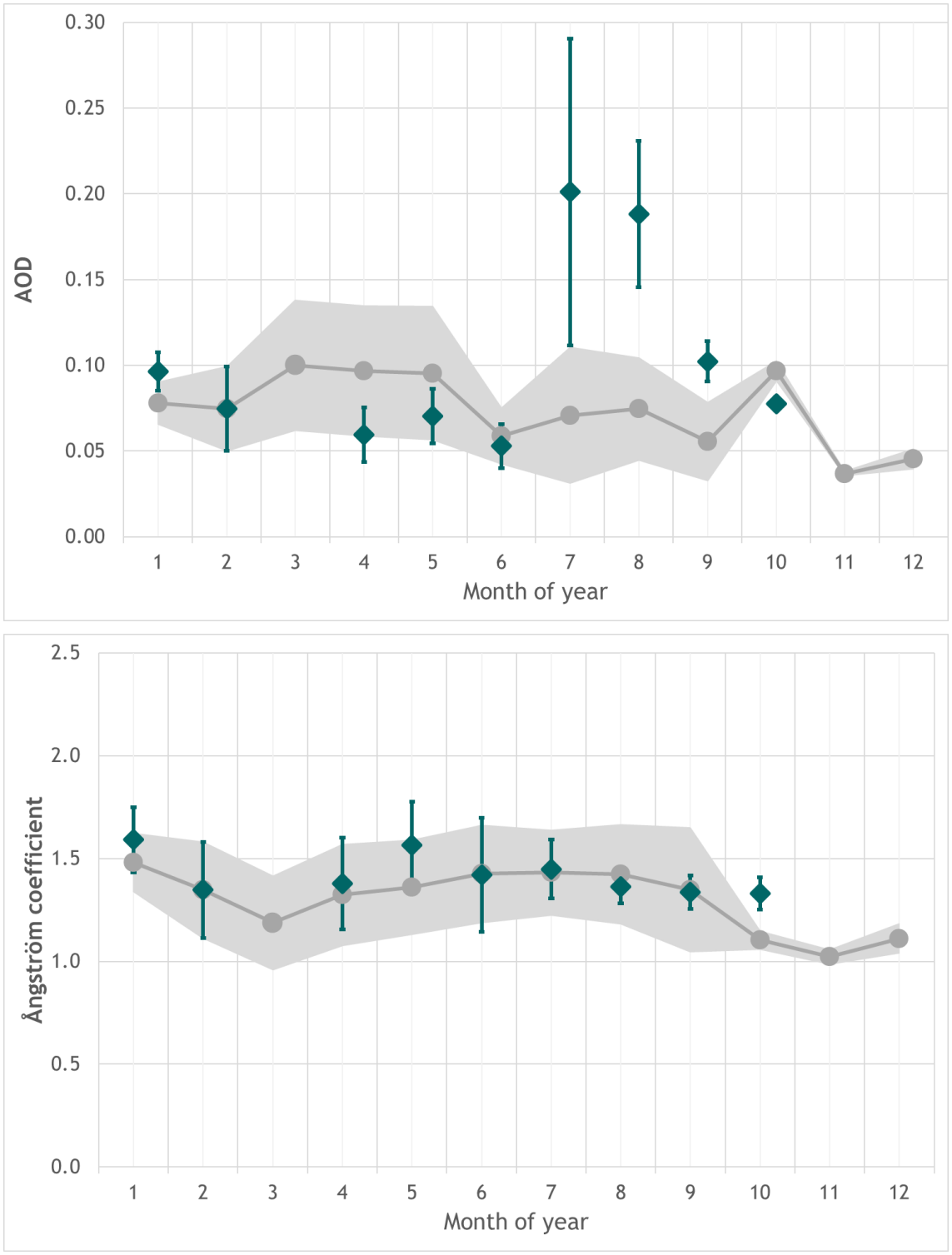

Figure 61: Seasonal variation of the aerosol optical depth (AOD) (upper panel) and Ångström coefficient (lower panel) observed in Ny-Ålesund in 2019. Values marked in grey are the mean and standard deviations for the time period 2002-2019; the 2019 monthly mean and standard deviations are shown in green.

Table 6: Monthly mean values for 2019 and mean for the time period 2002-2019, plus standard deviations, for aerosol optical depth (AOD) and Ångström coefficient observed in Ny-Ålesund. In addition, the number of days with cloud free and quality assured observations are given. Values in January, February, November and December, and partially in March and October, are derived from lunar PFR observations.

	Jan	Feb	Mar	Apr	May	Jun	Jul	Aug	Sep	Oct	Nov	Dec
Aerosol optical depth (AOD)												
2019	**0.10 ±0.01**	**0.07 ±0.02**		**0.06 ±0.02**	**0.07 ±0.02**	**0.05 ±0.01**	**0.20 ±0.09**	**0.19 ±0.04**	**0.10 ±0.01**	**0.08 ±0.00**		
Mean 02-19	**0.08 0.01**	**0.07 ±0.02**	**0.10 ±0.04**	**0.10 ±0.04**	**0.10 ±0.04**	**0.06 ±0.02**	**0.07 ±0.04**	**0.07 ±0.03**	**0.06 ±0.02**	**0.10 ±0.01**	**0.04 ±0.00**	**0.05 ±0.01**
Ångström coefficient (Å)												
2019	**1.59 ± 0.16**	**1.35 ± 0.23**		**1.238 ± 0.22**	**1.57 ± 0.21**	**1.42 ± 0.28**	**1.45 ± 0.14**	**1.36 ± 0.08**	**1.34 ± 0.08**	**1.33 ± 0.08**		
Mean 02-19	**1.48 ±0.14**	**1.35 ±0.23**	**1.19 ±0.23**	**1.32 ±0.24**	**1.36 ±0.23**	**1.43 ±0.24**	**1.43 ±0.21**	**1.42 ±0.24**	**1.35 ±0.30**	**1.10 ±0.04**	**1.02 ±0.03**	**1.11 ± 0.07**
Number of days with cloud-free and quality assured observations (AERONET level 2)												
2019	**9**	**3**		**10**	**19**	**18**	**9**	**16**	**7**	**1**		
Total 02-19	**16**	**3**	**70**	**207**	**204**	**193**	**209**	**168**	**133**	**3**	**2**	**2**

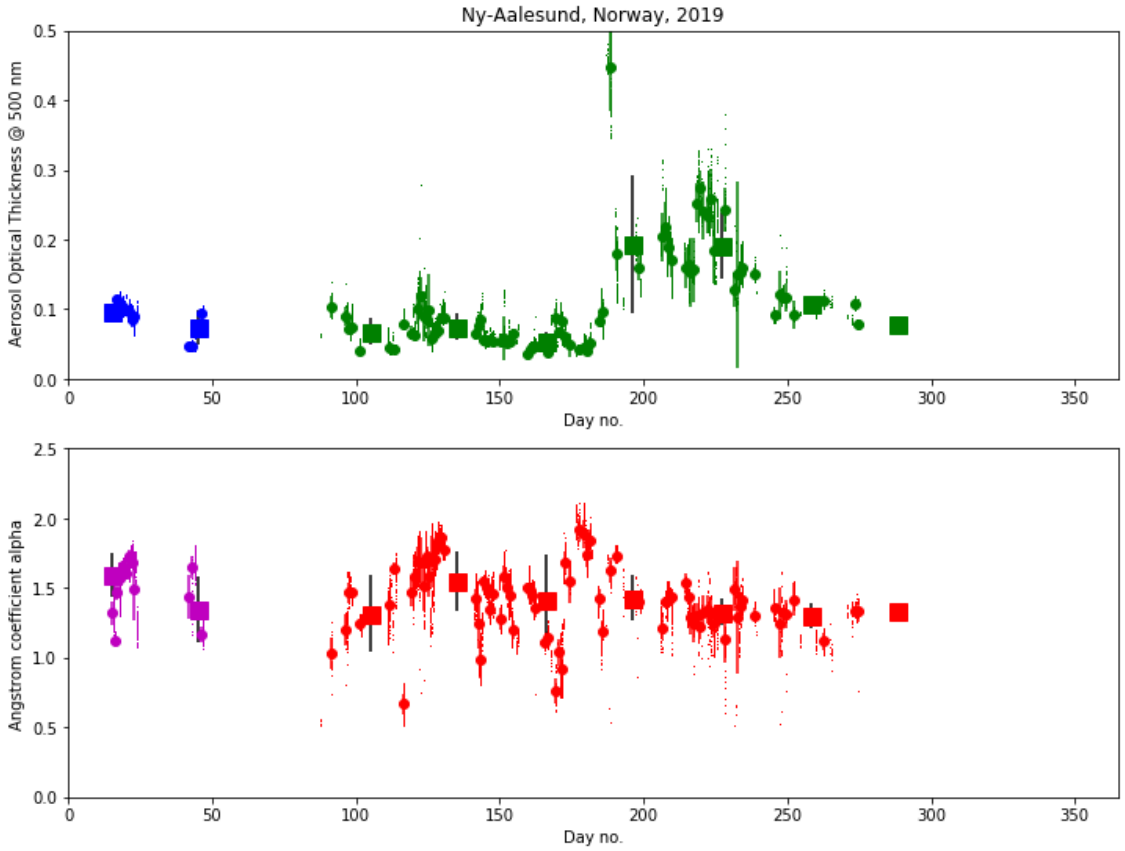

Figure 62: AOD and AE data, combining solar (green, red) and lunar (blue, magenta) observations. Single measurements are marked by dots, daily averages by filled circles and monthly means by filled squares. Standard deviations of single measurements used for means calculations are marked by error bars.

3.6.3 Column optical aerosol properties measured by ground-based remote sensing at Troll Station, Antarctica

In austral summer 2006/2007, NILU established an atmospheric observatory at the Norwegian Troll Station (72°01'S, 2°32'E, 1270 m a.s.l.). During the first years of operation, the observatory was located close to the main building of Troll, which caused frequent episodes of local pollution inhibiting aerosol and pollution measurements which focus on long-range transport. For this reason, in January 2014, the atmospheric monitoring station was moved to Trollhaugen, which is more than 2 km away from the main station and at an elevation of more than 280 m above the station. The original instrumentation included a sun PFR instrument from PMOD/WRC (instrument #513); it has been operated quasi-continuously since, but with largely improved measurement statistics after the move of the atmospheric observatory to Trollhaugen.

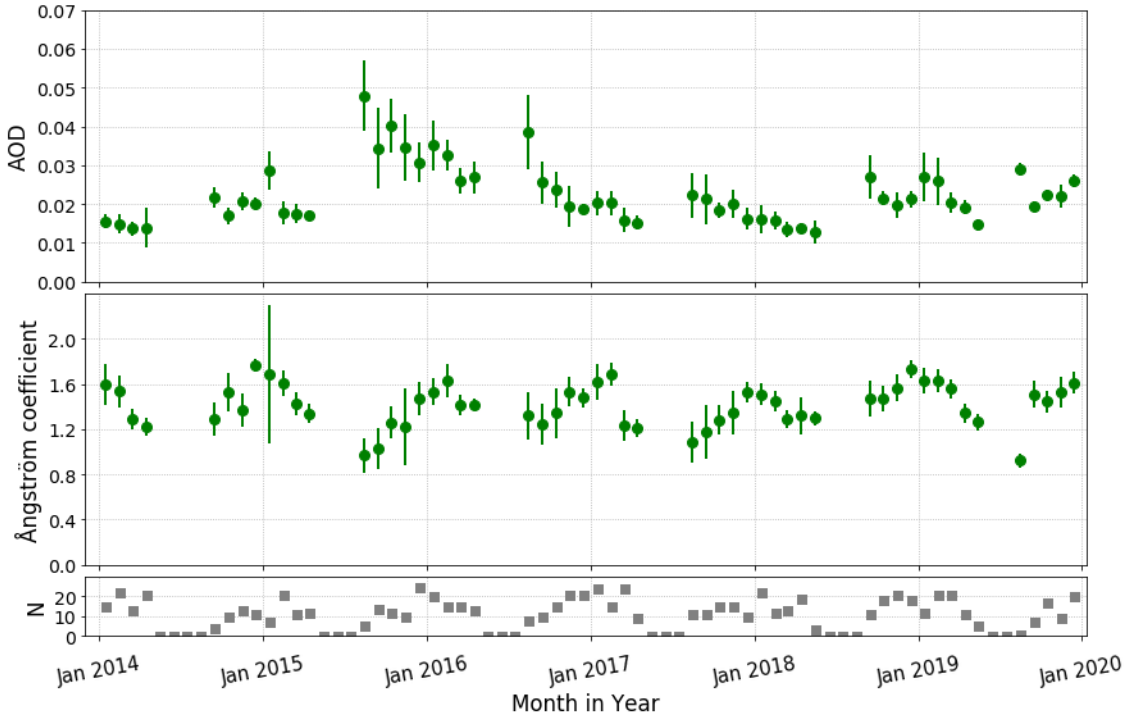

Figure 63: 2014 - 2019 time series of aerosol optical depth (AOD) at 500.5 nm wavelength in the atmospheric column above Trollhaugen Observatory, Antarctica (upper panel), Ångström coefficient (centre panel), and number of days per month with measurements. Monthly mean values and standard deviations are given

Here we present the measurements collected since the move, i.e., from the years 2014 to 2019. Figure 58 shows the series of monthly means of both AOD at 500.5 nm, the multi-wavelength Ångström coefficient, and the number of days with usable observations. Generally, the AOD values are significantly lower than at high Northern latitudes. Most months exhibit mean values between 0.013 and 0.023, except the austral spring and autumn in 2015/2016 and a few other outliers. In most years, the January-April values (autumn) are lower than the August-December (spring) values. The standard deviations of the means are markedly smaller than at Northern hemisphere (including Arctic) stations. Ångström exponents vary between ca. 1.2 and 1.7, again except the second half of 2015 with values down to 1.1. The number of measurements is generally lower after austral winter (August - November) than before; this may be due to the enhanced presence of stratospheric clouds in austral winter which are filtered out by cloud algorithms.

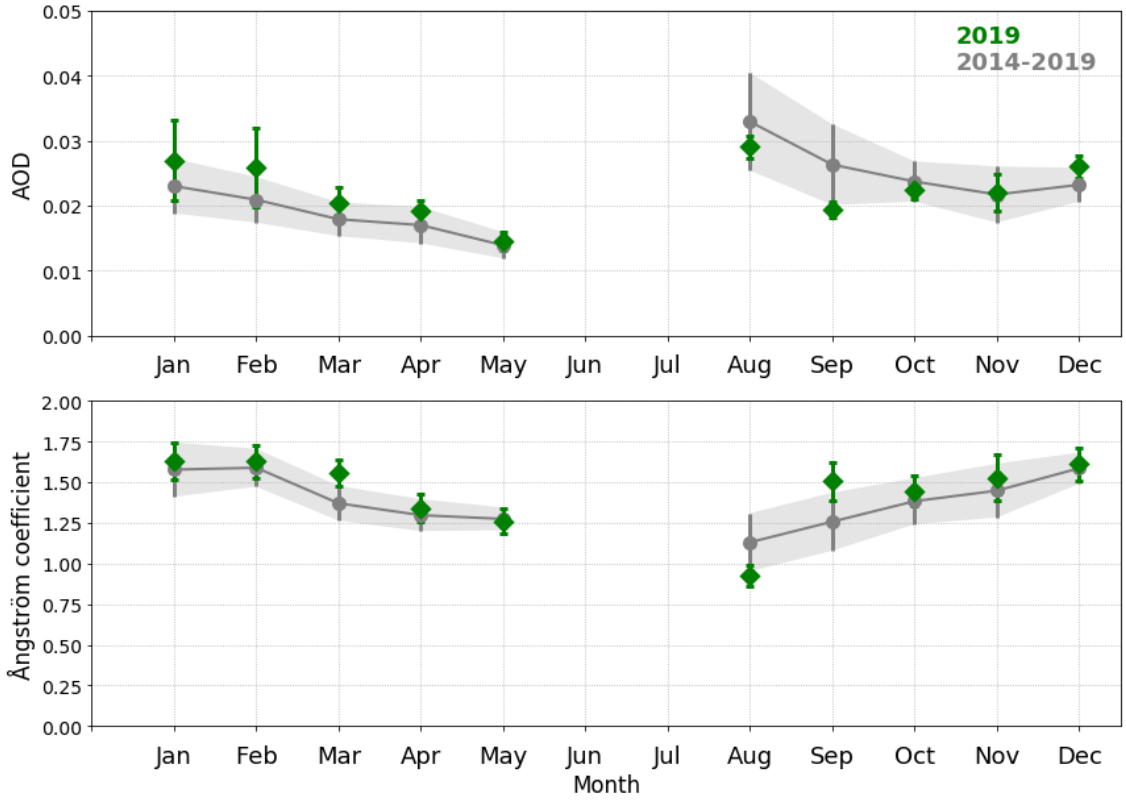

Figure 64: Seasonal variation of the aerosol optical depth (AOD) (upper panel) and Ångström coefficient (lower panel) observed at Troll Station, Antarctica. Values marked in grey are the mean and standard deviations for the time period 2009-2019; the 2019 monthly mean and standard deviations are shown in green.

Figure 64 shows the seasonal variation of AOD and Ångström coefficient for 2019 and the average values over the 6-year series with standard deviations. While the AOD monthly means in the first half of 2019 (i.e., austral summer/autumn) were generally larger than in the 6-year record, values were mostly below the 6-year mean after the austral winter (September – December). In January and February, the somewhat higher monthly AOD means are caused by two marked episodes of AOD values of up to 0.045 (which is quite high at this pristine site) around 16 January and 7 February, as one can see in Figure 65. It might be worth investigating whether these are related to biomass burning in the Southern hemisphere, e.g., bush and forest fires in Australia. The Ångström exponent values were mostly somewhat larger than the multi-annual mean except in March and September, when they were significantly larger and outside the standard deviation range.

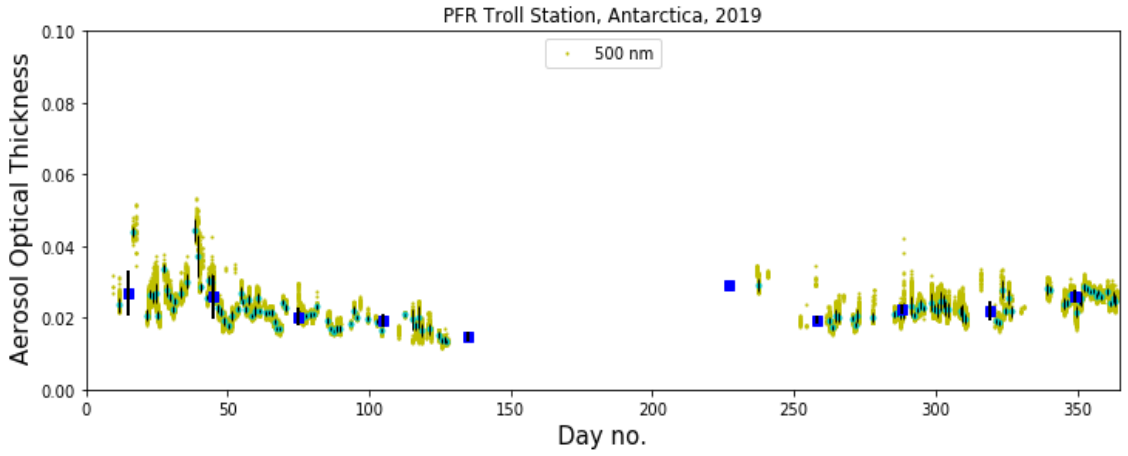

Figure 65: Aerosol optical depth (AOD) observations from Troll. The graph shows both monthly means (dark blue squares), daily means with variations (light blue marks with black "error" bars) and single measurements (yellow-green marks).

Table 7: Monthly mean values for 2019 and means for the time period 2014-2019 plus standard deviations, for aerosol optical depth (AOD) and Ångström coefficient observed at Trollhaugen Observatory. In addition, the number of days with cloud-free and quality-assured observations is given.

	Jan	Feb	Mar	Apr	May	Jun	Jul	Aug	Sep	Oct	Nov	Dec
Aerosol optical depth (AOD)												
2019	**0.027 ±0.006**	**0.026 ±0.006**	**0.020 ±0.003**	**0.019 ±0.002**	**0.014 ±0.001**			**(0.029 ±0.001)**	**0.019 ±0.001**	**0.022 ±0.001**	**0.022 ±0.003**	**0.026 ±0.002**
Mean 14-19	**0.023 ±0.004**	**0.021 ±0.004**	**0.018 ±0.003**	**0.017 ±0.003**	**0.015 ±0.001**			**0.033 ±0.008**	**0.026 ±0.006**	**0.024 ±0.003**	**0.022 ±0.004**	**0.023 ±0.003**
Ångström coefficient (Å)												
2019	**1.63 ± 0.11**	**1.63 ± 0.10**	**1.56 ± 0.08**	**1.34 ± 0.08**	**1.26 ± 0.08**			**(0.92 ± 0.01)**	**1.51 ± 0.12**	**1.44 ± 0.09**	**1.53 ± 0.14**	**1.61 ± 0.10**
Mean 14-19	**1.58 ±0.17**	**1.59 ±0.12**	**1.37 ±0.11**	**1.30 ±0.10**	**1.26 ±0.08**			**1.13 ±0.18**	**1.26 ±0.18**	**1.38 ±0.14**	**1.45 ±0.17**	**1.59 ± 0.10**
Number of days with cloud-free and quality assured observations (AERONET level 2)												
2019	**12**	**21**	**21**	**11**	**5**			**1**	**7**	**17**	**9**	**20**
Total 14-19	**100**	**108**	**98**	**88**	**8**			**25**	**58**	**89**	**89**	**110**

3.7 Summary of aerosol column properties

As pointed out in the introduction, this kind of measurements gives information about the total load of aerosols in the radiation path between the sun (or another external light source, like the moon and bright stars) and the instrument. This necessitates an extremely careful and frequent calibration of the instrument and regular updates on the respective external light source. The only solution to fulfil these criteria has been to have dual instruments at sites with continuous light (Birkenes) and very limited accessibility (Troll), and complementary instruments at sites with long periods without the main light source (the sun; Ny-Ålesund). From the end of 2018, this has been in place at all our sites.

With respect to Birkenes, there is no statistically significant trend in the eleven years of AOD observations, which is not surprising, taking into account the large variability both on an annual and monthly basis between 2009 and 2015. The most remarkable feature in the 2019 data is the high load of aerosols during parts of the summer, but also in February and April. All of these coincide with severe forest fires in parts of Scandinavia and other areas in Eurasia.

Also in Ny-Ålesund, the 2019 monthly mean AOD values are characterized by very high values during summer, while in other months they are markedly below the long-term average. The high summer AOD values can be directly connected to very severe forest fires both in Northern Russia and the Northern regions of North America. In contrast to previous years the aerosol load persisted over a long time (more than 2 months).

AOD observations at the Trollhaugen Observatory in Antarctica in 2019 mostly fit into the picture of an extremely clean atmosphere at this site, with monthly average AOD values below 0.02. However, also here episodes with significantly enhanced AOD (up to 0.045) occurred in austral summer, and an influence of the increasing number and severity of forest fires in SH regions (South America, South Africa, Australia) cannot be excluded.

4 References

Aas, Wenche, S. Eckhardt, M. Fiebig (2020) Monitoring of long-range transported air pollutants in Norway. Annual Report 2019. Kjeller, NILU (NILU report, 4/2020) (Miljødirektoratet rapport, M-1710/2020).

Asmi, A., Collaud Coen, M., Ogren, J. A., Andrews, E., Sheridan, P., Jefferson, A., Weingartner, E., Baltensperger, U., Bukowiecki, N., Lihavainen, H., Kivekäs, N., Asmi, E., Aalto, P. P., Kulmala, M., Wiedensohler, A., Birmili, W., Hamed, A., O'Dowd, C., G Jennings, S., Weller, R., Flentje, H., Fjaeraa, A. M., Fiebig, M., Myhre, C.E.L., Hallar, A. G., Swietlicki, E., Kristensson, A., Laj, P. (2013) Aerosol decadal trends - Part 2: In-situ aerosol particle number concentrations at GAW and ACTRIS stations. *Atmos. Chem. Phys.*, *13*, 895-916. doi:10.5194/acp-13-895-2013.

Baasandorj, M., Hall, B. D., Burkholder, J. B. (2012) Rate coefficients for the reaction of $O(^1D)$ with the atmospherically long-lived greenhouse gases NF_3, SF_5CF_3, CHF_3, C_2F_6, c-C_4F_8, *n*-C_5F_{12}, and *n*-C_6F_{14}. *Atmos. Chem. Phys., 12,* 11753-11764. doi:10.5194/acp-12-11753-2012.

Coen, M. Collaud., Andrews, E., Alastuey, A., Arsov, T. P., Backman, J., Brem, B. T., Bukowiecki, N., Couret, C., Eleftheriadis, K., Flentje, H., Fiebig, M., Gysel-Beer, M., Hand, J. L., Hoffer, A., Hooda, R., Hueglin, C., Joubert, W., Keywood, M., Kim, J. E., Kim, S.-W., Labuschagne, C., Lin, N.-H., Lin, Y., Lund Myhre, C., Luoma, K., Lyamani, H., Marinoni, A., Mayol-Bracero, O. L., Mihalopoulos, N., Pandolfi, M., Prats, N., Prenni, A. J., Putaud, J.-P., Ries, L., Reisen, F., Sellegri, K., Sharma, S., Sheridan, P., Sherman, J. P., Sun, J., Titos, G., Torres, E., Tuch, T., Weller, R., Wiedensohler, A., Zieger, P. and Laj, P. (2020) Multidecadal trend analysis of in situ aerosol radiative properties around the world. *Atmos. Chem. Phys., 20,* 8867-8908. doi: 10.5194/acp-20-8867-2020.

Coen, M. C., Andrews, E., Asmi, A., Baltensperger, U., Bukowiecki, N., Day, D., Fiebig, M., Fjaeraa, A. M., Flentje, H., Hyvärinen, A., Jefferson, A., Jennings, S. G., Kouvarakis, G., Lihavainen, H., Myhre, C. L, Malm, W. C., Mihapopoulos, N., Molenar, J. V., O'Dowd, C., Ogren, J. A., Schichtel, B. A., Sheridan, P., Virkkula, A., Weingartner, E., Weller, R., Laj, P. (2013) Aerosol decadal trends - Part 1: In-situ optical measurements at GAW and IMPROVE stations. *Atmos. Chem. Phys., 13,* 869-894. doi:10.5194/acp-13-869-2013.

Coen, M.C., Weingartner, E., Apituley, A., Ceburnis, D., Fierz-Schmidhauser, R., Flentje, H., Henzing, J. S. (2010) Minimizing light absorption measurement artifacts of the Aethalometer: evaluation of five correction algorithms. *Atmos. Meas. Tech, 3,* 457–474. doi: 10.5194/amt-3-457-2010.

Dalsøren, S. B., Myhre, C. L., Myhre, G., Gomez-Pelaez, A. J., Søvde, O. A., Isaksen, I. S. A., Weiss, R. F., Harth, C. M. (2016) Atmospheric methane evolution the last 40 years. *Atmos. Chem. Phys., 16,* 3099-3126. doi:10.5194/acp-16-3099-2016.

Dalsøren, S. D., Myhre, G., Hodnebrog, Ø., Myhre, C. L., Stohl, A., Pisso, I., Schwietzke, S., Höglund-Isaksson, L., Helmig, D., Reimann, S., Sauvage, S., Schmidbauer, N., Read, K. A., Carpenter, L. J., Lewis, A. C., Punjabi, S., Wallasch, M. (2018) Discrepancy between simulated and observed ethane and propane levels explained by underestimated fossil emissions. *Nature Geosci., 11,* 178-184. doi:10.1038/s41561-018-0073-0.

Delene, D.J., Ogren, J.A. (2002) Variability of aerosol optical properties at four North American surface monitoring sites. *J. Atmos. Sci., 59,* 1135-1150.

Dlugokencky, E.J., Hall, B. D., Montzka, S. A., Dutton, G., Mühle, J., Elkins, J. W. (2019) Long-lived greenhouse gases [in “State of the Climate in 2019”]. *Bull. Amer. Meteor. Soc.,* 101, No 8, S48–52. doi: 10.1175/2020BAMSStateoftheClimate.1.

Dlugokencky, E.J., Hall, B. D., Montzka, S. A., Dutton, G., Mühle, J., Elkins, J. W. (2018) Long-lived greenhouse gases [in “State of the Climate in 2017”]. *Bull. Amer. Meteor. Soc.,* 99, S46-49. doi:10.1175/2018BAMSStateoftheClimate.1.

Drinovec, L., Močnik, G., Zotter, P., Prévôt, A. S. H., Ruckstuhl, C., Coz, E., Rupakheti, M., Sciare, J., Müller, T., Wiedensohler, A., Hansen, A. D. A. (2015) The "dual-spot" Aethalometer: an improved measurement of aerosol black carbon with real-time loading compensation. *Atmos. Meas. Tech, 8,* 1965-1979. doi:10.5194/amt-8-1965-2015.

Etiope, G., Ciccioli, P. (2009) Earth's Degassing: A Missing Ethane and Propane Source. *Science 323,* 478. doi:10.1126/science.1165904.

Etminan, M.,Myhre, G., Highwood, E. J., Shine, K. P. (2016) Radiative forcing of carbon dioxide, methane, and nitrous oxide: A significant revision of the methane radiative forcing, *Geophys. Res. Lett*., 43, 12,614-12,623, doi:10.1002/ 2016GL071930.

Fiebig, M., Hirdman, D., Lunder, C. R., Ogren, J. A., Solberg, S., Stohl, A., Thompson, R. L. (2014) Annual cycle of Antarctic baseline aerosol: controlled by photooxidation-limited aerosol formation. *Atmos. Chem. Phys., 14,* 3083-3093. doi: 10.5194/acp-14-3083-2014

Fisher, R. E., France, J. L., Lowry, D., Lanoisellé, M., Brownlow, R., Pyle, J. A., Cain, M., Warwick, N., Skiba, U. M., Drewer, J., Dinsmore, K. J., Leeson, S. R., Bauguitte, S. J.-B., Wellpott, A., O'Shea, S. J., Allen, G., Gallagher, M. W., Pitt, J., Percival, C. J., Bower, K., George, C., Hayman, G. D., Aalto, T., Lohila, A., Aurela, M., Laurila, T., Crill, P. M., McCalley, C. K. and Nisbet, E. G. (2017) Measurement of the 13C isotopic signature of methane emissions from northern European wetlands. *Global Biogeochem. Cycles, 31,* 605-623, doi:10.1002/2016GB005504.

France, J. L., Cain, M., Fisher, R. E., Lowry, D., Allen, G., O'Shea, S. J., Illingworth, S., Pyle, J., Warwick, N., Jones, B. T., Gallagher, M. W., Bower, K., Le Breton, M., Percival, C., Muller, J., Welpott, A., Bauguitte, S., George, C., Hayman, G. D., Manning, A. J., Myhre, C. L., Lanoisellé, M., Nisbet, E. G. (2016) Measurements of δ 13C in CH4 and using particle dispersion modeling to characterize sources of Arctic methane within an air mass. *J. Geophys. Res. Atmos., 121,* 14,257-14,270, doi:10.1002/2016JD026006.

Gliß, J., Mortier, A., Schulz, M., Andrews, E., Balkanski, Y., Bauer, S. E., Benedictow, A. M. K., Bian, H., Checa-Garcia, R., Chin, M., Ginoux, P., Griesfeller, J. J., Heckel, A., Kipling, Z., Kirkevåg, A., Kokkola, H., Laj, P., Le Sager, P., Lund, M. T., Lund Myhre, C., Matsui, H., Myhre, G., Neubauer, D., van Noije, T., North, P., Olivié, D. J. L., Sogacheva, L., Takemura, T., Tsigaridis, K. and Tsyro, S. G. (2020) Multi-model evaluation of aerosol optical properties in the AeroCom phase III Control experiment, using ground and space based columnar observations from AERONET, MODIS, AATSR and a merged satellite product as well as surface in-situ observations from GAW sites. *Atmos. Chem. Phys*., doi: 10.5194/acp-2019-1214.

IPCC (2013) Summary for policymakers. In: *Climate Change 2013: The Physical Science Basis. Contribution of Working Group I to the Fifth Assessment Report of the Intergovernmental Panel on Climate Change*. Ed. by Stocker, T.F., Qin, D., Plattner, G.-K., Tignor, M., Allen, S.K., Boschung, J., Nauels, A., Xia, Y., Bex, V., Midgley, P.M. Cambridge, Cambridge University Press. pp. 3-29.

Hall, B. D., Montzka, S. A., Dutton, G., Mühle, J., Elkins, J. W. (2017) Long-lived greenhouse gases [in "State of the Climate in 2016"]. *Bull. Amer. Meteor. Soc., 98* (8), S43-S46, doi:10.1175 /2017BAMSStateoftheClimate.1.

Hall, B. D., Montzka, S. A., Dutton, G., Miller, B. R., Elkins, J. W. (2020) Ozone-depleting substances [in "State of the Climate in 2019"]. *Bull. Amer. Meteor. Soc., 101* (8), S75-S76, https://doi.org/10.1175/BAMS-D-20-0104.1

Hartmann, D.L., Klein Tank, A. M. G., Rusticucci, M., Alexander, L.V., Brönnimann, S., Charabi, Y., Dentener, F. J., Dlugokencky, E. J., Easterling, D. R., Kaplan, A., Soden, B. J., Thorne, P. W., Wild, M., Zhai, P. M. (2013) Observations: atmosphere and surface. In: *Climate Change 2013: The Physical Science Basis. Contribution of Working Group I to the Fifth Assessment Report of the Intergovernmental Panel on Climate Change*. Ed. by Stocker, T. F., Qin, D., Plattner, G.-K., Tignor,

M., Allen, S. K., Boschung, J., Nauels, A., Xia, Y., Bex, V., Midgley, P.M. Cambridge, Cambridge University Press. pp. 159-254.

Heintzenberg, J. (1980) Particle size distribution and optical properties of Arctic haze. *Tellus, 32,* 251-260. doi: 10.3402/tellusa.v32i3.10580

Helmig, D., Rossabi, S., Hueber, J., Tans, P., Montzka, S. A., Masarie, K., Thoning, K., Plass-Duelmer, C., Claude, A., Carpenter, L. J., Lewis, A. C., Punjabi, S., Reimann, S., Vollmer, M. K., Steinbrecher, R., Hannigan, J. W., Emmons, L. K., Mahieu, E., Franco, B., Smale, D., Pozzer, A. (2016) Reversal of global atmospheric ethane and propane trends largely due to US oil and natural gas production. *Nature Geosci., 9,* 490-495. doi:10.1038/ngeo2721.

Hewitt, C. Nicholas (ed.) (1999) Reactive Hydrocarbons in the Atmosphere. San Diego, CA, Academic Press. p. 313.

Hodnebrog, Ø., M. Etminan J. S. Fuglestvedt G. Marston G. Myhre C. J. Nielsen K. P. Shine T. J. Wallington Global warming potentials and radiative efficiencies of halocarbons and related compounds: A comprehensive review, (2013) *Reviews of Geophysics*, *51,* 300-378. doi./10.1002/rog.20013

Hossaini, R., Chipperfield, M. P., Montzka, S. A., Leeson, A. A., Dhomse, S. and Pyle, J. A (2017) The increasing threat to stratospheric ozone from dichloromethane. *Nat. Commun., 8,* 15962, doi:10.1038/ncomms15962.

Isaksen, I. S. A., Hov, Ø. (1987) Calculation of trends in the tropospheric concentration of O_3, OH, CO, CH_4 and NO_x. *Tellus*, *39B*, 271-285.

Jackson, R.B., Saunois, M., Bousquet, P., Canadell, J.G., Poulter, B., Stavert, A.R., Bergamaschi, P., Niwa,Y., Segers, A., and Tsuruta, A. (2020) *Environ. Res. Lett., 15,* 071002. doi:10.1088/1748-9326/ab9ed2

Laj, P., Bigi, A., Rose, C. Andrews, E. Lund Myhre, C. Collaud Coen, M. Lin, Y. Wiedensohler, A. Schulz, M. Ogren, J. A. Fiebig, M. Gliß, J. Mortier, A. Pandolfi, M. Petäja, T. Kim, S.-W. Aas, W. Putaud, J.-P. Mayol-Bracero, O. Keywood, M., Labrador, L. Aalto, P. Ahlberg, E. Alados Arboledas, L. Alastuey, A. Andrade, M. Artíñano, B. Ausmeel, S. Arsov, T. Asmi, E. Backman, J. Baltensperger, U., Bastian, S., Bath, O., Beukes, J. P., Brem, B. T., Bukowiecki, N., Conil, S., Couret, C., Day, D., Dayantolis, W., Degorska, A., Eleftheriadis, K., Fetfatzis, P., Favez, O., Flentje, H., Gini, M. I., Gregorič, A., Gysel-Beer, M., Hallar, A. G., Hand, J., Hoffer, A., Hueglin, C., Hooda, R. K., Hyvärinen, A., Kalapov, I., Kalivitis, N., Kasper-Giebl, A., Kim, J. E., Kouvarakis, G., Kranjc, I., Krejci, R., Kulmala, M., Labuschagne, C., Lee, H.-J., Lihavainen, H., Lin, N.-H., Löschau, G., Luoma, K., Marinoni, A., Martins Dos Santos, S., Meinhardt, F., Merkel, M., Metzger, J.-M., Mihalopoulos, N., Nguyen, N. A., Ondracek, J., Pérez, N., Perrone, M. R., Petit, J.-E., Picard, D., Pichon, J.-M., Pont, V., Prats, N., Prenni, A., Reisen, F., Romano, S., Sellegri, K., Sharma, S., Schauer, G., Sheridan, P., Sherman, J. P., Schütze, M., Schwerin, A., Sohmer, R., Sorribas, M., Steinbacher, M., Sun, J., Titos, G., Toczko, B., Tuch, T., Tulet, P., Tunved, P., Vakkari, V., Velarde, F., Velasquez, P., Villani, P., Vratolis, S., Wang, S.-H., Weinhold, K., Weller, R., Yela, M., Yus-Diez, J., Zdimal, V., Zieger, P., and Zikova, N. (2020) A global analysis of climate-relevant aerosol properties retrieved from the network of Global Atmosphere Watch (GAW) near-surface observatories. *Atmos. Meas Tech., 13*, 4353-4392, doi: 10.5194/amt-13-4353-2020.

Montzka, S. A., Dutton, G. S., Yu, P., Ray, E., Portmann, R. W., Daniel, J. S., Kuijpers, L., Hall, B. D., Mondeel, D., Siso, Nance, J. D., Rigby, M., Manning, A. J., Hu, L., Moore, F., Miller, B. R., Elkins, J. W. (2018) An unexpected and persistent increase in global emissions of ozone-depleting CFC-11. *Nature, 557,* 413-417.

Mortier, A., Gliss, J., Schulz, M., Aas, W., Andrews, E., Bian, H., Chin, M., Ginoux, P., Hand, J., Holben, B., Hua, Z., Kipling, Z., Kirkevåg, A., Laj, P., Lurton, T., Myhre, G., Neubauer, D., Olivié, D., von Salzen, K., Takemura, T. and Tilmes, S. (2020) Evaluation of climate model aerosol trends with

ground-based observations over the last two decades -- an AeroCom and CMIP6 analysis. *Atmos. Chem. Phys*. doi: 10.5194/acp-2019-1203.

Myhre, C. L., Hermansen, O., Fiebig, M., Lunder, C., Fjæraa, A. M., Svendby, T., Platt, M., Hansen. G., Schmidbauer, N., Krognes, T. (2016) Monitoring of greenhouse gases and aerosols at Svalbard and Birkenes in 2015 - Annual report. Kjeller, NILU (Miljødirektoratet rapport, M-694/2016) (NILU report, 31/2016).

Myhre, C. L., Ferré, B., Platt, S. M., Silyakova, A., Hermansen, O., Allen, G., Pisso, I., Schmidbauer, N., Stohl, A., Pitt, J., Jansson, P., Greinert, J., Percival, C., Fjaeraa, A. M., O'Shea, S., Gallagher, M., Le Breton, M., Bower, K., Bauguitte, S., Dalsøren, S., Vadakkepuliyambatta, S., Fisher, R., Nisbet, E., Lowry, D., Myhre, G., Pyle, J., Cain, M., Mienert, J. (2016) Large methane release from the Arctic seabed west of Svalbard, but small release to the atmosphere. *Geophys. Res. Lett*., *43,* 4624–4631. doi:10.1002/2016GL068999.

Myhre, G., Myhre C. L., Forster, P. M., Shine, K. P. (2017) Halfway to doubling of CO2 radiative forcing. *Nature Geosci., 10,* 710--711. doi:10.1038/ngeo3036.

Myhre, G., Myhre, C. L., Samset, B. H., Storelvmo, T. (2013a) Aerosols and their relation to global climate and climate sensitivity. *Nature Education Knowledge, 4,* 5,7. URL: http://www.nature.com/scitable/knowledge/library/aerosols-and-their-relation-to-global-climate-102215345

Myhre, G., Shindell, D., Bréon, F.-M., Collins, W., Fuglestvedt, J., Huang, J., Koch, D., Lamarque, J.-F., Lee, D., Mendoza, B., Nakajima, T., Robock, A., Stephens, G., Takemura, T., Zhang, H. (2013b) Anthropogenic and natural radiative forcing. In: *Climate Change 2013: The Physical Science Basis. Contribution of Working Group I to the Fifth Assessment Report of the Intergovernmental Panel on Climate Change*. Ed. by Stocker, T.F., Qin, D., Plattner, G.-K., Tignor, M., Allen, S.K., Boschung, J., Nauels, A., Xia, Y., Bex, V., Midgley, P.M. Cambridge, Cambridge University Press. pp. 659-740.

Ng, N. L., Kroll, J.H., Chan, A. W. H., Chhabra, P. S., Flagan, R. C., Seinfeld, J. H. (2007) Secondary organic aerosol formation from m-xylene, toluene, and benzene. *Atmos. Chem. Physics, 7,* 3909–3922.

Nicewonger, M. R., Verhulst, K. R., Aydin, M., Saltzman, E. S. (2016) Preindustrial atmospheric ethane levels inferred from polar ice cores: A constraint on the geologic sources of atmospheric ethane and methane. *Geophys. Res. Lett., 43,* 214-221. doi:10.1002/2015GL066854.

Oram, D. E., Mani, F. S., Laube, J. C., Newland, M. J., Reeves, C. E., Sturges, W. T., Penkett, S. A., Brenninkmeijer, C. A. M., Röckmann, T., and Fraser, P. J. (2012) Long-term tropospheric trend of octafluorocyclobutane (c-C_4F_8 or PFC-318), *Atmos. Chem. Phys., 12,* 261-269. doi:10.5194/acp-12-261-2012.

Platt, S. M., Eckhardt, S., Ferré, B., Fisher, R. E., Hermansen, O., Jansson, P., Lowry, D., Nisbet, E. G., Pisso, I., Schmidbauer, N., Silyakova, A., Stohl, A., Svendby, T. M., Vadakkepuliyambatta, S., Mienert, J., and Lund Myhre, C. (2018) Methane at Svalbard and over the European Arctic Ocean. *Atmos. Chem. Phys., 18,* 17207--17224. 10.5194/acp-18-17207-2018

Prather, M., Ehhalt, D., Dentener, F., Derwent, R. G., Dlugokencky, E., Holland, E., Isaksen, I. S. A., Katima, J., Kirchhoff, V., Matson, P., Midgley, P. M., Wang, M. (2001) Atmospheric chemistry and greenhouse gases. In: *Climate Change 2001: The Scientific Basis, Contribution of Working Group I to the Third Assessment Report of the Intergovernmental Panel on Climate Change.* Ed. by: Houghton, J. T., Ding, Y., Griggs, D. J., Noguer, M., van der Linden, P. J., Dai, X., Maskell, K., Johnson, C. A. Cambridge, Cambridge University Press. pp. 239-287.

Pisso, I., Myhre, C. L., Platt, S. M., Eckhardt, S., Hermansen, O., Schmidbauer, N., Mienert, J., Vadakkepuliyambatta, S., Bauguitte, S., Pitt, J., Allen, G., Bower, K.N., O'Shea, S., Gallagher, M. W., Percival, C.J., Pyle, J., Cain, M., Stohl, A. (2016) Constraints on oceanic methane emissions west of

Svalbard from atmospheric in situ measurements and Lagrangian transport modelling. *J. Geophys. Res., 121,* 14188-14200. doi:10.1002/2016JD025590.

R Core Team (2018) R: A language and environment for statistical computing. Vienna, Austria, R Foundation for Statistical Computing. URL: https://www.R-project.org/.

Ramonet, M. , P. Ciais, F. Apadula, J. Bartyzal, Bartyzel, , A. Bastos, , P. Bergamaschi, P.E. Blanc, D. Brunner, L. C. di Torchiarolo, F. Calzolari, H. Chen, L. Chmura, A. Colomb, S. Conil, P. Cristofanelli, E. Cuevas, R. Curcoll, M. Delmotte1, A. di Sarra, L. Emmenegger, G. Forster, A. Frumau, C. Gerbig, F. Gheusi, S. Hammer, L. Haszpra12, J. Hatakka, L. Hazan, M. Heliasz, S. Henne, A. Hensen, O. Hermansen, P. Keronen, R.Kivi, K. Komínková, D. Kubistin, O. Laurent, T. Laurila, J.V. Lavric, I. Lehner, K.E.J. Lehtinen, A. Leskinen, M. Leuenberger, I. Levin, M. Lindauer, M. Lopez, C. LundMyhre, I. Mammarella, G. Manca, A. Manning, M.V. Marek, P. Marklund, D. Martin, F. Meinhardt, N. Mihalopoulos, M. Mölder, J.A. Morgui, J. Necki, S. O'Doherty, C. O'Dowd, M. Ottosson, C. Philippon, S. Piacentino, J.M. Pichon, C. Plass-Duelmer, A. Resovsky, L.Rivier, X. Rodó, M.K. Sha, H.A. Scheeren, D. Sferlazzo, T.G. Spain, K.M. Stanley, M. Steinbacher, P. Trisolino, A. Vermeulen, G. Vítková, D. Weyrauch, I. Xueref-Remy, K. Yala, C. Yver Kwok. The fingerprint of the summer 2018 drought in Europe on ground-based atmospheric CO2 measurements. *Phil.l Trans. R. Soc. B, 375,* 20190513. doi:10.1098/rstb.2019.0513

Repo, M. E., Susiluoto, S., Lind, S. E., Jokinen, S., Elsakov, V., Biasi, C., Virtanen, T., Pertti, J., Martikainen, P. J. (2009) Large N_2O emissions from cryoturbated peat soil in tundra. *Nature Geosci., 2*, 189-192. doi: 10.1038/ngeo434.

Rigby, M., Park, S., Saito, T., Western, L. M., Redington, A. L., Fang, X. , Henne, S., Manning, A. J., Prinn, R. G., Dutton, G. S., Fraser, P. J., Ganesan, A. L., Hall, B. D., Harth, C. M., Kim, J., Kim, K.-R., Krummel, P. B., Lee, T., Li, S., Liang, Q., Lunt, M. F., Montzka, S. A., Mühle, J., O'Doherty, S., Park, M.-K., Reimann, S., Salameh, P. K., Simmonds, P., Tunnicliffe, R. L., Weiss, R. F., Yokouchi, Y. , Young, D. (2019) Increase in CFC-11 emissions from eastern China based on atmospheric observations. *Nature*, *569*, 546-550. doi: 10.1038/s41586-019-1193-4 .

Saunois, M., Stavert, A. R., Poulter, B., Bousquet, P., Canadell, J. G., Jackson, R. B., Raymond, P. A., Dlugokencky, E. J., Houweling, S., Patra, P. K., Ciais, P., Arora, V. K., Bastviken, D., Bergamaschi, P., Blake, D. R., Brailsford, G., Bruhwiler, L., Carlson, K. M., Carrol, M., Castaldi, S., Chandra, N., Crevoisier, C., Crill, P. M., Covey, K., Curry, C. L., Etiope, G., Frankenberg, C., Gedney, N., Hegglin, M. I., Höglund-Isaksson, L., Hugelius, G., Ishizawa, M., Ito, A., Janssens-Maenhout, G., Jensen, K. M., Joos, F., Kleinen, T., Krummel, P. B., Langenfelds, R. L., Laruelle, G. G., Liu, L., Machida, T., Maksyutov, S., McDonald, K. C., McNorton, J., Miller, P. A., Melton, J. R., Morino, I., Müller, J., Murguia-Flores, F., Naik, V., Niwa, Y., Noce, S., O'Doherty, S., Parker, R. J., Peng, C., Peng, S., Peters, G. P., Prigent, C., Prinn, R., Ramonet, M., Regnier, P., Riley, W. J., Rosentreter, J. A., Segers, A., Simpson, I. J., Shi, H., Smith, S. J., Steele, L. P., Thornton, B. F., Tian, H., Tohjima, Y., Tubiello, F. N., Tsuruta, A., Viovy, N., Voulgarakis, A., Weber, T. S., van Weele, M., van der Werf, G. R., Weiss, R. F., Worthy, D., Wunch, D., Yin, Y., Yoshida, Y., Zhang, W., Zhang, Z., Zhao, Y., Zheng, B., Zhu, Q., Zhu, Q., and Zhuang, Q. (2020), The Global Methane Budget 2000–2017. *Earth Syst. Sci. Data, 12,* 1561-1623. doi:10.5194/essd-12-1561-2020.

Simmonds, P. G., Manning, A. J., Cunnold, D. M., Fraser, P. J., McCulloch, A., O'Doherty, S., Krummel, P. B., Wang, R. H. J., Porter, L. W., Derwent, R. G., Greally, B., Salameh, P., Miller, B. R., Prinn, R. G., Weiss, R. F. (2006) Observations of dichloromethane, trichloroethene and tetrachloroethene from the AGAGE stations at Cape Grim, Tasmania, and Mace Head, Ireland. *J. Geophys. Res., 111*, D18304. doi:10.1029/2006JD007082.

Svendby, Tove M., G. H. Hansen, A. Bäcklund, and A.-C. Nilsen (2020) Monitoring of the atmospheric ozone layer and natural ultraviolet radiation. Annual report 2019. Kjeller, NILU (Norwegian Environment Agency report, M-1768) (NILU report 11/2020).

Thompson R.L. G. Broquet, C. Gerbig, T. Koch, M. Lang, G. Monteil, S. Munassar, A. Nickless, M. Scholze, M. Ramonet, U. Karstens, E. van Schaik, Z. Wu and C. Rödenbeck, (2020) Changes in net ecosystem exchange over Europe during the 2018 drought based on atmospheric observations. *Phil. Trans. R. Soc. B, 375,* 20190512. doi:10.1098/rstb.2019.0512

Thompson, R. L., Sasakawa, M., Machida, T., Aalto, T., Worthy, D., Lavric, J. V., Myhre, C. L., Stohl, A. (2017) Methane fluxes in the high northern latitudes for 2005–2013 estimated using a Bayesian atmospheric inversion. *Atmos. Chem. Phys.*, 17, 3553-3572. doi:10.5194/acp-2016-660.

Thompson, R. L., Dlugockenky, E., Chevallier, F., Ciais, P., Dutton, G., Elkins, J. W., Langenfelds, R. L., Prinn, R. G., Weiss, R. F., Tohjima, Y., Krummel, P. B., Fraser, P., Steele, L. P. (2013) Interannual variability in tropospheric nitrous oxide. *Geophys. Res. Lett, 40*, 4426-4431. doi:10.1002/grl.50721.

Tørseth, K., Aas, W., Breivik, K., Fjæraa, A. M., Fiebig, M., Hjellbrekke, A. G., Myhre, C. L., Solberg, S., Yttri, K. E. (2012) Introduction to the European Monitoring and Evaluation Programme (EMEP) and observed atmospheric composition change during 1972–200. *Atmos. Chem. Phys., 12,* 5447-5481. doi:10.5194/acp-12-5447-2012.

Umezawa, T., Baker, A. K., Oram, D., Sauvage, C., O'Sullivan, D., Rauthe-Schöch, A., Montzka, S. A., Zahn, A., Brenninkmeijer, C. A. M. (2014) Chloromethane in the upper troposphere observed by the CARIBIC passenger aircraft bservatory: Large-scale distributions and Asian summer monsoon outflow. *J. Geophys. Res. Atmos., 119,* 5542-5558, doi:10.1002/2013JD021396.

Vollmer, M. K., Young, D., Trudinger, C. M., Muhle, J., Henne, S., Rigby, M., Park, S., Li, S., Guillevic, M., Mitrevski, B., Harth, C. M., Miller, B. R., Reimann, S., Yao, B., Steele, L. P., Wyss, S. A., Lunder, C. R., Arduini, J., McCulloch, A., Wu, S., Rhee, T. S., Wang, R. H. J., Salameh, P. K., Hermansen, O., Hill, M., Langenfelds, R. L., Ivy, D., O'Doherty, S., Krummel, P. B., Maione, M., Etheridge, D. M., Zhou, L., Fraser, P. J., Prinn, R. G.; Weiss, R. F., Simmonds, P. G. (2018) Atmospheric histories and emissions of chlorofluorocarbons CFC-13 (CClF3), ΣCFC-114 (C2Cl2F4), and CFC-115 (C2ClF5). *Atmos. Chem. Phys.*, *18*, 979-1002, doi:10.5194/acp-18-979-2018

Wiedensohler, A., Birmili, W., Nowak, A., Sonntag, A., Weinhold, K., Merkel, M., Wehner, B., Tuch, T., Pfeifer, S., Fiebig, M., Fjäraa, A. M., Asmi, E., Sellegri, K., Depuy, R., Venzac, H., Villani, P., Laj, P., Aalto, P., Ogren, J. A., Swietlicki, E., Williams, P., Roldin, P., Quincey, P., Hüglin, C., Fierz-Schmidhauser, R., Gysel, M., Weingartner, E., Riccobono, F., Santos, S., Grüning, C., Faloon, F., Beddows, D., Harrison, R., Monahan, C., Jennings, S. G., O'Dowd, C. D., Marinoni, A., Horn, H.-G., Keck, L., Jiang, J., Scheckman, J., McMurry, P.H., Deng, Z., Zhao, C. S., Moerman, M., Henzing, B., de Leeuw, G., Löschau, G., Bastian, S. (2012) Mobility particle size spectrometers: harmonization of technical standards and data structure to facilitate high quality long-term observations of atmospheric particle number size distributions. *Atmos. Meas. Tech.*, *5,* 657-685. doi:10.5194/amt-5-657-2012.

Wilkinson, M. D., Dumontier, M., Aalbersberg, I. J., Appleton, G., Axton, M., Baak, A., Blomberg, N., Boiten, J. W., Santos, L. B. D., Bourne, P. E., Bouwman, J., Brookes, A. J., Clark, T., Crosas, M., Dillo, I., Dumon, O., Edmunds, S., Evelo, C. T., Finkers, R., Gonzalez-Beltran, A., Gray, A. J. G., Groth, P., Goble, C., Grethe, J. S., Heringa, J., Hoen, P. A. C., Hooft, R., Kuhn, T., Kok, R., Kok, J., Lusher, S. J., Martone, M. E., Mons, A., Packer, A. L., Persson, B., Rocca-Serra, P., Roos, M., van Schaik, R., Sansone, S. A., Schultes, E., Sengstag, T., Slater, T., Strawn, G., Swertz, M. A., Thompson, M., van der Lei, J., van Mulligen, E., Velterop, J., Waagmeester, A., Wittenburg, P., Wolstencroft, K., Zhao, J., and Mons, B. (2016)The FAIR Guiding Principles for scientific data management and stewardship*. Sci. Data, 3,* 160018.doi: /10.1038/sdata.2016.18.

WMO (2019) Greenhouse Gas Bulletin. The state of greenhouse gases in the atmosphere using global observations through 2018. Geneva, World Meteorological Organization (GHG Bulletin No. 15, 25 November 2019). URL: https://library.wmo.int/index.php?lvl=notice_display&id=21620#.X1i3NN7VI2w

WMO (2018) Scientific assessment of ozone depletion: 2018. Geneva, World Meteorological Organization (Global Ozone Research and Monitoring Project-Report No. 58). URL: https://www.esrl.noaa.gov/csd/assessments/ozone/2018/

WMO (2017) Greenhouse Gas Bulletin. The state of greenhouse gases in the atmosphere using global observations through 2016. Geneva, World Meteorological Organization (GHG Bulletin No. 13, 30 October 2017). URL: https://library.wmo.int/opac/doc_num.php?explnum_id=4022

WMO (2016) Greenhouse Gas Bulletin. The state of greenhouse gases in the atmosphere using global observations through 2015. Geneva, World Meteorological Organization (GHG Bulletin No. 12, 24 October 2016). URL: http://library.wmo.int/pmb_ged/ghg-bulletin_12_en.pdf

WMO (2015) Greenhouse Gas Bulletin. The state of greenhouse gases in the atmosphere using global observations through 2014. Geneva, World Meteorological Organization (GHG Bulletin No. 11, 9 November 2015). URL: http://library.wmo.int/pmb_ged/ghg-bulletin_11_en.pdf

WMO (2014) Greenhouse Gas Bulletin. The state of greenhouse gases in the atmosphere using global observations through 2013. Geneva, World Meteorological Organization (GHG Bulletin No. 10, 9 September 2014). URL: http://library.wmo.int/opac/index.php?lvl=notice_display&id=16396#.VGHPz5-gQtK

WMO (2014b) Scientific assessment of ozone depletion: 2014. Geneva, World Meteorological Organization (Global ozone research and monitoring project, Report No. 55). **URL:** https://www.esrl.noaa.gov/csd/assessments/ozone/2014/chapters/2014OzoneAssessment.pdf

WMO (2013) Greenhouse Gas Bulletin. The state of greenhouse gases in the atmosphere using global observations through 2012. Geneva, World Meteorological Organization (GHG Bulletin No. 9, 6 November 2013). URL: http://www.wmo.int/pages/prog/arep/gaw/ghg/documents/GHG_Bulletin_No.9_en.pdf

WMO (2012) Greenhouse Gas Bulletin. The state of greenhouse gases in the atmosphere using global observations through 2011. Geneva, World Meteorological Organization (GHG Bulletin No. 8, 19 November 2012). URL: http://www.wmo.int/pages/prog/arep/gaw/ghg/documents/GHG_Bulletin_No.8_en.pdf

WMO (2011) Scientific assessment of ozone depletion: 2010. Geneva, World Meteorological Organization (Global ozone research and monitoring project, Report No. 52).

Xu, Y., Zaelke, D., Velders, G.J.M., Ramanathan, V. (2013) The role of HFCs in mitigating 21st century climate change. *Atmos. Chem. Phys., 13,* 6083-6089. doi:10.5194/acp-13-6083-2013.

Zeileis A. (2004) Econometric Computing with HC and HAC Covariance Matrix Estimators. *J. Stat. Software*, *11,* 1-17. doi: 10.18637/jss.v011.i10.

Zeileis, A. (2006) Object-oriented computation of sandwich estimators. *J. Stat. Software*, *16,* 1-16. doi:10.18637/jss.v016.i09.

Appendix I

Data Tables

Table A 1: Annual mean concentration for all greenhouse gases included in the programme at Zeppelin and Birkenes. All concentrations are mixing ratios in ppt, except for methane and carbon monoxide (ppb) and carbon dioxide (ppm). The annual means are based on a combination of the measurements and the fitted values; during periods with lacking observations we have used the fitted mixing ratios in the calculation of the annual mean. All underlying measurement data are open and accessible and can be downloaded directly from the database: http://ebas.nilu.no/

Component	2001	2002	2003	2004	2005	2006	2007	2008	2009	2010	2011	2012	2013	2014	2015	2016	2017	2018	2019
Carbon dioxide - Zeppelin												394.8	397.5	399.6	401.4	404.4	408.0	409.3	411.9
Carbon dioxide - Birkenes									391.6	394.0	396.6	397.9	400.7	402.8	405.2	409.8	411.2	415.2	416.1
Methane - Zeppelin	1843.6	1842.8	1855.5	1852.9	1852.4	1853.4	1863.5	1873.3	1888.8	1881.3	1880.0	1892.0	1898.1	1910.0	1920.2	1931.8	1938.9	1938.5	1952.9
Methane - Birkenes									1880.6	1886.9	1895.6	1900.5	1902.5	1917.3	1926.2	1941.9	1945.3	1953.0	1961.2
Carbon monoxide	129.3	126.1	140.2	130.6	128.6	126.4	120.2	120.2	118.0	128.9	116.0	120.7	113.2	113.4	112.8	112.4	114.3	113.6	115.4
Nitrous oxide										323.6	324.2	325.1	326.1	327.2	328.0	329.0	330.0	331.3	332.1
Chlorofluorocarbons																			
CFC-11	259.0	257.2	255.2	253.5	251.3	249.3	246.6	244.7	242.7	240.7	238.4	236.9	235.2	234.0	232.3	231.2	230.1	229.2	228.1
CFC-12	547.2	547.5	547.7	545.7	546.9	546.3	542.3	541.5	537.7	534.4	531.5	528.6	525.4	522.0	518.6	515.9	512.4	508.8	505.7
CFC-113	81.5	80.8	80.0	79.4	78.8	77.9	77.4	76.8	76.2	75.5	74.7	74.1	73.5	73.0	72.3	71.7	71.1	70.6	70.1
CFC-115	8.21	8.18	8.22	8.28	8.42	8.39	8.38	8.40	8.43	8.42	8.41	8.44	8.43	8.45	8.51	8.53	8.59	8.67	8.75
Hydrochlorofluorocarbons																			
HCFC-22	158.8	164.3	170.6	175.7	181.3	189.0	196.2	204.5	212.5	219.8	225.9	231.2	236.5	241.3	245.4	248.8	252.1	253.8	255.7
HCFC-141b	16.8	17.9	18.7	19.2	19.5	19.9	20.5	21.2	21.6	22.2	23.1	24.0	24.7	25.4	25.6	25.9	25.8	25.6	25.7
HCFC-142b	14.4	15.0	15.9	16.6	17.2	18.2	19.3	20.3	21.3	22.0	22.7	23.0	23.3	23.4	23.6	23.5	23.4	23.2	23.1
Hydrofluorocarbons																			
HFC-125	2.2	2.6	2.9	3.3	4.0	4.9	5.8	6.9	8.0	9.6	11.8	13.5	15.6	17.9	20.3	22.9	25.9	28.9	32.3
HFC-134a	21.0	26.0	30.8	35.5	39.9	44.2	48.6	53.5	57.8	63.5	68.5	73.6	78.9	84.5	90.1	96.5	103.1	108.6	114.8
HFC-152a	2.6	3.5	4.3	5.1	5.8	6.8	7.8	8.6	9.0	9.5	10.0	10.2	10.2	10.2	10.1	10.3	10.2	10.3	10.5
HFC-23										23.5	24.7	25.7	26.7	27.7	28.7	29.6	30.7	31.9	33.2

Component	2001	2002	2003	2004	2005	2006	2007	2008	2009	2010	2011	2012	2013	2014	2015	2016	2017	2018	2019
HFC-365mfc										0.74	0.79	0.87	0.92	1.02	1.10	1.19	1.24	1.28	1.31
HFC-227ea										0.71	0.79	0.88	0.99	1.10	1.21	1.34	1.47	1.60	1.76
HFC-236fa										0.09	0.10	0.11	0.13	0.14	0.15	0.16	0.17	0.18	0.20
HFC-245fa										1.58	1.80	1.98	2.20	2.39	2.57	2.79	3.04	3.25	3.53
HFC-32										5.49	6.56	7.70	9.29	10.93	12.83	15.17	18.25	21.52	25.24
HFC-4310mee										0.21	0.22	0.24	0.25	0.26	0.27	0.28	0.28	0.29	0.30
HFC-143a										11.95	13.18	14.56	16.03	17.63	19.10	20.75	22.51	23.90	25.54
Perfluorinated compounds																			
PFC-14															82.42	83.29	84.28	85.25	86.10
PFC-116										4.12	4.20	4.27	4.37	4.45	4.55	4.64	4.74	4.82	4.91
PFC-218										0.56	0.57	0.59	0.60	0.61	0.63	0.64	0.66	0.67	0.69
PFC-318										1.28	1.33	1.38	1.43	1.47	1.53	1.59	1.66	1.73	1.80
Sulphurhexafluoride	4.95	5.14	5.37	5.61	5.82	6.09	6.31	6.64	6.93	7.19	7.50	7.78	8.11	8.43	8.75	9.09	9.46	9.79	10.14
Nitrogen trifluoride																1.61	1.76	1.98	2.22
Sulfuryl fluoride										1.73	1.81	1.91	2.03	2.12	2.22	2.33	2.45	2.53	2.63
Halons																			
H-1211	4.39	4.43	4.48	4.53	4.52	4.48	4.43	4.39	4.33	4.26	4.18	4.09	3.97	3.87	3.77	3.65	3.55	3.45	3.37
H-1301	2.99	3.07	3.14	3.17	3.21	3.22	3.24	3.28	3.29	3.32	3.33	3.35	3.36	3.37	3.39	3.38	3.39	3.38	3.39
H-2402										0.47	0.46	0.45	0.44	0.43	0.43	0.42	0.41	0.41	0.41
Other halocarbons																			
Chloromethane	506.5	521.2	526.4	522.7	519.2	520.8	523.2	525.0	526.3	520.7	509.6	515.2	519.1	514.4	512.5	521.7	516.7	514.4	508.0
Bromomethane	9.08	9.12	8.88	8.88	8.55	8.58	8.33	7.78	7.37	7.29	7.20	7.05	6.98	6.86	6.67	6.73	6.56	6.58	6.78
Dichloromethane	31.74	31.57	32.33	32.16	31.83	33.33	35.34	37.50	38.58	42.19	42.14	45.28	53.72	54.44	54.14	56.63	61.26	60.73	58.89
Trichloromethane	11.18	10.71	10.66	10.31	10.33	10.41	10.58	10.41	10.87	11.53	11.99	12.23	12.77	13.50	13.69	14.25	15.31	14.70	12.20
Carbon tetrachloride										86.63	85.28	84.46	83.50	82.51	81.71	80.60	79.44	78.78	78.02

Component	2001	2002	2003	2004	2005	2006	2007	2008	2009	2010	2011	2012	2013	2014	2015	2016	2017	2018	2019
Trichloroethane	37.94	32.02	27.28	22.87	19.17	15.95	13.33	11.07	9.23	7.74	6.48	5.37	4.51	3.79	3.33	2.82	2.34	2.00	1.71
Trichloroethene*	0.74	0.67	0.56	0.51	0.50	0.47	0.33	0.37	0.53	0.54	0.55	0.49	0.55	0.50	0.45	0.42	0.38	0.27	0.16
Tetrachloroethene**	4.69	4.22	4.06	3.87	3.37	2.91	3.13	2.71	2.97	3.13	2.83	2.68	2.55	2.58	2.60	2.56	2.48	2.30	2.27
Volatile Organic Compounds (VOC)																			
Ethane										1472.0	1471.9	1583.0	1568.8	1647.5	1638.8	1580.8	1576.8	1524.9	1602.4
Propane										498.4	528.4	565.8	578.9	571.5	543.9	565.8	582.9	499.3	454.7
Butane										177.5	187.1	199.0	204.3	193.2	182.2	167.6	192.9	143.5	140.1
Pentane										58.9	61.4	63.2	67.7	64.3	62.0	57.9	60.8	38.9	43.8
Benzene										84.8	72.7	74.3	69.5	71.4	68.3	67.5	62.5	62.9	61.1
Toluene										34.9	29.3	28.6	26.7	28.7	26.0	25.7	18.2	21.0	18.9

*Trichloroethene: Larger uncertainties in the numbers due to low concentrations, memory effects and blanks in the instrument. The reference numbers (scale UB-98) have also larger uncertainties for the same reasons.
**Tetrachloroethene: Larger uncertainties in the 2001-2010 numbers due to larger variability in the measurements with the ADS-GCMS instrument.

Table A 2: All calculated trends per year, error and regression coefficient for the fit. The trends are all in ppt per year, except for CH_4, N_2O, and CO which are in ppb and CO_2 is in ppm. The negative trends are in blue, and the positive trends are shown in red. Generally the period is from 2001 to 2018, but for some compounds the measurements started after September 2010. For these compounds the trends are in general more uncertain.

Component	Formula	Trend /yr	Error	R^2
Carbon dioxide - Zeppelin	CO_2	2.46	0.04	0.96
Carbon dioxide - Birkenes		2.54	0.06	0.75
Methane - Zeppelin	CH_4	6.15	0.10	0.90
Methane - Birkenes		8.38	0.24	0.65
Carbon monoxide	CO	-1.17	0.22	0.80
Nitrous oxide	N_2O	0.98	0.01	0.99
Chlorofluorocarbons				
CFC-11	CCl_3F	-1.79	0.008	0.99
CFC-12	CF_2Cl_2	-2.51	0.025	0.98
CFC-113	CF2ClCFCl2	-0.64	0.002	0.99
CFC-115	CF_3CF_2Cl	0.02	0.001	0.73
Hydrochlorofluorocarbons				
HCFC-22	$CHClF_2$	5.81	0.031	0.997
HCFC-141b	$C_2H_3FCl_2$	0.53	0.020	0.971
HCFC-142b	CH_3CF_2Cl	0.54	0.011	0.987
Hydrofluorocarbons				
HFC-125	CHF_2CF_3	1.65	0.006	0.999
HFC-134a	CH_2FCF_3	5.14	0.009	0.999
HFC-152a	CH_3CHF_2	0.43	0.011	0.965
HFC-23	CHF_3	1.04	0.003	0.998
HFC-365mfc	$CH_3CF_2CH_2CF_3$	0.07	0.000	0.981
HFC-227ea	CF_3CHFCF_3	0.12	0.000	0.998
HFC-236fa	$CF_3CH_2CF_3$	0.01	0.000	0.985
HFC-245fa	$CHF_2CH_2CF_3$	0.21	0.001	0.997
HFC-32	CH_2F_2	2.15	0.007	0.999
HFC-4310mee	$C_5H_2F_{10}$	0.01	0.000	0.936
HFC-143a	CH_3CF_3	1.53	0.004	0.997
Perfluorinated compounds				
PFC-14	CF_4	0.893	0.1109	0.995
PFC-116	C_2F_6	0.089	0.0003	0.996
PFC-218	C_3F_8	0.014	0.0001	0.976
PFC-318	c-C_4F_8	0.057	0.0002	0.995
Sulphurhexafluoride	SF_6	0.291	0.0004	0.999
Nitrogen trifluoride	NF_3	0.204	0.0818	0.991
Sulfuryl fluoride	SO_2F_2	0.102	0.0009	0.993

Component	Formula	Trend /yr	Error	R^2
Halons				
H-1211	$CBrClF_2$	-0.065	0.0003	0.995
H-1301	$CBrF_3$	0.020	0.0004	0.776
H-2402	$CBrF_2CBrF_2$	-0.007	0.0001	0.961
Halogenated compounds				
Chloromethane	CH_3Cl	-0.373	0.2145	0.871
Bromomethane	CH_3Br	-0.161	0.0056	0.885
Dichloromethane	CH_2Cl_2	1.927	0.0613	0.934
Trichloromethane	$CHCl_3$	0.242	0.0220	0.691
Carbon tetrachloride	CCl_4	-0.954	0.0182	0.935
Trichloroethane	CH_3CCl_3	-1.807	0.0083	0.999
Trichloroethene*	$CHClCCl_2$	-0.017	0.0035	0.396
Tetrachloroethene**	CCl_2CCl_2	-0.111	0.0076	0.512
Volatile Organic Compounds (VOC)				
Ethane***	C_2H_6	9.76	4.12	0.88
Propane***	C_3H_8	-2.96	3.13	0.82
Butane***	C_4H_{10}	-4.78	1.48	0.74
Pentane***	C_5H_{12}	-2.03	0.54	0.68
Benzene***	C_6H_6	-2.08	0.43	0.87
Toluene***	$C_6H_5CH_3$	-1.51	0.37	0.71

**Trichloroethene: Larger uncertainties in the numbers due to low concentrations, memory effects and blanks in the instrument. The reference numbers (scale UB-98) have also larger uncertainties for the same reasons.*

***Tetrachloroethene: Larger uncertainties in the 2001-2010 numbers due to larger variability in the measurements with the ADS-GCMS instrument.*

**** Larger uncertainty for VOC due to shorter timeseries*

Table A 3: 2010 - 2019 seasonal and annual means of integral particle concentrations in the ultrafine, fine and coarse particle size range for Birkenes, Trollhaugen, and Zeppelin stations, as far as available.

		Birkenes				Trollhaugen[1]		Zeppelin	
Year	Season	N_{ait} / cm^{-3}	N_{acc} / cm^{-3}	N_{coa} / cm^{-3}	N_{tot} / cm^{-3}	N_{ait} / cm^{-3}	$^{2}N_{acc}$ / cm^{-3}	N_{ait} / cm^{-3}	$^{2}N_{acc}$ / cm^{-3}
2009/10	Winter	440	384	0.087	824				
2010	Spring	1030	324	0.311	1354				
2010	Summer	1511	488	0.323	1999				
2010	Autumn	835	299	0.260	1135				
2010	Whole Year	973	362	0.256	1336				
2010/11	Winter	454	285	0.311	739				
2011	Spring	1127	369	0.639	1496				
2011	Summer	1391	438	0.572	1829				
2011	Autumn	1594	464	0.966	2059				
2011	Whole Year	1047	371	0.565	1418				
2011/12	Winter	424	213	0.305	637				
2012	Spring	1107	271	0.386	1378				
2012	Summer	1314	392	0.485	1706				
2012	Autumn	661	152	0.365	814				
2012	Whole Year	889	263	0.375	1152				
2012/13	Winter	383	183	0.183	566				
2013	Spring	1190	352	0.411	1543				
2013	Summer	1519	447	0.467	1967				
2013	Autumn	701	162	0.417	864				
2013	Whole Year	1020	304	0.391	1324				
2013/14	Winter	699	333	0.347	1033				
2014	Spring	1464	402	0.334	1866	183	32		
2014	Summer	1723	625	0.343	2349	43	19		
2014	Autumn	1122	446	0.385	1568	207	28		
2014	Whole Year	1279	456	0.338	1735	183	34		
2014/15	Winter	549	192	0.307	741	368	67		
2015	Spring	1425	332	0.348	1757	134	25		
2015	Summer	1979	559	0.395	2539	38	23		
2015	Autumn	1130	422	0.257	1553	221	28		
2015	Whole Year	1326	390	0.340	1717	171	32		
2015/16	Winter	542	233	0.297	776				
2016	Spring	1328	442	0.449	1770	170	26		
2016	Summer	1455	484	0.517	1940	47	18	156	64
2016	Autumn	895	290	0.312	1185	262	35	47	31
2016	Whole Year	1063	357	0.392	1421	231	37	---	---
2016/17	Winter	526	223	0.232	750	473	74	---	---
2017	Spring	855	216	0.271	1072	157	31	96	126
2017	Summer	1605	402	0.424	2007	51	20	282	70
2017	Autumn	852	250	0.228	1103	265	27	56	63
2017	Whole Year	943	272	0.267	1216	238	38	---	---
2017/18	Winter	450	244	0.092	694	482	78	27	44
2018	Spring	1370	589	---	1960	170	24	107	85
2018	Summer	1910	537	---	2449	45	18	225	66
2018	Autumn	915	195	---	1112	273	28	30	25
2018	Whole Year	1151	444	---	1596	233	35	92	55
2018/19	Winter	545	229	---	774	427	64	18	60
2019	Spring	1268	450	---	1718	183	25	78	95
2019	Summer	1683	457	---	2140	34	14	224	68
2019	Autumn	726	167	---	893	233	29	29	28
2019	Whole Year	1049	321	---	1369	202	31	87	64

[1] Cells shaded in grey mark values obtained with an older instrument version that can't be compared directly with later values. Numbers given for the time when the respective season is present in the Northern hemisphere. Actual seasons in Southern hemisphere are shifted by 6 months.

[2]The accumulation mode integral particle concentration N_{acc} at Trollhaugen and Zeppelin extends only up to 0.8 µm particle diameter due to lack of an instrument covering larger particles. For Birkenes, N_{acc} includes particles up to 1 µm diameter

Table A 4: 2010 - 2019 seasonal and annual means of optical aerosol properties scattering coefficient, absorption coefficient, and single scattering albedo for Birkenes, Trollhaugen, and Zeppelin stations, as far as available.

		Birkenes			Trollhaugen[1]			Zeppelin		
Year	Season	σ_{sp} (550 nm) / Mm^{-1}	σ_{ap} (550 nm) / Mm^{-1}	ϖ_0 (550 nm)	σ_{sp} (550 nm) / Mm^{-1}	σ_{ap} (550 nm) / Mm^{-1}	ϖ_0 (550 nm)	σ_{sp} (550 nm) / Mm^{-1}	σ_{ap} (550 nm) / Mm^{-1}	ϖ_0 (550 nm)
2009/10	Winter	16.82	3.09	0.88						
2010	Spring	12.33	0.78	0.93						
2010	Summer	11.30	0.70	0.94						
2010	Autumn	7.26	0.71	0.90						
2010	Whole Year	11.52	1.24	0.91						
2010/11	Winter	16.96	2.18	0.89						
2011	Spring	18.67	1.26	0.93						
2011	Summer	15.43	0.74	0.95						
2011	Autumn	29.74	2.87	0.92						
2011	Whole Year	20.26	1.69	0.93						
2011/12	Winter	11.29	1.00	0.91						
2012	Spring	15.10	0.86	0.93						
2012	Summer	12.62	0.67	0.95						
2012	Autumn	9.80	0.65	0.92						
2012	Whole Year	12.22	0.83	0.92						
2012/13	Winter	12.48	1.84	0.84						
2013	Spring	17.03	1.48	0.90						
2013	Summer	13.81	1.15	0.92						
2013	Autumn	8.89	1.25	0.85						
2013	Whole Year	13.73	1.40	0.88						
2013/14	Winter	22.89	2.64	0.87						
2014	Spring	12.95	2.09	0.87	0.74	-0.05	0.95			
2014	Summer	15.85	1.26	0.92	1.39	0.04	0.98			
2014	Autumn	18.76	3.41	0.82	1.02	0.15	0.93			
2014	Whole Year	16.99	2.30	0.87	1.01	0.09	0.95			
2014/15	Winter	13.98	1.30	0.89	0.74	0.04	0.94			
2015	Spring	12.72	1.48	0.89	0.65	0.02	0.97			
2015	Summer	12.45	1.46	0.90	2.44	0.02	0.98		0.30	
2015	Autumn	15.69	2.45	0.95	1.32	0.07	0.94		0.14	
2015	Whole Year	14.36	1.56	0.90	1.32	0.04	0.96			
2015/16	Winter	13.59	1.24	0.88	0.87	0.05	0.94		0.38	
2016	Spring	14.86	1.10	0.91	0.78	0.17	0.97		0.39	
2016	Summer	11.93	0.77	0.94	2.01	0.00	0.99		0.09	
2016	Autumn	11.47	1.46	0.85	1.54	0.04	0.95		0.12	
2016	Whole Year	12.26	1.12	0.89	1.31	0.06	0.97		0.24	
2016/17	Winter	12.27	2.24	0.81	0.82	0.05	0.94		0.40	
2017	Spring	8.71			0.76	0.02	0.97		0.48	
2017	Summer	8.58			1.57	0.01	0.99		0.10	
2017	Autumn	8.09	1.21	0.85	1.22	0.05	0.94		0.29	
2017	Whole Year	9.07			1.10	0.03	0.96		0.33	
2017/18	Winter	13.56	1.66	0.83	0.72	0.04	0.95		0.34	
2018	Spring	17.10	2.45	0.87	0.60	0.03	0.97		0.32	
2018	Summer	13.62	1.23	0.91	1.78	0.06	0.98		0.12	
2018	Autumn	14.08	2.04	0.86	1.31	0.04	0.95		0.10	
2018	Whole Year	14.54	1.90	0.86	1.10	0.04	0.96		0.21	
2018/19	Winter	---	---	---	0.73	0.04	0.94		0.45	
2019	Spring	---	---	---	0.81	0.03	0.97		0.46	
2019	Summer	---	---	---	1.81	0.01	0.99		0.19	
2019	Autumn	6.26	0.93	0.85	1.61	0.04	0.96		0.13	
2019	Whole Year	---	---	---	1.26	0.03	0.97		0.33	

Values stated in cells shaded in grey are re-evaluated according to latest inter-comparisons within ACTRIS and therefore deviate from values given in earlier years.

[1]Numbers given for the time when the respective season is present in the Northern hemisphere. Actual seasons in Southern hemisphere are shifted by 6 months.

Table A 5: Monthly means and standard deviation of aerosol optical depth (AOD) at 500 nm at Ny-Ålesund.

Month/ Year	Jan	Feb	Mar	Apr	May	Jun	Jul	Aug	Sep	Oct	Nov	Dec
Aerosol optical depth (AOD)												
2002				0.06 ±0.01	0.08 ±0.03	0.06 ±0.02	0.07 ±0.12	0.07 ±0.08	0.06 ±0.05			
2003			0.15 ±0.12	0.11 ±0.05	0.15 ±0.06	0.10 ±0.03	0.04 ±0.01	0.05 ±0.02	0.06 ±0.03			
2004			0.06 ±0.00	0.12 ±0.08	0.13 ±0.09	0.06 ±0.01	0.10 ±0.07	0.05 ±0.02	0.04 ±0.02			
2005			0.08 ±0.03	0.12 ±0.07	0.10 ±0.03	0.05 ±0.02	0.05 ±0.02	0.04 ±0.03	0.03 ±0.01			
2006			0.12 ±0.03	0.16 ±0.07		0.04 ±0.00	0.05 ±0.02	0.05 ±0.04	0.04 ±0.03			
2007				0.10 ±0.05	0.10 ±0.12	0.07 ±0.03	0.05 ±0.01	0.05 ±0.02	0.04 ±0.03			
2008			0.13 ±0.05	0.14 ±0.06	0.14 ±0.04	0.06 ±0.02	0.06 ±0.02	0.09 ±0.03	0.16 ±0.03			
2009					0.11 ±0.03	0.08 ±0.02	0.11 ±0.04	0.10 ±0.02	0.09 ±0.01			
2010			0.11±0. 03	0.08 ±0.03	0.08 ±0.01	0.06 ±0.01	0.05 ±0.01	0.05 ±0.01				
2011					0.08 ±0.02	0.08 ±0.01	0.05 ±0.01	0.06 ±0.02	0.05 ±0.01			
2012			0.10 ±0.03	0.10 ±0.02	0.10 ±0.03	0.06 ±0.02	0.06 ±0.02	0.07 ±0.03	0.07 ±0.03			
2013			0.11 ±0.04	0.09 ±0.04	0.06 ±0.02	0.05 ±0.01	0.06 ±0.02	0.05 ±0.01	0.04 ±0.02			
2014				0.07 ±0.01	0.10 ±0.02	0.06 ±0.02	0.06 ±0.03	0.08 ±0.01	0.11 ±0.05			
2015			0.05 ±0.02	0.10 ±0.03	0.07 ±0.02	0.05 ±0.01	0.15 ±0.20	0.05 ±0.02	0.05 ±0.01			
2016			0.08 ±0.03	0.06 ±0.02	0.08 ±0.03	0.07 ±0.02	0.04 ±0.01	0.05 ±0.04	0.03 ±0.01			
2017				0.07 ±0.03	0.07 ±0.03	0.04 ±0.01	0.04 ±0.01	0.05 ±0.01	0.07 ±0.01			
2018	0.05 ±0.01		0.05 ±0.01	0.08 ±0.02	0.07 ±0.02	0.04 ±0.01	0.03 ±0.01	0.08 ±0.07	0.05 ±0.02	0.10 ±0.01	0.04 ±0.00	0.05 ±0.01
2019	0.10 ±0.01	0.07 ±0.02		0.06 ±0.02	0.07 ±0.02	0.05 ±0.01	0.20 ±0.09	0.19 ±0.04	0.10 ±0.01	0.08 ±0.00		
Mean (2002-2019)	**0.08 ±0.01**	**0.07 ±0.02**	**0.10 ±0.04**	**0.10 ±0.04**	**0.10 ±0.04**	**0.06 ±0.02**	**0.07 ±0.04**	**0.07 ±0.03**	**0.06 ±0.02**	**0.10 ±0.01**	**0.04 ±0.00**	**0.05 ±0.01**

Table A 6: Monthly means and standard deviation of the Ångström coefficient (Å) at Ny-Ålesund. There are no observations of this parameter during the winter months due to polar night.

Month/ Year	Jan	Feb	Mar	Apr	May	Jun	Jul	Aug	Sep	Oct	Nov	Dec
Aerosol optical depth (AOD)												
2002				0.9 ±0.1	1.4 ±0.1	1.2 ±0.3	1.2 ±0.2	1.3 ±0.4	1.2 ±0.5			
2003			0.9 ±0.5	1.3 ±0.3	1.3 ±0.2	1.5 ±0.1	1.5 ±0.3	1.4 ±0.5	1.4 ±0.3			
2004			1.3 ±0.1	1.2 ±0.3	1.4 ±0.5	1.7 ±0.2	1.6 ±0.4	1.5 ±0.3	1.3 ±0.3			
2005			1.1 ±0.3	1.4 ±0.4	1.0 ±0.2	1.6 ±0.3	1.7 ±0.2	1.4 ±0.7	1.5 ±0.4			
2006			0.9 ±0.1	0.9 ±0.3		1.7 ±0.2	1.4 ±0.3	1.3 ±0.6	1.4 ±0.3			
2007				1.4 ±0.4	1.4 ±0.6	1.7 ±0.2	1.6 ±0.2	1.7 ±0.3	1.5 ±0.4			
2008			1.4 ±0.2	1.3 ±0.2	1.4 ±0.2	1.4 ±0.4	1.2 ±0.2	1.3 ±0.3	1.4 ±0.3			
2009					1.3 ±0.4	1.4 ±0.2	1.3 ±0.3	1.2 ±0.1	1.1 ±0.1			
2010			1.0 ±0.3	1.4 ±0.2	1.3 ±0.2	1.3 ±0.3	1.4 ±0.2	1.0 ±0.1				
2011					1.7 ±0.3	1.8 ±0.1	1.5 ±0.1	1.4 ±0.3	1.6 ±0.2			
2012			1.1 ±0.2	1.3 ±0.2	1.2 ±0.2	1.1 ±0.1	1.3 ±0.2	1.4 ±0.2	1.5 ±0.2			
2013			1.3 ±0.2	1.2 ±0.3	1.4 ±0.2	1.6 ±0.3	1.3 ±0.2	1.4 ±0.2	1.2 ±0.5			
2014				1.4 ±0.1	1.4 ±0.1	1.3 ±0.3	1.5 ±0.1	1.5 ±0.1	1.5 ±0.2			
2015			1.32 ±0.17	1.23 ±0.26	1.47 ±0.14	1.50 ±0.20	1.47 ±0.16	1.56 ±0.16	1.18 ±0.52			
2016			1.30 ±0.21	1.56 ±0.12	1.57 ±0.06	1.49 ±0.19	1.45 ±0.28	1.52 ±0.18	1.43 ±0.22			
2017				1.46 ±0.20	1.46 ±0.21	1.38 ±0.09	1.57 ±0.11	1.54 ±0.09	1.36 ±0.06			
2018	1.34 ±0.12		1.41 ±0.08	1.35 ±0.15	1.22 ±0.31	1.47 ±0.17	1.43 ±0.08	1.41 ±0.10	1.16 ±0.12	1.03 ±0.03	1.02 ±0.03	1.11 ±0.07
2019	1.59 ± 0.16	1.35 ± 0.23		1.25 ± 0.27	1.47 ± 0.23	1.35 ± 0.23	1.38± 0.18	1.30 ± 0.10	1.28 ± 0.06	1.19 ± 0.12		
Mean (2002-2019)	**1.48 ±0.14**	**1.35 ±0.23**	**1.19 ±0.23**	**1.32 ±0.25**	**1.36 ±0.23**	**1.43 ±0.24**	**1.43 ±0.21**	**1.42 ±0.24**	**1.35 ±0.30**	**1.10 ±0.04**	**1.02 ±0.03**	**1.11 ±0.07**

Table A 7: Number of days with AOD observations at Ny-Ålesund made within the months.

Month/Year	Jan	Feb	Mar	Apr	May	Jun	Jul	Aug	Sep	Oct	Nov	Dec
Number of days with cloud-free and quality assured observations												
2002				4	15	11	6	9	14			
2003			3	12	16	8	15	17	12			
2004			2	8	13	9	5	12	12			
2005			12	17	24	15	10		11			
2006			6	12		5	12	4	13			
2007				16	9	12	17	10	9			
2008			15	12	14	20	16	13	2			
2009					7	10	17	8	8			
2010			7	18	7	10	12	3	1			
2011					2	2	7	4	6			
2012			6	18	12	15	16	11	4			
2013			5	13	10	10	8	7	9			
2014				13	9	9	9	14	4			
2015			5	17	15	9	17	13	6			
2016			6	14	8	7	12	10	7			
2017				13	19	11	12	6	3			
2018	7		3	10	5	12	9	11	5	2	2	2
2019	9	3		10	19	18	9	16	7	1		
Total (2002-2019)	**16**	**3**	**70**	**207**	**204**	**193**	**209**	**168**	**133**	**3**	**2**	**2**

Table A 8: Monthly means and standard deviation of aerosol optical depth (AOD) at 500 nm at Birkenes.

Month/Year	Jan	Feb	Mar	Apr	May	Jun	Jul	Aug	Sep	Oct	Nov	Dec
Aerosol optical depth (AOD)												
2009				0.29 ±0.00	0.09 ±0.05	0.09 ±0.05	0.18 ±0.06	0.17 ±0.07	0.10 ±0.04	0.08 ±0.03		
2010					0.10 ±0.04	0.09 ±0.04	0.10 ±0.07	0.10 ±0.05	0.05 ±0.02	0.07 ±0.03	0.04 ±0.01	
2011	0.02 ±0.01	0.03 ±0.01	0.07 ±0.02	0.21 ±0.19	0.13 ±0.07	0.10 ±0.04	0.13 ±0.06	0.09 ±0.05				
2012			0.07 ±0.05	0.05 ±0.02	0.08 ±0.04	0.09 ±0.04	0.07 ±0.03	0.08 ±0.03	0.07 ±0.01	0.06 ±0.03	0.04 ±0.00	
2013							0.17 ±0.17	0.12 ±0.09	0.05 ±0.03	0.05 ±0.03		
2014			0.15 ±0.14	0.11 ±0.06	0.10 ±0.03	0.08 ±0.03	0.13 ±0.06	0.15 ±0.07	0.14 ±0.06			
2015			0.04 ±0.02	0.07 ±0.02	0.07 ±0.03	0.06 ±0.02	0.10 ±0.07	0.09 ±0.06	0.04 ±0.02	0.03 ±0.03	0.04 ±0.01	
2016	0.01 ±0.00	0.03 ±0.01	0.03 ±0.02	0.05 ±0.03							0.02 ±0.00	
2017*				0.08 ±0.01	0.06 ±0.03	0.04 ±0.03	0.06 ±0.03	0.09 ±0.07	0.09 ±0.03	0.06 ±0.03		
2018*				0.09 ±0.07	0.11 ±0.05	0.07 ±0.06	0.08 ±0.06	0.10 ±0.08	0.06 ±0.04			
2019	0.03 ±0.01	0.07 ±0.09	0.04 ±0.02	0.11 ±0.08	0.06 ±0.03	0.12 ±0.11	0.19 ±0.06	0.16 ±0.04			0.07 ±0.03	0.05 ±0.00
Mean 2009 -2019	**0.02 ±0.01**	**0.04 ±0.04**	**0.07 ±0.04**	**0.10 ±0.06**	**0.09 ±0.04**	**0.08 ±0.05**	**0.12 ±0.07**	**0.12 ±0.06**	**0.08 ±0.03**	**0.06 ±0.03**	**0.04 ±0.01**	**0.05 ±0.00**

* version 3 data analysis (Aeronet)

Table A 9: Monthly means and standard deviation of the Ångström coefficient (Å) at Birkenes

Month/Year	Jan	Feb	Mar	Apr	May	Jun	Jul	Aug	Sep	Oct	Nov	Dec
Ångström coefficient (Å)												
2009				1.5 ±0.0	1.2 ±0.3	1.4 ±0.3	1.4 ±0.4	1.1 ±0.2	1.0 ±0.2	1.1 ±0.2		
2010					1.3 ±0.3	1.4 ±0.3	1.4 ±0.2	1.4 ±0.2	1.3 ±0.3	1.3 ±0.3	1.3 ±0.23	
2011	1.0 ±0.2	1.0 ±0.1	1.0 ±0.3	1.2 ±0.5	1.3 ±0.3	1.5 ±0.3	1.6 ±0.3	1.6 ± 0.1				
2012			1.1 ±0.4	1.6 ±0.3	1.4 ±0.4	1.7 ±0.1	1.6 ±0.3	1.5 ±0.3	1.1 ±0.3	1.4 ±0.4	0.8 ±0.3	
2013							1.3 ± 0.2	1.2 ±0.3	0.8 ±0.2	0.8 ±0.3		
2014			0.87 ±0.48	1.04 ±0.33	1.07 ±0.27	1.02 ±0.24	1.38 ±0.33	1.14 ±0.25	1.19 ±0.16			
2015			0.93 ±0.16	1.06 ±0.13	1.11 ±0.20	1.30 ±0.20	1.49 ±0.20	1.37 ±0.26	1.30 ±0.23	1.23 ±0.25	0.84 ±0.33	
2016	0.68 ±0.07	1.00 ±0.2	0.90 ±0.3	1.13 ±0.2							1.11 ±0.08	
2017*				1.77 ±0.07	1.39 ±0.35	1.39 ±0.37	1.73 ±0.34	1.48 ±0.37	0.93 ±0.18	0.78 ±0.20		
2018				1.02 ± 0.24	1.31 ± 0.25	1.23 ± 0.31	1.54 ± 0.28	1.36 ± 0.23	1.11 ±0.25			
2019	0.83 ±0.23	0.96 ±0.45	1.01 ±0.31	1.47 ± 0.28	1.29 ± 0.23	1.43 ± 0.17	1.60 ± 0.16	1.41 ± 0.15			1.04 ±0.29	1.08 ±0.14
Mean 2009-2019	**0.83 ±0.15**	**1.00 ±0.23**	**0.96 ±0.33**	**1.28 ±0.24**	**1.26 ±0.26**	**1.37 ±0.23**	**1.51 ±0.27**	**1.37 ±0.24**	**1.09 ±0.22**	**1.09 ±0.26**	**1.01 ±0.24**	**1.08 ±0.14**

* version 3 data analysis (Aeronet)

Table A 10: Number of days with AOD observations at Birkenes made within the months.

Month/Year	Jan	Feb	Mar	Apr	May	Jun	Jul	Aug	Sep	Oct	Nov	Dec
Number of days with cloud-free and quality assured observations (lev 2; lev 1.5 for 2013)												
2009				1	22	25	11	13	15	12		
2010					13	16	18	15	16	10	6	
2011	7	2	20	23	18	20	15	13				
2012			11	12	10	7	16	18	9	12	2	
2013							26	18	13	7		
2014			12	17	16	25	20	13	7			
2015			6	1	14	21	21	16	9	11	3	
2016	1	9	11	8							1	
2017*				2	17	15	17	11	6	8		
2018*				8	27	20	22	15	10			
2019	**6**	**9**	**14**	**23**	**23**	**11**	**5**	**10**			**3**	**3**
Total	**14**	**20**	**74**	**95**	**160**	**160**	**171**	**143**	**85**	**60**	**15**	**3**

* version 3 data analysis (Aeronet)

Table A 11: Monthly means and standard deviation of aerosol optical depth (AOD) at 500 nm at Trollhaugen Observatory.

Month/Year	Jan	Feb	Mar	Apr	May	Jun	Jul	Aug	Sep	Oct	Nov	Dec
Aerosol optical depth (AOD)												
2014	0.016 ±0.002	0.015 ±0.002	0.014 ±0.002	0.014 ±0.005					0.022 ±0.003	0.017 ±0.002	0.021 ±0.002	0.020 ±0.002
2015	0.029 ±0.003	0.018 ±0.003	0.018 ±0.002	0.017 ±0.001				0.048 ±0.009	0.034 ±0.010	0.040 ±0.007	0.035 ±0.009	0.031 ±0.005
2016	0.035 ±0.006	0.033 ±0.004	0.026 ±0.003	0.027 ±0.004				0.039 ±0.010	0.026 ±0.005	0.024 ±0.005	0.019 ±0.005	0.019 ±0.001
2017	0.020 ±0.003	0.020 ±0.003	0.016 ±0.003	0.015 ±0.002				0.022 ±0.006	0.021 ±0.006	0.019 ±0.002	0.020 ±0.004	0.016 ±0.003
2018	0.016 ±0.004	0.016 ±0.002	0.013 ±0.002	0.014 ±0.001	0.013 ±0.003				0.027 ±0.006	0.022 ±0.002	0.020 ±0.003	0.021 ±0.002
2019	0.027 ±0.006	0.026 ±0.006	0.020 ±0.003	0.019 ±0.002	0.015 ±0.001			0.029 ±0.002	0.019 ±0.001	0.022 ±0.001	0.022 ±0.003	0.026 ±0.002
Mean 2014-2019	**0.023 ±0.004**	**0.021 ±0.004**	**0.018 ±0.003**	**0.017 ±0.003**	**0.014 ±0.002**			**0.033 ±0.008**	**0.026 ±0.006**	**0.024 ±0.003**	**0.022 ±0.004**	**0.023 ±0.003**

Table A 12: Monthly means and standard deviation of the Ångström coefficient (Å) at Trollhaugen.

Month/Year	Jan	Feb	Mar	Apr	May	Jun	Jul	Aug	Sep	Oct	Nov	Dec
Ångström coefficient (Å)												
2014	1.59 ±0.18	1.54 ±0.14	1.29 ±0.09	1.22 ±0.08					1.29 ±0.15	1.52 ±0.17	1.37 ±0.15	1.76 ±0.06
2015	1.69 ±0.61	1.60 ±0.12	1.43 ±0.10	1.34 ±0.09				0.97 ±0.15	1.03 ±0.18	1.26 ±0.14	1.22 ±0.34	1.47 ±0.15
2016	1.53 ±0.12	1.63 ±0.14	1.41 ±0.09	1.42 ±0.05				1.32 ±0.21	1.25 ±0.18	1.34 ±0.22	1.53 ±0.13	1.48 ±0.09
2017	1.61 ±0.16	1.68 ±0.10	1.23 ±0.14	1.21 ±0.08				1.08 ±0.18	1.18 ±0.24	1.28 ±0.13	1.35 ±0.19	1.53 ±0.10
2018	1.51 ±0.10	1.45 ±0.09	1.29 ±0.08	1.32 ± 0.17	1.30 ± 0.06				1.47 ±0.16	1.47 ±0.11	1.56 ±0.12	1.73 ±0.08
2019	1.63 ±0.11	1.63 ±0.10	1.56 ±0.08	1.34 ± 0.08	1.26 ± 0.08			0.92 ±0.07	1.51 ±0.12	1.44 ±0.09	1.53 ±0.14	1.61 ±0.10
Mean 2014-2019	**1.58 ±0.17**	**1.59 ±0.12**	**1.37 ±0.11**	**1.30 ±0.10**	**1.27 ±0.07**			**1.13 ±0.18**	**1.26 ±0.18**	**1.38 ±0.14**	**1.45 ±0.17**	**1.59 ±0.10**

Table A 13: Number of days with AOD observations at Trollhaugen made within the months

Month/Year	Jan	Feb	Mar	Apr	May	Jun	Jul	Aug	Sep	Oct	Nov	Dec
Number of days with cloud-free and quality assured observations (lev 2; lev 1.5 for 2013)												
2014	15	22	13	21					4	10	**13**	**11**
2015	7	21	11	12				5	14	12	10	25
2016	20	15	15	13				8	10	15	21	21
2017	24	15	24	9				11	11	15	15	10
2018	22	14	14	22	3				12	20	21	13
2019	12	21	21	11	5			1	7	17	9	20
Total	**100**	**108**	**98**	**88**	**8**			**25**	**58**	**89**	**89**	**110**

Appendix II

Description of instruments and methodologies

On the instrumental methods used for the measurements of the various greenhouse gases at Birkenes and Zeppelin Observatories

In this section of the appendix, the instrumental methods used for the measurements of the various greenhouse gases are presented. Additionally, we explain the theoretical methods used in calculation of the trends.

The next table provides details about greenhouse gas measurements and recent improvement and extensions.

Table A 14: Instrumental details for greenhouse gas measurements at Zeppelin and Birkenes.

Component		Instrument and method	Time res.	Calibration procedures	Start - End	Comment
Methane (Birkenes)	CH_4	Picarro CRDS G1301 CO2/CH4/H2O	1 h 5 s	Working std. calibrated against GAW stds at EMPA	19. May 2009 – Jan 2018	
Methane (Birkenes)	CH_4	Picarro CRDS G2401 CO2/CH4/CO	1 h 5 s	ICOS reference standards	1.Jan 2018 ->	Data coverage in 2019: 95%
Methane (Zeppelin)	CH_4	GC-FID	1h	NOAA reference standards	Aug 2001-Apr 2012	
Methane (Zeppelin)	CH_4	Picarro CRDS	1 h 5 sec	ICOS reference standards	20.Apr. 2012 ->	Data coverage 2019: 94%
Nitrous oxide (Zeppelin)	N_2O	GC-ECD	30 min	NOAA reference standards	27. Mar 2010 – 31. Dec 2015	
Nitrous oxide (Zeppelin)	N_2O	Picarro CRDS	1 h 5 sec	ICOS reference standards	1.Jan 2016 ->	Data coverage 2019 98%
Carbon monoxide (Zeppelin)	CO	GC-HgO/UV	20 min	Every 20 min, working std. calibrated vs. GAW std.	Sep. 2001 - 2012	Data coverage 2019: 94%
Carbon monoxide (Zeppelin)	CO	Picarro CRDS	1 h 5 sec	ICOS reference standards.	20.Apr 2012 ->	Data coverage 2019: 95%
Carbon monoxide (Birkenes)	CO	Picarro CRDS G2401 CO2/CH4/CO	1 h 5 sec	ICOS reference standards.	1.Jan 2018 ->	CO_2 measured by ITM Stockholm University (SU) until 2012
Carbon dioxide (Zeppelin)	CO_2	Li-Cor	1 h	NOAA reference standards	1989 - 2012	Data coverage 2019: 94%
Carbon dioxide (Zeppelin)	CO_2	Picarro CRDS	1 h 5 sec	ICOS reference standards	20.Apr. 2012 ->	
Carbon dioxide (Birkenes)	CO_2	Picarro CRDS G1301 CO2/CH4/H2O	1 h 5 s	Working std. calibrated against GAW stds at EMPA	19. May 2009 –– Jan 2018>	Data coverage in 2019: 95%
Carbon dioxide (Birkenes)	CO_2	Picarro CRDS G2401 CO2/CH4/CO	1 h 5 s	ICOS reference standards	1.Jan 2018 ->	Data coverage 2019: 94%
CFC-11 CFC-12 CFC-113 CFC-115 HFC-125 HFC-134a HFC-152a HFC-365mfc HCFC-22 HCFC-141b HCFC-142b H-1301 H-1211 H-2402	$CFCl_3$ CF_2Cl_2 $CF_2ClCFCl_2$ CF_3CF_2Cl CHF_2CF_3 CH_2FCF_3 CH_3CHF_2 $CF_3CH_2CHF_2C$ H_3 CHF_2Cl CH_3CFCl_2 CH_3CF_2Cl CF_3Br CF_2ClBr	ADS-GCMS	4 h	Every 4 hours, working std. calibrated vs. AGAGE std.	4.Jan 2001-2010	The measurements of the CFCs, TCE and PCE have higher uncertainty and are not within the required precision of AGAGE. See next section for details.

Component		Instrument and method	Time res.	Calibration procedures	Start - End	Comment
Chloromethane	CH_3Cl	ADS-GCMS	4h	Every 4 hours, working std. calibrated vs. AGAGE std.	4.Jan 2001-2010	
Bromomethane	CH_3Br					
Dichloromethane	CH_2Cl_2					
Trichloromethane	$CHCl_3$					
Trichloroethane	CH_3CCl_3					
Trichloroethene	$CHClCCl_2$					
Tetrachloroethene	CCl_2CCl_2					
Sulphurhexafluoride	SF_6					
Nitrogen trifluoride	NF_3	Medusa-GCMS No. 19	2 h	Every 2 hours, working std. calibrated vs. AGAGE std	1. September 2010	Data coverage 2019: 87% (except for CFC-11, CFC-12, H-1211 (60%), Carbontetra-Chloride (50%),Benzene and Toluene where data coverage in 2019 were 10%)
PFC-14	CF_4					
PFC-116	C_2F_6					
PFC-218	C_3F_8					
PFC-318	$c\text{-}C_4F_8$					
Sulphurhexafluoride	SF_6					
Sulfuryl fluoride	SO_2F_2					
HFC-23	CHF_3					
HFC-32	CH_2F_2					
HFC-125	CHF_2CF_3					
HFC-134a	CH_2FCF_3					
HFC-143a	CH_3CF_3					
HFC-152a	CH_3CHF_2					
HFC-227ea	CF_3CHFCF_3					
HFC-236fa	$CF_3CH_2CF_3$					
HFC-245fa	$CF_3CH_2CHF_2$					
HFC-365mfc	$CH_3CF_2CH_2CF_3$					
HFC-43-10mee	$CF_3(CHF)_2CF_2CF_3$					
HCFC-22	$CHClF_2$					
HCFC-141b	CH_3CCl_2F					
HCFC-142b	CH_3CClF_2					
CFC-11	CCl_3F					
CFC-12	CCl_2F_2					
CFC-113	CCl_2FCClF_2					
CFC-115	$CClF_2CF_3$					
H-1211	$CBrClF_2$					
H-1301	$CBrF_3$					
H-2402	$C_2Br_2F_4$					
Chloromethane	CH_3Cl					
Bromomethane	CH_3Br					
Dichloromethane	CH_2Cl_2					
Trichloromethane	$CHCl_3$					
Trichloroethane	CH_3CCl_3					
Dibromomethane	CH_2Br_2					
Trichloroethene	$CHClCCl_2$					
Tetrachloroethene	CCl_2CCl_2					
Carbon tetrachloride	CCl_4					
Ethane	C_2H_6					
Propane	C_3H_8					
Butane	C_4H_{10}					
Pentane	C_5H_{12}					
Benzene	C_6H_6					
Toluene	$C_6H_5CH_3$					
Ozone	O_3		5 min			

The overall data coverage for 2019 was 87 %. But for CFC-11, CFC-12 and H-1211 there were issues with the instrument from September 2019, so these data had to be rejected for the rest of the year (solved in Feb 2020). Earlier problems with unstable reference values in the reference standard for Carbontetrachloride were solved in June 2019 and an ongoing unsolved issue in the trapping system for air samples of Trichloroethene, Benzene and Toluene was solved in November 2019.

DATA QUALITY AND UNCERTAINTIES

HALOCARBONS

In 2001 – 2010 measurements of a wide range of hydrochlorofluorocarbons, hydrofluorocarbons (HCFC-141b, HCFC-142b, HFC-134a etc.), methyl halides (CH_3Cl, CH_3Br, CH_3I) and the halons (e.g. H-1211, H-1301) were measured with good scientific quality by using ADS-GCMS. The system also measured other compounds like the chlorofluorocarbons (CFCs), but the quality and the precision of these measurements were not at the same level. Table A 15shows a list over those species measured with the ADS-GCMS at Zeppelin Observatory from 2001 - 2010. The species that are in blue are of acceptable scientific quality and in accordance with recommendations and criteria of the AGAGE network for measurements of halogenated greenhouse gases in the atmosphere. Those listed in red have higher uncertainties and are not within the required precision of AGAGE. There are various reasons for these increased uncertainties; unsolved instrumental problems e.g. possible electron overload in detector (for the CFC's), influence from other species, detection limits (CH_3I, $CHClCCl_2$) and unsolved calibration problems ($CHBr_3$) or instrumental issues (CCl_2CCl_2). At September 1st 2010, the ADS-GCMS was replaced by a Medusa-GCMS system. The uncertainties improved for almost all species (Table A 11 for details), but there are periods where measurements of the CFC's were still not satisfactory due to a failure in the detector and still high blank values and memory effects in the instruments leads to higher uncertainties in the CHClCCl2 (TCE) measurements .

Table A 15: ADS-GCMS measured species at Zeppelin from 4 January 2001 to 1 September 2010. Good scientific quality data in Blue; Data with reduced quality data in Red. The data are available through http://ebas.nilu.no. Please read and follow the stated data policy upon use.

Compound	Typical precision (%)	Compound	Typical precision (%)
SF_6	1.5	H1301	1.5
HFC134a	0.4	H1211	0.4
HFC152a	0.6	CH_3Cl	0.6
HFC125	0.8	CH_3Br	0.8
HFC365mfc	1.7	CH_3I	5.1
HCFC22	0.2	CH_2Cl_2	0.4
HCFC141b	0.5	$CHCl_3$	0.3
HCFC142b	0.5	$CHBr_3$	15
HCFC124	2.3	CCl_4	0.5
CFC11	0.3	CH_3CCl_3	0.6
CFC12	0.3	$CHClCCl_2$	1.2
CFC113	0.2	CCl_2CCl_2	0.7
CFC115	0.8		

Table below gives an overview over the species measured with the Medusa-GCMS systems at the AGAGE stations and the typical precision with the different instruments. The Medusa-GCMS instrument at the Zeppelin Observatory has the same precision as shown in the Table A 16.

Table A 16: AGAGE measured species.

Compound	Typical precision (%)	Compound	Typical precision (%)
NF_3	1	CFC-11	0.15
CF_4	0.15	CFC-12	0.05
C_2F_6	1	CFC-113	0.2
C_3F_8	3	CFC-115	0.8
c-C4F8	1.5	H-1301	1.7
SF_6	0.6	H-1211	0.4
SO_2F_2	2	H-2402	2
HFC-23	0.7	CH_3Cl	0.2
HFC-32	3	CH_3Br	0.6
HFC-134a	0.5	CH_2Cl_2	0.5
HFC-152a	1.4	CH_2Br_2	1.5
HFC-125	0.7	CCl_4	1
HFC-143a	1	CH_3CCl_3	0.7
HFC-227ea	2.2	$CHClCCl_2$	3
HFC-236fa	10	CCl_2CCl_2	0.5
HFC-245fa	3	C_2H_6	0.3
HFC-365mfc	5	C_3H_8	0.6
HFC-43-10mee	3	C_4H_{10}	0.6
HCFC-22	0.3	C_6H_6	0.3
HCFC-141b	0.5	C_7H_8	0.6
HCFC-142b	0.4		

METHANE

Methane is measured at both Birkenes and Zeppelin using a Picarro CRDS (Cavity Ring-Down Spectrometer) monitor which is calibrated against ICOS reference standards (NOAA scale). The instrument participates in ring tests and applies to the ICOS system for calibration and measurement control. The continuous data are also compared to weekly flask samples sent to NOAA CMDL, Boulder Colorado. All data are available for download from EBAS database http://ebas.nilu.no.

$\delta^{13}C_{CH4}$

Air samples from Zeppelin are collected in 1 L steel or aluminium canisters at the same air inlet as CH_4. Two samples per week are sent to the Greenhouse Gas Laboratory at Royal Holloway University of London. Methane mole fraction was measured using a Picarro 1301 cavity ring down spectrometer (CRDS). Methane δ13C analysis is carried out using a modified gas chromatography isotope ratio mass spectrometry system for all samples (Trace Gas and Isoprime mass spectrometer, Isoprime Ltd.) with 0.05‰ repeatability. All measurements for the canisters are made in triplicate. See Fischer et al, 2017 and Myhre et al, 2016 for more details.

N_2O MEASUREMENTS

N_2O at Zeppelin is now measured using a new mid-IR Cavity Ring Down instrument (since December2017) which is calibrated against ICOS reference standards (NOAA scale). The instrument participates in ring tests and applies to the ICOS system for calibration and measurement control. The continuous data are also compared to weekly flask samples sent to NOAA CMDL, Boulder Colorado.

This new instrument is doing continuous measurements with improved precision and higher measurement frequency (< 1 min).

CO_2 MEASUREMENTS

Carbon dioxide (CO_2) at Birkenes and Zeppelin is monitored using a Picarro Cavity Ring-Down Spectrometer for continuous measurements, calibrated against a set of ICOS reference standards (NOAA scale). The instrument participates in ring tests and applies to the ICOS system for calibration and measurement control. The continuous data are also compared to weekly flask samples sent to NOAA CMDL, Boulder Colorado. All data will be available for download from the EBAS database http://ebas.nilu.no.

CO MEASUREMENTS

Carbon monoxide (CO) at Birkenes and Zeppelin is monitored using a Picarro Cavity Ring-Down Spectrometer for continuous measurements, calibrated against a set of ICOS reference standards (NOAA scale). The instrument participates in yearly ring tests and applies to the ICOS system for calibration and measurement control. The continuous data are also compared to weekly flask samples sent to NOAA CMDL, Boulder Colorado. All data will be available for download from the EBAS database http://ebas.nilu.no.

^{14}C IN CO2 MEASUREMENTS

As part of the ICOS program, isotope ^{14}C in CO2 is sampled every 2-weeks. CO2 is absorbed by sodium hydroxide solution (NaOH 4mol/l) in a rotating Raschig-tube. The liquid sodium hydroxide samples are transferred into glass bottles and sent to the ICOS Central Radiocarbon Laboratory for analysis of the 14C/C ratio in the absorbed CO2. Sampling started in 2017.

IMPLEMENTATION OF MEASUREMENTS FROM BIRKENES AND ZEPPELIN INTO ICOS RESEARCH INFRASTRUCTURE

The Integrated Carbon Observation System (ICOS) is a European research infrastructure forming an observation system that will measure and assess the global carbon budget, including atmospheric CO_2, CH_4 and CO concentrations, while ensuring independent and reliable measurements. ICOS-Norway (https://no.icos-cp.eu) contributes to the network of atmospheric measurements with two observatories, Birkenes and Zeppelin.

ICOS has divided their sites into two labels Class 1 and Class 2, dependent on instrumental setup. At Class 1 sites a wider range of measurements of different species are required. Whilst for Class 2 fewer parameters are mandatory. The labelling process evaluates the site set up, the instrumentation with its calibration set-up and data handling, as a quality certificate of the data output from the ICOS site (Figure 66). The labelling process is time consuming as the instrument (Picarro) needs to be evaluated for minimum 1 month at the central ICOS lab, ICOS Atmospheric Thematic Centre (ATC) in France. Another central ICOS lab, ICOS Central Analytical Laboratories (CAL) in Germany, provides calibration cylinders and it takes 4 months to produce them. The same lab provides calibration cylinders and it takes 4 months to produce them. After having the instrument and calibration routines established at the site, the measurements will have to go through a 6 months evaluation period before approval as an ICOS site. In total it typically takes about 1.5 years to get an ICOS certificate.

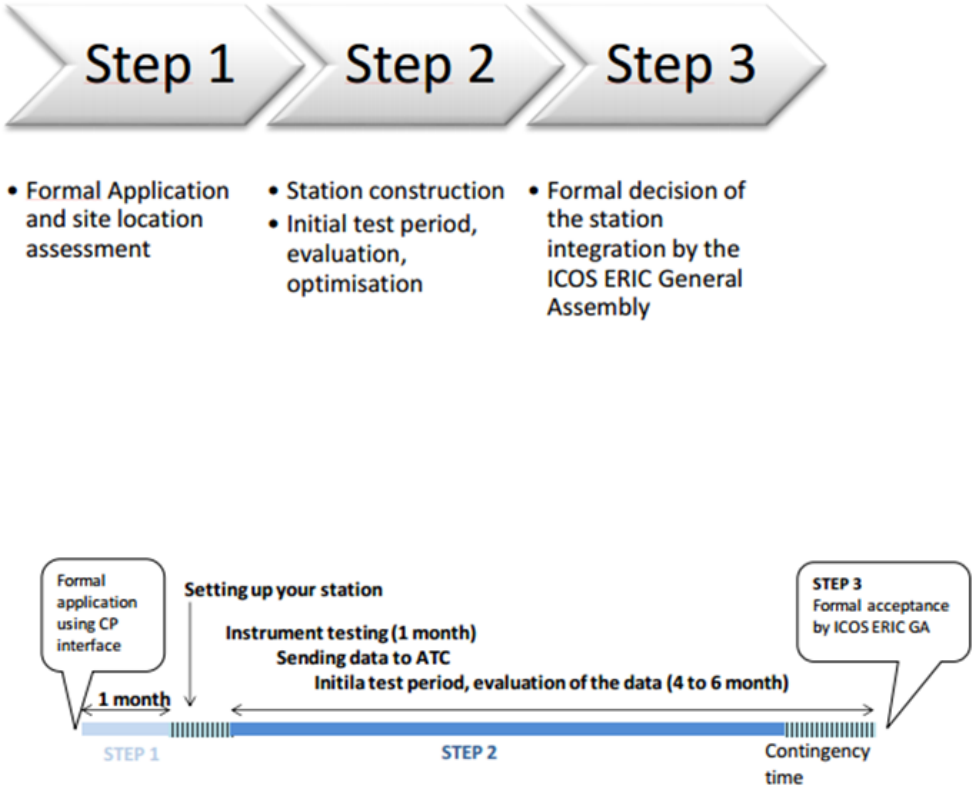

Figure 66: Outline of the labelling process for ICOS stations according to the atmosphere thematic centre (ATC).

The ATC has established the following recommended parameters for ICOS Class 1 and Class 2 sites:

Category	Gases, continuous	Gases, periodical	Meteorology, continuous	Eddy Fluxes
Class 1 Mandatory parameters	• **CO_2, CH_4, CO** : at each sampling height	• **CO_2, CH_4, N_2O, SF_6, CO, H_2, ^{13}C and ^{18}O in CO_2**: weekly sampled at highest sampling height†	• **Air temperature, relative humidity, wind direction, wind speed**: at highest and lowest sampling height*	
		• **^{14}C** (radiocarbon integrated samples): at highest sampling height	• **Atmospheric Pressure**	
			• **Planetary Boundary Layer Height**** †	
Class 2 Mandatory parameters	• **CO_2, CH_4** : at each sampling height		• **Air temperature, relative humidity, wind direction, wind speed**: at highest and lowest sampling height*	
			• **Atmospheric Pressure**	
Recommended parameters***	• **^{222}Rn, N_2O, O_2/N_2 ratio**	• **CH_4 stable isotopes, O_2/N_2 ratio** for Class 1 stations: weekly sampled at highest sampling height		• **CO_2** : at one sampling height
	• **CO** for Class 2 stations			

* Atmospheric temperature and relative humidity recommended at all sampling heights

** Only required for continental stations.

*** Recommended for its scientific value but support from ATC in terms of protocols, data base, spare analyzer will not be ensured as long as the parameters are not mandatory.

The Zeppelin Observatory was labelled as an ICOS Class 1 site in 2018. Meanwhile, for sites such as Birkenes, classed as a 'continental site' by ICOS, the ATC requires that measurements are from air sampled at 100 m above ground or higher, typically using sampling inlets installed on a mast, with additional sampling at 10 m, and between 40-70 m. The purpose of this is to minimise the influence of vegetation (i.e. photosynthesis) on CO_2 measurements. For Zeppelin, a mountain top site, the only requirement was that sampling is 'sufficiently high to avoid contamination e.g. by local sources'.

Due to the location of the Birkenes Observatory on a small hill at 40 m, construction of foundations for a 100 m would be challenging and expensive. Thus, NILU initiated negotiations with ATC to lower the required sampling height on the basis that the Observatory is already elevated by 40 m. The ATC agreed to lower the required sampling height to 75 m, a more feasible mast height requiring less extensive foundations, stating in writing: "The Birkenes Observatory location and site infrastructure fulfil the ICOS requirements and recommendations specified in the latest ICOS Atmospheric Station Specifications document (version 1.3, November 2017) when the tower will be installed."

As of August 28th 2020 construction of the 75 m mast was complete (Figure 2 and Figure 67) and the installation of equipment on the mast (meteorological equipment, sample inlets etc.) were mostly done by the second week of September. The very first measurements from the 75-meter mast were performed on the 14th of September. The finalization of the installation is scheduled to the beginning of October. Note that the new mast has also required changes to the station infrastructure i.e. changing the location of the station entrance, upgraded protection from lightning strikes and falling ice, as well as changes in health and safety procedures (the station may no longer be accessed if there is a risk of thunder storms).

Figure 67: Birkenes Observatory with the new 75 m mast installed August-September 2020 to comply with the ICOS requirements.

Status of the labelling process for Birkenes and Zeppelin Observatories:

- The Zeppelin Observatory has achieved Class 1 status and is now fully integrated in the network
- Birkenes has the analyzer (Picarro) installed and run continuous measurements of CH_4, CO_2 and CO.
- The analyzer has been at ICOS ATC for 1 month evaluation.
- ICOS calibration tanks and calibration routines have been implemented at Birkenes
- Mandatory meteorological parameters are measured with the upgraded equipment to meet the ICOS precision criteria at Birkenes.
- Permission granted by the landowner and Avinor to install a tall sampling tower (up to 100m) at Birkenes.
- 75 m mast installed
- Equipment being installed on the mast in September 2020
- Approval of class 2 label at Birkenes by ATC confirmed pending operational status of measurements at the mast

At class 1 sites an automatic flask sampler is mandatory and has been installed at the Zeppelin station. The flask sampling program is still under development by ICOS and sampling will start as soon as this is in place.

AIR INLET AT ZEPPELIN

In 2011 the air inlet for the GHG measurements at Zeppelin were improved to reduce possible influence from the station and visitors at the station. The inlet was moved away from the station and installed in a 15 m tower nearby for the following components:

- N_2O
- CH_4
- CO_2
- CO
- Halogenated compounds
- NOAA flaks sampling program
- Isotope flask sampling of CO_2 and CH_4

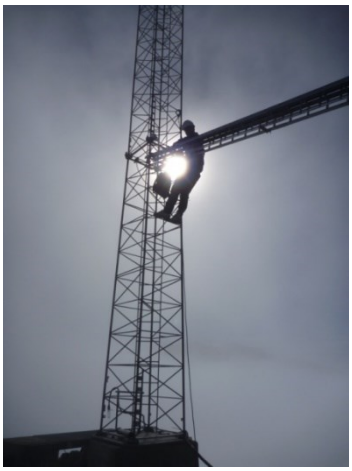

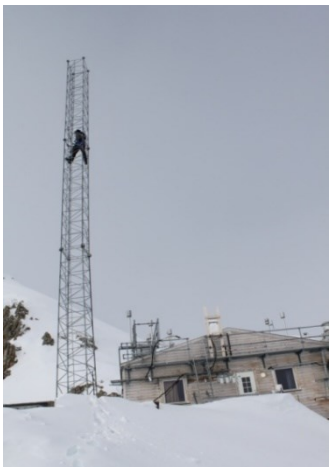

DETERMINATION OF BACKGROUND DATA

Based on the daily mean concentrations an algorithm is selected to find the values assumed as clean background air. If at least 75% of the trajectories within +/- 12 hours of the sampling day are arriving from a so-called clean sector, defined below, one can assume the air for that specific day to be non-polluted. The remaining 25% of the trajectories from European, Russian or North American sector are removed before calculating the background.

CALCULATION OF TRENDS FOR GREENHOUSE GASES AND VOCS

To calculate the annual trends the observations have been fitted as described in Simmonds et al. (2006) by an empirical equation of Legendre polynomials and harmonic functions with linear, quadratic, and annual and semi-annual harmonic terms:

$$f(t) = a + b\left(\frac{N}{12}\right)\cdot P_1\left(\frac{t}{N}-1\right) + \frac{1}{3}\cdot d\left(\frac{N}{12}\right)^2 \cdot P_2\left(\frac{t}{N}-1\right) + c_1\cdot\cos\left(\frac{2\pi t}{12}\right) + s_1\sin\left(\frac{2\pi t}{12}\right) + c_2\cos\left(\frac{4\pi t}{12}\right) + s_2\sin\left(\frac{4\pi t}{12}\right)$$

The observed *f* can be expressed as functions of time measures from the 2N-months interval of interest. The coefficient *a* defines the average mole fraction, *b* defines the trend in the mole fraction and *d* defines the acceleration in the trend. The *c* and *s* define the annual and inter-annual cycles in mole fraction. N is the mid-point of the period of investigation. P_i are the Legendre polynomials of order *i*.

This equation is used for all GHGs except for the halocarbons, where the fit between the empirical equation and observations improves if the semi-annual harmonic terms are replaced by an additional Legendre polynomial.

We are applying a new and improved method for estimating the *uncertainties* in the estimated annual trends from the time series regression modelling. In previous years, these uncertainties were estimated using a standard method from ordinary linear regression, where it was implicitly assumed that the residuals of the fitted regression models were uncorrelated. However, the use of such standard methods is known to often underestimate the true uncertainties in the estimated parameters if these assumptions are not true, i.e. if the residuals are autocorrelated, which to a large extent is the case for the regression models being fitted here.

In the current report we have replaced the standard method with a new method for estimation of uncertainties in the estimated annual trend that takes into account the presence of autocorrelated errors in the fitted model residuals. The new method also takes into account possible presence of heteroscedasticity, which means that the variances of the residuals might vary with the level of the time series, which also affects the uncertainties of the estimated trend. To this end we use the routine **vcovHAC** in the **sandwich** package in R (R Core Team, 2018) as described in Zeileis (2006; 2004), to estimate standard deviation of all estimated parameters of the time series regression models. Here HAC is short for Heteroscedastic and Autocorrelation Consistent.

It is important to emphasize that the new method only alters the estimated *uncertainties* of the annual trend estimates. The annual trend estimates themselves are not influenced by this update and have been correctly estimated using standard linear regression also in previous year's reports.

ON THE SURFACE IN SITU OBSERVATIONS OF AEROSOL MICROPHYSICAL AND OPTICAL PROPERTIES AT BIRKENES, ZEPPELIN AND TROLLHAUGEN OBSERVATORY

Table A 17: Overview of atmospheric aerosol parameters measured by surface in situ observations operated at which station

	Birkenes	Trollhaugen	Zeppelin
Particle Number Size Distribution (fine size range D_p < 0.8 µm)	X	X	X
Particle Number Size Distribution (coarse size range D_p > 0.8 µm)	X		X
Particle Number Size Distribution, refractory particle fraction (fine size range D_p < 0.8 µm)			X
Aerosol Scattering Coefficient (spectral)	X	X	
Aerosol Absorption Coefficient (spectral)	X	X	X

Concerning surface in situ observations of microphysical and optical properties of atmospheric aerosol, the table on the left gives an overview over the parameters observed at Birkenes, Trollhaugen, and Zeppelin stations and operated by NILU.

To achieve high quality data with appropriate uncertainty and precisions, this requires networked instruments to participate in inter-comparisons at ACTRIS aerosol calibration centre in Leipzig, Germany, in regular intervals. This activity has proven to be necessary in order to ensure comparable measurements within the distributed infrastructure. The frequency of these inter-comparisons, once every 2-3 years, is balanced with minimising the downtime associated with these quality assurance measures. In 2016, instruments targeting the direct aerosol climate effect were in the focus of inter-comparisons. Both the integrating nephelometer and the newer filter absorption photometer, measuring the spectral aerosol particle scattering and absorption coefficients respectively, were scheduled for being inter-compared, with satisfactory outcome in both cases.

With respect to microphysical aerosol properties, the particle number size distribution (PNSD) at surface-level is observed at all 3 stations covered in this report, at least over parts of the relevant range in particle size. The relevant particle sizes cover a range of 0.01 µm – 10 µm in particle diameter. The diameter range of 1.0 µm – 10 µm is commonly referred to as coarse mode, the range D_p < 1.0 µm as fine mode. The fine mode is separated further into Aitken-mode (0.01 µm < D_p < 0.1 µm) and accumulation mode (0.1 µm < D_p < 1 µm). The distinction of these modes is justified by different predominant physical processes as function of particle size. In the Aitken-mode, particles grow by condensation of precursor gases from the gas-phase, and coagulate among themselves or with accumulation mode particles. Accumulation mode particles grow by taking up Aitken-mode particles or by mass uptake while being activated as cloud droplets, and they are removed by precipitation. Coarse mode particles in turn are formed by break-up of biological or crustal material, including pollen, bacteria, and fungus spores, and removed by gravitational settling and wet removal. The PNSD of an aerosol is needed for quantifying any interaction or effect of the aerosol since all of them depend strongly on particle size.

To measure the PNSD over the full relevant size range, several measurement principles need to be combined. A Differential Mobilty Particle Spectrometer (DMPS) measures the particle number size distribution, now in the range of 0.01 – 0.8 µm particle diameter after several improvements of the instruments at all three stations, i.e. almost the full fine mode. In a DMPS, the particles in the sample air stream are put into a defined state of charge by exposing them to an ionised atmosphere in thermal equilibrium. The DMPS uses a cylindrical capacitor to select a narrow size fraction of the particle phase. The particle size of the selected size fraction is determined by the voltage applied to the capacitor. The particle number concentration in the selected size fraction is then counted by a Condensation Particle Counter (CPC). A mathematical inversion that considers charge probability, diffusional losses of

particles in the system, transfer function of the capacitor, and counting efficiency of the CPC is then used to calculate the particle number size distribution.

The PNSD of particles with diameters 0.25 µm < D_p < 30 µm is measured with an Optical Particle Spectrometer (OPS). In the OPS, the particles in the sample stream are focussed through a laser beam. The instrument registers number and amplitude of the pulses of light scattered by the particles. The particle pulses are sorted into a histogram by their amplitude, where the pulse amplitude yields the particle diameter and the pulse number the particle concentration, i.e. together the PNSD. Both, the DMPS and the OPS, yield method specific measures of the particle diameter, the electrical mobility and the optical particle diameter, respectively. When related to the spherical equivalent geometric particle diameter commonly referred to, both particle size measures depend on particle shape (causing a 5% systematic uncertainty in particle diameter), the optical particle diameter in addition on particle refractive index (causing a 20% systematic uncertainty in particle diameter). Where possible, the PNSDs provided by DMPS and OPS are joined into a common PNSD, in this report. To quality assure this process, PNSDs are accepted only if DMPS and OPS PNSD agree within 25% in particle diameter in their overlap size range. Together, both instruments provide a PNSD that spans over 3 orders of magnitude in particle diameter, and over 6 orders of magnitude in particle concentration.

Optical aerosol parameters quantify the direct aerosol climate effect. The observation programme at Birkenes includes the spectral particle scattering coefficient $\sigma_{sp}(\lambda)$ and the spectral particle absorption coefficient $\sigma_{ap}(\lambda)$. The scattering coefficient quantifies the amount of light scattered by the aerosol particle population in a sample per distance a light beam travels through the sample. The absorption coefficient is the corresponding property quantifying the amount of light absorbed by the particle population in the sample. An integrating nephelometer is used for measuring $\sigma_{sp}(\lambda)$ at 450, 550, and 700 nm wavelength. In this instrument, the optical sensors look down a blackened tube that is filled with aerosol sample. The tube is illuminated by a light source with a perfect cosine intensity characteristic perpendicularly to the viewing direction. It can be shown mathematically that this setup integrates the scattered light seen by the optical sensors over all scattering angles. The nephelometer at Birkenes has successfully undergone quality assurance by intercomparison within the EU research infrastructure ACTRIS in 2015. In 2017 we detected drift in the older filter absorption photometer operated at Birkenes since 2009 through carefully implemented quality control within ACTRIS. The drift was detected by operating the older filter absorption photometer in parallel with a newer, more stable make and model in order to ensure a continuous, rupture-free aerosol absorption time series at Birkenes. In addition, the newer instrument was sent to an inter-comparison within the European research infrastructure for short-lived climate forcers ACTRIS. These exercises connect individual instruments to a network-wide primary standard, ensuring traceability and comparability of observations at stations in the network. The old instrument exhibiting the drift has since been decommissioned.

For the nephelometer at Trollhaugen, such intercomparisons are impossible because of the remote Antarctic location and associated logistical challenges. However, the Trollhaugen instrument undergoes the same regular on-site quality assurance as the Birkenes instrument, including regular calibration verification traceable to physical first principles (calibration with high-purity carbon dioxide, where scattering coefficient of carbon dioxide can be calculated from fundamental quantum mechanics).

The spectral particle absorption coefficient $\sigma_{ap}(\lambda)$ is measured by filter absorption photometers. A filter absorption photometer infers $\sigma_{ap}(\lambda)$ by measuring the decrease in optical transmissivity of a filter while the filter is loaded with the aerosol sample. The transmissivity time series is subsequently translated into an absorption coefficient time series by using Lambert-Beer's law, the same law also used in optical spectroscopy. The filter absorption photometers deployed at Birkenes are a custom-built 1 wavelength Particle Soot Absorption Photometer (PSAP), and a commercial 3-wavelength PSAP. The 1-wavelength PSAP received quality assurance by intercomparison within ACTRIS in 2013 discovering calibration stability issues. The 3-wavelength PSAP has undergone ACTRIS intercalibration successfully

in 2015, i.e. without discovering any issues. Thus, both instruments are interpreted in combination to benefit from both, quality assurance in a research network and spectral capabilities. For 2013 and later, the data of the 3-wavelength PSAP are used, for 2010-2012, the data of the older 1-wavelength are used after being corrected by comparison with the newer instrument during the overlap period. For comparison with the nephelometer, the PSAP data has been transferred to a wavelength of 550 nm using the measured spectral dependence (3-wavelength PSAP), or by assuming an absorption Ångström coefficient $å_{ap}$ of -1 (1-wavelength PSAP, adding 2% systematic uncertainty to the data).

For measuring $\sigma_{ap}(\lambda)$ at Zeppelin, a more recently developed filter absorption photometer, an aethalometer type AE33, has been deployed in 2015. The AE33 features a larger spectral range of 370 – 950 nm as compared to other instruments, and offers a 7-wavelength resolution across this range. Previous aethalometer models suffered from high systematic uncertainties due to uncorrected dependencies on filter loading (e.g. Collaud Coen et al.,2010). Comparisons and calibrations within ACTRIS have shown that this systematic uncertainty has been reduced significantly in the AE33 model by an internal loading compensation (Drinovec et al., 2015). Due to this successful instrument evaluation, the instrument programme at Birkenes has been upgraded by an AE33 in 2017 as well.

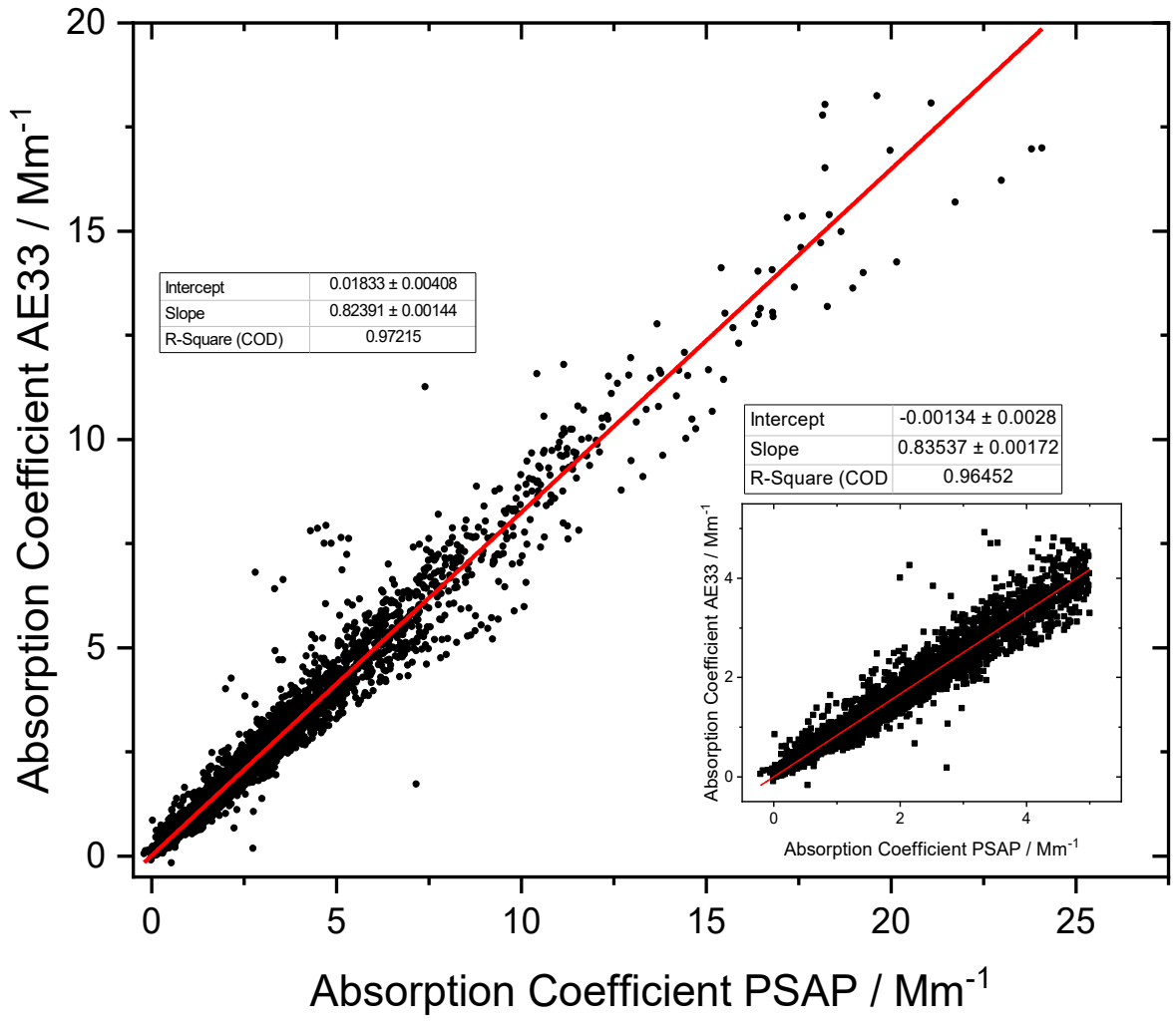

Figure 68: Comparison of particle absorption coefficient data measured the Particle Absorption Photometer (PSAP) deployed at Birkenes in 2012, and the AE33 aethalometer deployed there in 2017. The wavelength of the absorption coefficient has been interpolated to 550 nm for both instruments. The data are compared as scatter plot with regression line (red), large panel for the total range of values, small panel for values ≤ 5 Mm^{-1}.

Figure 68 compares the particle absorption coefficient between the Particle Absorption Photometer (PSAP) deployed at Birkenes in 2012, and the AE33 aethalometer deployed there in 2017 with a scatter plot including regression line. The analysis shows a correlation coefficient R^2 of 0.97 for the whole range of values, i.e. 97% of the variation in the data of one instrument is explained by the respective variation of the other instrument. This result ensures that the new instrument will continue the time series consistently. The slope of the regression line deviates from 1. Corresponding calibration factors are currently being established by the ACTRIS Research Infrastructure.

Even though the older filter absorption photometer underwent quality assurance by off-site intercomparison within ACTRIS in 2013, a drift of the reading of the older compared to the newer instrument can be observed between 2013 – 2015. These stability issues of the older filter absorption photometer were discovered already during the 2013 intercomparison. Consequently, also the newer filter absorption photometer was subjected to an ACTRIS intercomparison in 2015. The intercomparison discovered no issues with the newer instrument and confirmed stability of calibration. As a result, the whole σ_{ap} time series obtained with the old filter absorption photometer has been corrected with the 2012 instrument as reference, yielding a consistent aerosol absorption time series for Birkenes for the years 2010 - 2017. In 2017, the 2012 absorption photometer experienced problems related to an unstable measurement of the sample flow, leading to low data coverage in summer 2017. Due to the importance of the aerosol absorption measurement in relation to emissions from biomass combustion for domestic heating, it was decided to install the new 7-wavelength version in parallel, and keep both instruments running as mutual backup.

All in situ observations of aerosol properties representing the ground-level are conducted for the aerosol at dry-state (RH < 40%) for obtaining inter-comparability across the network.

DETAILS ABOUT AEROSOL OPTICAL DEPTH MEASUREMENTS

The amount of particles in the air during sunlit conditions is continuously monitored by means of Precision-Filter-Radiometer (PFR) sun photometers, located at the Sverdrup station in Ny-Ålesund and at Trollhaugen Atmospheric Observatory, Troll Station, Antarctica, and a Cimel instrument at Birkenes. The observations in Ny-Ålesund and at Troll Station are performed in collaboration with PMOD/WRC (N. Kouremeti, S. Kazadzis), Davos, Switzerland. The main instrument characteristics are given below.

AERONET - Cimel C-318

- Sun (9 channels) and sky radiances
- Wavelength range: 340-1640 nm
- 15 min sampling
- No temperature stabilization
- AOD uncertainty: 0.01-0.02

PFR-GAW- Precision Filter Radiometer

- Direct sun measurements (4 channels)
- Wavelength range: 368 - 862 nm
- 1 min averages
- Temperature stabilized
- AOD uncertainty: 0.01

Figure 69: Photos and typical features of the standard instrument of the AERONET (left panel) and GAW PFR network instruments (right panel)

The sun-photometer measurements in Ny-Ålesund are part of the global network of aerosol optical depth (AOD) observations, which started in 1999 on behalf of the WMO GAW program. The instrument is located on the roof of the Sverdrup station, Ny-Ålesund, close to the EMEP station on the Zeppelin Mountain (78.9°N, 11.9°E, 474 m a.s.l.). The Precision Filter Radiometer (PFR) has been in operation since May 2002. In Ny-Ålesund, the sun is below 5° of elevation from 10 October to 4 March, limiting the period with sufficient sunlight to the spring-early autumn season. However, during the summer months it is possible to measure day and night if the weather conditions are satisfactory. The instrument measures direct solar radiation in four narrow spectral bands centred at 862 nm, 501 nm, 411 nm, and 368 nm. Data quality control includes instrumental control like detector temperature and solar pointing control as well as objective cloud screening. Measurements made at full minutes are averages of 10 samples for each channel made over a total duration of 1.25 seconds. SCIAMACHY TOMSOMI and OMI ozone columns as well as meteorological data from Ny-Ålesund are used for the retrieval of aerosol optical depth (AOD).

At Birkenes Observatory, aerosol optical depth measurements started in spring 2009, utilizing an automatic sun and sky radiometer (CIMEL type CE-318) of the global Aerosol Robotic Network (AERONET) at NASA-GSFC, with spectral interference filters centred at selected wavelengths: 340 nm, 380 nm, 440 nm, 500 nm, 675 nm, 870 nm, 1020 nm, and 1640 nm. The measurement frequency is approximately 15 minutes (this depends on the air-mass and time of day). Calibration is performed about once per year, at the Atmospheric Optics Group at the University of Valladolid (GOA-UVa), Spain. GOA manages the calibration for the AERONET sun photometers of the European sub-network of AERONET. Raw data are processed and quality assured centrally by AERONET. Data reported for 2009 - 2017 are quality-assured AERONET level 2.0 data, which means they have been pre- and post-field-calibrated, automatically cloud cleared and have been manually inspected by AERONET.

From 2017, only the new analysis algorithm (version 3) is used at the central AERONET analysis unit at NASA GSFC. In this version, the data quality control, including cloud screening, has been improved and a temperature correction has been applied to all wavelength channels. A comparison between the

data from all years of operations at Birkenes (2019 – 2016) analysed with version 3 and version 2 revealed an increase of 25% in number of usable data, especially in the winter half-year. While during the summer months, the agreement between the two versions is better than 2% for both AOD and (470, 870nm) Ångström coefficient, there are significant deviations (>10%) in the months with less than 1000 observations over the whole period (November – February). A comprehensive analysis of the differences between the two versions and possible effects on trend studies is in progress; a paper by the NASA GSFC team will be published in the near future.

Due to the large gaps in data acquisition caused by the obligatory annual calibrations at the University of Valladolid combined with technical problems and occasionally unfavourable weather conditions at Birkenes, NILU decided to purchase a second Cimel instrument which will be operated alternately with the current instrument. It will be taken into operation in fall 2018.

OUTLOOK ON OBSERVATIONS OF AEROSOL OPTICAL DEPTH IN NY-ÅLESUND BEYOND 2019

A major obstacle to obtaining a year-round AOD climatology in the Arctic arises from the long polar night. To fill gaps in the aerosol climatology at Ny-Ålesund, a lunar photometer will be operated on a quasi-permanent basis in the frame of the SIOS infrastructure project. This is a collaborative initiative between NILU, PMOD/WRC and ISAC-CNR. Seasonal deployments of a lunar photometer owned by PMOD/WRC were already made in the winters of 2014/15 and 2016/17. The multiple-season deployment started in autumn 2018.

Figure 70: Moon PFR on the Kipp & Zonen tracker during the day (left, parking position) and during night-time measurements (right).

The PFR instrument modified by PMOD-WRC was installed on a tracker model Kipp & Zonen provided usually hosting a sun photometer. Figure 70 shows the instrument on the tracker during day-time and night-time. Six lunar cycles were monitored: the first during February 2014, while the other 5 during winter 2014-2015. We collected data on 66 measurement periods, from Moon-rise to Moon-set or from minimum-to-minimum elevation as in Polar Regions no set-rise events are possible. Among these, we obtained 17 distinct good measurement periods, due to the frequent occurrence of clouds. For further details see e.g. Mazzola at al., 2015.

Appendix III

Abbreviations

Abbreviation	Full name
ACSM-ToF	Aerosol Chemical Speciation Monitor
ACTRIS	Aerosols, Clouds, and Trace gases Research InfraStructure Network
ADS-GCMS	Adsorption-Desorption System – Gas Chromatograph Mass Spectrometer
AeroCom	Aerosol Comparisons between Observations and Models
AERONET	Aerosol Robotic Network
AGAGE	Advanced Global Atmospheric Gases Experiment
AIRS	Atmospheric Infrared Sounder
AMAP	Arctic Monitoring and Assessment
AOD	Aerosol optical depth
AWI	Alfred Wegener Institute
BC	Black carbon
CAMP	Comprehensive Atmospheric Monitoring Programme
CCN	Cloud Condensation Nuclei
CCNC	Cloud Condensation Nucleus Counter
CFC	Chlorofluorocarbons
CICERO	Center for International Climate and Environmental Research – Oslo
CIENS	Oslo Centre for Interdisciplinary Environmental and Social Research
CLTRAP	Convention on Long-range Transboundary Air Pollution
CO	Carbon monoxide
CPC	Condensation Particle Counter
DMPS	Differential Mobility Particle
EMEP	European Monitoring and Evaluation Programme
ENVRI^{plus}	Environmental Research Infrastructures Providing Shared Solutions for Science and Society
EOS	Earth Observing System
ERF	Effective radiative forcing ERF
ERFaci	ERF due to aerosol–cloud interaction
EU	European Union
EUSAAR	European Supersites for Atmospheric Aerosol Research
FLEXPART	FLEXible PARTicle dispersion model
GAW	Global Atmosphere Watch
GB	Ground based
GHG	Greenhouse gas
GOA-UVA	Atmospheric Optics Group of Valladolid University

Abbreviation	Full name
GOSAT	Greenhouse Gases Observing Satellite
GOSAT-IBUKI	Greenhouse Gases Observing Satellite "IBUKI"
GWP	Global Warming Potential
HCFC	Hydrochlorofluorocarbons
HFC	Hydrofluorocarbons
ICOS	*Integrated Carbon Observation System*
InGOS	Integrated non-CO2 Greenhouse gas Observing System
IPCC	Intergovernmental Panel on Climate Change
ISAC-CNR	Institute of Atmospheric Sciences and Climate (ISAC) of the Italian National Research Council
ITM	Stockholm University - Department of Applied Environmental Science
JAXA	Japan Aerospace Exploration Agency
LLGHG	Well-mixed greenhouse gases
MOCA	Methane Emissions from the Arctic OCean to the Atmosphere: Present and Future Climate Effects
MOE	Ministry of the Environment
NARE	Norwegian Antarctic Research Expeditions
NASA	National Aeronautics and Space Administration
NEOS-ACCM	Norwegian Earth Observation Support for Atmospheric Composition and Climate Monitoring
NIES	National Institute for Environmental Studies
NOAA	National Oceanic and Atmospheric Administration
NRS	Norsk Romsenter
OC	Organic Carbon
ODS	Ozone-depleting substances
OH	Hydroxyl radical
OPS	Optical Particle Spectrometer
OSPAR	Convention for the Protection of the marine Environment of the North-East Atlantic
PFR	Precision filter radiometer
PMOD/WRC	Physikalisch-Meteorologisches Observatorium Davos/World Radiation Center
PNSD	Particle number size distribution
ppb	Parts per billion
ppm	Parts per million
ppt	Parts per trillion
PSAP	Particle Soot Absorption Photometers

Abbreviation	Full name
RF	Radiative forcing
RI	Research Infrastructure
RIMA	Red Ibérica de Medida fotométrica de Aerosoles
SACC	Strategic Aerosol Observation and Modelling Capacities for Northern and Polar Climate and Pollution
SCIAMACHY	SCanning Imaging Absorption spectroMeter for Atmospheric CHartographY
SIS	Strategisk instituttsatsing
SMPS	Scanning Mobility Particle
TES	Tropospheric Emission Spectrometer
TOA	Top Of Atmosphere
TOMS OMI	Total Ozone Mapping Spectrometer Ozone Monitoring instrument
UN	United Nations
UNFCCC	United Nations Framework Convention on Climate Change
VOC	Volatile organic compounds
WDCA	World Data Centre for Aerosol
WDCS	World Data Centre of Aerosols
WMGHG	Well-mixed greenhouse gases
WMO	World Meteorological Organization

NILU – Norwegian Institute for Air Research

NILU – Norwegian Institute for Air Research is an independent, non-profit institution established in 1969. Through its research NILU increases the understanding of climate change, of the composition of the atmosphere, of air quality and of hazardous substances. Based on its research, NILU markets integrated services and products within analysing, monitoring and consulting. NILU is concerned with increasing public awareness about climate change and environmental pollution.

NILU's values: *Integrity - Competence - Benefit to society*
NILU's vision: *Research for a clean atmosphere*

NILU – Norwegian Institute for Air Research
P.O. Box 100, NO-2027 KJELLER, Norway

E-mail: nilu@nilu.no
http://www.nilu.no

ISBN: 978-82-425-3018-9
ISSN: 2464-3327

Norsk institutt for luftforskning
Norwegian Institute for Air Research